



Vrije Universiteit Brussel

FACULTY OF PHARMACY AND MEDICINE  
CENTER FOR PHARMACEUTICAL RESEARCH  
DEPARTMENT OF ANALYTICAL CHEMISTRY AND PHARMACEUTICAL TECHNOLOGY

## **Near-infrared and Raman spectroscopy for the in-line monitoring of protein unfolding during freeze-drying processes**

Thesis presented to obtain the degree of Doctor in Pharmaceutical Sciences

Sigrid Pieters

Academic Year 2012-2013

Promotors:

Prof. Dr. Yvan Vander Heyden (VUB)  
Prof. Dr. Thomas De Beer (UGent)













Vrije Universiteit Brussel

FACULTY OF PHARMACY AND MEDICINE  
CENTER FOR PHARMACEUTICAL RESEARCH  
DEPARTMENT OF ANALYTICAL CHEMISTRY AND PHARMACEUTICAL TECHNOLOGY

---

## **Near-infrared and Raman spectroscopy for the in-line monitoring of protein unfolding during freeze-drying processes**

---

Thesis presented to obtain the degree of Doctor in Pharmaceutical Sciences

Sigrid Pieters

---

Academic Year 2012-2013

Promotors:

Prof. Dr. Yvan Vander Heyden (VUB)  
Prof. Dr. Thomas De Beer (UGent)





---

## Preface

---

*This thesis is the result of 4.5 years of study and research, an intense experience with many ups and downs. Thanks to the indispensable support, guidance and expertise of certain people, I was able to find my way through this vast project. It is now the moment to express my gratitude to all who supported me from near or far.*

*I would like to thank Prof. Yvan Vander Heyden and Prof. Thomas De Beer, my promoters, for giving me the chance to work on this interesting and hot topic, and for realizing the many practical arrangements and cooperations behind this project. I appreciate their excellent supervision and the time they took to answer all my questions and carefully revise my texts and papers.*

*I am grateful to Prof. Wouter Saeys for his professional assistance in the tablets project. Even the most complex things became clear after being explained by him, and some of his ideas inspired me to solve my lyo problems.*

*An absolute highlight of my PhD was my stay abroad at Irstea. Here, I was able to couple the expansion of my knowledge on spectroscopy, chemometrics and French to the pleasures of the Mediterranean life. An absolute win-win situation! I sincerely thank Dr. Jean-Michel Roger for his great supervision during my stay there. I also would like to thank Alexia for the car pooling every day, and Bernard for the clear explanations on the statistics. I am also grateful to Prof. Steven D. Brown for sharing the office with me. I enjoyed our talks, both chemometrics and non-chemometrics related.*

*Thank you, Iulia, for being such a great office-colleague and friend!*

*Debby, Bieke, Tanika, Johan, Bart, Katrijn, Peggy, Katrien, Dima, Goedele, Mohammad, Hasret, Ans, Melanie, Indiana, Christophe and Ahmed, thanks a lot for the nice work environment at the VUB and the unforgettable (special) coffee breaks. A special word of thanks to Greet for taking over my student tasks during the last months, and to Mohammad for his indispensable help with the matlab. I will of course never forget the hilarious conversations he had in our office with Iulia.*

*Anneleen, Margot, Lien, Laurent and Tinne, thank you for the help in the PAT lab. I especially would like to thank Laurent for the practical assistance with the lyo, and Lien for the help with the Raman.*

*I am indebted to my master thesis students Dorien, Oliwia and Tara for their commitment and the successful outcome of their thesis.*

*Thank you so much Goedele, Mohammad, Hadewych, Ellen, Lise, Kristien and Gaëlle, for the support, which I especially needed during the last months.*

*I want to express my gratitude to the Research Foundation - Flanders (FWO ) for financing my PhD studies and my research stay in Montpellier.*

*I am grateful to my family, family in law and friends for the continuous support and for the understanding when I had to decline again during the last months. I want to thank my parents and grand-parents for stimulating me, without any pressure, to find my way in life. Thanks to my brother Pascal, for always being there and in general for his awesomeness.*

*Last but definitely not least, I want to thank two persons who are very special to me. First, I would like to express my warm gratitude to my beloved grandfather, who is unfortunately no longer with us since last February. There are no words that can express my feelings of thankfulness for the unconditional support and for being that great companion for so many years. I am so grateful that you were in my life, and could not imagine a better grandfather!*

*Now is the time to thank Jan. Where should I begin, there are so many things where I owe you thanks. With regards to my thesis, your continuous support, your coaching sessions to calm me down when my research seemed jammed, and the help with the layout of my thesis are some of the things that are so much appreciated. Thank you so much for the unforgettable time in Montpellier, for the little things that lighten up my days, for being open-minded, for just being yourself.*

*Sigrid Pieters,  
June 26<sup>th</sup>, 2013*

---

# Table of contents

---

Abbreviations, symbols and notations.....	11
Abstract.....	16
Chapter 1: INTRODUCTION, OBJECTIVES AND OUTLINE.....	17
1.1. The Process Analytical Technology (PAT) initiative .....	17
1.1.1. The idea behind PAT .....	17
1.1.2. Analysis from the lab to the work floor.....	19
1.2. Theoretical aspects of molecular spectroscopy.....	21
1.2.1. Spectroscopy in quality analysis .....	21
1.2.2. Principles of Mid- and Near-infrared spectroscopy .....	23
1.2.3. Principles of Raman spectroscopy .....	26
1.2.4. Spectroscopic methods .....	28
1.3. Freeze-drying of proteins .....	29
1.3.1. Introduction to freeze-drying.....	29
1.3.2. Current PAT for freeze-drying .....	31
1.3.2. Critical Quality Attributes of lyophilized protein formulations .....	33
1.4. Objectives and outline of this work .....	40
1.5. References .....	42
Chapter 2: GENERAL CONSIDERATIONS .....	51
2.1. Implementation of NIR and Raman spectroscopy as process analyzers in freeze-drying processes: what to consider? .....	51
2.1.1. Environment.....	51
2.1.2. Instrument choice and conditions.....	52
2.1.3. Sampling and interfacing.....	55
2.2. A reference for detecting protein unfolding.....	57
2.2.1. FTIR: a state of the art technique for protein secondary structure characterization and detecting protein unfolding.....	57
2.2.2. The reference method to determine protein unfolding .....	63
2.2.3. Further assessment of protein unfolding.....	73

2.3. References .....	74
Chapter 3: NEAR-INFRARED SPECTROSCOPY FOR IN-LINE MEASURING PROTEIN UNFOLDING DURING FREEZE-DRYING .....	79
3.1. NIR spectroscopy for detecting protein unfolding .....	79
3.2. NIR spectroscopy for in-line measuring water loss .....	81
3.3. Defining a process trajectory for in-line monitoring protein unfolding versus dehydration .....	83
3.4. References .....	98
Chapter 4: RAMAN SPECTROSCOPY FOR MEASURING PROTEIN UNFOLDING .....	101
4.1. Raman spectroscopy for detecting protein unfolding.....	101
4.2. Raman spectroscopy and multivariate analysis for the rapid discrimination between native-like and non-native states in freeze-dried protein formulations .....	104
4.3. References .....	115
Chapter 5: MEASURING PROTEIN UNFOLDING IN RAMAN SPECTRA IN THE PRESENCE OF INTERFERENCES.....	117
5.1. Introduction.....	117
5.2. The robustness of multivariate calibration (MVC) models.....	117
5.3. In-line monitoring protein unfolding during freeze-drying processes using Raman spectroscopy.....	145
5.4. References .....	181
Chapter 6: SUMMARY, CONCLUSIONS & FUTURE PERSPECTIVES.....	183
6.1. Summary and conclusions.....	183
6.2. Suggestions for future research with NIR spectroscopy.....	189
6.3. Suggestions for future research with Raman spectroscopy .....	191
Annex .....	193
Curriculum Vitae .....	203
List of publications .....	205

---

## Abbreviations, symbols and notations

---

### *Abbreviations and Symbols*

$\alpha/\beta$ ratio	ratio between $\alpha$ -helix and $\beta$ -sheet content
ACLS	Augmented Classical Least Squares
ANN	Artificial Neural Network
ANOVA	Analysis of Variance
AWA	Apparent Water Absorbance
AO	Area of Overlap
API	Active Pharmaceutical Ingredient
ATR	Attenuated Total Reflectance
AUC	Analytical Ultracentrifugation
BSPC	Batch Statistical Process Control
CCD	Charged Coupled Device
CD	Circular Dichroism
CLS	Classical Least Squares
CMC	Chemistry, Manufacturing and Controls
CQA	Critical Quality Attribute
CTD	Common Technical Document
CV	Cross validation
DEN	Non-native state
$\Delta G$	Gibbs free energy
DOP	Dynamic Orthogonal Projection
EMA	European Medicines Agency
EMSC	Extended Multiplicative Scatter Correction
EPO	External Parameter Orthogonalization
FDA	Food and Drug Administration
FN	False Negatives
FP	False Positives
FT	Fourier Transformation
FTIR	Fourier-Transform Infrared
GLM	General Linear Model
GLP	Good Laboratory Practices
GMP	Good Manufacturing Practices
Gu.HCl	Guanidine hydrochloride
HIS	Histidine buffer
HPLC-MS	High Performance Liquid Chromatography - Mass Spectrometry
ICH	International Conference on Harmonisation
IgG	Immunoglobulin G
IPC	In-process control

IR	Infrared
IT	Information Technology
LDH	Lactate Dehydrogenase
LV	Latent variable
MIR	Mid-infrared
MRP	Maillard reaction product
MSC	Multiplicative Scatter Correction
MSPC	Multivariate Statistical Process Control
MTM	Manometric Temperature Measurement
MVA	Multivariate Analysis
MVC	Multivariate Calibration
NA	Noise Augmentation
NAP	Net Analyte Preprocessing
NAS	Net Analyte Signal
NaSCN	Sodium thiocyanate
NDA	New Drug Application
NIR	Near-infrared
NL	Native-like state
NMR	Nuclear Magnetic Resonance
NOC	Normal Operational Conditions
OSC	Orthogonal Signal Correction
PAC	Process Analytical Chemistry
PACLS	Prediction - Augmented Classical Least Squares
PAT	Process Analytical Technology
PC	Principal Component
PCA	Principal Component Analysis
PEG	Polyethylene glycol
Phe	Phenylalanine
PHOS	Phosphate buffer
PLS	Partial Least Squares
PLS-LDA	Partial Least Squares - Linear Discriminant Analysis
PLSR	Partial Least Squares Regression
PVP	Polyvinylpyrrolidone
QA	Quality Assurance
QbD	Quality by Design
QC	Quality Control
RMSECV	Root Mean Square Error of Cross Validation
RMSEP	Root Mean Square Error of Prediction
RNase	ribonuclease
ROC	Receiver Operating Characteristics
RTR	Real Time Release
SE-HPLC	Size-Exclusion High Performance Liquid Chromatography



SEP	Standard Error of Prediction
SERS	Surface Enhanced Raman Spectroscopy
SNV	Standard Normal Variates
SVD	Singular Value Decomposition
T <sub>c</sub>	Collapse Temperature
TDC	Transition Dipole Coupling
TDLAS	Tunable Diode Laser Absorption Spectroscopy
T <sub>g</sub>	Glass Transition Temperature
T <sub>g</sub> '	Glass Transition Temperature of freeze-concentrate
TN	True Negatives
TOP	Transfer by Orthogonal Projection
TP	True Positives
TRIS	TRIS buffer
Trp	Tryptophane
Tyr	Tyrosine
UV	Ultra-Violet
VC	Coefficient of Variation

### *Notations*

Matrices	Capital bold characters, e.g. <b>X</b>
Vectors	Small bold characters, e.g. <b>y</b>
Scalars	Small italic characters, e.g. <i>k</i>
Estimates of model parameters	Hat, e.g. $\hat{x}$
Vector space	Arrow, e.g. $\vec{T}$



---

## Abstract

---

One objective of the FDA's Process Analytical Technology (PAT) initiative is to move the analysis of critical quality attributes (CQA's) from the quality control (QC) laboratory towards the manufacturing process environment (i.e. analysis based on in- , on- and at-line measurements). Because of their non-invasive nature, their extremely simple and ultra-fast analysis, and because of the fact that they can transfer light over meters through fiber optics, Near-infrared (NIR) and Raman spectroscopy have become major players, even the prototype, in many in-line and on-line PAT applications. In this doctoral dissertation, the potential of NIR and Raman spectroscopy has been investigated for a novel application: the automated and real-time detection of protein unfolding in freeze-dried formulations and during freeze-drying processes (in-line monitoring). Protein unfolding during freeze-drying is a CQA as it may precede the formation of non-covalently bound aggregates in the reconstituted and thus administered drug product. Since the latter may cause immunogenicity and reduced potency it is a necessity to minimize protein unfolding during freeze-drying for delivering safe and effective lyophilized protein drug products. The goal is to have a quality indication by evaluating the protein's conformational state at an early stage (preferably when the process is still running and still can be adjusted) without destroying the sample or interfering the process. Based on the interaction of light with sample molecules, characteristic chemical and physical information, visualized as a spectrum, could be obtained. A first objective was to recognize the useful information about the protein's conformational status out of the complex spectra. Methods were developed to use this information in an optimal way for distinguishing between samples with and without remarkable protein unfolding. To allow using spectral (and thus multivariate) methods for evaluating future samples (e.g. from novel batches or different formulations) or to perform in-line measurements during the freeze-drying process, the influences of spectral interferences were investigated. Strategies for dealing with uninformative systematic effects were developed in order to increase the robustness of the multivariate methods and to allow in-line use during the freeze-drying process.



---

# Chapter 1: INTRODUCTION, OBJECTIVES AND OUTLINE

---

## 1.1. The Process Analytical Technology (PAT) initiative

### 1.1.1. The idea behind PAT

In response to the growing need for continuous improvement and innovation, the Food and Drug Administration (FDA) launched in September 2004 a guideline on PAT. It forms the basis of the pharmaceutical Good Manufacturing Practice (GMP) rules for the 21<sup>st</sup> century [1]. PAT has been defined as: "A system for designing, analyzing, and controlling manufacturing through timely measurements (i.e. during processing) of critical quality and performance attributes of raw and in-process materials and processes with the goal of ensuring final product quality". Hereby, the FDA's guideline recommends the following tools for innovating the pharmaceutical manufacturing industry: (1) multivariate tools for design, data acquisition, and analysis, (2) process analyzers, (3) process control tools, (4) continuous improvement and knowledge management tools [1].

"The pharmaceutical industry has a little secret: Even as it invents futuristic new drugs, its manufacturing techniques lag far behind those of potato-chip and laundry-soap makers."

Wall Street Journal (September 3, 2003) [2]

Most current pharmaceutical manufacturing processes are batch processes. The traditional way of pharmaceutical batch manufacturing uses a fixed manufacturing process to ensure that the end products will meet their specifications, which are tightly fixed in regulatory documents that need approval from authorities. As most processes are black boxes, process validation is primarily based on the quality of the end products of initial full-scale batches. A new batch can be released after comprehensive raw material and end product testing of representative samples in the lab ("quality-by-testing") has confirmed that the specifications are met.

A disadvantage of this conservative approach is the rigid regulatory system. Even the smallest change in Chemistry, Manufacturing and Controls (CMC), e.g. to the process, the drug product, raw materials, facilities, equipment or analysis methods, requires time- and effort-intensive regulatory filing. This discourages drug product manufacturers to change outdated and inefficient processes and increases the administrative burden during pharmaceutical development and up-scaling. By issuing the PAT guidelines, the FDA has taken the first step towards a more proactive approach for regulatory filing, which must motivate the pharmaceutical industry to modernize. It proposes a more risk- and science-based approach for acquiring improved process understanding and product quality [3]. The idea is mainly inspired by innovation strategies from other industries, including "Process Analytical Chemistry" (PAC), parametric release and Six Sigma [4]. During the last decade, the International Conference on Harmonization (ICH) has also started promoting PAT by issuing its own guidelines [5-7], which were adopted by the European Medicines Agency (EMA) [8-10]. The idea of PAT has also been extended under the more holistic term "Quality by Design" (QbD), being defined as a systematic approach to development that begins with predefined objectives and emphasizes product and process understanding, and process control, based on sound science and quality risk management. The PAT initiative, when fully accomplished, may have major positive implications in different areas of pharmaceutical manufacturing, e.g. in the development of pharmaceutical manufacturing processes and products (engineering), quality assurance (QA) and regulatory affairs (Table 1.1.) [11].

Almost one decade later than the initial launch of the PAT concept in 2004, there has been a progressively growing interest in PAT by research institutions, regulatory authorities and industry partners. However, as expected the progress of the practical implementation of this new concept is slow, and new problems have raised on the way. Obstacles include increased regulatory uncertainty (i.e. regulatory submissions may be reviewed in different ways), the need for a mindset change, the need for a multidisciplinary approach, strong investments in analyzer-, information technology (IT)- and process infrastructure, the need for revalidating existing processes, etc... An interesting uprising trend resulting from the PAT idea is that batch processes are being converted to continuous ones [12].

**Table 1.1. Some important illustrations of the ideas behind the PAT initiative in different areas of pharmaceutical manufacturing, and their aspired implications.**

Areas	Traditional approach	PAT-based approach	Aspired implications
Regulatory affairs	- Product testing to document (e.g. CTD, NDA) quality	- More flexible and science-based specifications (i.e. design spaces) - More flexible regulatory filing built on the premise that manufacturers demonstrate that they understand their processes	- May help breaking the impasse involving time- and effort-intensive regulatory filing of change controls - Encourages process optimization and continuous improvement efforts within a facilities quality system
Quality assurance	- Intensive deviation and out-of-specification investigations	- Right first time and risk-based quality assurance strategy	- Less batch rejections and recalls
Process engineering and development	- Fixed black box processes	- Continuously real-time controlled and mechanistically well-understood processes	- More cost-effective manufacturing processes - Decreased cycle times

Abbreviations: CTD (Common Technical Document), NDA (New Drug Application)

### 1.1.2. Analysis from the lab to the work floor

PAT is a broad concept embracing many aspects of pharmaceutical manufacturing. This thesis contributes to one particular aspect of PAT, i.e. moving the testing of core quality parameters from the laboratory (off-line testing) to the work floor (in-, on- or at-line testing). The ICH Q8 guideline [5] defines CQA's as being physical, chemical, biological, or microbiological properties or characteristics that should be within an appropriate limit, range or distribution to ensure the desired product quality. They are generally associated with the drug substance, excipients, intermediates and drug products.

Fig. 1.1. schematically represents the different possible measurement set-ups, i.e. in-line, on-line and at-line, during a manufacturing process. In-line measurements (invasive or not-invasive) can be made directly in the process stream, without removing the sample from the process. On-line measurements require an automatic sampling device to divert the samples from the process to the measurement equipment, e.g. by using recirculation lines, tubing, discharge points... The samples are often returned to the process stream. In- and on-line set-ups may allow continuous measurements. The at-line set-up requires the withdrawal of the samples from the process stream. The analysis, which is often

destructive, happens in the proximity of the process equipment within the time scale of manufacturing [13]. Of course, it will depend on the process, sample and analyzer which set-up is the most suitable.

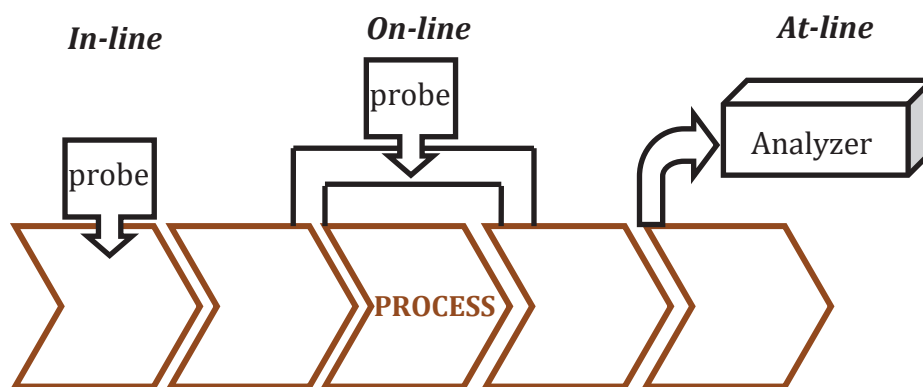


**Fig. 1.1. Different product measurement possibilities, i.e. in-line, on-line and at-line, during a manufacturing process.**

In-process monitoring also exists in the traditional way of pharmaceutical manufacturing. It mostly involves the timely measurements and control of interferential parameters (such as pressure, temperature, etc...) that can be easily measured, or, in case there are separate process steps, the testing of intermediate products in the lab. However, monitoring CQA's continuously and in real-time is seldom part of a traditional pharmaceutical manufacturing process.

For obtaining continuous real-time information on CQA's during manufacturing processes the use of PAT-tools (process analytical instruments) is indispensable. These tools may include various instruments and sensors, provided that they can offer an ultra-fast acquisition of data leading directly to valuable information on the quality attributes of interest. NIR and Raman spectroscopy may fulfill these requirements for many pharmaceutical applications [14]. They acquire lots of information-rich multivariate spectra and therefore usually need to be treated with multivariate analysis (MVA) techniques. The possibility to use such high data densities is quite new and still expanding, because computer processors and data storage capacities have substantially evolved over the last decades.



By continuously monitoring CQA's while manufacturing, one can obtain process understanding, making the manufacturing process less a black box. This may enable the development of more efficient and science-based processes. It may also permit setting up superior quality systems that use this knowledge to anticipate possible risks and mitigate them to best effort. Ultimately, PAT is heading for processes where all CQA's are continuously monitored and controlled, in order to allow real-time release (RTR) [15].

## **1.2. Theoretical aspects of molecular spectroscopy**

### **1.2.1. Spectroscopy in quality analysis**

The principle of spectroscopy relies on irradiating the sample with electromagnetic radiation of a particular energy level. Based on interaction between the radiation and the material chemical and/or physical information about the sample can be obtained. In (bio-) pharmaceutical analysis and quality control, different types of spectroscopy are commonly used. Table 1.2 summarizes the main characteristics of these spectroscopic techniques. From the table it can be seen that only infrared, Raman and tertrahertz spectroscopy may have potential for PAT applications. While mid-infrared (MIR) spectroscopy is well-known for identifying various materials and drug substances [16], NIR and Raman spectroscopy are probably the best known and most widespread PAT-tools today. Tertrahertz spectroscopy is an upcoming PAT-tool for analyzing crystalline materials but not for amorphous ones. There are numerous examples of applications in various fields, e.g. in the (petro-) chemical, food and agricultural industry, showing their accomplishments [17-26]. Because of the FDA's PAT initiative, they have also been increasingly used in the last decade for (real-time) measurements of critical process and product quality attributes during or after pharmaceutical manufacturing processes [14, 27-39]. The key of their success may be that they can provide a wealth of information on chemical structures and physical characteristics of materials in an (ultra-) rapid and non-destructive way. It may have great business value when a traditional slow and/or costly final release method could be replaced by such a rapid method requiring no or hardly any sample preparation. These advantages may also allow one to obtain information on the relevant quality attributes during the process itself, in order to gain process understanding or perform real-time fault detection.

Table 1.2. Characteristics of the spectroscopic techniques being applied in (bio-) pharmaceutical analysis

Type of spectroscopy	Wavelength range of the electromagnetic spectrum used to irradiate the sample (cm)	Type of interaction of the radiation with material	Process involved in the interaction of the radiation with material	Pros	Cons
<b>Gamma-ray</b>	$10^{-10}$	absorption	change in nuclear configuration	NA	
<b>X-ray</b>	$10^{-8}$	absorption	change in electron distribution	- detailed visualization of the molecular and atomic structure of matter (also proteins)	- requires a crystalline state of the material
<b>UV-visible</b>	$10^{-5}$	absorption	change in electron distribution	- assay (Lambert-Beer's law)	- requires diluted solutions
<b>Circular dichroism</b>	$10^{-5}$	absorption	displacement and circulation of charge	- total protein assay at 280 nm	- requires solutions
<b>Fluorescence</b>	$10^{-5}$	excitation of the electrons in molecules causes emission of light	change in configuration and electronic state	- determination of protein conformation	- requires solutions
<b>Raman</b>	$10^{-4} - 10^{-5}$	non-elastic scatter	change in configuration	- far-UV-CD for determination of protein conformation	
<b>Near-infrared</b>	$10^{-4}$	absorption	change in configuration	- assay (Lambert-Beer's law)	- laser energy can decompose labile samples
				- non-invasive, no or little sample preparation	- lower chemical structural selectivity than MIR
				- high chemical structural selectivity	- bands difficult to interpret
				- non-invasive, non-destructive	
				- ease of sampling through packaging materials	
				- gives chemical and physical information on sample	
<b>Mid-infrared</b>	$10^{-3}$	absorption	change in configuration	- high chemical structural selectivity (identification of materials)	- requires sample preparation or contact with ATR crystal
<b>Far-infrared/ Terahertz</b>	$10^{-2}$	absorption	change in configuration and orientation	- non-invasive, non-destructive	- not for amorphous material
				- chemical analysis of solid dosage forms	
<b>Microwave</b>	1	absorption	change in orientation	NA	
<b>Radiowave</b>	10	absorption	change in spin	NA	

### 1.2.2. Principles of Mid- and Near-infrared spectroscopy

As sample molecules constitute of smaller units (i.e. atoms, electrons, protons), each chemical bond in the sample will vibrate with its own specific resonance frequency. Electromagnetic radiation that passes the sample will interact with it when the energy content (frequency) of the photon corresponds to the resonance frequency of one of these bonds. The absorption of the radiation will transition the molecule to a higher vibrational energy level. A spectrum is obtained by plotting the absorbance (or transmittance) against the light frequencies (expressed as wavelengths or wavenumbers). Vibrations resulting in changes in dipole moment of a molecule will result in absorption bands in the (N)IR spectrum. Therefore, the selection rule applies that symmetrical molecules will have fewer 'infrared-active' vibrations than asymmetrical molecules, e.g. water is a strong (N)IR absorber [14, 40-41]. As absorptions correspond to the frequencies of vibrations of different bonds within the sample molecules, they can be used to identify particular functional groups.

#### 1.2.2.1. Fundamental vibrations (MIR) from $4000$ to $400\text{ cm}^{-1}$ ( $2500$ to $25\,000\text{ nm}$ )

Absorption of the MIR radiation results from fundamental vibrations ( $\nu = 1$ ) involving a change in a chemical bond, i.e. in bond length (stretching vibration) or bond angle (bending vibration) [40, 42]. Some bonds can stretch in-phase (symmetrical stretching) or out-of-phase (asymmetrical stretching) (Fig. 1.2). The resonance frequencies of most molecular bonds correspond to radiation from the MIR region (Fig.1.3). Because of the large number of molecular absorptions, the "fingerprint region" from  $2000$  to  $1000\text{ cm}^{-1}$  is well-known for sample identification [40].

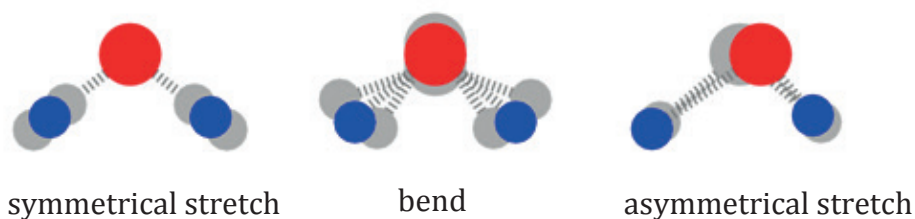
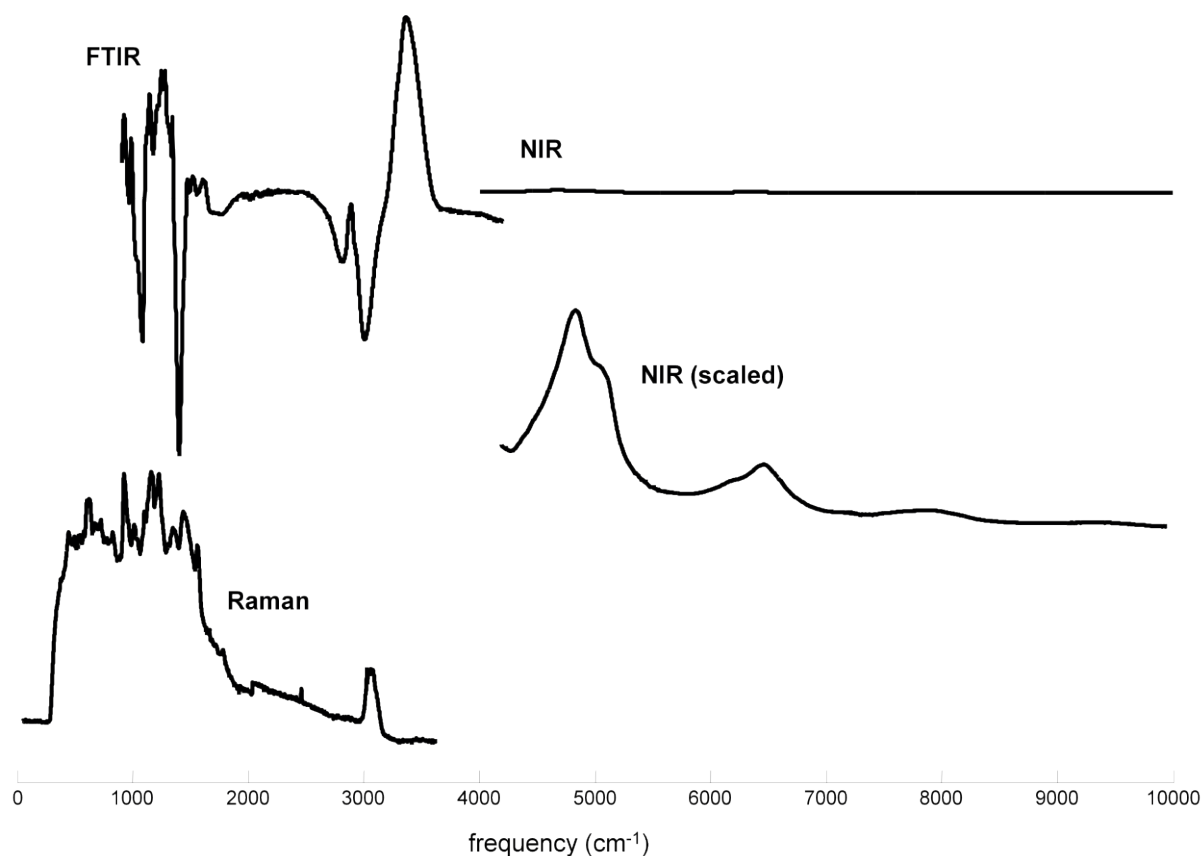


Fig. 1.2. Different types of fundamental vibrations shown for a  $\text{H}_2\text{O}$  molecule. Adapted from [43].

### 1.2.2.2. Overtone and combination bands (NIR) from 12821 to 4000 $\text{cm}^{-1}$ (780 to 2500 nm)

For absorption of NIR light there is the need for molecular transitions to higher vibrational states. Overtones result from multiples, e.g. two or three times, the fundamental absorption frequency. The energy levels associated with NIR overtones ( $\nu = 2$  or  $3$ ) are shown in Fig. 1.4. Combination bands arise when two (or more) fundamental vibrations involving the same functional group absorb energy simultaneously. The resulting band will be sum of the contributing frequencies. This also explains why NIR spectra have weaker bands than MIR spectra, as is observed in Fig. 1.3. The bands involved are typically due to C-H, N-H and O-H stretching vibrations [14, 40].



**Fig. 1.3. Attenuated Total Reflection (ATR) - Fourier Transform (FT) IR, reflectance FT-NIR and dispersive Raman (785 nm laser) spectra of a freeze-dried Immunoglobulin (IgG) sample, plotted on one energy scale. The intensity scales of the FTIR and NIR spectra above are the same, while the same NIR spectrum below is scaled to visualize its features. The Raman spectrum is also scaled as it showed a much higher intensity than the FTIR spectrum due to the large background on which the Raman signals are superimposed.**

### 1.2.2.3. Hydrogen bonds

In both MIR and NIR, hydrogen bonds alter vibrational energy states, shifting existing absorption bands. Hydrogen bonds are weak bonds formed by the interaction between hydrogen and electron donating atoms such as nitrogen and oxygen. The formation of such bonds changes the bond stiffness and thus the structure of the molecules attached to the atoms forming the hydrogen bond. This results in altered vibrational frequencies of the different bonds in these molecules, which shifts the peaks in the spectrum depending on the strength of hydrogen bonds in the sample. This is, for instance, demonstrated by different MIR absorption frequencies within the amide I band ( $1700\text{--}1600\text{ cm}^{-1}$ ), corresponding to different protein secondary structures [44]. Although they use the same molecular bond vibrations (i.e. mainly C=O stretch vibration of the peptide bond), the absorption frequencies of the different secondary structures (e.g.  $\alpha$ -helix,  $\beta$ -sheets, turns, unordered structures...) have different positions within this band. This results from different hydrogen bonding states, characterizing these secondary structures, that affect the C=O stretching vibration. The stronger the hydrogen bonds in the secondary structure element, the lower the absorption frequency. As the degree of hydrogen bonding is also affected by solvents and temperature, these bonds can uniquely influence the infrared spectrum [40].

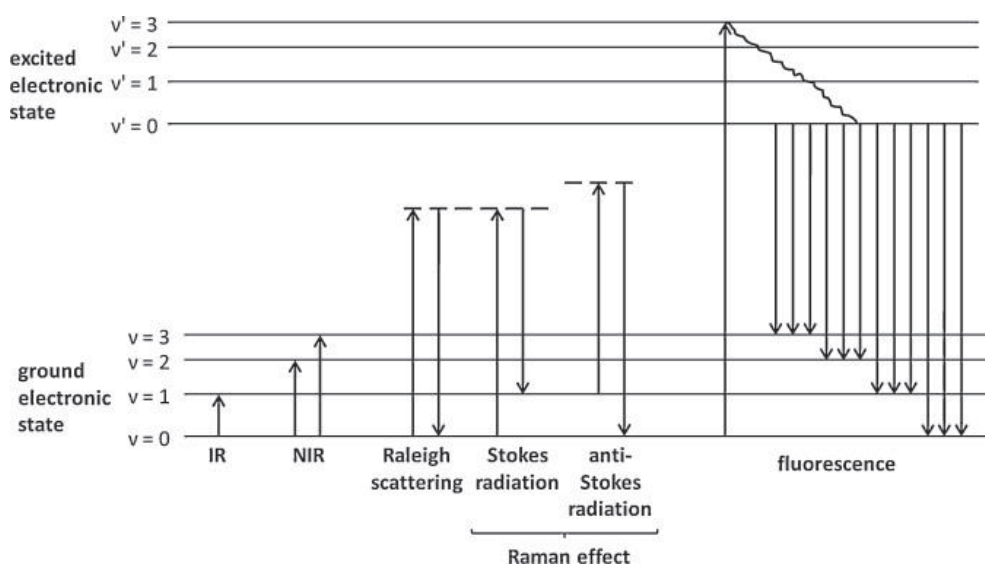


Fig. 1.4. IR and NIR absorption, the Raman effect and fluorescence [14].

As molecules may incorporate many different bonds, and each bond may absorb at several vibrational frequencies as well, this can make an (N)IR spectrum look very complex. However, this complex spectrum can be a selective means (especially in the case of MIR) providing a "fingerprint" for the molecule. Compared to MIR, NIR spectra will have broader and weaker bands, thus they will be less suitable for a qualitative analysis of a sample. Yet they are frequently used in combination with MVA for quantitative analysis of samples. An interfering effect being present in most (N)IR spectra of pharmaceuticals is light scattering. Light scattering is dependent on material properties, i.e. particle number, size, and shape [40]. Spectral pre-processing methods are therefore often necessary to get the useful information out of the spectra, and it should be realized that light scattering violates one of the assumptions for the validity of Lambert-Beer's law. Therefore, calibrations with (N)IR spectra for the determination of the concentration of an ingredient are mostly developed with inverse calibration methods instead of with classical least squares methods.

### **1.2.3. Principles of Raman spectroscopy**

When a sample is irradiated with monochromatic laser light, molecules are excited to a virtual electronic state that generally lies below the first excited electronic energy level for the molecules (Fig. 1.4.). Laser frequencies in the visible (e.g. 532 nm) or near-infrared (e.g. 785 nm, 1064 nm) range are typically used. When molecules relax back to the original state they may produce scattered photons. Most of the scattered photons will have the same energy (frequency) as the incident laser light. This phenomenon is called Rayleigh or elastically scattering. However, a small fraction of the scattered photons, approximately 1 in  $10^8$ , will be scattered with a change in frequency. These inelastically scattered photons constitute the Raman effect. The difference between the incident and scattered frequencies is the result of an excitation of the molecular system, often an excitation of a vibrational mode. The Raman spectrum plots the intensity of the inelastically scattered photons versus the frequency difference between incident laser and scattered frequencies. If the molecule is in an excited vibrational state when scattering of an incident photon occurs, the photon may gain energy when scattered,

leading to anti-Stokes Raman scattering. Conversely, in Stokes Raman scattering the scattered photons lose energy compared to the incident photons [14, 45].

Both Raman and IR spectroscopy depend on molecular vibrations. Whereas Raman spectroscopy probes vibrational transitions of molecules indirectly by light scattering, IR spectroscopy detects them directly via absorption of the incident electromagnetic light. Molecules will be Raman active when a change in polarizability occurs during their normal modes. Polarizability is the ease to distort an electron cloud by the electric component,  $E$ , of an electromagnetic wave, and changes with respect to the bond length during vibrations. Good Raman scatterers are symmetrical molecules (e.g. cyclohexane), homonuclear functionalities (e.g. C=C, C-C, S-S) and multiple bonds. Similar energy ranges are observed in Raman and MIR (fundamental vibrations), hence they probe the same chemical information (Fig. 1.3). However, as they apply different selection rules, they can be complementary techniques [14, 45]. For molecules of high symmetry, the Raman and MIR spectra differ the most. Raman and MIR spectra can be completely complementary for molecules with a center of inversion symmetry (e.g. benzene,  $CS_2$ ,  $N_2$ ) and thus will contain no bands in common. In less symmetrical molecules there will be relatively more overlap compared to complementary information.

A striking difference between Raman scattering and IR absorption is the probability of occurrence of each phenomenon. Raman scattering is  $10^{10}$  times less likely to occur than light absorption. This makes Raman scattering an inherently weak effect, limiting detection sensitivity. The lower the incident laser wavelength, the stronger the Raman scatter will be. But there are also other competing effects, such as luminescent effects (e.g. stray light, fluorescence...). In modern Raman spectrometers stray light can be efficiently filtered. Fluorescence may originate from the analyte of interest or from sample impurities, and its intensity depends on the chosen wavelength of the laser light. In some cases, fluorescence emission may cause in the Raman spectra a strong background on which the Raman signals are superimposed. Fluorescence may probably contribute to the large background in the Raman spectra of proteins (Fig. 1.3), due to the presence of aromatic amino acids that exhibit fluorescence, such as Tryptophane (Trp), Tyrosine (Tyr) and Phenylalanine (Phe). In the worst case, fluorescence emission can be

so strong that it completely overwhelms the much weaker Raman signals. Then Raman spectroscopy at that laser wavelength is not a suitable option for the given analysis. Near-infrared lasers (i.e. 785 nm, 1064 nm) may minimize the occurrence of fluorescence, and are therefore commonly applied in many Raman spectroscopic applications [14, 45-46].

#### **1.2.4. Spectroscopic methods**

Raman and (N)IR spectroscopy are thus similar in the fact that they all use the interaction of electromagnetic light with the sample molecules to obtain chemical (and sometimes also physical) information from the sample. Yet IR and Raman spectroscopy use different physical phenomena, i.e. absorption versus scattering of the radiation. MIR differs from NIR by using a different range of the electromagnetic spectrum. Consequently, each technique can provide unique information about the sample, while each technique will have its own advantages and disadvantages. These tools provide spectra as output for the measurements. Thus, the output is multivariate and can be used as a "fingerprint" to identify or classify substances, or to provide (semi)-quantitative information.

As the spectra may provide an abundance of information, with physical and chemical interferences, most spectroscopic methods require MVA or chemometrics. The Guideline on the use of NIR spectroscopy by the pharmaceutical industry and data requirements for new submissions and variations (EMA/CHMP/CVMP/QWP/17760/2009 Rev2) provides a regulatory framework for developing and validating such multivariate methods [47]. The guideline makes a distinction between multivariate calibration (MVC) methods, replacing golden standard methods, and so called *conformity check* methods in PAT applications. Both methods can be qualitative or quantitative in nature. The MVC method should be validated with respect to the reference method, and generally evaluates similar figures of merit as in univariate calibration, e.g. standard error of prediction (SEP), specificity, linearity, range, precision, sensitivity, selectivity, signal-to-noise ratio, robustness, limits of detection and quantification [47-48]. The *conformity check* methods may cover all kinds of diagnostic or in-process control (IPC) methods,



and are specific to the nature of the considered manufacturing process. For such methods it may often not be possible to validate with respect to a reference method (e.g. because of potential sampling errors). Therefore, their validation requirements are less predefined and will depend on what is believed to be important from the users perspective for that specific process [47]. A *conformity check* method may create a trajectory for (a part of) the process onto a chosen space that should be relevant for the CQA's specification [49]. From this trajectory one can perform a risk analysis, e.g. when is my process running on track and when not? An important aspect of the trajectory quality is the information content, i.e. the relevant-to-irrelevant variation ratio should be maximized [49]. Validation of the *conformity check* method may include justifying why such a trajectory may be appropriate for the intended use (and establish acceptable limits), demonstrate the correlation with the quality attribute, and assess the circumstances where that correlation may be put at risk.

### 1.3. Freeze-drying of proteins

#### 1.3.1. Introduction to freeze-drying

Freeze-drying or lyophilization is a popular drying technique performed at low temperature and low pressure. It is commonly applied for the drying of heat labile pharmaceuticals, such as protein pharmaceuticals. The dried solid cake may provide a more long term stability for the pharmaceutical during storage and distribution. The freeze-drying process consists essentially of three important consecutive phases, i.e. freezing, primary drying and secondary drying (Fig. 1.5) [50-51].

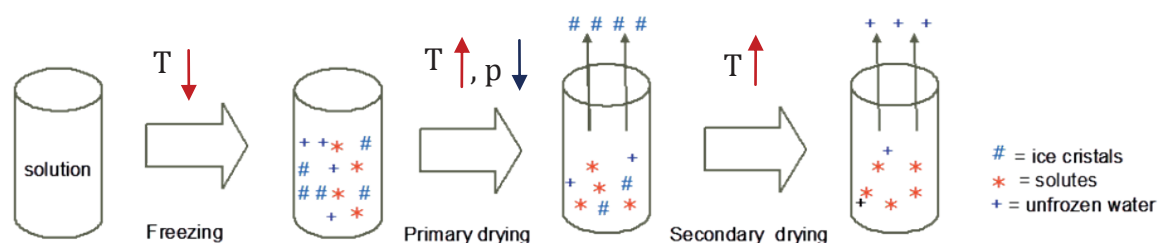


Fig. 1.5. Different phases in a freeze-drying process.

During the freezing phase, the shelf temperature is decreased below its solid-liquid phase transition temperature. As the temperature decreases, most of the water will be converted to ice crystals, while the solutes become more concentrated (i.e. freeze concentration) until they crystallize or until the viscosity exceeds a critical point (i.e. the glass transition). The associated temperature with the latter phenomenon is the glass transition temperature  $T_g'$  of the maximally freeze-concentrated solution. Below the glass transition a solid amorphous phase (glass) is formed in the interstitials of the ice crystals. Proteins do not crystallize during freezing, but form an amorphous glass. A small fraction of the original water will stay present as non-frozen water in this system [50-52]. Generally, freezing is performed between -40 to -50°C (Fig. 1.6).

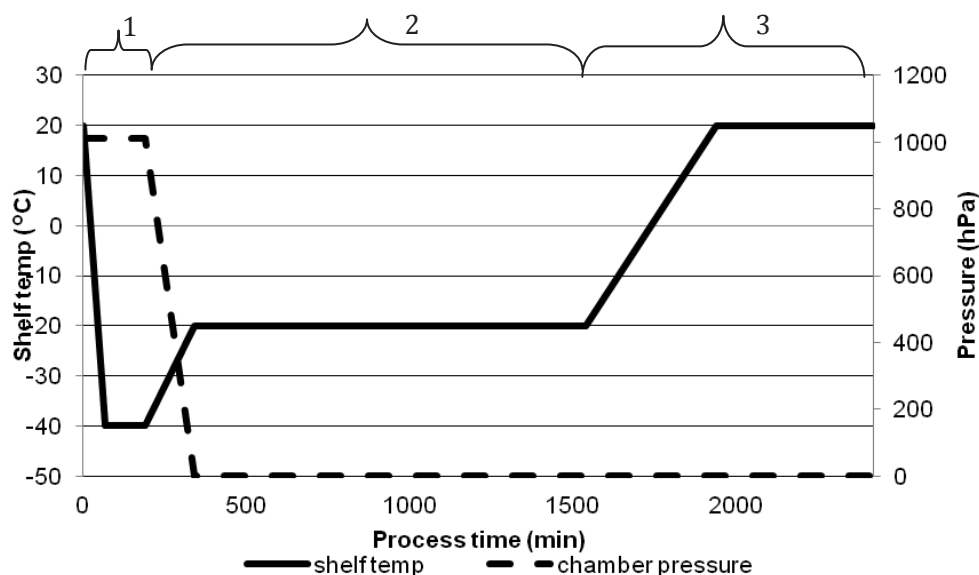


Fig. 1.6. Example of temperature and pressure settings in a freeze-drying process. Step 1 is the freezing, step 2 the primary drying and step 3 the secondary drying.

The goal of primary drying is to sublime the ice. Therefore, a vacuum is created in the chamber and the shelf temperature is raised (e.g. to -20°C in Fig. 1.6) to provide more energy to the system for sublimation. It is important that the temperature for sublimation does not exceed the product's collapse temperature ( $T_c$ ), which is generally 1 to 3°C higher than the  $T_g'$ . This is necessary to avoid that the product will lose its macroscopic structure (i.e. macro-collapse), which may result in an inelegant cake being unacceptable from a commercial point of view [53]. To minimize the risk for collapse,

another good practice is that the sublimation process should be completely finished (in all vials of the batch) before moving on to the secondary drying [50-51, 54]. However, maintaining the temperature below  $T_g'$  makes the primary drying phase long (typically > 24 hours) and expensive. Therefore, there is a growing interest to explore more aggressive freeze-drying cycles. They use temperatures exceeding the collapse temperature in formulations that are prone to micro-collapse (visual appearance is not an issue), i.e. completely amorphous formulations (protein content >20 mg/ml) or partially crystalline formulations (where the crystals provide a structural framework for the cake). Possible advantages may be that the cycle time can be largely reduced (meaning reduced costs), the process can be simplified (i.e. one cycle for all proteins, combine primary and secondary drying), and tall cakes might not longer be a problem. A possible downside is a choke flow in stoppers and condenser. Research is currently focused on studying the impact of this action on the entire quality of the product [55-59].

The unfrozen water content at the end of primary drying generally ranges between 10-30% of the initial water content (on a dried solid basis, depending on the formulation). As this water cannot be eliminated by sublimation, it is aimed removing it by desorption during the secondary drying phase. To promote drying during this phase, the temperature is increased (e.g. to 20°C in Fig. 1.6) while the vacuum stays. The ideal final residual moisture content will be product-dependent. Generally, under-drying should be avoided because too much water will decrease the long term stability of the end product [50-51]. Over-drying holds also a risk for proteins because it may change the conformational state [60]. As every product needs its optimized freeze-drying and formulation conditions, developing a proper freeze-drying cycle for a drug product is an empirical and complex task [54, 61].

### **1.3.2. Current PAT for freeze-drying**

As the freeze-drying process is essentially based on mass and heat transfer principles, the development of any freeze-drying cycle requires the careful knowledge of product temperature (to avoid melting or collapse) and moisture content (to determine primary

and secondary drying end points) profiles during the process [62-63]. For instance, if secondary drying is started too early (i.e. before the end of primary drying), the product may collapse or melt. If secondary drying is delayed, the cycle is not cost-effective. As the PAT initiative promotes an efficient monitoring and control system for developing the freeze-drying cycle, most current PAT tools focus on the real-time and accurate measurement of process operating parameters (e.g. product temperature, sublimation rate and moisture content). Ideally, sensors and devices should be easily implementable in a sterile environment, regardless the scale of the freeze-dryer [63]. Among the thermocouples, the wireless (e.g. Tempris®) are uprising technologies. Other popular emerging PAT tools include Manometric Temperature Measurement (MTM) and Tunable Diode Laser Absorption Spectroscopy (TDLAS). By measuring the pressure rise between the freeze-drying chamber and the condenser (by MTM), or the water vapor concentration and flow velocity (by TDLAS), the product temperatures can be derived from mathematical equations that consider heat and mass transfer. They also allow determining end points for primary and secondary drying in a non-invasive way for the entire batch [55, 59, 64-68].

Whereas the above techniques (e.g. MTM and TDLAS) focus on monitoring the entire batch, NIR and Raman spectroscopy focus on the product behavior in individual vials. Their niche may rather be to provide a continuous product evaluation during the freeze-drying process in a non-invasive way. De Beer et al. [69-70] showed their suitability for in-line detecting process end points, product characterization (i.e. solid state of excipients) and physical phenomena occurring during freeze-drying (process understanding). Hereby, NIR and Raman spectroscopy complemented, but also mutually confirmed each other, suggesting that a combined use of both process analyzers can cover most of the critical process aspects [71-72]. Given the inter- and even intra-vial variability, it can be argued whether it makes sense to monitor one particular (part of a) vial in thousands. In order to address this problem, recently, the first multi-point NIR system in a freeze-dryer has been presented [73]. This study, employing the latest technological advances in freeze-dryer and spectroscopic instrumentation, takes the first hurdle towards a judicious practical implementation of NIR spectrometers in freeze-driers. It may allow combining the specific product information gathered from

multiple (and well chosen) single vials by the NIR probes. This may permit studying inter-and intra-vial differences during the drying phase of the process. Moreover, this set-up can be easily combined with sensors providing batch information, such as MTM and TDLAS.

Nowadays, some QC labs already start making use of NIR spectroscopy for the residual water content determination in freeze-dried end products [74]. Besides that NIR analysis is much faster and requires less work than the golden standard release method (i.e. Karl-Fisher), the measurement is non-destructive and non-invasive (i.e. the vial does not need to be opened). For certain applications this can have great advantages. For instance, the residual moisture content in freeze-dried infectious material can be determined in a sealed vial. Analyzing the sample with a non-destructive test is also interesting because the sample is not lost and, when necessary, the analysis of the very same sample can be repeated with another test. Other possible applications may include studying over-drying in protein materials, study inter-and intra-batch moisture content variations in order to detect processing problems, study the drying equivalence across the shelves during the validation of the freeze-dryer... Drawbacks are that each container format and formulation, or fill depth need its own calibration curve, and the integrity in the freeze-dried cakes is a requirement.

### **1.3.2. Critical Quality Attributes of lyophilized protein formulations**

Protein pharmaceuticals have become a major class of therapeutic molecules, and it is expected that their market share will increase in the next decades. In 2011, approximately 20% of the FDA approved therapeutic biologicals were freeze-dried [75]. Important quality attributes of the final freeze-dried protein drug products include the reconstitution time, the residual moisture content, the morphology and appearance, the physical stability (i.e. conformational stability) of the folded protein, and the chemical stability over storage time (i.e. loss of potency and the possible formation of new uncharacterized degradation products) [52, 58]. In this thesis, we will specifically focus on one CQA, i.e. **the physical stability of proteins**.

In contrast to the conventional small molecular weight drugs, proteins are fragile structures with a complex 3D-configuration. This configuration is thermodynamically stabilized. A protein consists of different structural levels (Fig. 1.7). The primary structure exists of amino acids that are covalently bound by peptide (or amide) bonds, forming an amino acid sequence. This forms the backbone of the protein. The peptide bond is formed when a carboxyl group of one amino acid reacts with the amino group of another, causing the release of a water molecule. The resulting molecule is called an amide (Fig. 1.8).

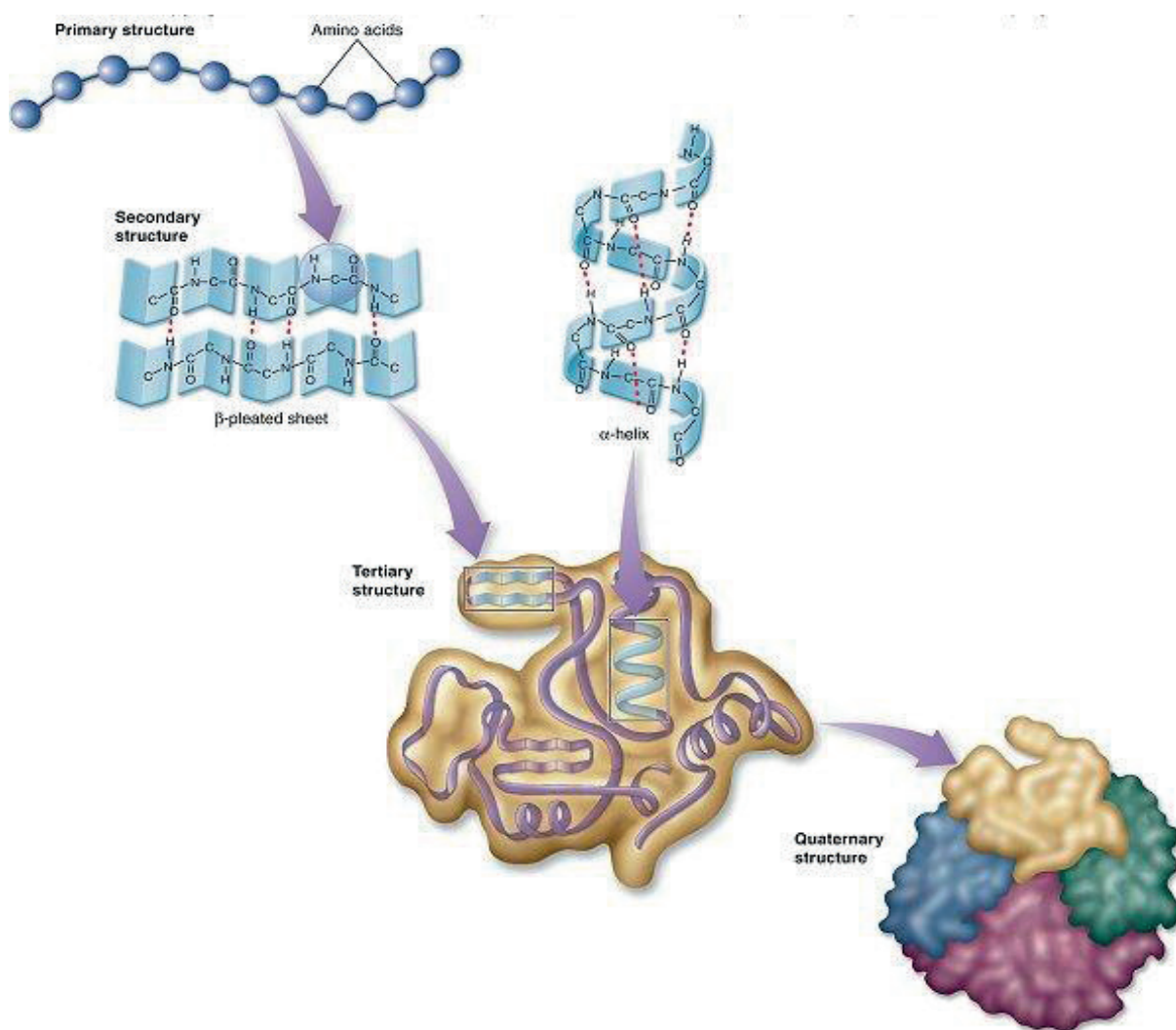


**Fig. 1.7. Schematic overview of the different structural levels of proteins [76].**

The higher order, i.e. secondary to quaternary, structural levels are stabilized through much weaker non-covalent bonds. The secondary structure is formed by hydrogen

bonds between the different amino acids of the sequence. The oxygen of the backbone carbonyl group of an amino acid hydrogen bonds to the backbone NH group of another one in a certain way forming secondary structures. Examples of secondary structures are  $\alpha$ -helix and  $\beta$ -sheet structures. The tertiary structure is the folded 3D-configuration of the protein, constituting of the different secondary structures. It is primarily held together by hydrophobic bonds between amino acid side chains, but also by other bonds, such as hydrogen bonds and salt bridges. For certain proteins, there is a quaternary structure. It associates several polypeptide chains (subunits) by non-covalent bonds, including hydrophobic interactions, hydrogen bonds and van der Waals interactions [77-78].

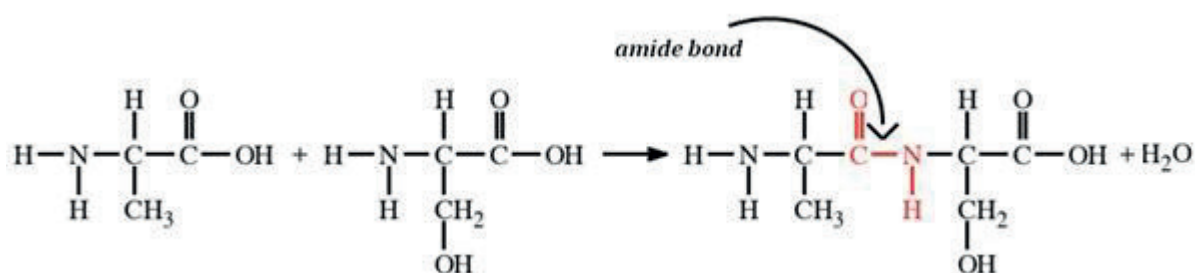


**Fig. 1.8. Formation of a peptide bond linking two amino acids together.**

Biological drug products need a thorough characterization, generally performed during development stages of the product. This includes the determination of the physico-chemical properties, biological activity, immunochemical properties, purity and impurities. Different techniques are necessary for the structural and physico-chemical characterization of the protein [79]. To gain information on the primary structure of proteins the procedure may comprise N-terminal sequencing by Edman degradation, C-terminal analysis, and peptide mapping followed by reversed phase High Performance Liquid Chromatography - Mass Spectrometry (HPLC-MS). Secondary structural information on proteins can be obtained via several techniques, e.g. fluorescence spectroscopy, far- Ultra-Violet (UV) circular dichroism (CD), Fourier-Transform infrared (FTIR) spectroscopy, Raman spectroscopy... However, only FTIR and Raman spectroscopy are useful to analyze proteins in the amorphous state (e.g. freeze-dried state). Tertiary structural information is usually obtained via Nuclear Magnetic Resonance (NMR), X-ray crystallography, and near UV-CD. Common methods for



determining the quaternary structure involve size exclusion-HPLC (SE-HPLC) and light scattering techniques. Obviously, to characterize the conformational state of proteins, one analytical method will not satisfy. Usually, a combination of several is used [77, 79-81].

The stability of proteins entails two different aspects. The chemical stability of a protein involves changes of the covalent structure, and is usually irreversible. The physical (or conformational) stability of the folded state involves non-covalent changes (i.e. in the secondary to quaternary structure), and can be either reversible or irreversible. In this work, the physical stability of proteins is considered. From a thermodynamically point of view, there is a dynamic equilibrium between two states, i.e. the native and the ensemble of unfolded states [82]. The difference in Gibbs free energy ( $\Delta G$ ) between the unfolded states and the native one reflects the thermodynamic stability of a protein. The native protein conformation needs to be energetically preferred in order to exert its biological activity. In physiological circumstances, this is normally accomplished because the native state has a lower Gibbs free energy level than the highly disordered unfolded states. Major factors favoring this are (1) the conversion from a highly disordered state to an ordered state goes with a large loss of entropy, (2) the shift of hydrophobic groups from a polar environment (exposed) to a non-polar environment in the protein interior (buried), and (3) the formation of stabilizing interactions with and within the protein, such as (surrounding) hydrogen bonds, salt bridges and Van der Waals interactions [83]. Fig. 1.9 depicts a natively folded protein stabilized by hydrogen bonds with the surrounding water molecules.

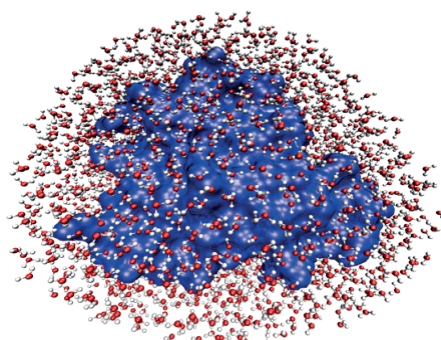


**Fig. 1.9. A natively folded and fully hydrated protein [84].**



However, because of the weak, non-covalent nature of the interactions constituting the secondary to quaternary structure, the native state is only marginally stabilized over the unfolded states. Consequently, when native proteins are exposed to even mild stress, e.g. caused by a change in their micro-environment, the partially unfolded states might become the preferred. This phenomenon is known as physical denaturation or protein unfolding, and usually happens via intermediate conformations (Fig. 1.10). The nature of the intermediate states can vary from transiently expanded species within the native ensemble to types with dramatic changes in the secondary structural element distribution.

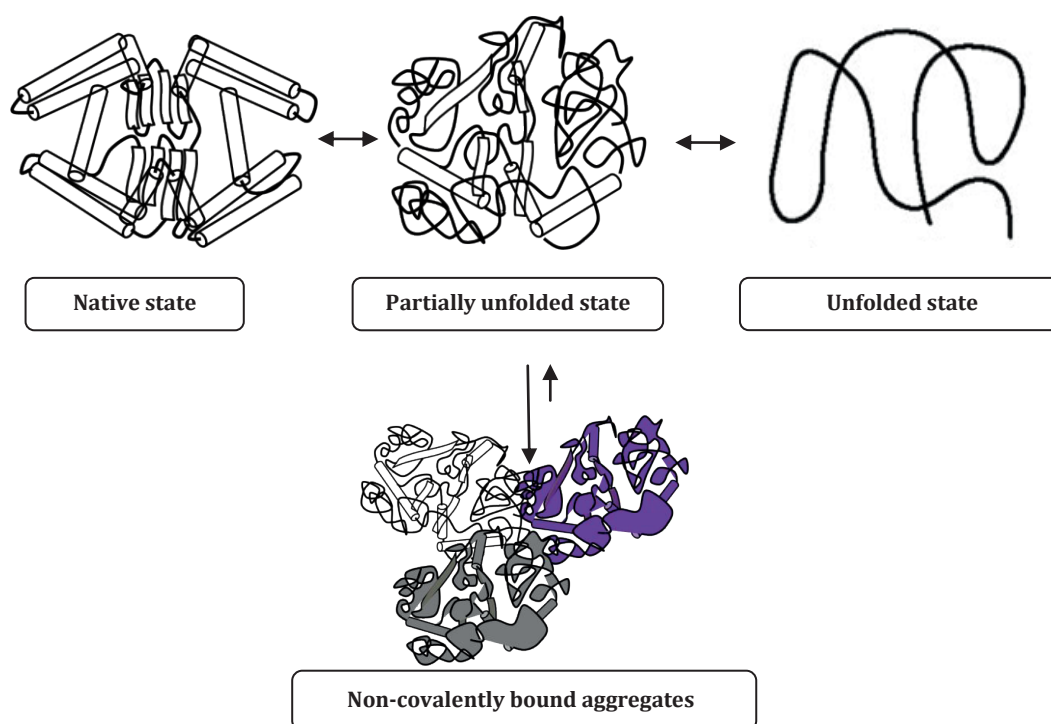


**Fig. 1.10. The relationship between the native and the (partially) unfolded states in proteins. Adapted from [91] and [92].**

Freeze-drying provides an arsenal of stresses that might physically destabilize proteins [61, 85]. Suspected causes during freeze concentration are cold denaturation, pH shifts, high ionic strength, and adsorption to interfaces [86-87]. During drying a well-known risk is dehydration, i.e. the (partial) removal of the hydration shell surrounding the protein [88-90]. This is also the reason why proteins are susceptible to over-drying, i.e.

when too much of the surrounding liquid shell is withdrawn, the protein may lose its native conformation.

A well-designed freeze-drying process for a protein formulation should induce minimal protein unfolding [61]. As a protein requires at least 40% hydrate water to be active, a protein will never be active in its dried state. Therefore, the dried native-like state differs mainly from a native state due to (partly) dehydration of the protein. When many conformational changes happen during the freeze-drying, the dried end product may comprise a high fraction of partially unfolded protein molecules. Those partially unfolded molecules might present a certain quality and safety hazard during the reconstitution of the product, as they increase the chance to produce non-covalent hydrophobic aggregates [93].

During reconstitution, it is expected that the addition of water will make the freeze-dried protein molecules to refold back to their native conformation. In most cases, they do, even when there is a small amount of protein unfolding in the freeze-dried product (i.e. reversible unfolding). However, when too much or too severe unfolding was present in the freeze-dried protein molecules, they might not refold back to the native conformation (i.e. irreversible unfolding). For most proteins, this involves significant disordered secondary structures [94]. As a result, the activity of the reconstituted protein may be reduced or absent. Also, during the reconstitution of partially unfolded proteins there is a risk that the hydrophobic side chains of exposed amino acids (which are buried in a native protein) start interacting with those from other protein molecules (Fig. 1.10). The latter may hamper the proper refolding of the protein and favor the association of partially unfolded protein molecules [92-93, 95]. This is known as physical protein aggregation (i.e. inter-molecular non-covalent bonds are formed) in the reconstituted and thus administered product. In the human body, aggregates of therapeutic proteins are often antigenic and may thus cause immunogenic reactions. The hydrophobic aggregation reaction will depend on the intrinsic properties of the protein molecules (e.g. hydrophobicity), but the aggregation rate will also be triggered by the high protein concentration in the freeze-dried cake to be reconstituted. A way to prevent this is by controlling its precursor step, i.e. maintaining the native conformation

during processing as much as possible, in order to avoid unfolding and thus exposure of hydrophobic sites. In view of the product's safety and efficacy, the accepted content of aggregates in a biological drug product will depend on its nature and its dose [96].

As aggregate formation can be avoided by minimizing protein unfolding during freeze-drying, this is a key aspect for formulation and lyophilization process development of any freeze-dried protein-based therapeutic [61]. For that reason, stabilizing excipients are frequently added to the formulation of protein pharmaceuticals, i.e. lyo- and cryo-protectants need to protect the protein from unfolding during the freeze-drying process [85, 97-98]. However, it should not be forgotten that the mitigation and control of aggregate formation is not only limited to this last step, the freeze-drying. It should cover the complete manufacturing process, as various stresses may as well be present during cell culture, harvest, purification, contact with equipment, freeze-thaw, storage, and vial filling [99]. The variety of different sizes and types of aggregates (e.g. covalent versus non-covalent, soluble versus insoluble...) that might be formed during the different processing steps requires different analytical techniques to detect and characterize them. Popular techniques are SE-HPLC, analytical ultracentrifugation (AUC), light scattering techniques, microscopy, and visual inspection [95].

## 1.4. Objectives and outline of this work

The extremely fast and non-invasive analysis of NIR and Raman spectroscopy make them useful for in-line monitoring of the product behavior during freeze-drying processes. The aim of this work is to evaluate the feasibility of NIR and Raman spectroscopy for the real-time and in-line monitoring of protein unfolding during freeze-drying processes. The conformational state of proteins in the freeze-dried product is a CQA as it directly impacts the efficacy and safety of the administered product. The correlation between protein unfolding during freeze-drying (generally involving a distortion in the secondary structures) and the risk for protein aggregation (or misfolding) at the time of reconstitution has been repeatedly demonstrated with different model proteins. Therefore, protein unfolding should be minimized during the freeze-drying process. To monitor this desired information during the process, it was for each technique under study in particular investigated (1) whether it can provide information on the desired quality attribute (i.e. determination of a suitable spectral response), (2) whether this information can be obtained directly from experimentally obtained spectra, and (3) whether this information still can be obtained accurately in the presence of expected interferences (e.g. process interferences).

The techniques under study are benchmarked to FTIR spectroscopy, being one of the state of the art techniques for determining changes in protein secondary structure. As molecular spectroscopic techniques can never fully characterize the conformational state of proteins (different methods will always be necessary for this purpose), the methods we aim for should rather give a *quality indication* on the conformational state of the proteins, just as FTIR does in the freeze-dried product. Hence, they will not replace final product quality testing. The ultimate goal is to have this quality indication early, when process settings still can be adjusted to obtain a freeze-dried end product with minimal protein unfolding.

In **chapter 2**, some general considerations are made before NIR and Raman spectroscopy are evaluated. Reflections are made on what to consider for the implementation of spectroscopic sensors for in-line monitoring protein samples during

a freeze-drying process. The instrument choice and conditions, the sampling strategy and the practical set-up are justified. As an adequate off-line reference method is necessary to independently evaluate whether or not there is protein unfolding in the studied samples, it was attempted to define a straightforward approach for quantifying, or at least qualifying, protein unfolding in the freeze-dried samples by using amide I FTIR spectroscopy. Two classes were defined, i.e. one with minimal ("native-like") and one with obvious ("non-native") changes in the secondary structural element distribution.

**Chapter 3** starts with a literature overview on NIR spectroscopy for detecting protein conformational changes. Because of the modest sensitivity of the NIR region to probe protein secondary structures, the focus was moved from considering varying intensities at multiple absorption frequencies (i.e. the classical approach in spectroscopic multivariate analysis) towards considering the frequency shifting of a relevant protein vibrational mode (i.e. the amide A/II band shifting due to variations in hydrogen bond strength caused by protein unfolding). Besides demonstration of the correlation between this spectral response and protein unfolding, it was also assessed whether this spectral response was selective when obtained in the presence of changing (process) interferences and in different formulations. Finally, this proof-of-concept study validates whether samples with and without protein unfolding (i.e. secondary structural changes detected with FTIR) during freeze-drying can be distinguished based on their process trajectory developed from the continuously in-line acquired NIR spectra.

In **chapter 4**, Raman spectroscopy is reviewed as one of the state of the art techniques for characterizing protein conformation. Although it provides information-rich spectra with respect to the conformation of freeze-dried proteins, it generally requires blank and background corrections for visual interpretation or univariate monitoring of selected features. This would be impractical and unacceptable for in-line monitoring purposes. Therefore, a first aim was to investigate the feasibility of MVA to obtain information on protein unfolding directly from the experimental Raman spectra. Exploratory analysis and supervised classification were explored for the discrimination

between two conformational state classes, i.e. native-like and non-native ones, in freeze-dried protein formulations.

To make the Raman model robust, spectral variations from interferences being likely to be present in future samples should be included in the model. In **chapter 5**, it was first attempted to make the Raman classification model robust for batch and formulation interferences, as they may cause spectral variations that impair the Raman analysis. To identify which interferences may largely influence the variability in the Raman spectra of freeze-dried formulations, a two-way variance analysis (evaluating batch and formulation type) was performed. In a next step, it was aspired to make the MVC model more robust for the identified interferences, by comparing both a classical (i.e. exhaustive calibration) and an orthogonal projection approach.

Finally, it was evaluated whether Raman spectroscopy can be applied for obtaining *in-line* and *real-time* information on protein unfolding during the freeze-drying process. A strategy was proposed for multivariate statistical process monitoring of protein unfolding from the in-line acquired Raman spectra. The strategy used orthogonal projections to make the statistical model independent from the progress of the process.

This thesis ends with a summary, some conclusions on this work, and some suggestions for future research (**chapter 6**).

In the **Annex**, we propose a cost-effective strategy for the development of a Partial Least Squares Regression (PLSR) model to predict the Active Pharmaceutical ingredient (API) content in tablets from NIR spectra. Since this study did not contribute to answering the research question of the thesis, it was considered separately from the rest of this thesis.

## 1.5. References

[1] U.S., Department of Health, Human Services, Food, Drug Administration, Center for Drug Evaluation Research, Center for Veterinary Medicine, Office of Regulatory Affairs, Guidance for industry: PAT - A framework for innovative pharmaceutical manufacturing and quality assurance, 2004.

<http://www.fda.gov/downloads/Drugs/Guidances/ucm070305.pdf> (accessed on 15/04/2013).

[2] L. Aboud, S. Hensley, New prescription for drug makers: Update the plants, *The Wall Street Journal*, September 3, 2003.

[3] D.C. Hinz, Process analytical technologies in the pharmaceutical industry: the FDA's PAT initiative, *Anal. Bioanal. Chem.* 384 (2006) 1036-1042.

[4] J. Workman, B. Lavine, R. Chrisman, M. Koch, Process analytical chemistry, *Anal. Chem.* 81 (2011) 4623-4643.

[5] International Conference on Harmonisation of technical requirements for registration of pharmaceuticals for human use, ICH Harmonised Tripartite Guideline, Q8(R2) Pharmaceutical Development, 2009.

[http://www.ich.org/fileadmin/Public\\_Web\\_Site/ICH\\_products/Guidelines/Quality/Q8\\_R1/Step4/Q8\\_R2\\_Guideline.pdf](http://www.ich.org/fileadmin/Public_Web_Site/ICH_products/Guidelines/Quality/Q8_R1/Step4/Q8_R2_Guideline.pdf) (accessed on 14/04/2013).

[6] International Conference on Harmonisation of technical requirements for registration of pharmaceuticals for human use, ICH Harmonised Tripartite Guideline, Q9 Quality Risk Management, 2005. [http://www.ich.org/fileadmin/Public\\_Web\\_Site/ICH\\_products/Guidelines/Quality/Q9/Step4/Q9\\_Guideline.pdf](http://www.ich.org/fileadmin/Public_Web_Site/ICH_products/Guidelines/Quality/Q9/Step4/Q9_Guideline.pdf) (accessed on 14/04/2013).

[7] International Conference on Harmonisation of technical requirements for registration of pharmaceuticals for human use, ICH Harmonised Tripartite Guideline, Q10 Pharmaceutical Quality System, 2008.

[http://www.ich.org/fileadmin/Public\\_Web\\_Site/ICH\\_products/Guidelines/Quality/Q10/Step4/Q10\\_Guideline.pdf](http://www.ich.org/fileadmin/Public_Web_Site/ICH_products/Guidelines/Quality/Q10/Step4/Q10_Guideline.pdf) (accessed on 14/04/2013).

[8] European Medicines Agency, EMA/CHMP/167068/2004, Pharmaceutical Development Q8 (R2), 2009. [http://www.ema.europa.eu/docs/en\\_GB/document\\_library/Scientific\\_guideline/2009/09/WC500002872.pdf](http://www.ema.europa.eu/docs/en_GB/document_library/Scientific_guideline/2009/09/WC500002872.pdf) (accessed on 15/04/2013).

[9] European Medicines Agency, EMA/INS/GMP/79766/2011, - Quality risk management (ICH Q9), 2011. [http://www.ema.europa.eu/docs/en\\_GB/document\\_library/Scientific\\_guideline/2009/09/WC500002873.pdf](http://www.ema.europa.eu/docs/en_GB/document_library/Scientific_guideline/2009/09/WC500002873.pdf) (accessed on 15/04/2013).

[10] European Medicines Agency, EMA/INS/GMP/79818/2011, - Pharmaceutical Quality System (ICH Q10), 2011. [http://www.ema.europa.eu/docs/en\\_GB/document\\_library/Scientific\\_guideline/2009/09/WC500002871.pdf](http://www.ema.europa.eu/docs/en_GB/document_library/Scientific_guideline/2009/09/WC500002871.pdf) (accessed on 15/04/2013).

[11] A.S. Houssain, Engineering a proactive decision system for pharmaceutical quality: integrating science of design, process analytical technology and quality system, presentation given at IFPAC 2005, Crystal City, VA.

[12] J. Chen, R. Mattes, K. Bakeev, S. Doherty, R.E. Cooley, R. Vangenechten, PAT/NIR roundtable, *American Pharmaceutical Review*, November issue 2010.

[13] R. Guenard, G. Thurau, Implementation of process analytical technologies, in: K.A. Bakeev (Ed.), *Process Analytical Technology*, John Wiley & Sons Ltd, United Kingdom, 2010, pp. 17-36.



- [14] T. De Beer, A. Burggraefe, M. Fonteyne, L. Saerens, J.P. Remon, C. Vervaet, Near infrared and Raman spectroscopy for the in-process monitoring of pharmaceutical production processes, *Int. J. Pharm.* 417 (2011) 32-47.
- [15] L.X. Yu, Pharmaceutical quality by design: product and process development, understanding, and control, *Pharm. Res.* 25 (2008) 781-791.
- [16] Council of Europe, European Pharmacopoeia, 7<sup>th</sup> edition, Strasbourg, 2010.
- [17] F. van den Berg, C.B. Lyndgaard, K.M. Sorensen, S.B. Engelsen, Process Analytical Technology in the food industry, *Trends in Food Science & Technology* 31 (2013) 27-35.
- [18] R. Riovanto, M. De Marchi, M. Cassandro, M. Penasa, Use of near infrared transmittance spectroscopy to predict fatty acid composition of chicken meat, *Food Chem.* 134 (2012) 2459-2464.
- [19] D.I. Ellis, V.L. Brewster, W.B. Dunn, J.W. Allwood, A.P. Golovanov, R. Goodacre, Fingerprinting food: current technologies for the detection of food adulteration and contamination, *Chem. Soc. Rev.* 41 (2012) 5706-5727.
- [20] J.P. Wold, M. O'Farrell, M. Hoy, J. Tschudi, On-line determination and control of fat content in batches of beef trimmings by NIR imaging spectroscopy, *Meat Sci.* 89 (2011) 317-324.
- [21] J. Wetterlind, B. Stenberg, R.A. Rossel, Soil analysis using visible and near infrared spectroscopy, *Methods Mol. Biol.* 953 (2013) 95-107.
- [22] G. Mirschel, K. Heymann, O. Savchuk, B. Genest, T. Scherzer, In-line monitoring of the thickness of printed layers by near-infrared (NIR) spectroscopy at a printing press, *Appl. Spectrosc.* 66 (2012) 765-772.
- [23] J.B. Holm-Nielsen, C.J. Lomborg, P. Oleskowicz-Popiel, K.H. Esbensen, On-line near-infrared monitoring of glycerol-boasted anaerobic digestion processes: evaluation of process analytical technologies, *Biotechnol. Bioeng.* 99 (2008) 302-313.
- [24] A.P. Craig, A.S. Franca, J. Irudayaraj, Surface-enhanced Raman spectroscopy applied to food safety, *Annu. Rev. Food Sci. Technol.* 4 (2013) 369-380.
- [25] M.W. Davey, W. Saeys, E. Hof, H. Ramon, R.L. Swennen, J. Keulemans, Application of visible and near-infrared reflectance spectroscopy (Vis/NIRS) to determine carotenoid contents in banana (*Musa spp.*) fruit pulp, *J. Agric. Food Chem.* 57 (2009) 1742-1751.
- [26] M. Lesteur, E. Latrille, V.B. Maurel, J.M. Roger, C. Gonzalez, G. Junqua, J.P. Steyer, First step towards a fast analytical method for the determination of Biochemical Methane Potential of solid wastes by near-infrared spectroscopy, *Bioresour. Technol.* 102 (2011) 2280-2288.
- [27] J. Aaltonen, K.C. Gordon, C.J. Strachan, T. Rades, Perspectives in the use of spectroscopy to characterise pharmaceutical solids, *Int. J. Pharm.* 364 (2008) 159-169.
- [28] G. Fevotte, In situ Raman spectroscopy for in-line control of pharmaceutical crystallization and solids elaboration processes: a review, *Chem. Eng. Sci. Des.* 85 (2007) 906-920.
- [29] A. Heinz, C.J. Strachan, K.C. Gordon, T. Rades, Analysis of solid-state transformations of pharmaceutical compounds using vibrational spectroscopy, *J. Pharm. Pharmacol.* 61 (2009) 971-988.



- [30] J. Luypaert, D.L. Massart, Y. Vander Heyden, Near-infrared spectroscopy applications in pharmaceutical analysis, *Talanta* 72 (2007) 865-883.
- [31] E. Rasanen, N. Sandler, Near-infrared spectroscopy in the development of solid dosage forms, *J. Pharm. Pharmacol.* 59 (2007) 147-159.
- [32] G. Reich, Near-infrared spectroscopy and imaging: basic principles and pharmaceutical applications, *Adv. Drug. Del. Rev.* 57 (2005) 1109-1143.
- [33] C.J. Strachan, T. Rades, K.C. Gordon, J. Rantanen, Raman spectroscopy for quantitative analysis of pharmaceutical solids, *J. Pharm. Pharmacol.* 59 (2007) 179-192.
- [34] Z.Q. Wen, Raman spectroscopy for protein pharmaceuticals, *J. Pharm. Sci.* 96 (2007) 2861-2878.
- [35] S. Tummula, J.W. Shabaker, S.S.W. Leung, Building process knowledge using inline spectroscopy, reaction calorimetry and reaction modeling - the integrated approach, *Curr. Opin. Drug. Disc. Dev.* 8 (2005) 789-797.
- [36] M. Fonteyne, S. Soares, J. Vercruysse, E. Peeters, A. Burggraef, C. Vervaet, J.P. Remon, N. Sandler, T. De Beer, Prediction of quality attributes of continuously produced granules using complementary PAT tools, *Eur. J. Pharm. Biopharm.* 82 (2012) 429-436.
- [37] L. Saerens, L. Dierickx, T. Quiten, P. Adriaenssens, R. Carleer, C. Vervaet, J.P. Remon, T. De Beer, In-line NIR spectroscopy for the understanding of polymer-drug interaction during pharmaceutical hot-melt extrusion, *Eur. J. Pharm. Biopharm.* 81 (2012) 230-237.
- [38] P.Y. Sacré, E. Deconinck, L. Saerens, T. De Beer, P. Courselle, R. Vancauwenberghe, P. Chiap, J. Crommen, J.O. De Beer, Detection of counterfeit Viagra® by Raman microscopy imaging and multivariate analysis, *J. Pharm. Biomed. Anal.* 56 (2011) 454-461.
- [39] L. Saerens, L. Dierickx, B. Lenain, C. Vervaet, J.P. Remon, T. De Beer, Raman spectroscopy for the in-line polymer-drug quantification and solid state characterization during a pharmaceutical hot-melt extrusion process, *Eur. J. Pharm. Biopharm.* 77 (2011) 158-163.
- [40] B. Stuart, *Infrared spectroscopy: fundamentals and applications*, John Wiley & Sons, United Kingdom, 2004, pp. 244.
- [41] G. Radtke, K. Knop, B.C. Lippold, Near infrared (NIR) spectroscopy: fundamentals and applications from a pharmaceutical point, *Pharm. Ind.* 61 (1999) 848-857.
- [42] R. Tantipolphan, T. Rades, N.J. Medlicott, Insights into the structure of protein by vibrational spectroscopy, *Curr. Pharm. Anal.* 4 (2008) 53-68.
- [43] <http://www.leakbird.com/science/water-color-blue-science-absorption-coefficient-backreaction-functio> (accessed on 25/05/2013).
- [44] A. Barth, C. Zscherp, What vibrations tell us about proteins, *Q. Rev. Biophys.* 35 (2002) 369-430.
- [45] R.L. McCreery, Raman spectroscopy for chemical analysis, J.D. Winefordner (Ed.), volume 157, John Wiley & Sons, New York, United States, 2000, pp 420.
- [46] T. Vankeirsbilck, A. Vercauteren, W. Baeyens, G. Van der Weken, Applications of Raman spectroscopy in pharmaceutical analysis, *TrAC* 21 (2002) 869-877.

- [47] European Medicines Agency, EMEA/CHMP/CVMP/QWP/17760/2009 Rev2, Guideline on the use of near infrared spectroscopy (NIRS) by the pharmaceutical industry and the data requirements for new submissions and variations, 2012.  
[http://www.ema.europa.eu/docs/en\\_GB/document\\_library/Scientific\\_guideline/2012/02/WC500122769.pdf](http://www.ema.europa.eu/docs/en_GB/document_library/Scientific_guideline/2012/02/WC500122769.pdf) (accessed on 15/04/2013).
- [48] A.C. Olivieri, N.M. Faber, J. Ferré, R. Bouqué, J.H. Kalivas, H. Mark, Uncertainty estimation and figures of merit for multivariate calibration, *Pure Appl. Chem.* 78 (2006) 633-661.
- [49] A. Bogomolov, Multivariate process trajectories: capture, resolution and analysis, *Chemom. Intell. Lab. Syst.* 108 (2011) 49-63.
- [50] F. Franks (Ed.), *Freeze-drying of pharmaceuticals and biopharmaceuticals*, 1<sup>st</sup> edition, The Royal Society of Chemistry, Cambridge, UK (2007), pp. 201.
- [51] S.L. Nail, S. Jiang, S. Chongprasert, S.A. Knopp, Fundamentals of freeze-drying, *Pharm. Biotechnol.* 14 (2002) 281-360.
- [52] J.C. Kasper, W. Friess, The freezing step in lyophilization: physico-chemical fundamentals, freezing methods and consequences on process performance and quality attributes of biopharmaceuticals, *Eur. J. Pharm. Biopharm.* 78 (2011) 248-263.
- [53] G. Levi, M. Karel, Volumetric shrinkage (collapse) in freeze-dried carbohydrates above their glass transition temperature, *Food Res. Int.* 28 (1995) 145-151.
- [54] X. Tang, M.J. Pikal, Design of freeze-drying processes for pharmaceuticals: practical advice, *Pharm. Res.* 21 (2004) 191-200.
- [55] R.E. Johnson, M.E. Oldroyd, S.S. Ahmed, H. Gieseler, L.M. Lewis, Use of manometric temperature measurements (MTM) to characterize the freeze-drying behavior of amorphous protein formulations, *J. Pharm. Sci.* 99 (2010) 2863-2873.
- [56] A. Parker, S. Rigby-Singleton, M. Perkins, D. Bates, D. Le Roux, C.J. Roberts, C. Madden-Smith, L. Lewis, D.L. Teagarden, R.E. Johnson, S.S. Ahmed, Determination of the influence of primary drying rates on the microscale structural attributes and physicochemical properties of protein containing lyophilized products, *J. Pharm. Sci.* 99 (2010) 4616-4629.
- [57] L.M. Lewis, R.E. Johnson, M.E. Oldroyd, S.S. Ahmed, L. Joseph, I. Saracovan, S. Sinha, Characterizing the freeze-drying behavior of model protein formulations, *AAPS PharmSciTech* 11 (2010) 1580-1590.
- [58] R. Johnson, L. Lewis, Freeze-drying protein formulations above their collapse temperatures: possible issues and concerns, *American Pharmaceutical Review*, April issue (2011)
- [59] J.C. Kasper, W. Friess, The freezing step in lyophilization: physico-chemical fundamentals, freezing methods and consequences on process performance and quality attributes of biopharmaceuticals, *Eur. J. Pharm. Biopharm.* 78 (2011) 248-263.
- [60] M.J. Pikal, S. Shah, Intravial distribution of moisture during the secondary drying stage of freeze-drying, *PDA J. Pharm. Sci. Technol.* 51 (1997) 17-24.
- [61] J.F. Carpenter, M.J. Pikal, B.S. Chang, T.W. Randolph, Rational design of stable lyophilized protein formulations: some practical advice, *Pharm. Res.* 14, 1997, 969-975.

- [62] D. Fissore, R. Pisano, V. Rasetto, D. Marchisio, A.A. Barresi, A. Vallan, S. Corbellini, Applying process analytical technology (PAT) to lyophilization processes, *Chemistry Today* 27 (2009) 7-11.
- [63] S.M. Patel, M. Pikal, Process Analytical Technologies (PAT) in freeze-drying of parenterals, *Pharmaceutical Development and Technology* 14 (2009) 567-587.
- [64] S.C. Schneid, H. Gieseler, W.J. Kessler, M.J. Pikal, Non-invasive product temperature determination during primary drying using tunable diode laser absorption spectroscopy, *J. Pharm. Sci.* 98 (2009) 3406-3418.
- [65] H. Gieseler, W.J. Kessler, M. Finson, S.J. Davis, P.A. Mulhall, V. Bons, D.J. Debo, M.J. Pikal, Pharmaceutical technology - Evaluation of tunable diode laser absorption spectroscopy for in-process water vapor mass flux measurements during freeze-drying, *J. Pharm. Sci.* 96 (2007) 1776-1793.
- [66] X.L.C. Tang, S.L. Nail, M.J. Pikal, Evaluation of manometric temperature measurement, a process analytical technology tool for freeze-drying: part III, heat and mass transfer measurement, *AAPS Pharmscitech* 7 (2006)
- [67] X.L.C. Tang, S.L. Nail, M.J. Pikal, Evaluation of manometric temperature measurement, a process analytical technology tool for freeze-drying: part II, measurement of dry layer resistance, *AAPS Pharmscitech* 7 (2006)
- [68] X.L.C. Tang, S.L. Nail, M.J. Pikal, Evaluation of manometric temperature measurement, a process analytical technology tool for freeze-drying: part I, product temperature measurement, *AAPS Pharmscitech* 7 (2006)
- [69] T.R.M De Beer, P. Vercruysse, A. Burggraeve, T. Quinten, J. Ouyang, X. Zhang, C. Vervaet, J.P. Remon, W.R.G Baeyens, In-line and real-time process monitoring of a freeze-drying process using Raman and NIR spectroscopy as complementary process analytical technology (PAT) tools, *J. Pharm. Sci.* 98 (2009) 3430-3446.
- [70] T.R.M De Beer, M. Alleso, F. Goethals, A. Coppens, Y. Vander Heyden, H. Lopez De Diego, J. Rantanen, F. Verpoort, C. Vervaet, J.P. Remon, W.R.G. Baeyens, Implementation of a process analytical technology system in a freeze-drying process using Raman spectroscopy for in-line process monitoring, *Anal. Chem.* 79 (2007) 7992-8003.
- [71] T.R.M. De Beer, M. Wiggernhorn, A. Hawe, J.C. Kasper, A. Almeida, T. Quinten, W. Friess, G. Winter, C. Vervaet, J.P. Remon, Optimization of a pharmaceutical freeze-dried product and its process using an experimental design approach and innovative process analyzers, *Talanta* 82 (2011) 1623-1633.
- [72] T.R.M. De Beer, M. Wiggernhorn, R. Veillon, C. Debacq, Y. Mayeresse, B. Moreau, A. Burggraeve, T. Quinten, W. Friess, G. Winter, C. Vervaet, J.P. Remon, W.R.G. Baeyens, Importance of using complementary process analyzers for the process monitoring, analysis and understanding of freeze-drying, *Anal. Chem.* 81 (2009) 7639-7649.
- [73] A. Kauppinen, M. Toiviainen, O. Korhonen, J. Aaltonen, K. Jarvinen, J. Paaso, M. Juuti, J. Ketolainen, In-line multipoint near-infrared spectroscopy for moisture content quantification during freeze-drying, *Anal. Chem.* 85 (2013) 2377-2384.

- [74] K.P. Malik, C. Duru, M. Ahmed, P. Matejtschuk, Analytical options for the measurement of residual moisture content in lyophilized biological materials, *American Pharmaceutical Review*, August issue (2010)
- [75] FDA's National Drug Code Directory.  
<http://www.accessdata.fda.gov/scripts/cder/ndc/default.cfm> (accessed on 18/04/2013)
- [76] L. Snyder, J.J. Kirkland, J.W. Dolan, *Biochemical and synthetic polymer separations, Introduction to modern liquid chromatography*, John Wiley & sons, New Jersey (2010) 569-664.
- [77] A.K. Banga, *Therapeutic peptides and proteins: formulation, processing and delivery systems* (2<sup>nd</sup> edition), Taylor and Francis group, Boca Raton, FL, 2006, pp 354.
- [78] J.M. Berg, J.L. Tymoczko, L. Stryer, *Biochemistry* (5th edition), W.H. Free man, New York, US, 2002, pp 1050.
- [79] European Medicines Agency, CPMP/ICH/365/96, - Specifications: Test procedures and acceptance criteria for biotechnological/ Biological products (ICH Q6B), 1999.  
[http://www.ema.europa.eu/docs/en\\_GB/document\\_library/Scientific\\_guideline/2009/09/WC500002824.pdf](http://www.ema.europa.eu/docs/en_GB/document_library/Scientific_guideline/2009/09/WC500002824.pdf) (accessed on 03/05/2013).
- [80] J.T. Pelton, L.R. McLean, Spectroscopic methods for analysis of protein secondary structure, *Anal. Biochem.* 277 (2000) 167-176.
- [81] S.K. Niazi, *Handbook of biogeneric therapeutic proteins: regulatory, manufacturing, testing, and patent issues*, Informa Healthcare, St Helier, Jersey, 2005, pp 265-289.
- [82] V. Ragoonanan, A. Aksan, Protein stabilization, *Transfus. Med. Hemother.* 34 (2007) 246-252.
- [83] D.P. Goldenberg, Protein folding and assembly, In *Encyclopedia of Biological Chemistry* (Lennarz, W. J. & Lane, M., eds.), Academic Press/Elsevier Science, San Diego, volume 3, 2004, pp. 493-499.
- [84] H. Frauenfelder, A unified model of protein dynamics, *Proceedings of the National Academy of Sciences of the United States of America* 106 (2009) 5129-5134.
- [85] J.F. Carpenter, K.I. Izutsu, T.W. Randolph, Freezing- and drying -induced perturbations of protein structure and mechanisms of protein protection by stabilizing additives, *Freeze-drying/lyophilization of pharmaceutical and biological products*, Informa Health Care, New York (2004) 147-187.
- [86] J.C. Kasper, W. Friess, The freezing step in lyophilization: physico-chemical fundamentals, freezing methods and consequences on process performance and quality attributes of biopharmaceuticals, *Eur. J. Pharm. Biopharm.* 78, 2011, 248-263.
- [87] B.S. Bhatnagar, R.H. Bogner, M.J. Pikal, Protein stability during freezing: Separation of stresses and mechanisms of protein stabilization, *Pharm. Develop. Techn.* 12 (2007) 505-523.
- [88] J.J. Hill, E.Y. Shalaeve, G. Zografi, Thermodynamic and dynamic factors involved in the stability of native protein structure in amorphous solids in relation to levels of hydration, *J. Pharm. Sci.* 94 (2005) 1636-1667.
- [89] A.M. Abdul-Fattah, D.S. Kalonia, M.J. Pikal, The challenge of drying method selection for protein pharmaceuticals: product quality implications, *J. Pharm. Sci.* 96 (2007) 1886-1916.

- [90] A.M. Abdul-Fattah, V. Truong-le, L. Yee, L. Nguyen, D.S. Kalonia, M.T. Cicerone, M.J. Pikal, Drying-induced variations in physico-chemical properties of amorphous pharmaceuticals and their impact on stability (I): Stability of a monoclonal antibody, *J. Pharm. Sci.* 96 (2007) 1983-2008.
- [91] D.J. Selkoe, Folding proteins in fatal ways, *Nature* 426 (2003) 900-904.
- [92] W. Wang, Protein aggregation and its inhibition in biopharmaceutics, *Int. J. Pharm.* 289 (2005) 1-30.
- [93] S. Srisailam, T.K.S. Kumar, T. Srimathi, C. Yu, Influence of backbone conformation on protein aggregation, *J. Am. Chem. Soc.* 124 (2002) 1884-1888.
- [94] Z.Q. Wen, Raman spectroscopy of protein pharmaceuticals, *J. Pharm. Sci.* 96 (2007) 2861-2878.
- [95] S. Zöls, R. Tantipolphan, M. Wiggenghorn, G. Winter, W. Jiskoot, W. Friess, A. Hawe, Particles in therapeutic protein formulations, part 1: Overview of analytical methods, *J. Pharm. Sci.* 101 (2012) 914-935.
- [96] S.K. Niazi, *Handbook of biogeneric therapeutic proteins: regulatory, manufacturing, testing, and patent issues*, Informa Healthcare, St Helier, Jersey, 2005, pp 265-289.
- [97] L. Chang, M.J. Pikal, Mechanisms of protein stabilization in the solid state, *J. Pharm. Sci.* 98 (2009) 2886-2908.
- [98] L. Chang, D. Shepherd, J. Sun, D. Ouellette, K.L. Grant, X. Tang, M.J. Pikal, Mechanism of protein stabilization by sugars during freeze-drying and storage: Native structure preservation, specific interaction, and/or immobilization in a glassy matrix?, *J. Pharm. Sci.* 94 (2005) 1427-1444.
- [99] A.S. Rathore, V. Joshi, N. Yadav, Aggregation of monoclonal antibody products: formation and removal, *BioPharm International*, March issue (2013).



---

## Chapter 2: GENERAL CONSIDERATIONS

---

### **2.1. Implementation of NIR and Raman spectroscopy as process analyzers in freeze-drying processes: what to consider?**

For any spectroscopic process analyzer that one wants to implement into a process stream some general requirements will have to be considered [1-2]. For the implementation of a spectroscopic sensor in a freeze-dryer, important things to consider have been summarized in Fig. 2.1. Although strongly linked, these aspects will be considered in different paragraphs and chapters along this thesis. First, there are requirements on the robustness of the equipment when exposed to the process environment (2.1.1). Also, critical decisions have to be made concerning practical aspects, such as the instrument choice and conditions (2.2.2) and the sampling and interfacing (2.2.3.). In the respective chapters for NIR (chapter 3) and Raman spectroscopy (chapters 4-5) we consider the following important aspects: (1) can the techniques provide information on the desired quality attribute (i.e. determination of a suitable spectral response), (2) can this information be obtained directly from the experimentally obtained spectra, and (3) can this information still be obtained in the presence of expected interferences (e.g. process interferences, different batches, different formulations).

#### **2.1.1. Environment**

Traditionally, analytical equipment has been used only inside the quality control lab under Good Laboratory Practices (GLP) conditions. With the PAT concept, it is aspired to use such equipments in the production environment under GMP conditions. As freeze-drying is a sterile process, the part of the equipment (e.g. the measurement probe, the fiber optic cables) in the freeze-dryer requires to be sterile. The equipment should also operate adequately in the presence of the expected temperature and pressure variations (robustness). In a freeze-dryer it is also perfectly possible to have no ambient light, which causes artifacts in Raman spectra. In this work, the NIR and Raman fiber optic probes were inserted via a gap made in the laboratory scale freeze-dryer. Recently, multi-point spectrometers with several fiber-optic probes in freeze-dryers have been developed [3].

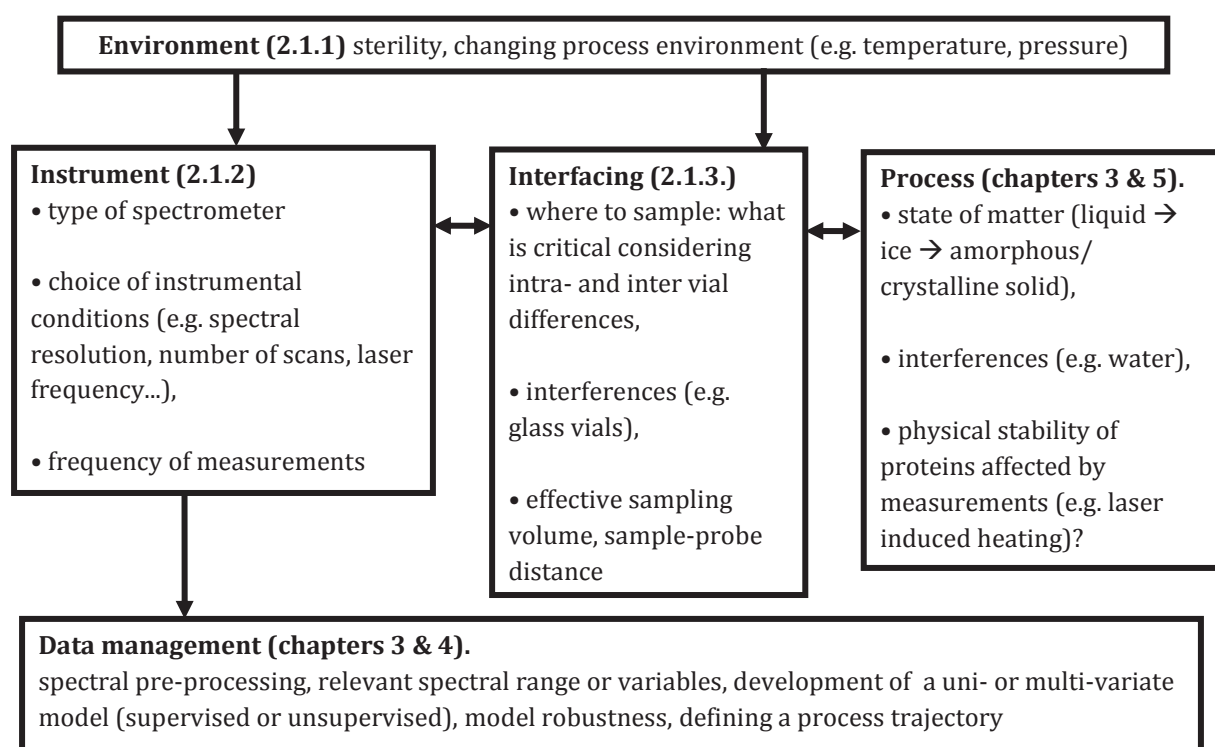


**Fig. 2.1. General requirements to consider for implementing spectroscopic process analyzers in a freeze-drying process.**

## 2.1.2. Instrument choice and conditions

A suitable process analyzer (or combination of process analyzers) should be able to efficiently monitor the desired critical process or product information. As there are different types of measurement techniques for (N)-IR and Raman spectroscopy, different types of instruments have been developed. We will shortly overview the characteristics of the instruments that were used in this work. Table 2.1. summarizes the main characteristics for each technique, being important for their use as potential process analyzers in a freeze-drying process.

### 2.1.2.1. ATR-FTIR spectrometer

In this work an Attenuated Total Reflectance (ATR)-FTIR spectrometer was used for the reference analyses. FTIR spectrometers are today the most popular type of infrared instrumentation. The idea is to split the light into two beams and measure the interference of their radiation. The detector measures a signal that is a function of the change in path length between these two beams. This obtained signal will finally be



converted by a mathematical method, called Fourier Transformation (FT), to the normal output, i.e. frequencies [4].

**Table 2.1. Characteristics of the different spectroscopic techniques used in this work, i.e. ATR-FTIR, reflectance FT-NIR and dispersive Raman spectroscopy with a 785 nm laser wavelength.**

Characteristic	ATR-FTIR	Reflectance FT-NIR	Dispersive Raman 785 nm
Vibrational modes	Fundamental	Overtones and combinations	Fundamental
Information content/ structural selectivity	High	Low	High
Water/ ice interference	High (subtraction often necessary)	Very high	Low
Invasiveness	Yes	No	No
Sampling through glass	No	Yes	Depends on the level of impurities in the glass
Sample preparation	Minimal with ATR	No	No
Sample destruction	Yes	No	Generally not (check for labile samples)
Sample state	Solid, liquid, gas	Mainly solid	Solid, liquid
Sample concentration	High (e.g. > 5 mg/ml in starting solution)	High (e.g. > 5 mg/ml in starting solution)	High (e.g. > 5 mg/ml in starting solution)
Remote sampling/ fiber optics	< 1 meter	> 1 meter	> 1 meter
Interferences	Can generally be subtracted, light scattering in solid samples	Spectral overlap, light scattering in solid samples	Luminescence (e.g. stray light, fluorescence)
Acquisition time	Seconds	Seconds	Seconds

ATR is a popular sampling technique used in conjunction with FTIR spectroscopy. It can greatly reduce the sample preparation time and effort. In an ATR cell the incident light is directed towards a crystal. When it penetrates the crystal it will undergo total internal reflection. Material that is in close contact with this crystal, and absorbs IR light, will make the beam lose energy at the wavelength where the material absorbs. The resulting attenuated radiation can be measured and plotted as a function of the frequencies [4]. Solid and liquid samples can be directly analyzed without any further sample preparation, however the short path length requires high protein

concentrations. As the technique requires contact with the sample (is invasive) it is not suitable to become a PAT tool for freeze-drying.

### 2.1.2.2. Reflectance FT-NIR spectrometer

Two popular means of sample presentation in (near)-infrared spectroscopy are transmittance and reflectance modes. In transmittance mode the sample is placed between the light source and the detector. The detector measures the fraction of the incident light that has passed the sample. In reflectance mode, the light source and detector are situated at one side relative to the sample, which has practical value for in- and on-line applications using fiber optic probes (the light returns to where it came from). Here one will measure the light that has been reflected by the sample. In this work, the FT-NIR instrument was in reflectance mode. This technique has the advantage that it can be used for highly absorbing and highly scattering matter. It has the disadvantage that the optimal optical path length is difficult to determine as it is variable depending on the (often variable) scattering properties of the sample.

### 2.1.2.3. Dispersive Raman spectrometer

Many different modes of Raman spectroscopy exist. They have been developed to enhance sensitivity (e.g. Surface Enhanced Raman spectroscopy or SERS), to minimize fluorescence contribution (e.g. FT-Raman spectroscopy) or to improve spatial resolution (e.g. Raman microscope). Different laser wavelengths (typically in the visible or NIR region) can also be used. The shorter the excitation laser wavelength, the stronger the intensity of the Raman signal, allowing higher sensitivity and shorter measurements times. However, fluorescence interference is more likely as the laser wavelength decreases. Thus the choice of the laser wavelength can dramatically influence the quality of the analysis, making the selection of the proper instrumental conditions for a certain sample crucial.

The Raman spectrometer we used in this work was the dispersive type with a laser wavelength of 785 nm, being a fair compromise between sensitivity and fluorescence issues. Charged Coupled Device (CCD) detectors are typically used for dispersive Raman. The collected Raman scattering is separated into its constituent frequencies by focusing

it onto a diffraction grating. Then the differentiated light is directed onto the CCD device [5].

### **2.1.3. Sampling and interfacing**

Both techniques (NIR and Raman spectroscopy) allow non-invasive sampling, which is a requirement not to disturb the freeze-drying process. An important practical aspect is the determination of the locations where to sample for obtaining the desired information, i.e. are we measuring a representative part of the sample?

#### 2.1.3.1. Remote measurements with fiber optic probes

The NIR and Raman instruments are equipped with fiber-optic probes. This enables remote measurements, i.e. inside the freeze-dryer chamber (Fig. 2.2). Optical fibers are very thin flexible strands made from pure glass (silica). They can carry light over a longer distance. Mid-infrared light is difficult to conduct through any existing optical fiber for more than a few meters, while this is no problem for NIR light or Raman scattering. This light is easily transmittable through fibers for hundreds of meters.

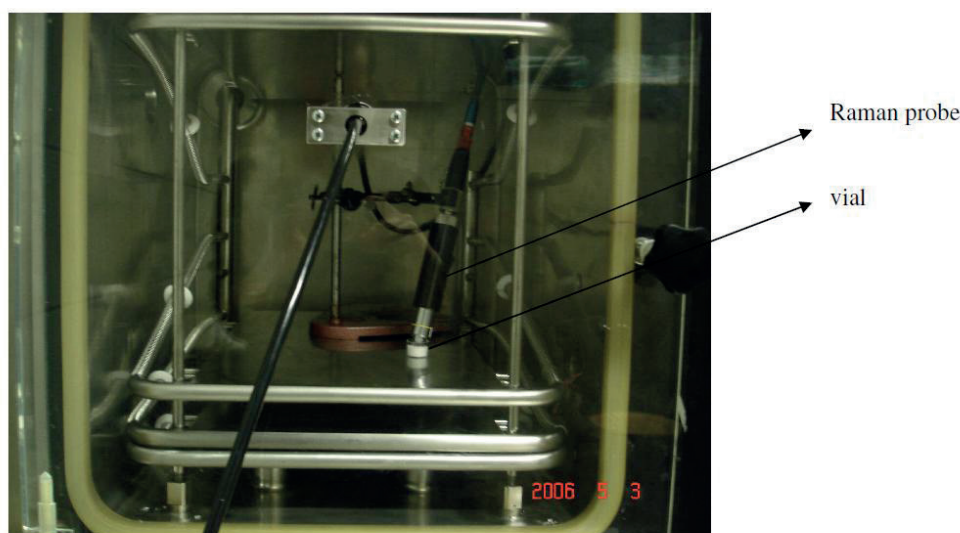


**Fig. 2.2. Experimental set-up of the in-line monitoring experiment, here shown for the Raman probe.**

#### 2.1.3.2. In-line set-up: when and where to sample?

Although both the NIR and Raman spectrometers with fiber optic probes allow non-invasive measurements without sample preparation or destruction (i.e. in-line

measurements), it is important to decide *when* and *where* to sample during the freeze-drying process. A continuous measurement set-up may allow a continuous inspection of the sample during the process. Since spectral acquisition for both NIR and Raman spectroscopy takes only a few seconds (e.g. less than one minute), all in-line experiments were conducted with one measurement per process minute. Hence, this may allow us to claim that we are measuring in 'real-time', although strictly spoken there is always a little time delay of less than one minute. But considering the fact that freeze-drying is an extremely slow process (i.e. the average time of a process is around 2 days), this time delay can be ignored.

Another important aspect is where to measure. As both NIR and Raman spectroscopy allow non-invasive measurement of only a fraction of the product (i.e. the part of the cake illuminated by the light spot), the measured spot should be selected well. It should provide us representative information about the quality attribute at the most critical places of the sample. Although it is known that product temperature and moisture content show intra- and inter-vial differences [6], this has not explicitly been studied for the protein conformation so far. However, regions in the product with lower residual water content may provide a higher risk for protein unfolding, since protein dehydration is one of the stress factors inducing this. Pikal et al. [6] found that during secondary drying, places providing a lower resistance passage for water vapor were more susceptible to over-drying than others, as they allowed faster drying. The top core section of the product contained relatively less moisture than the bottom core section, whereas the outer sections (i.e. near the vial wall) showed consistently to have lower moisture contents. The latter was ascribed to a cake shrinkage at the product-glass vial interface during drying, opening a pathway for water vapor. Moreover, secondary drying will start earlier at the outers of the cake, as sublimation will end there earlier than in the core (Fig. 2.3) [7]. Thus in these local regions, secondary drying will also last relatively longer, also increasing the risk for over-drying.

It was possible to measure with NIR spectroscopy from the side through the glass vial (Fig. 2.3). Although some studies proved the opposite [8-10], it was not possible to measure with dispersive Raman spectroscopy through the type I glass vials we used,

because of a large background, totally overruling the Raman signals (data not shown). Probably, the impurities of the glass vial are critical for the spectral background. Therefore, the Raman probe was placed above the open vial (Figs. 2.2 and 2.3). As these regions may be the most critical for over-drying, challenging the physical stability of the proteins the most, they were suggested to be the most suitable for the intended purpose. Because of the intra-vial differences it must be taken into account that the process proceeds differently depending on where one measures. This should also be considered when analyzing the spectroscopic data obtained from a process.

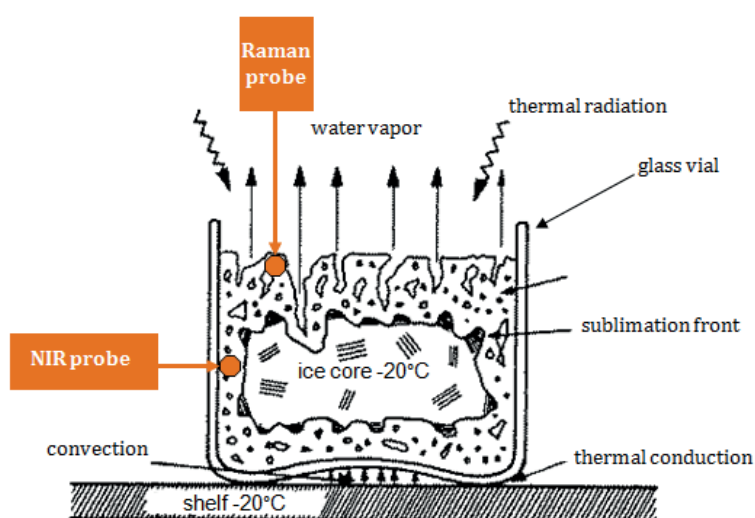


Fig. 2.3. Experimental set-up of the in-line monitoring experiments with NIR and Raman spectroscopy. This cartoon provides a snap shot during primary drying. Adapted from [7].

## 2.2. A reference for detecting protein unfolding

### 2.2.1. FTIR: a state of the art technique for protein secondary structure characterization and detecting protein unfolding

It was the goal to evaluate the feasibility of NIR and Raman spectroscopy for detecting protein unfolding in freeze-dried formulations, or during freeze-drying, because this would be their niche (for protein conformational analysis in solution many other techniques exist). Hence, the reference technique should also be applied on the same freeze-dried (and thus amorphous) protein samples to evaluate whether or not protein unfolding happened during the freeze-drying process. Among the many analytical techniques that exist to characterize the protein conformation, infrared and Raman

spectroscopy are the only options for the analysis on secondary structures of proteins in the freeze-dried state. The other techniques require the proteins to be in solution (e.g. CD, fluorescence spectroscopy, activity assay) or in a pure crystalline state (X-ray diffraction), but are not suitable for analysis of the freeze-dried amorphous state. As FTIR spectroscopy has been widely acknowledged for the analysis of secondary structures of proteins in freeze-dried products, this technique was chosen as the reference technique to analyze the conformational state of the proteins in the freeze-dried products.

The MIR region consists of nine bands that represent different vibration modes of the protein backbone. They are called amide A, B and I-VII (Table 2.2). The amide A band involves an N-H stretching vibration, exclusively localized on the N-H group. Usually, the amide A forms a Fermi resonance doublet with the amide II overtone (amide B). The frequencies of the amides A and B strongly depend on the strength of the hydrogen bonds, but are not used to determine protein secondary structure. For the latter the amide I and II bands are the most frequently used (Fig. 2.4). They are less complex and less influenced by side-chains contributions than the amide III and IV, making them more suitable for protein structural analysis and protein stability studies [4, 11-12]. Studies with proteins with known secondary structures have been used to correlate the shape of these bands to their secondary structure content [13-14]. The amide V, VI and VII bands are associated with out-of-plane motions.

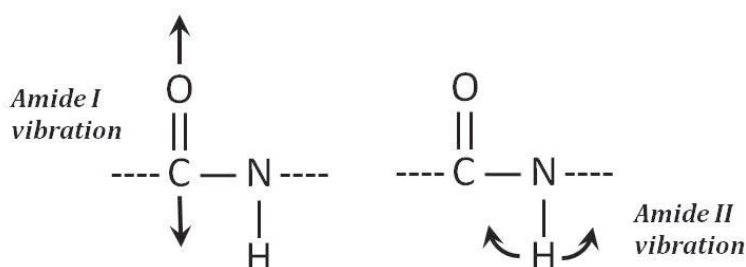


**Fig. 2.4.** The amide I vibration, mainly due to carbonyl stretching, and the amide II vibration, primarily due to N-H bending, being sensitive to protein backbone conformation.

The amide I band is the most intense absorption band for proteins. As the correlation between the secondary structure and the absorption frequencies is here the most

obvious, it is the most popular band for protein secondary structure determination [12]. The absorption frequencies in the amide I band are influenced by the molecular geometry (i.e. transition dipole coupling or TDC) and by the strength of the hydrogen bonds formed by the protein backbone (amide groups). TDC induces a splitting of the amide I band. The magnitude of the splitting depends on the distance between interacting dipoles and their orientation.

**Table 2.2. The nine characteristic infrared amide bands of proteins.**

Amide band	Wave number (cm <sup>-1</sup> )	Assignment
A	near 3300	N-H stretch
B	near 3170	in resonance with overtone amide II
I	1600-1700	80% C=O stretch, 10% C-N stretch, 10% N-H bend
II	1480-1575	60% N-H bend, 40% C-N stretch
III	1200-1400	30% C-N stretch, 30% N-H bend, 10% C=O stretch, 10% O=C-N bend, 20% other
IV	625-770	40% O=C-N, 60% other
V	near 725	N-H bend
VI	near 600	C=O bend
VII	near 200	C-N torsion

The frequency of the C=O bond is indirectly proportional to the strength of the formed hydrogen bonds. Stronger hydrogen bonds will result in a lower electron densities of the C=O groups, lowering the absorption frequencies in the amide I. As each type of secondary structural element is characterized by different hydrogen bond strengths, they give rise to different absorption frequencies within the amide I band. However, as these sub-bands are overlapping, the amide I band is visualized as one broad peak (Fig. 2.5A). The underlying absorption bands can be delineated by, for instance, Fourier self-deconvolution or second derivative calculations [11-12]. The minima in the second derivative spectrum indicate the positions of the overlapping components, corresponding to secondary structures [12]. For example,  $\alpha$ -helices, having weaker hydrogen bonds, absorb at higher frequencies than  $\beta$ -sheets (Fig. 2.5.B). Unordered or random structures are all structures that cannot be categorized as being helix, turn or sheet [15]. They usually appear as broad features because of their structural inhomogeneity [16-17].



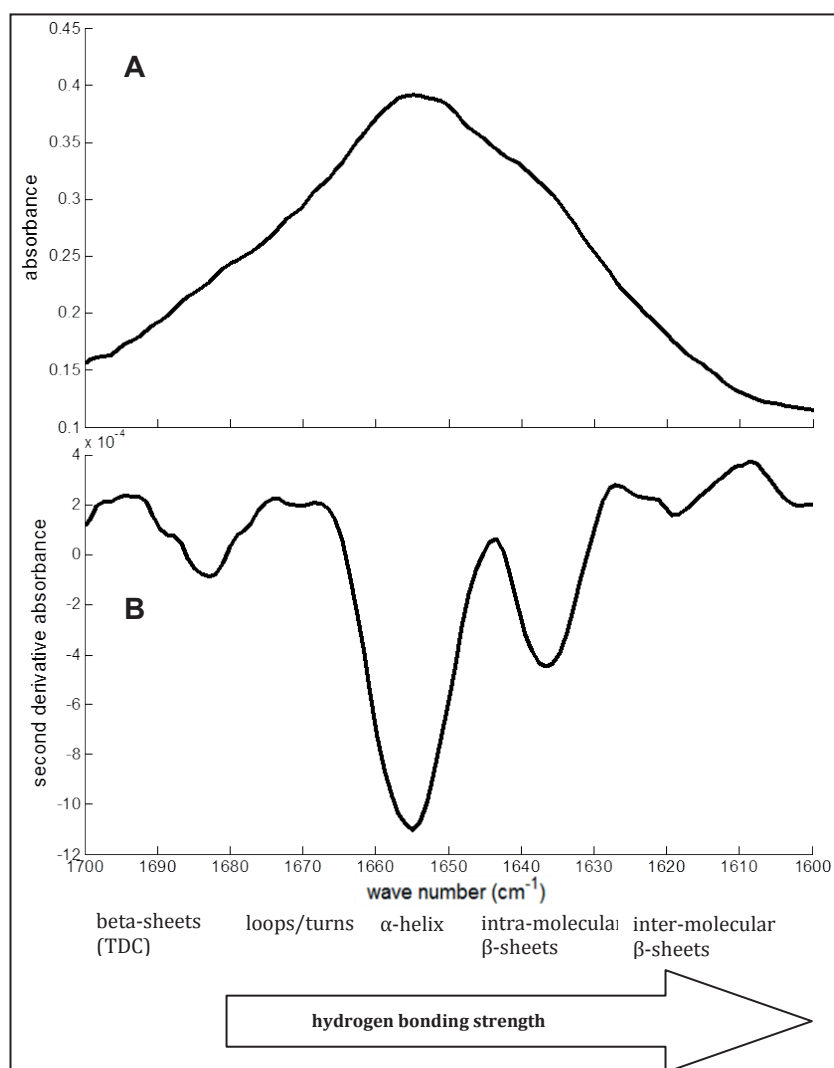


**Fig. 2.5.** The amide I band of a native-like freeze-dried lactate dehydrogenase (LDH) sample. (A) the blank corrected amide I band, (B) the second derivative spectrum of (A) with the frequency regions for the different secondary structural elements indicated.

The amide I band is less suitable for obtaining information on the protein tertiary and quaternary structures. Changes in the tertiary structure are manifested in the amide I band as a general broadening of the underlying sub-bands corresponding to the native secondary structures, since the bandwidth is a measure of conformational freedom and homogeneity [12, 18]. For instance, Matsuura et al. [19] observed a band broadening and decreased band resolution when a protein was converted to its molten globule state (i.e. a native-like but loosened structure). Changes in quaternary structure, and also aggregate formation, involve changes in inter-molecular interactions. The amide I band gives limited information on this type of interaction, i.e. via the absorption signal near 1620  $\text{cm}^{-1}$  (intermolecular beta-sheets). However, as not all types of aggregates can be



detected this way, a combination of different techniques is mostly necessary to draw conclusions on the presence or absence of aggregates [11-12]. Thus, the amide I band is generally being used to detect changes in secondary structural element distribution.

FTIR spectroscopy is besides CD and other spectroscopic techniques (e.g. Raman, fluorescence) one of the state of the art techniques for characterizing and detecting changes (in comparability studies) in the protein secondary structure [11]. A generally accepted methodology for protein characterization using the amide I band is a curve fitting approach. It relies on delineating and decomposing of the amide I band into its underlying secondary structural elements. A popular band narrowing technique is Fourier self-deconvolution, maintaining the relative intensities of each component. A drawback is that self-deconvolution procedures require parameters to be subjectively determined [12].

A parameter to quantify the different secondary structures is, for instance, the % relative area of each secondary structure [4]. Another way is making a calibration. The latter can be done by means of PLSR [20], or based on pattern recognition techniques such as artificial neural networks (ANN's) [12-21]. The spectral assignments of the different secondary structures are based on model proteins having been characterized by X-ray crystallography. Amide I FTIR spectroscopy is also frequently used in comparability studies, i.e. to assess a protein's physical stability when going from condition A to condition B. For proteins in solution, this technique is mostly combined with CD. The aim of comparability studies can be to investigate the differences before and after processing or stressing [11-12, 22]. The amide I band is here generally delineated by calculating the second derivative absorption spectrum. Contrary to Fourier self-deconvolution, the second derivative procedure does not preserve the relative intensities of the absorption bands. As it can also increase the level of noise, it is commonly combined with smoothing functions (e.g. Skavitzky-Golay) [11].

A great advantage of FTIR spectroscopy is that it is able to analyze protein samples under all kinds of physical conditions, such as aqueous, frozen, dried, insoluble precipitates, etc [23]. It is, next to Raman spectroscopy, one of the few techniques that

allows protein conformational state analysis in the freeze-dried state. However, although the amide I band is highly sensitive to protein secondary structure, not all changes in the amide I band can be ascribed to them [12, 24]. A protein's amide I spectrum is influenced by both protein conformation and some environmental factors.

Common interferences in the amide I band are water absorptions (especially in aqueous solutions) and excipient (e.g. buffer) components. By subtracting procedures these interferences can be corrected for [15, 25-27]. However, contributions of certain amino acid side chains may still interfere the amide I band (e.g. around 1610-1600  $\text{cm}^{-1}$ ) [27-29]. In practice, one is aware of these possible contributions but spectral analysis is generally performed without any correction factor for this [27].

It should be realized that any change in the hydrogen bond strength (regardless its origin) formed by the amide groups constituting the protein backbone can cause changes in the amide I. Thus, for instance, when comparing proteins with a different hydration state (i.e. changed hydrogen bonding between solvent exposed amide groups and water), or when going from a native to a molten globule state (i.e. is a native-like state that has loosened intra-molecular hydrogen bonds compared to the native state), one will observe changes in the amide I band that are not related to changes in secondary structural element distribution. They may manifest as subtle frequency shifts (i.e. due to small changes in hydrogen bonding strength), as well as small intensity shifts and peak broadening (i.e. due to changes in conformational freedom) of the peaks corresponding to secondary structures [12].

The spectral intensities in the amide I band may also be influenced by differences in physical conditions (such as morphology, degree of amorphous state...). Especially in the dried state, they can have a large effect [24]. This is generally apparent as a non-zero baseline. Often, a baseline correction is performed to minimize these differences between spectra [30-31]. Reference [31] recommends performing a baseline correction by connecting the two most positive points within the second derivative amide I spectrum (Fig. 2.6).

Since the second derivative absorption spectra do not preserve the original relative intensities of the underlying compounds, there is also need for an area normalization prior to comparison of two spectra [30]. Area normalization will also remove slight effects of differences in path length and protein concentration. Depending on the accessory and crystal, ATR sampling can induce artifacts in the FTIR spectra, such as small frequency shifts and changes in band width [12, 30].

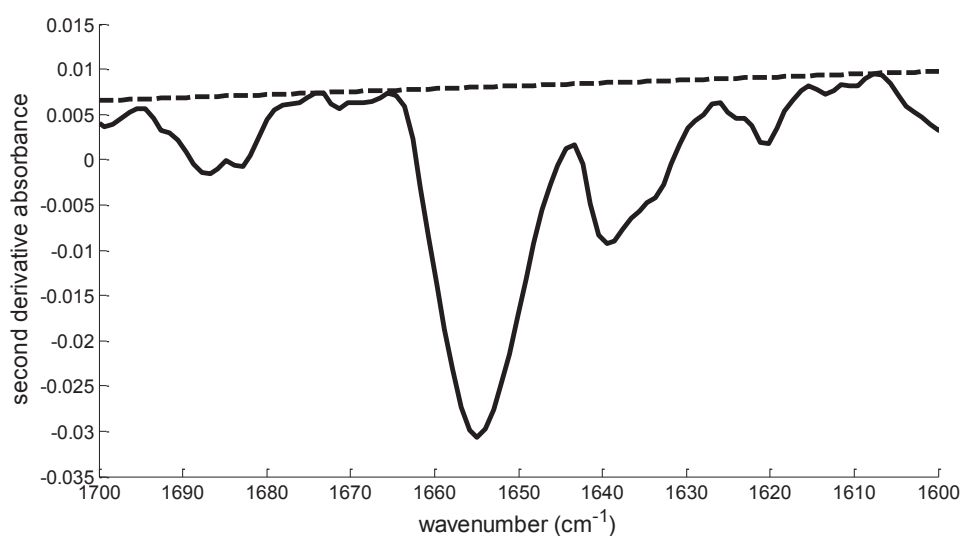


**Fig. 2.6. Baseline correction in the second derivative absorbance amide I spectrum of an LDH sample. The baseline is drawn by connecting the 2 maxima of the spectrum, as is recommended in ref. [31].**

## 2.2.2. The reference method to determine protein unfolding

### 2.2.2.1. Introduction

Combined with ATR, FTIR requires minimal sample preparation. However, the technique is destructive for freeze-dried samples, and invasive, which makes it unsuitable to become a PAT tool for in-line analysis during freeze-drying. In the reported studies, where it was used as an in-situ tool for detecting protein unfolding, samples in solution were studied [32], or at-line analysis during freeze-drying processes was performed [33-34].

In this work, FTIR spectroscopy (amide I band) is used off-line (i.e. at the end of freeze-drying) as a reference technique to decide whether or not there is protein unfolding induced by freeze-drying (comparability study). The second derivative absorption amide I spectra of the freeze-dried products (i.e. after freeze-drying stress) are

compared with the native state spectrum in solution (i.e. before freeze-drying stress). Comparison of the spectra can be done qualitatively (e.g. by visual comparison using expert knowledge) or quantitatively. Popular quantitative approaches are calculating the spectral correlation coefficient between two spectra [35], the area of overlap with the spectrum of the native state (% similarity between two spectra) [30], or the difference spectra (i.e. by subtracting a spectrum of a protein in one state from that same protein in another state). Such difference spectra provide a signature of the change in the spectrum which can be interpreted, and quantified by calculating the band area [11-12].

The aim of this thesis is to assess the feasibility of two potential in-line monitoring techniques, i.e. NIR and Raman spectroscopy, for detecting protein unfolding during freeze-drying processes. As protein aggregation during reconstitution is preceded by partial protein unfolding, generally involving changes in the secondary structure [36], this study requires thus in essence two types of freeze-dried samples, i.e. those where the freeze-drying process induced either obvious or minimal changes in the secondary structural element distribution in the freeze-dried product. Such samples were produced by varying process- and/or formulation conditions, thus stressing the protein molecules in different ways. Apart from their effect on the protein's physical stability, varying process and formulation conditions will also have their influence on other sample characteristics, e.g. the hydration state of the protein (e.g. affected by the residual moisture content and the presence or absence of lyoprotectants that interact with the protein molecules), the cake structure, the amorphous versus crystalline ratio... Hence, the samples required for this work will be very diverse, not only in protein conformation but also in other sample characteristics. As both may influence the amide I spectra, a proper reference method should be able to selectively detect protein unfolding in all samples.

In the following experiment, two approaches, a qualitative and quantitative one, are compared to detect protein unfolding in 99 freeze-dried lactate dehydrogenase (LDH) samples, being produced in different formulation and/or freeze-drying conditions. As a result, this set covered a continuum of different conformational states (i.e. native-like

and various types of unfolded states) and environmental states (differences in protein hydration and physical states).

### 2.2.2.2. Experimental

#### *2.2.2.2.1. Materials*

LDH from rabbit muscle Type II in ammonium sulfate was obtained from Sigma-Aldrich (Saint Louis, MO, USA). Prior to freeze-drying, 2 mL type I vials (Nipro, Authon-du-Perche, France) were filled with 720 µl formulation containing approximately 9 mg/ml LDH. Table 2.3 shows the different LDH formulations that were prepared in this study. Formulations 1-12 were used in the design of experiments (DoE) and contained a 40 mM buffer pH 7.4, either sodium phosphate (Sigma Aldrich, Steinheim, Germany) (PHOS), L-histidine (HIS) or TRIS (Merck, Darmstadt, Germany). Some formulations contained a lyoprotectant, i.e. 5% sucrose (Suedzucker, Mannheim, Germany) and/or a cryoprotectant, i.e. 1% PEG 4000 (Fagron, Barsbüttel, Germany). Besides the DoE formulations, others (formulations 13-19) contained NaSCN, NaCl or ethanol (Sigma Aldrich, Steinheim, Germany), or were formulated in water.

**Table 2.3. Different LDH formulations (appr. 9 mg/ml LDH) prepared in this study.**

Formulation number	Excipient composition
1	HIS
2	HIS, sucrose
3	HIS, PEG
4	HIS, sucrose, PEG
5	PHOS
6	PHOS, sucrose
7	PHOS, PEG
8	PHOS, sucrose, PEG
9	TRIS
10	TRIS, sucrose
11	TRIS, PEG
12	TRIS, sucrose, PEG
13	50 mM NaSCN
14	150 mM NaSCN
15	300 mM NaSCN
16	600 mM NaSCN
17	0.9% NaCl
18	1.0% ethanol
19	water

Abbreviations: HIS= histidine buffer, PHOS = phosphate buffer, TRIS = TRIS buffer, all 40 mM at pH 7.4.

*2.2.2.2.2. Freeze-drying*

Freeze-drying was performed using an Amsco FINN-AQUA GT4 freeze-dryer (GEA, Koeln, Germany). Eight batches were produced with different cooling methods and secondary drying temperatures (Table 2.4). The cooling methods included: (1) slow cooling at a rate of 0.2°C/min (SL), (2) fast cooling with pre-cooled shelf at -45°C (FA), (3) cooling at 1°C/min and after freezing an annealing step of 10h at -7°C (ANN), (4) cooling at 1°C/min with cooling stop for 60 min at -10°C (CH). Freezing was always performed for 2h at -45°C, primary drying for 20h at -20°C and 100 µbar, and secondary drying for 6h at 100 µbar with temperature ramps of 0.2°C/min in between. The full factorial experimental design led to 96 freeze-dried samples (8 runs x 12 formulations) (Tables 2.3 and 2.4). Seven additional samples (formulations 13-19) were added to runs 1 and 2 to produce more extremely denatured LDH. This resulted in a total of 110 freeze-dried samples that were analyzed with FTIR spectroscopy. Since the amide I bands in the FTIR spectra of some freeze-dried samples could not be interpreted, those were omitted and the data set comprised 99 freeze-dried samples.

**Table 2.4. Design of the freeze-drying runs performed.**

Batch	Freezing method	Secondary drying temperature (°C)	Formulations*
1	SL	40	1-19
2	ANN	40	1-19
3	CH	5	1-12
4	ANN	5	1-12
5	FA	40	1-12
6	FA	5	1-12
7	CH	40	1-12
8	SL	5	1-12

Abbreviations: SL = slow cooling, FA = fast cooling, ANN = annealing, CH = cooling hold

\* See table 1.

*2.2.2.2.3. FTIR spectroscopy*

FTIR spectroscopy functioned as a reference technique to evaluate potential changes in protein secondary structure in the freeze-dried solid. FTIR spectroscopy measurements were conducted on a Varian Scimitar 800 FTIR spectrometer, equipped with a Specac Golden Date diamond ATR module (Varian Scimitar, Middelburg, The Netherlands). The spectra were recorded from 4000 to 500 cm<sup>-1</sup> in ATR mode at a resolution of 2 cm<sup>-1</sup>. Each measurement was the average of 100 scans. The FTIR spectra of the same freeze-dried samples and the corresponding blanks were first background (air) corrected and

converted to absorbance format. The resulting FTIR absorbance spectra were subsequently corrected for the spectral contributions of the blank formulations. Finally, the second derivative with 17-point Savitzky-Golay smoothing was performed and the FTIR spectra were area normalized over the amide I region (1700-1600 cm<sup>-1</sup>) for direct comparison. Individual peak positions were identified and assigned according to the literature.

#### 2.2.2.2.4. Qualitative approach

Using a qualitative approach, one is able to differentiate between groups having certain characteristics. Visual comparison of the experimental versus native spectra is a common approach to assess whether there are observable changes in the distribution of secondary structural elements [12, 27, 29, 31, 38-41]. The area normalized second derivative absorbance amide I FTIR spectra are used for this purpose. A qualitative approach should at least allow to distinguish between samples where the amide I spectrum shows *minimal* (which we defined as native-like or NL state) and *obvious* (which we defined as non-native or denatured (DEN) state) visible changes in the distribution of the secondary structural elements compared to the native state amide I spectrum. Interpretation of the amide I spectra is based on expert knowledge and considers the possible interferences that were above described. Therefore, based on two criteria the native-like class was defined: (1) no apparent changes observed in the distribution of the native secondary structural elements (i.e. in the ratio between  $\alpha$ -helix and  $\beta$ -sheet peaks observed in the native amide I spectrum), and (2) no obvious formation of non-native structures, compared to the native state spectrum. Samples that did not meet these requirements were categorized as non-native (DEN). This classification does not give information on the tertiary or quaternary structures, because FTIR is not an appropriate technique to extract such information.

#### 2.2.2.2.5. Quantitative approach

Using a quantitative approach [30, 35], one aspires obtaining a numerical response related to protein unfolding. It can give information on the amount of protein unfolding, which can be convenient when limits or specifications need to be set. We evaluated the

area of overlap (AO) with the native state (% similarity) as a parameter to quantify protein unfolding in our studied freeze-dried formulations. This parameter does not have the disadvantages of the spectral correlation coefficient and is therefore assumed to be more appropriate [30]. To allow calculating the % similarity between two spectra, a baseline correction, and subsequent area normalization of the blank corrected second derivative (with 17 point Savitzky-Golay smoothing) absorbance amide I spectra are required [30]. Baseline correction was performed by connecting the two most positive points within the second derivative amide I spectrum (Fig. 2.6) [31]. In Fig. 2.6, the area of overlap between two spectra (i.e. the amide I spectra of a freeze-dried formulation versus the native state in solution) is visually represented. Based on this parameter, the NL example spectrum and native state spectrum had 73.4% similarity.

#### *2.2.2.2.6. Principal Component Analysis (PCA)*

PCA is a multivariate descriptive method that reduces the data dimensionality by creating orthogonal latent variables (being linear combinations of the original variables), called principal components (PC's). The PC's are defined in such a way that they explain most the (remaining) variability in the data and are orthogonal to each other. By means of singular value decomposition the matrix is decomposed into loadings and scores. The loading vector gives qualitative information about the samples by describing what type of information characterizes them, i.e. which variables are important. The associated weighted averages of the original variables are the scores, providing quantitative information, i.e. the amount of each loading vector in each sample [14, 17]. The goal is to capture the systematic variations in the data set by the first  $n$  PC's, while excluding the random variations (i.e. noise), described by the higher PC's. Before PCA the blank corrected area normalized second derivative amide I spectra were mean centered.

#### 2.2.2.3. Results and discussion

LDH was used as a model protein. According to X-ray analysis, LDH consists theoretically of 56.81%  $\alpha$ -helix, 25.32%  $\beta$ -sheet and 2.92% intermolecular  $\beta$ -sheet [20]. This  $\alpha/\beta$  ratio was also approximately observed in the native [37] and native-like amide I FTIR spectra (Fig. 2.7).



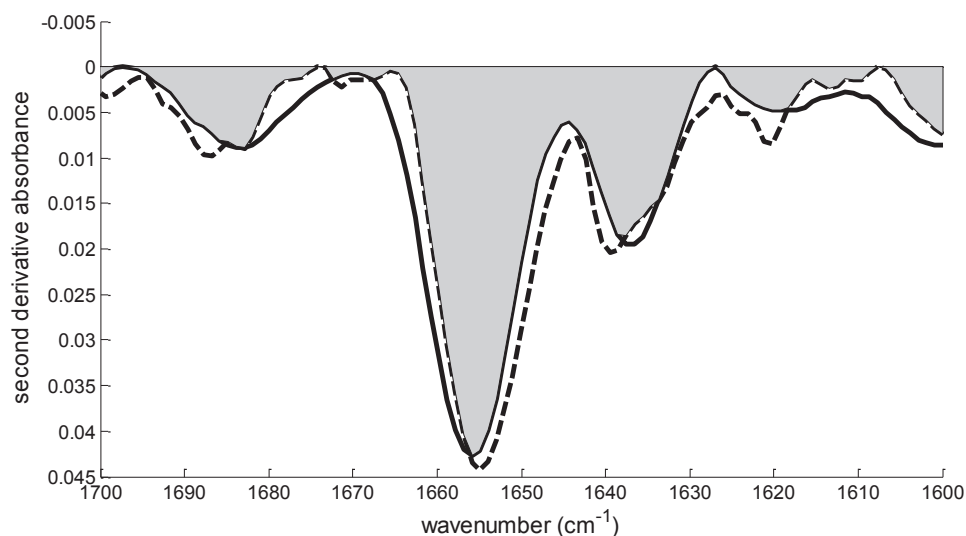


**Fig. 2.7. Baseline corrected and area normalized second derivative amide I spectra of native LDH in solution (dashed line) and NL freeze-dried LDH (full line). The area of overlap is indicated in grey and corresponds to 73.4% similarity.**

Fig. 2.8 compares both quantitative (AO method) and qualitative (visual inspection) approaches on the same data set of 99 spectra. The results of the AO method are visible on the y axis (i.e. % similarity with the native state), while the color pattern indicates the classification result obtained by the visual inspection of the spectra. The average NL spectrum has a % similarity of 66.1% with the native state in solution. Not unexpected, the % similarities of the DEN samples were generally lower than those of the NL samples (49.9% on average). However, for some samples there was a discrepancy between the qualitative and quantitative approaches.

The reason for this inconsistency may be that the AO parameter (and also other reported quantitative parameters) does not allow making a distinction between the origin of the spectral changes. Any spectral change will contribute in the same way to the reduced % similarity between two spectra, as these quantitative methods make the assumption that all spectral changes in the amide I band arise from changes in secondary structural element distribution. As explained in section 2.3.1, this will not be the case.

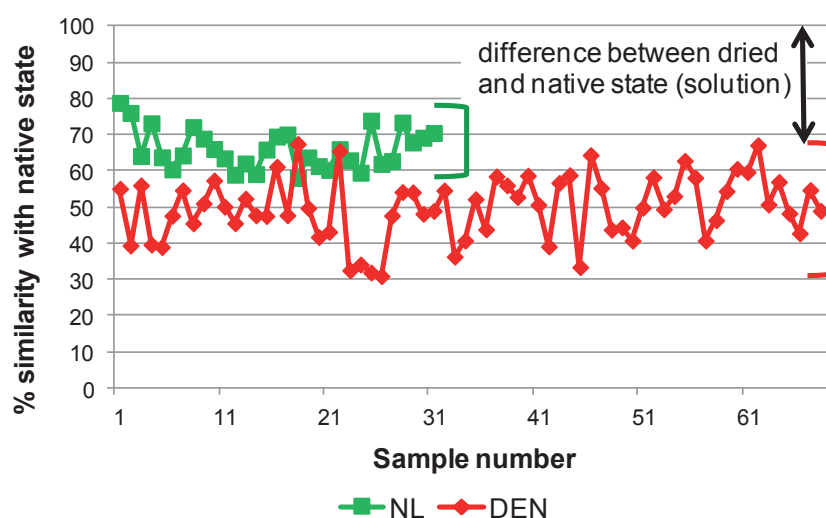


**Fig. 2.8.** % similarities with the native state for different NL and DEN freeze-dried LDH samples in different formulations and using different freeze-drying conditions (having different environmental conditions). The black arrow shows the % similarity reduction due to the difference between the dried and native state in solution. The green and red brackets show the within NL and DEN group range in % similarity, respectively.

Van de Weert et al. [24] observed the same when determining the % similarities (AO method) of the baseline corrected and area normalized amide I spectra of a protein formulation in different physical states (e.g. solution versus freeze-dried, and freeze-dried supplied versus freeze-dried). Although no true changes in secondary structural element distribution could be detected in the dried state, the % similarities were strongly reduced because of environmental effects. One large contributor to the reduction of the % similarity was considered to be the changes in hydrogen bonding characteristics [24]. In our samples, the hydration status of the protein in the native state in solution and in the freeze-dried states are also strongly different, which may cause large changes in % similarities between them (Fig. 2.8), even when there are minimal secondary structural changes (Fig. 2.7).

Among the % similarities of the amide I spectra of NL samples there was also a certain variability, i.e. the coefficient of variation (VC) was 8.3%. This may be the result of physical changes due to differences in the formulations and freeze-drying conditions. For instance, different residual moisture contents and the presence or absence of lyoprotectants may affect the hydration status of the protein. Another cause for the variations in % similarities within the NL group is the various physical conditions (i.e.

amorphous versus crystalline ratio...) of the samples, also affecting the spectral background, each in their own way. As the area of overlap method needs a manual baseline correction (and the performance of the method strongly relies on the correctness of this step [24, 42]) an operator-induced bias during this step is more prone when various freeze-dried samples (with different physical characteristics) have to be analyzed. The VC of the DEN samples was 17.5%. The reason for this is possibly that the amide I spectra of these samples are influenced by the same environmental variability as dried NL samples, plus the variability due to the changes in the protein secondary structure.

Thus, the AO method has a reduced selectivity for detecting solely the changes related to the secondary structural element distribution (the ones we are interested in) in the presence of varying environmental conditions (e.g. hydration status, physical state) in the studied freeze-dried formulations. Whereas this may not be problematic when comparing two protein samples in the aqueous solution state [42-44], this bias becomes more pronounced when comparing samples in different physical states (where the measured signal has significant contributions from other sources) (Fig. 2.7) [24]. The quantitative method was therefore considered inappropriate for analyzing the more complex dried samples in this study.

Whereas the qualitative approach is more selective, possible disadvantages are the lower sensitivity to detect subtle spectral changes and the possible subjectivity associated with band assignments [27]. In some cases, the amide I band may show very obvious signs of changes in secondary structural element distribution, whereas in other cases (i.e. with reduced signs of protein unfolding) it may be more difficult to assign a NL or DEN class label to a sample. When there are samples with different conformational states, a principal component analysis (PCA) can be helpful to minimize the risk to introduce a subjective bias in the class labelling. A PCA was performed on the visually labeled amide I spectra of the complete sample set and should independently confirm the correctness of the class labeling. As variations in the protein conformation of these samples (and thus also in the conformation sensitive amide I FTIR spectra) of the data set exist, they must be present as a type of systematic variation, represented by some of

the first principal components (PC's). Hence, the scores of the NL and the DEN samples should be separated, as is the case in the PC1-PC2 scores plot shown in Fig. 2.9. This separation is the result of the systematic variation originating from the different conformational states (over a varying range) of the proteins in the data set. As both NL and DEN samples are expected to have similar other spectral variations (e.g. due to changes in environmental and physical conditions, such as hydration state and physical state of the sample), these will not cluster the NL and DEN labelled samples into separate groups. The scores of some samples with small signs of protein unfolding were very close to the NL group, which can be interpreted by the fact that there was a continuum of states (from NL to various types and amounts of partially unfolded states) in this case study.

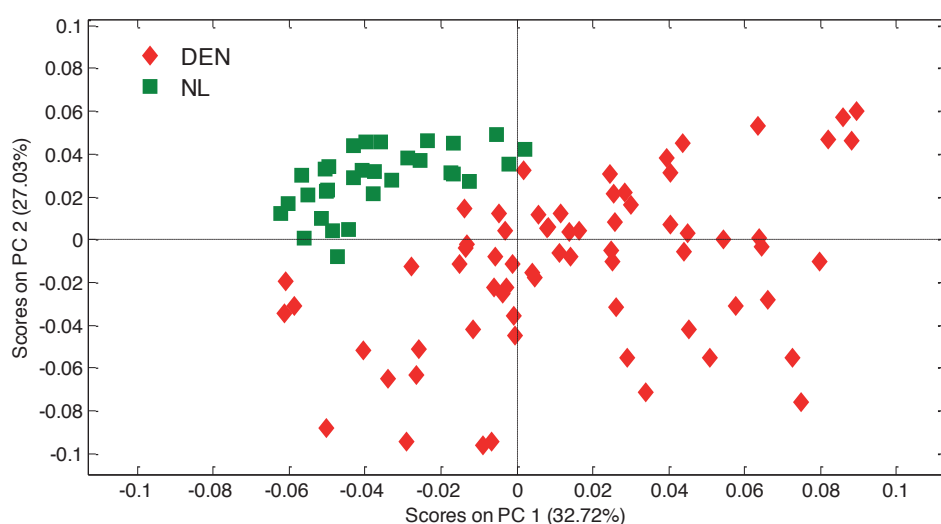


**Fig. 2.9. PCA score plot (PC1-PC2) of the second derivative amide I FTIR spectra of a data set of freeze-dried LDH formulations. The spectra are independently labeled based on the visual interpretation of the amide I band (FTIR) as either NL (in open squares) or DEN (in filled triangles).**

#### 2.2.2.4. Conclusion

Considering the pro's and con's of both qualitative and quantitative approaches for determining protein unfolding in freeze-dried samples (summarized in Table 2.5), the qualitative one was preferred in this work, where dried samples with different conformational states and physical differences need to be analyzed. A direct implication is that we continue working with class memberships. Based on visual expert knowledge, a distinction can be made between variations in the amide I spectra due to secondary

structural element distribution changes and environmental changes. PCA can reduce the subjectivity of this approach and is therefore recommended in a data set with a range of protein conformational states (i.e. with different secondary structural element distribution) and environmental variations. A quantitative approach, i.e. % similarity calculation between two spectra, never takes into account the origin of the changes. Any change, whether it is relevant or not, contributes equally to the decrease in % similarity. The quantitative method (or a variant to quantify protein unfolding based on spectral similarity) is very popular in the literature. However, the samples are mostly analyzed in solution (not having the problem of different hydration states and physical differences) [22, 42-43], or in case of freeze-dried samples, only one formulation is compared (e.g. before and after the process) to demonstrate that the protein is denatured (i.e. a decrease in % similarity is a priori expected) [31, 34, 45].

**Table 2.5. Summary of the characteristics of the studied qualitative and quantitative approaches to determine protein unfolding.**

	<b>Qualitative approach</b>	<b>Quantitative approach</b>
Requirements	Blank corrected area normalized second derivative absorbance spectra	Blank and baseline corrected area normalized second derivative absorbance spectra
Assumptions	Relies on expert knowledge to define the origin of the spectral changes	Assumes that changes in the amide I spectra are always due to changes in secondary structure elements (which is not always true); Relies on a perfect baseline correction
Constraints	The output is a class membership	Any spectral change (regardless its origin) contributes the same to the reduction in % similarity
Advantages	Changes in secondary structures can be more selective determined apart from environmental changes	The output is a numerical response (may provide information on the amount of protein unfolding)
Limitations	Sensitivity? (How sensitive is the eye to detect spectral changes); Subjectivity? (PCA can help to reduce it)	Works fine for comparison of samples in aqueous solutions, but selectivity problems arise when there are also a lot of spectral differences due to environmental effects

### 2.2.3. Further assessment of protein unfolding

After determining the conformational state of the proteins in the freeze-dried product, an assessment of the protein conformational state in the reconstituted product will remain necessary. The latter may indicate whether the native state is regained in the reconstituted product, and thus determines the potential risk for obtaining an

unacceptable product. This risk for irreversible unfolding will be protein specific. One way to assess this is by measuring the biological activity of the protein, describing the ability of the drug substance to achieve a predefined biological effect. This can only be achieved when the protein is in its native conformation. Another way is by assessing the amide I FTIR spectra of the reconstituted product. The amide I spectrum of the native state in the reconstituted product are highly similar to the one of the solution before freeze-drying, as both proteins in solution are fully hydrated, and have no differences in physical state. If possible, it is recommended to use different techniques that determine the conformational state of the reconstituted protein and possible aggregate formation (in the solution more techniques can be used than in the solid state).

### 2.3. References

- [1] J. Rantanen, Process analytical applications of Raman spectroscopy, *J. Pharm. Pharmacol.* 59 (2007) 171-177.
- [2] T. De Beer, A. Burggraef, M. Fonteyne, L. Saerens, J.P. Remon, C. Vervaet, Near infrared and Raman spectroscopy for the in-process monitoring of pharmaceutical production processes, *Int. J. Pharm.* 417 (2011) 32-47.
- [3] A. Kauppinen, M. Toiviainen, O. Korhonen, J. Aaltonen, K. Jarvinen, J. Paaso, M. Juuti, J. Ketolainen, In-line multipoint near-infrared spectroscopy for moisture content quantification during freeze-drying, *Anal. Chem.* 85 (2013) 2377-2384.
- [4] B.H. Stuart, *Infrared spectroscopy: fundamentals and applications*, John Wiley & Sons, Chichester, United Kingdom, 2004, pp. 244.
- [5] R.L. McCreery, *Raman spectroscopy for chemical analysis*, J.D. Winefordner (Ed.), volume 157, John Wiley & Sons, New York, United States, 2000, pp 420.
- [6] M.J. Pikal, S. Shah, Intravial distribution of moisture during the secondary drying stage of freeze drying, *PDA J. Pharm. Sci. Technol.* 51 (1997) 17-24.
- [7] L. Sukowski, PhD thesis: NIR based process analytical technology: In-line residual moisture determination for a complete batch inspection of lyophilized end-products, University of Basel, 2003.
- [8] Z. Wen, X. Cao, J. Philips, Application of Raman spectroscopy in biopharmaceutical manufacturing, *American Pharmaceutical Review*, May issue, 2010.
- [9] R.L. McCreery, A.J. Horn, J. Spencer, E. Jefferson, Noninvasive identification of materials inside USP vials with Raman spectroscopy and Raman spectral library, *J. Pharm. Sci.* 87 (1998) 1-8.
- [10] R. Alexander, Advantages of Raman spectroscopy when analyzing materials through glass or polymer containers and in aqueous solution, Application note Raman spectroscopy, Perkin Elmer.

[www.perkinelmer.com/Content/ApplicationNotes/APP\\_RamanAnalysisThroughGlassPolymerAqueous.pdf](http://www.perkinelmer.com/Content/ApplicationNotes/APP_RamanAnalysisThroughGlassPolymerAqueous.pdf) (accessed on 22/05/2013).

- [11] P. Garidel, H. Schott, Fourier-transform midinfrared spectroscopy for analysis and screening of liquid protein formulations, part 2: Detailed analysis and applications, *Bioprocess international*, June 2006, 48-55.
- [12] A. Barth, C. Zscherp, What vibrations tell us about proteins, *Quart. Rev. Biophys.* 35 (2002) 369-430.
- [13] D.M. Byler, H. Susi, Examination of the secondary structure of proteins by deconvolved FTIR spectra, *Biopolymers* 25 (1986) 469-487.
- [14] W.K. Surewicz, H.H. Mantsch, New insight into protein secondary structure from resolution-enhanced infrared spectra, *Biochim. Biophys. Acta*, 952 (1988) 115-130.
- [15] J.T. Pelton, L.R. McLean, Spectroscopic methods for analysis of protein secondary structure, *Anal. Biochem.* 277 (2000) 167-176.
- [16] A. Dong, B. Kendrick, L. Kreilgard, J. Matsuura, M. Manning, J.F. Carpenter, Spectroscopic study of secondary structure and thermal denaturation of recombinant human factor XIII in aqueous solution, *Arch. Biochem. Biophys.* 347 (1997) 213-220.
- [17] S.D. Allison, T.W. Randolph, M.C. Manning, K. Middleton, A. Davis, J.F. Carpenter, Effects of drying methods and additives on structure and function of actin: mechanisms of dehydration-induced damage and its inhibition, *Arch. Biochem. Biophys.* 358 (1998) 171-181.
- [18] S.T.R. Walsh, R.P. Cheng, W.W. Wright, D.O.V. Alonso, V. Daggett, J.M. Vanerkooi, W.F. DeGrado, The hydration of amides in helices; a comprehensive picture from molecular dynamics, IR, and NMR, *Protein Science* 12 (2003) 520-531.
- [19] J.E. Matsuura, A.E. Morris, R.R. Ketchem, E.H. Braswell, R. Klinke, W.R. Gombotz, R.L. Remmele, Biophysical characterization of a soluble CD40 ligand (CD 154) coiled-coil trimer: Evidence of a reversible acid-denatured molten globule, *Arch. Biochem. Biophys.* 392 (2001) 208-218.
- [20] S. Vonhoff, J. Condliffe, H. Schiffter, Implementation of an FTIR calibration curve for fast and objective determination of changes in protein secondary structure during formulation development, *J. Pharm. Biomed. Anal.* 51 (2010) 39-45.
- [21] J.A. Hering, P.R. Innocent, P.I. Haris, Automatic amide I frequency selection for rapid quantification of protein secondary structure from Fourier transform infrared spectra of proteins, *Proteomics* 2 (2002) 829-849.
- [22] E.H. Moller, M. Fano, M. van de Weert, S. Frokjaer, Comparability of protein pharmaceuticals and the suitability of methods for secondary structure analysis, *Pharmaceutical Technology Europe*, July 2006, 38-42.
- [23] J.F. Carpenter, S.J. Prestrelski, A. Dong, Application of infrared spectroscopy to development of stable lyophilized protein formulations, *Eur. J. Pharm. Biopharm.* 45 (1998) 231-238.
- [24] M. van de Weert, P.I. Haris, W.E. Hennink, D.J.A. Crommelin, Fourier transform infrared spectroscopic analysis of protein conformation: effect of sampling method and stress factors, *Anal. Biochem.* 297 (2001) 160-169.



- [25] S.E. Reid, D.J. Moffatt, J.E. Baenziger, The selective enhancement and subsequent subtraction of atmospheric water vapour contributions from Fourier transform infrared spectra of proteins, *Spectrochim. Acta A* 52 (1996) 1347-1356.
- [26] A. Dong, P. Huang, W.S. Caughey, Protein secondary structures in water from second-derivative amide I infrared spectra, *Biochemistry* 29 (1990) 3303-3308.
- [27] R. Tantipolphan, T. Rades, N.J. Medlicott, Insights into the structure of protein by vibrational spectroscopy, *Curr. Pharm. Anal.* 4 (2008) 53-68.
- [28] S.Y. Venyaminov, N.N. Kalnin, Quantitative IR spectrophotometry of peptide compounds in water (H<sub>2</sub>O) solutions: I- Spectral parameters of amino acid residue absorption bands, *Biopolymers* 30 (1990) 1243-1257.
- [29] J. Kong, S. Yu, Fourier transform infrared spectroscopic analysis of protein secondary structures, *Acta Biochim. Biophys. Sinica*, 39 (2007) 549-559.
- [30] B.S. Kendrick, A. Dong, S.D. Allison, M.C. Manning, J.F. Carpenter, Quantitation of the area of overlap between second derivative amide I infrared spectra to determine the structural similarity of a protein in different states, *J. Pharm. Sci.* 85 (1996) 155-158.
- [31] A. Dong, S.J. Prestrelski, S.D. Allison, J.F. Carpenter, Infrared spectroscopic studies of lyophilization- and temperature-induced protein aggregation, *J. Pharm. Sci.* 84 (1995) 415-424.
- [32] C.L. McFearn, J. Sankaranarayanan, A. Almutairi, Application of fiber-optic attenuated total reflection-FT-IR-methods for in-situ characterization of protein delivery systems in real-time, *Anal. Chem.* 83 (2011) 3943-3949.
- [33] R.L. Remmele Jr., C. Stushnoff, J.F. Carpenter, Real-time in situ monitoring of lysozyme during lyophilization using infrared spectroscopy: dehydration stress in the presence of sucrose, *Pharm. Res.* 14 (1997) 1548-1555.
- [34] J.J. Schwegman, J.F. Carpenter, S.L. Nail, Infrared microscopy for in situ measurement of protein secondary structure during freezing and freeze-drying, *J. Pharm. Sci.* 96 (2007) 179-195.
- [35] S.J. Prestrelski, N. Tedeschi, T. Arakawa, J.F. Carpenter, Dehydration-induced conformational transitions in proteins and their inhibition by stabilizers, Rational design of stable lyophilized protein formulations: some practical advice, *Biophys. J.* 65 (1993) 661-671.
- [36] Z.Q. Wen, Raman spectroscopy of protein pharmaceuticals, *J. Pharm. Sci.* 96 (2007) 2861-2878.
- [37] A. Al-Hussein, H. Gieseler, Investigation of histidine stabilizing effects on LDH during freeze-drying, *J. Pharm. Sci.* 102 (2013) 813-826.
- [38] J.T. Pelton, L.R. McLean, Spectroscopic methods for analysis of protein secondary structure, *Analytical Biochemistry* 277 (2000) 167-176.
- [39] P.I. Haris, F. Severcan, FTIR spectroscopic characterization of protein structure in aqueous and non-aqueous media, *J. Mol. Catal. B: Enzymatic* 7 (1999) 207-221.
- [40] K. Izutsu, N. Aoyagi, S. Kojima, Protection of protein secondary structure by saccharides of different molecular weights during freeze-drying, *Chem. Pharm. Bull.* 52 (2004) 199-203.
- [41] M. Jackson, H.H. Mantsch, The use and misuse of FTIR spectroscopy in the determination of protein structure, *Critical Reviews in Biochemistry and Molecular Biology* 30 (1995) 95-120.



- [42] J. D'Antonio, B.M. Murphy, M.C. Manning, W.A. Al-Azzam, Comparability of protein therapeutics: Quantitative comparison of second-derivative amide I infrared spectra, *J. Pharm. Sci.* 101 (2012) 2025-2033.
- [43] B.M. Teska, C. Li, B.C. Winn, K.K. Arthur, Y. Jiang, J.P. Gabrielson, Comparison of quantitative spectral similarity analysis methods for protein higher-order structure confirmation, *Analytical Biochemistry* 434 (2013) 153-165.
- [44] Y. Jiang, C. Li, X. Nguyen, S. Muzammil, E. Towers, J. Gabrielson, L. Nahri, Qualification of FTIR spectroscopic method for protein secondary structural analysis, *J. Pharm. Sci.* 100 (2011) 4631-4641.
- [45] T.H. Lee, W.T. Cheng, S.Y. Lin, Thermal stability and conformational structure of salmon calcitonin in the solid and liquid states, *Biopolymers* 93 (2009) 200-207.



---

## Chapter 3: NEAR-INFRARED SPECTROSCOPY FOR IN-LINE MEASURING PROTEIN UNFOLDING DURING FREEZE-DRYING

---

### 3.1. NIR spectroscopy for detecting protein unfolding

Although fundamental infrared vibrations can provide much molecular information, their combination and overtone modes in the NIR region are less intense and broader. However, unlike MIR, NIR enables the non-invasive and non-destructive measurements, necessary for potential in-line use during the freeze-drying process.

There has been controversy whether the NIR region has (enough) sensitivity for probing secondary structural changes in proteins. Researchers have been seeking for specific NIR marker bands for the secondary structure of proteins, similar to the amide I and II bands in FTIR spectroscopy and the amide I and amide III band in Raman spectroscopy [1-3]. But so far, no real marker band for the secondary structure of proteins has been established. Different frequency regions that could be correlated to  $\alpha$ -helix (i.e. 4090, 4365-4370, 4615 and 5755  $\text{cm}^{-1}$ ) and  $\beta$ -sheets (i.e. 4060, 4405, 4525-4540, 4865, 5915-5925  $\text{cm}^{-1}$ ) were pointed out [4], but a distinguishable absorption signal for intermolecular beta-sheets, loops, turns and unordered structures could not be determined [4-5]. Another study concludes that the NIR region is not suitable for determining secondary structures in proteins [2]. Obviously, the relationship of the shape and position of the combination absorption bands (usually the NIR second derivative spectrum is taken) with secondary structure is rather obscure and complex [6]. Besides, the NIR spectra are also influenced by water signals, physical sample characteristics and the hydration status of the protein [5]. When correlating (via PLSR2) NIR spectra from various proteins with different relative amounts of secondary structures obtained from the literature (X-ray determination) or with amide I spectra, it was concluded that NIR spectra were not very suitable for detecting and characterizing changes in protein secondary structures [5]. However, Bai et al. [3] found a high correlation ( $R^2 = 0.982$ ) when building PLSR1 models, for two model proteins, between their NIR spectra and the intensities of the main peak (i.e. the peak constituting the largest fraction of a secondary structural element type for a certain protein) in the

second derivative amide I spectra. This study did not provide a proof that chance correlation was excluded.

Most studies agreed that combination bands of protein fundamental vibrations, such as the amide A/II (near  $4860\text{ cm}^{-1}$ ) and amide B/II (near  $4600\text{ cm}^{-1}$ ) band, were sensitive to changes in the hydrogen bonding strength of the protein backbone [2, 5, 7-12]. They were generally manifested as frequency shifts of these bands. These shifts were interpreted as being related to protein unfolding (i.e. loosening of the intra-molecular hydrogen bonds formed by the protein backbone), but also to changes in the protein hydration status (i.e. hydrogen bonds formed by the protein backbone with environmental molecules, such as water and sucrose) (Fig. 3.1).

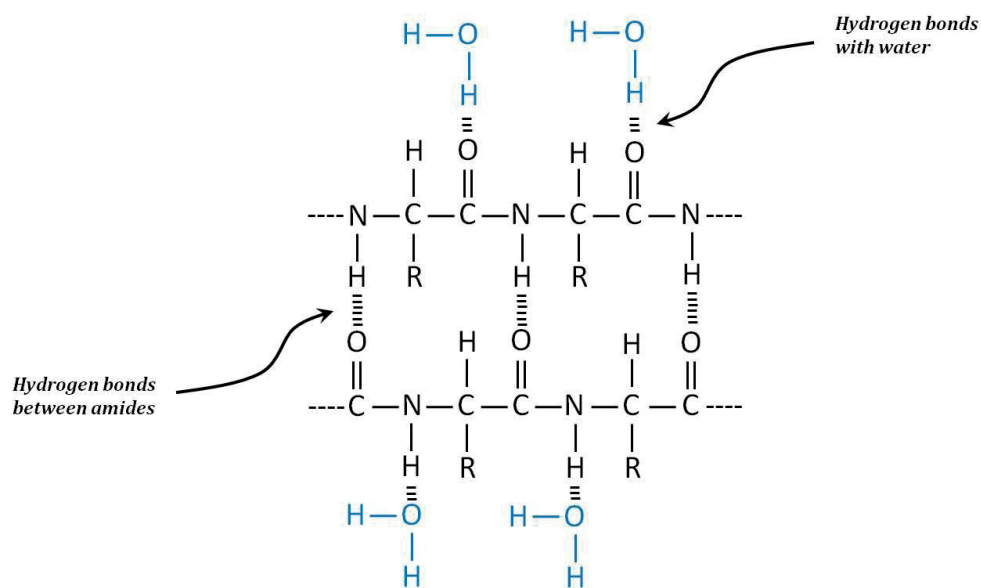


**Fig. 3.1.** The amide A/II frequency is influenced by two types of hydrogen bonds formed by the protein backbone, i.e. (A) those with other amide groups of the protein backbone constituting the folded protein structure (i.e. intra-molecular), and (B) those with surrounding molecules (e.g. water, lyoprotectants).

Therefore, the amide A/II combination band, arising from the amide A and the amide II protein backbone vibrations, has been proposed as a potential marker band for studying the relative strength of the hydrogen bonds of the protein backbone vibrations [2]. References [2] and [10] showed the dependence of the peak position of this band on the extent of the hydrogen bonding by the amide groups making up the folded protein

structure. Liu et al. [2] showed the frequency of amide A/II changes little with the secondary structure of proteins (various proteins with dissimilar secondary structure had amide A/II bands all near  $4860\text{ cm}^{-1}$ ) but upon thermal denaturation the amide A/II band shifted significantly upwards. When a protein molecule unfolds there is a general weakening of the intra-molecular hydrogen bonding strength, because it loses its cooperatively folded structure [13], which may be reflected by an increasing amide A/II band position [2]. On the other hand, when water or stabilizers interact with the protein's backbone by hydrogen bonding, the increased extent of hydrogen bonding induces a relative decrease in amide A/II frequency [10].

The above literature study indicates that NIR spectra may be less suitable for the determination of changes in the secondary structure of proteins. Preliminary experiments using PCA also confirmed that the NIR spectra could not be seen as a multivariate data source to distinguish between freeze-dried formulations with and without changes in the protein secondary structures (data not shown). Conversely, the high sensitivity of the amide A/II combination band frequency to hydrogen bonding might potentially be interesting to probe the relative expansion of the backbone hydrogen bond network when a protein unfolds. Besides this, it should be considered that the amide A/II frequency is also influenced by protein hydration or hydrogen bond interaction with other molecules (e.g. lyoprotectants) (Fig. 3.1).

### **3.2. NIR spectroscopy for in-line measuring water loss**

As freeze-drying is essentially a drying process, its primary goal is to remove most of the water from the surroundings of the protein molecules. During the last phase, i.e. the secondary drying, hydrate water will be removed from the protein by desorption. However, protein dehydration will influence the frequency of the amide A/II band (Fig. 3.1), regardless the process leads to protein unfolding or not. To separate both effects, an independent estimate of the loss of water during protein dehydration in the same sample spot illuminated by the NIR light is necessary. This was possible by monitoring the residual water content during secondary drying.

NIR spectroscopy is a popular means for the determination of the residual water content in various dried samples or during drying processes [14-15]. The band near  $5150\text{ cm}^{-1}$  results from a combination of asymmetric stretch and bend of the water molecule, and is the most prominent one among the numerous other water absorptions in the NIR spectrum. In some studies, NIR spectroscopy has been proposed to replace the time consuming Karl-Fisher titration or gravimetric methods for freeze-dried (protein) samples, by developing off-line MVC models [16-17]. However, supervised in-line MVC models require samples containing the full range of possible water and all other spectral variations in their calibration and validation set. Hence, regular sample extractions (e.g. via a sample thief) during the process would be required to develop and validate the MVC model [18]. Since we did not have a sample thief, we were not able to develop a supervised monitoring method. Unsupervised in-line monitoring methods are, from a practical point of view, easier to develop since they do not have these sampling issues. Methods monitoring the apparent absorbance of water (AWA), i.e. the intensity of the main peak near  $5160\text{ cm}^{-1}$  [19], the area of the same peak [20], or the normalized PC1 score value (PCA) [21] have been proposed. When applying the AWA [19] and PCA [21] methods on the same normalized process NIR spectra, a similar trend was noticed (Fig. 3.2). Only the absolute measured values, which were not of interest, were different.

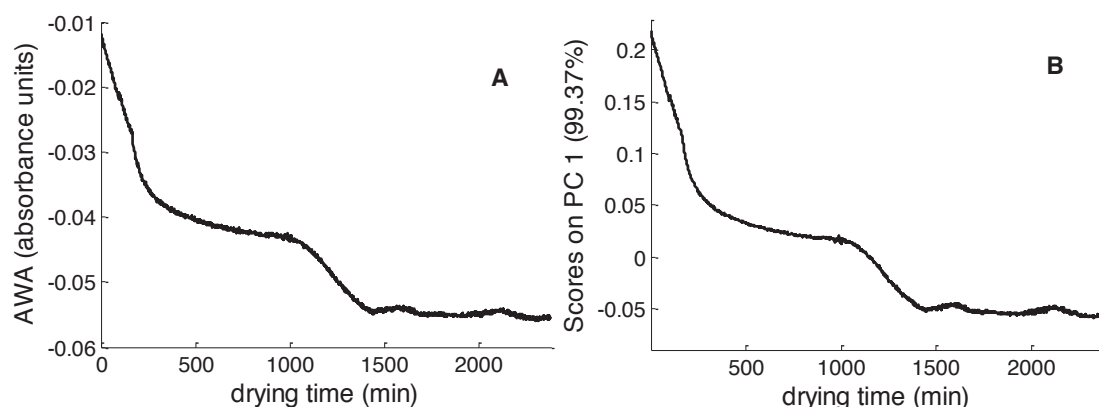


**Fig. 3.2. Application of the AWA (A) and PCA (B) methods on the same normalized process spectra obtained during secondary drying.**

### **3.3. Defining a process trajectory for in-line monitoring protein unfolding versus dehydration**

In the following paper (S. Pieters, T. De Beer, JC Kasper, D. Boulpaep, O. Waszkiewicz, M. Goodarzi, C. Tistaert, W. Friess, JP Remon, C. Vervaet, Y. Vander Heyden, Near-infrared spectroscopy for in-line monitoring of protein unfolding and its interactions with lyoprotectants during freeze-drying, *Analytical Chemistry* 84 (2012) 947-955), the feasibility of NIR spectroscopy for the in-line monitoring of protein unfolding during freeze-drying is evaluated.

## Near-Infrared Spectroscopy for In-Line Monitoring of Protein Unfolding and Its Interactions with Lyoprotectants during Freeze-Drying

Sigrid Pieters,<sup>†</sup> Thomas De Beer,<sup>‡</sup> Julia Christina Kasper,<sup>§</sup> Dorien Boulpaep,<sup>†</sup> Oliwia Waszkiewicz,<sup>†</sup> Mohammad Goodarzi,<sup>†</sup> Christophe Tistaert,<sup>†</sup> Wolfgang Friess,<sup>§</sup> Jean-Paul Remon,<sup>||</sup> Chris Vervaet,<sup>||</sup> and Yvan Vander Heyden<sup>\*,†</sup>

<sup>†</sup>Department of Analytical Chemistry and Pharmaceutical Technology, Center for Pharmaceutical Research, Free University of Brussels (VUB), Laarbeeklaan 103, 1090 Brussels, Belgium

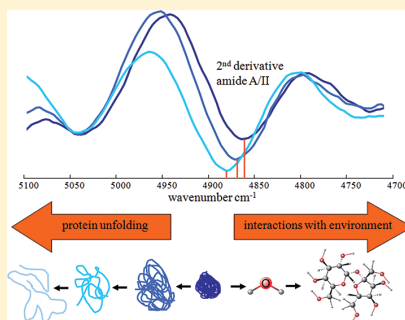
<sup>‡</sup>Laboratory of Pharmaceutical Process Analytical Technology, Ghent University, Harelbekestraat 72, 9000 Ghent, Belgium

<sup>§</sup>Department of Pharmacy, Pharmaceutical Technology and Biopharmaceutics, Ludwig-Maximilians University, Butenandtstrasse 5, 81377 Munich, Germany

<sup>||</sup>Laboratory of Pharmaceutical Technology, Department of Pharmaceutics, Ghent University, Harelbekestraat 72, B-9000 Ghent, Belgium

### Supporting Information

**ABSTRACT:** This work presents near-infrared spectroscopy (NIRS) as an in-line process analyzer for monitoring protein unfolding and protein-lyoprotectant hydrogen bond interactions during freeze-drying. By implementing a noncontact NIR probe in the freeze-drying chamber, spectra of formulations containing a model protein immunoglobulin G (IgG) were collected each process minute. When sublimation was completed in the cake region illuminated by the NIR probe, the frequency of the amide A/II band (near 4850 cm<sup>-1</sup>) was monitored as a function of water elimination. These two features were well correlated during protein dehydration in the absence of protein unfolding (desired process course), whereas consistent deviations from this trend to higher amide A/II frequencies were shown to be related to protein unfolding. In formulations with increased sucrose concentrations, the markedly decreased amide A/II frequencies seen immediately after sublimation indicated an increased extent of hydrogen bond interaction between the protein's backbone and surrounding molecules. At the end of drying, there was evidence of nearly complete water substitution for formulations with 1%, 5%, and 10% sucrose. The presented approach shows promising perspectives for early fault detection of protein unfolding and for obtaining mechanistic process information on actions of lyoprotectants.



To allow an acceptable shelf life, many pharmaceutical proteins require the removal of water from their environment. Freeze-drying is a suitable technique for this purpose, but when not having the different freeze-drying steps under control, the folded structure of proteins may be perturbed.<sup>1–5</sup> A direct link has been reported between the amount of unfolding that proteins experience during freeze-drying and the risk to misfolding or aggregation at any later stage, e.g., at the time of reconstitution and administration of the drug product. Since a wrong protein conformation may trigger severe immune responses or may result in reduced therapeutic activity, minimizing protein structural perturbations and maintaining the protein conformation “native-like” during freeze-drying is an important quality attribute.<sup>6,7</sup> Stress-specific stabilization studies have shown to be essential for the freeze-drying process and product development. However, the process itself is still partly a black box and the formulation behavior during freeze-drying is not yet fully understood. To make the

freeze-drying processes more efficient and to enable faster development of therapeutic protein formulations, there is a high need for technologies providing mechanistic information, preferably in real-time and in the process environment, on the protein's conformational stability. Reported attempts used at-line attenuated total reflectance Fourier transform-infrared (ATR-FT-IR) or needed specialized and adapted freeze-dryer equipment resulting in complex setups which do not fully represent the conditions of real-life samples in a production freeze-dryer.<sup>3,4,8,9</sup>

Because of its many beneficial features (e.g., being fast and noninvasive, requiring no sample preparation, supplying chemical and physical information...), near-infrared spectroscopy

**Received:** August 23, 2011

**Accepted:** November 28, 2011

**Published:** November 28, 2011



(NIRS) emerges as a frequently used technique in the pharmaceutical industry.<sup>10–12</sup> In combination with Raman and plasma emission spectroscopy, it proved to be a successful complementary and confirmatory tool for the in-line monitoring of critical process and product information during the freeze-drying of excipient mixtures.<sup>13–15</sup> Its sensitivity toward hydrogen bonding and water makes NIRS an attractive tool for studying (de)hydration and assaying the water content in various samples.<sup>10</sup> In protein structural research, infrared spectroscopy is a common technique where the NIR region has played a modest role. Applying *in situ* FT-IR using fiber-optics is from a practical point of view not evident in a freeze-dryer and its invasive character may disturb the process. Although the relation to protein secondary structure is less obvious in the NIR region and its sensitivity for characterizing the secondary structure in proteins has been questioned,<sup>16,17</sup> the amide A/II frequency (near 4850 cm<sup>-1</sup>) is influenced by the strength of the hydrogen bonds formed by the amide groups of proteins.<sup>16,18</sup> The amide A/II combination band stems from protein backbone vibrations from the amide A and amide II vibrations. Amide A vibrations arise from N–H stretching vibrations, whereas amide II vibrations are mainly due to N–H bending coupled with C–N stretching, with minor contributions of C–C and N–C stretching and C=O in plane bending.<sup>19</sup> Liu et al.<sup>16</sup> observed a significant upward frequency shift of this band upon heat denaturation of pepsin, whereas a lowering of the frequency was observed upon hydrogen bonding between ribonuclease and sucrose.<sup>20</sup>

A folded protein is a highly cooperative structure. Most, if not all, of the polypeptide backbone and side chain hydrogen bonds of the native protein are satisfied, either by H-bonding to other groups of the same protein (forming its folded structure) or to water (stabilizing its folded structure). In (partially) unfolded states, there is less cooperativity and relatively more amide groups will be exposed to the solvent.<sup>21</sup> The native protein conformation is thermodynamically stabilized and its relative stability depends on the difference in Gibbs free energy ( $\Delta G$ ) between the folded and unfolded states. Changes in the microenvironment of the protein, e.g., when the hydration shell surrounding the protein is (partly) removed during drying, may disturb this equilibrium. This can make the system globally unstable ( $\Delta G$  becomes negative), inducing a transition to (partially) unfolded states that will be energetically preferred.<sup>22</sup> How much the protein will be perturbed depends on the protein's intrinsic stability as well as on the formulation and processing conditions.<sup>1,4,6</sup> It is one of the many challenges for formulation scientists to control the protein's stability by selecting the proper process conditions and excipients in their right concentrations.<sup>6</sup>

Stabilizers aim at modifying the microenvironment of the protein to retain its native confirmation.<sup>2,23–27</sup> Currently, some mechanisms of lyoprotection have been proposed and debated, but neither explanation proved completely satisfactory.<sup>2,22,26</sup> It is suggested that during freeze-concentration the stabilizer will be preferentially excluded from the surface of the protein, i.e., the vicinity of the protein will contain a relative higher amount of water molecules and in this way thermodynamically stabilizing the native state of the protein. When water becomes scarcer, as is expected to happen during secondary drying, the water replacement hypothesis supposes that the stabilizer will satisfy the protein's need to hydrogen bond as a response to the water removal from its environment. In contrast to these thermodynamical mechanisms, the “vitrification” theory relies

on a pure kinetical supposition. As it is a prerequisite for unfolding that the protein can sufficiently move, this stabilization mechanism is based upon the molecular dispersion of the protein in a rigid glassy matrix. This effect strongly hampers the protein's mobility. The availability of in-line information on hydrogen bond interactions between the protein and its surrounding molecules (i.e., water and lyoprotectant molecules) during dehydration may increase the understanding of the actions of lyoprotectants.

The aim of this study is to assess whether NIRS may provide relevant in-process information on protein conformational stability and on the influence of lyoprotectants during freeze-drying. In particular, this study addresses two questions. Is NIRS capable of (i) in-line detecting protein unfolding apart from pure environmental effects and (ii) providing mechanistic process knowledge on the protein protection by lyoprotectants, i.e., when during processing and to what extent are there hydrogen bond interactions between the protein's backbone and its surrounding molecules. Immunoglobulin G (IgG) was used as a model protein.

## EXPERIMENTAL SECTION

**Materials.** A humanized IgG antibody was used as a model protein and freeze-dried at high concentrations (~35 mg/mL). IgG bulk solutions at a concentration of about 70 mg/mL (determined by UV spectrophotometry at 280 nm,  $a = 1.44$  mg mL<sup>-1</sup> cm<sup>-1</sup>) were prepared by dialysis in the appropriate buffer and were used for further formulation. Dialysis was performed with a Spectra/Por membrane, MWCO 6–8 000 obtained from Serva (Heidelberg, Germany). Sucrose was purchased from Suedzucker (Mannheim, Germany). Sodium thiocyanate was from Sigma Aldrich (Steinheim, Germany). L-Histidine, sodium citrate, and sodium acetate were from Merck (Darmstadt, Germany) and sodium dihydrogen phosphate from Riedel-de-Haen (Seelze, Germany). Kollidon 30 was obtained from BASF (Ludwigshafen, Germany). We used vials type 2R (type I glass, Fiolax clear, Schott, Müllheim Germany) with corresponding lyophilization stoppers (West, Eschweiler, Germany) as the primary container for all experiments. The filling volume of the vials was 1.5 mL. Reconstitution was performed with the same volumes of water.

**Freeze-Drying.** All freeze-drying experiments were performed in an Amsco FINN-AQUA GT4 freeze-dryer (GEA, Koeln, Germany). The freeze-drying cycle consisted of a freezing phase to –50 at 1 °C/min, followed by a 120 min hold at –50 °C. Primary drying was performed at –20 °C (increase in temperature with 0.2 °C/min) at 100  $\mu$ bar for 1200 min. For secondary drying, three different cycles were used, i.e., hold at 50 °C for at least 1200 min (cycle 1), hold at 20 °C for at least 480 min (cycle 2), and hold at 40 °C for at least 480 min (cycle 3). Cycles 1 and 2 used a temperature ramp of 0.1 °C/min, whereas cycle 3 used one of 0.2 °C/min. Secondary drying was always performed at 100  $\mu$ bar. All freeze-dried cakes had an elegant appearance without signs of collapse.

**Spectroscopic Conditions.** FT-IR spectroscopy, performed on a Tensor 27 Fourier-transform IR spectrometer (Bruker Optics, Ettlingen, Germany) using the Bio-ATR unit, was used to verify whether protein unfolding occurred. It was applied to the samples in solution before freeze-drying, to the solid freeze-dried, and to the reconstituted samples. The spectra were recorded from 4000 to 850 cm<sup>-1</sup> in attenuated total reflectance (ATR) mode at 20 °C. Each measurement was the average of 240 scans. During data acquisition, the optical bench

was purged with dry nitrogen to reduce interference from water vapor IR absorption. For the solid samples about 10 mg and for the liquid samples 30  $\mu$ L were placed into the Bio-ATR unit.

Diffuse reflectance NIR spectra were continuously in-line and noninvasively collected during freeze-drying using a Fourier-transform NIR spectrometer (Thermo Fisher Scientific, Nicolet Antaris II near-IR analyzer) equipped with an InGaAs detector, a quartz halogen lamp, and a fiber-optic noncontact probe. Every process minute a spectrum was acquired, which was collected in the 10 000–4 000  $\text{cm}^{-1}$  region with a resolution of 8  $\text{cm}^{-1}$  and averaged over 32 scans. The NIR noncontact probe was placed into the freeze-dryer chamber next to the monitored vial, as described in ref 13. Hence, measurements were performed from the side at the bottom of the vial. The noninvasive character of the measurements guarantees that neither the process nor the product is influenced by contact of the NIR probe. The detection spot area of the NIR probe was about 28  $\text{mm}^2$ . Hence, the effective sample size “captured” by the NIR probe only consisted of a small part of the cake volume. It was assumed that this part is representative of the whole cake.

**Data Handling.** Data handling was performed using in house-written m-files in Matlab 7.1 (The Mathworks, Natick, MA). Each FT-IR spectrum was background corrected for the appropriate placebo spectrum. The FT-IR and NIR spectra were processed by offset correction, vector normalization, and the second derivative with Savitzky–Golay smoothing. The amide I band (1700–1600  $\text{cm}^{-1}$ ) in the mid-infrared region was used to indicate changes in the secondary structure of the protein. In the NIR region, the frequency corresponding to the minimum of the amide A/II band in the second derivative spectra (near 4850  $\text{cm}^{-1}$ ) was monitored to investigate differences in the hydrogen bonding strength of the protein’s amide groups. An increase in frequency indicated a relative weakening of the hydrogen bonding and vice versa.<sup>16,20</sup> Missing frequency values were predicted by means of spline interpolation between data points.<sup>28</sup> This way, a data spacing of 1  $\text{cm}^{-1}$  was obtained, which allowed a better accuracy. To reduce noise in the time series the frequency values of the  $n$  previous measurements were averaged. For spectra from samples without sucrose,  $n$  was set at 5, while for the more noisy spectra from samples with high sucrose content  $n$  was 10. An apparent water absorbance (AWA) value<sup>29–31</sup> was calculated as the intensity of the band near 5160  $\text{cm}^{-1}$  in the baseline-corrected and normalized NIR spectra. This band, originating from a combination of OH-stretching and HOH bending vibrations, was used as an indicator of the unfrozen water moiety and provided an estimation of the apparent water loss from the measured sample region, i.e., the part of the sample illuminated by the NIR probe, throughout drying.

## RESULTS AND DISCUSSION

**Selection of Model Formulations.** To enable evaluating whether NIRS has potential for in-line detection of protein unfolding, two types of model formulations were used, i.e., those that effectively experience protein unfolding during freeze-drying and those that render native-like freeze-dried IgG. Therefore, different IgG formulations were freeze-dried and checked for protein unfolding before and after freeze-drying, as well as after reconstitution, using FT-IR spectroscopy.

The amide I band of the native IgG in 25 mM histidine buffer pH 6.2 mainly indicated  $\beta$ -sheet structures (bands near 1691 and 1636  $\text{cm}^{-1}$ ) and to a small extent loops and turns

(bands near 1681 and 1663  $\text{cm}^{-1}$ ), which is consistent with the literature.<sup>32</sup> Upon freeze-drying, with or without 10% sucrose, only small changes were seen in the amide I band, indicating that the secondary structure was barely affected (Supporting Information, Figure S-1). The changes were mainly related to a reduced intensity of the bands for loops or turns, which make up only a very small fraction of the IgG structural elements. Loops and turns usually lie on the surfaces of proteins and thus often participate in interactions of proteins with other molecules.<sup>33</sup> It seems plausible that these structures may be easily affected by dehydration of the protein. Besides these minor structural changes, we also observed a decrease in bandwidth as well as a shift to higher frequencies of the main peak near 1636  $\text{cm}^{-1}$ . These changes can be related to the dehydration of the protein.<sup>19,34</sup> Thus, a high level of native protein structure was retained in the dried solid of the studied formulations. The amide I bands of IgG formulated in other buffers (100 mM acetate pH 4.0, 100 mM phosphate pH 7.4, and 100 mM citrate pH 4.0) and freeze-dried using different drying cycles (cycles 1, 2 and 3) also lacked distinct signs of protein unfolding, i.e., no peaks were (dis)appearing in the amide I region (data not shown). In all above-described formulations, the full native protein conformation was recovered upon reconstitution.

When 50, 150, 300, and 600 mM sodium thiocyanate (NaSCN) was added to the formulation, distinct signs of protein unfolding increasing with the NaSCN concentration became visible in the amide I spectrum of the freeze-dried product (Supporting Information, Figure S-2). In the spectrum of the freeze-dried solid products, a broad band appeared near 1670  $\text{cm}^{-1}$ , and in the formulations with 300 and 600 mM NaSCN the absorption band near 1636  $\text{cm}^{-1}$  was significantly decreased. The broad band near 1670  $\text{cm}^{-1}$  can be attributed to an assembly of unordered structures, where none is present in a sufficient amount for obtaining a clear absorption signal.<sup>35</sup> Also, the band broadening indicates loss of structural homogeneity among the protein population.<sup>36</sup> Hence, there are clear signs that protein unfolding has taken place. In the reconstituted formulations containing 300 and 600 mM NaSCN, clear signs of protein misfolding and aggregation (absorption near 1620  $\text{cm}^{-1}$ ) were visible (irreversible protein denaturation). In contrast, IgG in the formulations containing 50 and 150 mM NaSCN refolded back to the native state upon reconstitution (reversible protein denaturation). Since the amide I spectra of the fresh and stored solutions (6 weeks) containing NaSCN indicated native-like IgG, it was ensured that protein unfolding was performed during freeze-drying.

The high stability of the model protein IgG obliged us to apply unusually severe conditions to induce protein unfolding during freeze-drying, but it must be emphasized that this will not be the case for all proteins. The conditions affecting protein conformational stability are very protein, process, and formulation specific. In this study, the above conditions rendered native-like, moderately, and more severely denatured IgG after freeze-drying and consequently served as adequate models to evaluate whether NIRS is able to detect protein unfolding in-line (Table 1).

**In-Line Monitoring Protein Unfolding.** Because ice leads to dominating signals in the NIR spectra, overwhelming the signals of our interest, monitoring was only feasible after completion of sublimation at the part of the sample illuminated by the NIR probe (Figure 1). Monitoring became possible early in the drying phase, i.e., after 50–100 min of primary drying, as

## Chapter 3: NEAR-INFRARED SPECTROSCOPY FOR IN-LINE MEASURING PROTEIN UNFOLDING DURING FREEZE-DRYING

Analytical Chemistry

Article

**Table 1.** Experimental Conditions Used for the Evaluation of NIRS for In-Line Monitoring Protein Unfolding during Freeze-Drying

experiment	formulation	process	conformational state of the freeze-dried product <sup>a</sup>	refolds to native state upon reconstitution? <sup>a</sup>
A	25 mM histidine pH 6.2	cycle 1	native-like	yes
B	25 mM histidine pH 6.2	cycle 2	native-like	yes
C	100 mM acetate pH 4.0	cycle 1	native-like	yes
D	100 mM acetate pH 4.0	cycle 2	native-like	yes
E	100 mM acetate pH 4.0	cycle 3	native-like	yes
F	25 mM histidine pH 6.2 + 50 mM NaSCN	cycle 2	moderately denaturated	yes
G	25 mM histidine pH 6.2 + 150 mM NaSCN	cycle 2	moderately denaturated	yes
H	25 mM histidine pH 6.2 + 300 mM NaSCN	cycle 2	strongly denaturated	no
I	25 mM histidine pH 6.2 + 600 mM NaSCN	cycle 2	strongly denaturated	no
J	100 mM acetate pH 4.0 + 600 mM NaSCN	cycle 1	strongly denaturated	no

<sup>a</sup>Evaluated via amide I band of the end product (FT-IR).

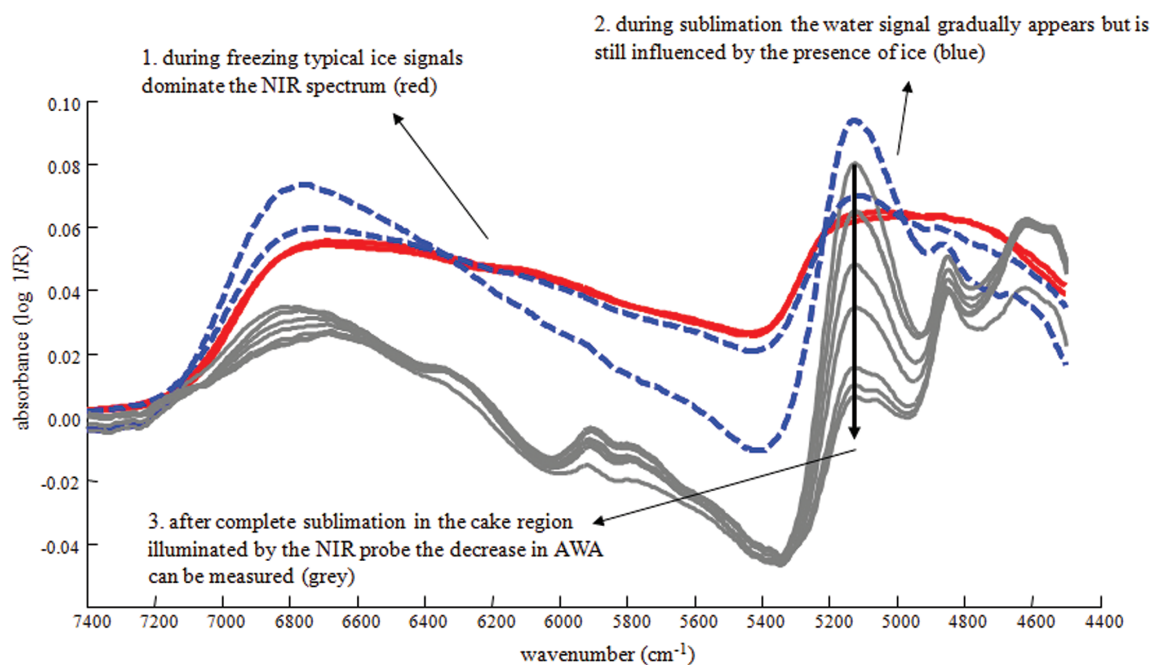


**Figure 1.** Representative baseline-corrected and normalized NIR spectra at the different stages during freeze-drying, i.e., freezing, sublimation and drying.

useful signals for the amide A/II band and water band were obtained then. This is because the ice typically sublimates first at the product–glass vial interface, where the NIR probe illuminates the sample.

Although NIR spectra are rich of physicochemical information,<sup>12–14,37</sup> process trajectories defined from principal component scores appeared not useful to discriminate between native-like and unfolded proteins during freeze-drying (data not shown). As the main information for protein unfolding lies in the shift of the amide A/II band,<sup>16</sup> which is also influenced by protein dehydration (see further), two “real” variables (i.e., the amide A/II frequency and the moisture content, here estimated by the AWA) were selected as the most relevant ones for the present problem.

It is important to know whether the amide A/II frequencies are influenced by other disturbing process and environmental effects, such as varying product temperatures. Also, protein

unfolding should be distinguished from protein dehydration. Dehydration involves a loss of hydrogen bonding between protein molecules and water and is an environmental effect inherent to any (freeze-) drying process, whereas intramolecular hydrogen bonds will lose strength when a protein unfolds and should be avoided.

As the shelf temperature was increased considerably during secondary drying (see Freeze-Drying), the effect of increasing the shelf temperature on the measured amide A/II frequency was studied. This is because an increasing shelf temperature will also increase the temperature of the product at the cake parts where sublimation has been completed. Already freeze-dried cakes with native-like IgG (with and without 10% sucrose) and with low residual water contents (from cycle 1) were placed in the freeze-drier and monitored during a shelf temperature increase from  $-20$  to  $50$  °C without vacuum. The unchanged AWA during these experiments confirmed no significant water

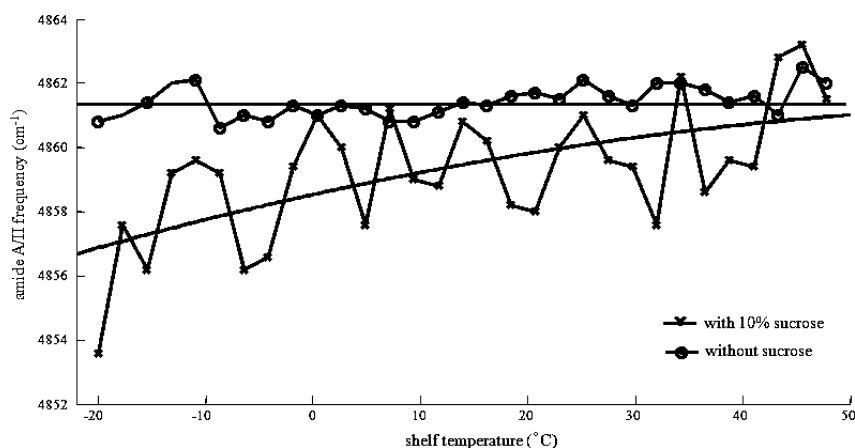


**Figure 2.** Effect of the shelf temperature increase from  $-20$  to  $50$  °C on the amide A/II frequency for freeze-dried IgG formulations in 100 mM acetate pH 4.0 with and without 10% sucrose. The respective trends for each formulation are indicated with the full black lines.

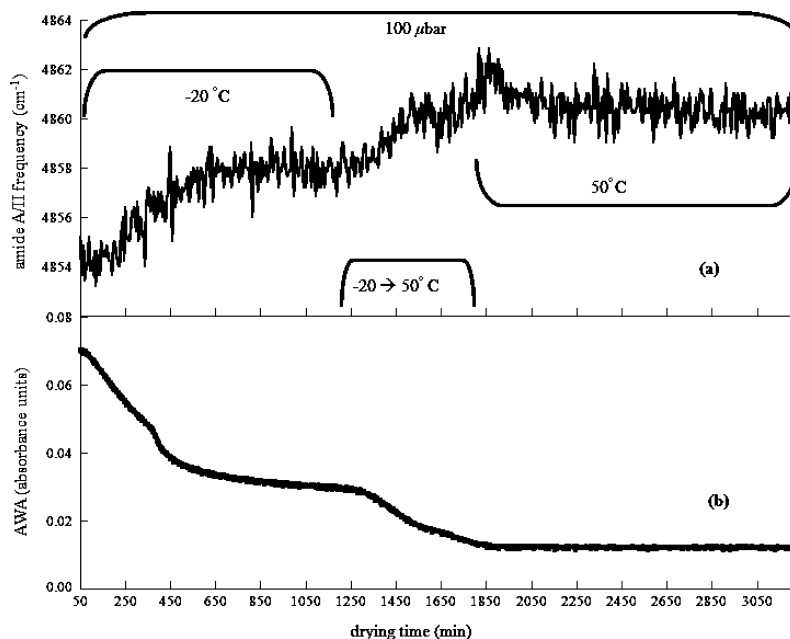


**Figure 3.** Effect of dehydration on the amide A/II frequency (a) and AWA (b) during drying of IgG in 100 mM acetate buffer pH 4.0 (cycle 1) leading to native-like freeze-dried IgG (experiment C). The conditions of the shelf temperature and pressure during the drying are indicated.

loss in the measured sample region (Supporting Information, Figure S-3). For the formulation containing no stabilizer that can hydrogen bond with the protein, the amide A/II frequency did not change with shelf temperature increase from  $-20$  to  $50$  °C (Figure 2). This effect could be due to the cooperative nature of the native protein, making its intramolecular hydrogen bond network less sensitive to thermal expansion.<sup>21</sup> In contrast, an increasing amide A/II frequency with increasing temperature was observed for the formulation containing 10% sucrose (Figure 2). This suggests that the hydrogen bonds of the protein's backbone formed with surrounding sucrose molecules experience thermal expansion.<sup>38</sup>

Next, the effect of pure dehydration was studied on both the amide A/II frequency and the AWA, using an excipient-free

formulation that rendered native-like freeze-dried IgG (experiment C). Figure 3b shows that water removal during drying at the illuminated sample spot causes a decrease in AWA, as is expected. There were two phases with elevated water removal rates, i.e., directly after ice sublimation when drying at  $-20$  °C (from approximately 50 to 500 min) and during the shelf temperature increase in secondary drying (from approximately 1250 to 1800 min). As proteins have both weak and strong binding sites to accommodate unfrozen water, the dehydration process may indeed progress in different phases. The water molecules coming from the weak and easily accessible binding sites (i.e., surface water) will be removed first.<sup>39</sup> This possibly happens in the first intense phase of water removal. Although sublimation is still ongoing elsewhere in the sample,



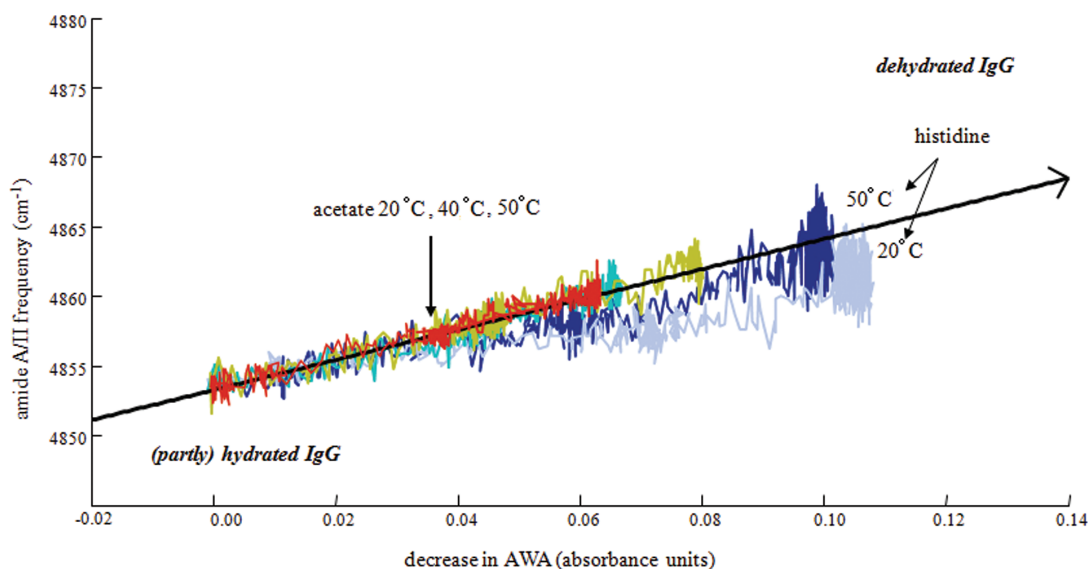


**Figure 4.** Amide A/II frequency versus decrease in AWA monitored during the drying of experiments rendering native-like freeze-dried IgG. Experiments A (dark blue trace) and B (light blue trace) were formulations in 25 mM histidine buffer pH 6.2 and secondary drying was performed at 50 and 20 °C, respectively. Experiments C (light green trace), D (red trace), and E (yellow trace) were formulated in 100 mM acetate buffer pH 4.0 and secondary drying was performed at 50 °C, 20 °C, and 40 °C, respectively.

dehydration may already start in local regions of the product where the ice is already removed.<sup>40</sup> After this phase the water removal slows down. Possibly, more energy is now needed to remove the remaining unfrozen water. Shortly after the shelf temperature starts increasing for secondary drying (at 1200 min of drying), another strong decrease in AWA appears. More strongly bound water and/or water molecules coming from less accessible places in the protein (i.e., buried water) may now be removed. Finally, the water removal rate slows down as there is less water.<sup>39</sup>

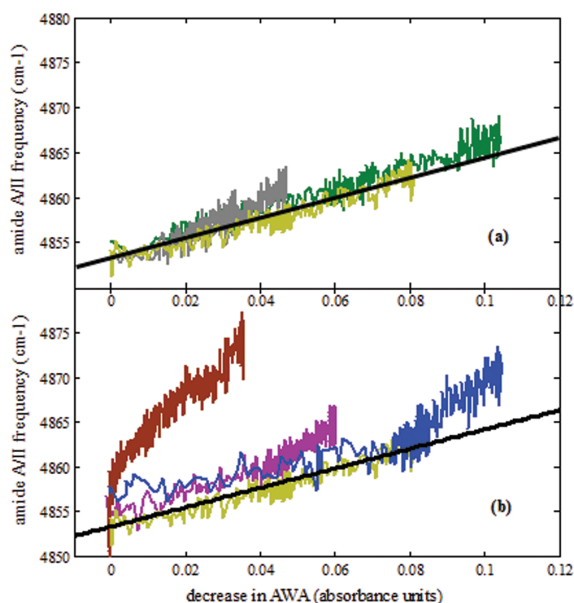
Interestingly, the same process phases were associated with an increased amide A/II band shifting to higher frequencies (Figure 3a). This may indicate a lowering in the extent of hydrogen bonding in the protein's backbone.<sup>16</sup> Since no marked protein unfolding was detected in the freeze-dried end product by FT-IR spectroscopy (data not shown), this shift in amide A/II frequency of the excipient free formulation must be attributed to protein dehydration. Indeed, more hydrated folded structures are supposed to absorb at lower frequencies than their dehydrated counterparts,<sup>19,41</sup> and water desorption during drying must originate at least partly from the protein's backbone. Time series of the amide A/II frequencies (a) and AWA values (b) for other formulations (Table 1), e.g., leading to either native-like, e.g., experiment E, or denaturated proteins, e.g., experiments G and J, indicated that time series profiles with similar shapes were obtained during drying (Supporting Information, Figure S-4). Because of the influence of dehydration on the amide A/II frequency, both variables, i.e., amide A/II frequency and AWA, are necessary to characterize the process trajectory for monitoring protein conformational stability during drying processes.

Figure 4 plots the amide A/II frequency versus the water elimination, expressed as AWA decreases during drying. In the absence of protein unfolding (i.e., experiments C, D, and E with respective  $r = 0.947$ ,  $0.952$ , and  $0.955$ ), the trajectories show a good correlation between both variables, even despite their

differences in drying conditions. This synchronous behavior of both variables represents the desired process course and can be attributed to water removal from the amorphous matrix, which dehydrates the protein molecules. For the formulations containing 25 mM histidine (experiments A and B), deviations from this trend appeared when further secondary drying, i.e., the amide A/II frequency shifts less with water removal (Figure 4). This is possibly because histidine contains an imidazole group, which may also interact with the protein backbone by hydrogen bonding,<sup>26,42</sup> this way acting as a water substitute (see further explanation in the next section).

Compared to the desired process course (e.g., yellow trace in Figure 5), the trajectories of experiments F, G, H, I, and J, where protein unfolding also occurred during drying (Figure 5), showed a more pronounced shifting of the amide A/II band (to higher frequencies) with water removal. Indeed, when a protein (partly) loses its folded structure, there is a relative decrease in hydrogen bonding strength, which may increase the amide A/II frequency.<sup>16</sup> Experiments F and G (gray and green trace in Figure 5a) experienced some moderate denaturation during drying, leading to small deviations from the desired process course ( $r = 0.905$  and  $0.924$ , respectively). Nonetheless, these modest degrees of denaturation during drying still led to acceptable end products, i.e., the proteins refolded back to their native conformation upon reconstitution. The larger deviations from the desired process course, as seen in the trajectories of experiments H, I, and J (purple, blue, and brown trace in Figure 5b, with respective  $r = 0.897$ ,  $0.875$ , and  $0.880$ ), represent conditions leading to strong and irreversible denaturated end products, being unacceptable from a quality point of view.

These results show that NIRS has potential for detecting protein unfolding during protein dehydration in freeze-drying processes. The trajectory obtained in the absence of protein unfolding can be set as the desired process course and consistent deviations from this trend toward higher amide A/II



**Figure 5.** Amide A/II frequency versus decrease in AWA monitored during the drying of (a) experiments F (gray trace) and G (green trace) leading to moderate and reversible denaturation and (b) experiments H (purple trace), I (blue trace), and J (brown trace) rendering strong and irreversible denaturation of IgG. Comparison is made to the track of experiment E (yellow trace with black fitted trend line) rendering native-like freeze-dried IgG.

frequencies may alarm to take actions for minimizing further protein unfolding during the process.

**In-Line Monitoring Protein–Lyoprotectant Interactions.** Lyoprotectants can be added to the formulation for

prevention of protein unfolding while water is removed from its environment. Hydrogen bond interactions of protein molecules with surrounding molecules are intended to stabilize the protein's native state, e.g., by (preferential) hydration, by forming molecular dispersions, and by replacing the lost water.<sup>23,25</sup> Because these interactions have been generally regarded as crucial for adequate lyoprotection, another aim in this study was to investigate whether shifts in the amide A/II frequency may provide in-line information/confirmation on the extent of these interactions and on when they occur during drying. Two types of molecules, supposed to have different modes of hydrogen bond interaction with proteins during freeze-drying, were used as lyoprotectants. Sucrose is assumed to effectively hydrogen bond with the protein during freeze-drying, and it is a good glass former.<sup>20</sup> Large polymers, such as PVP, are excellent glass formers but it is believed that steric hindrance effects prevent effective hydrogen bonding to the protein.<sup>3</sup> Formulations with sucrose showed different process trajectories compared to those from formulations without lyoprotectant or with PVP (Figures 6 and 7).

Directly after sublimation of the illuminated sample region, i.e., at no AWA decrease in Figure 6, the amide A/II frequencies were markedly lower in formulations with sucrose compared to those without lyoprotectant or with PVP. Moreover, the amide A/II frequencies were consistently lower with increasing sucrose content (Figure 7), suggesting a relative higher extent of hydrogen bonding between the protein's backbone and surrounding molecules, i.e., sucrose and water, in these systems.<sup>20</sup> Sucrose–protein bonds may have been formed during freeze-concentration. For the formulation with 10% PVP, there was no decrease in the amide A/II frequency compared to the formulation without lyoprotectant (Figure 6). This may be the result of its large molecular size hampering efficient hydrogen bonding to proteins.

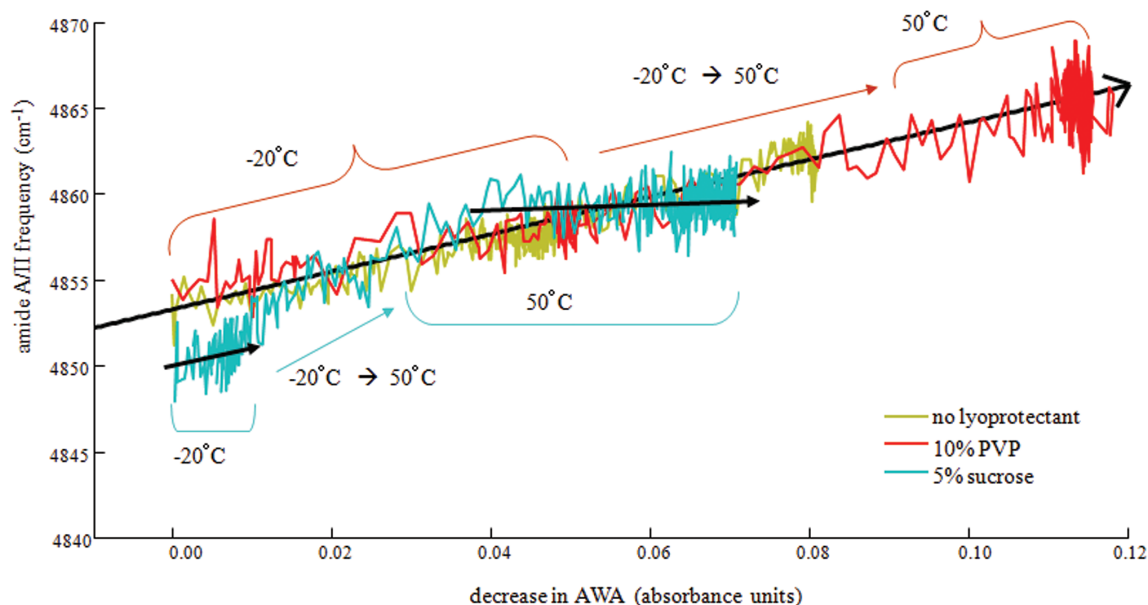


**Figure 6.** Amide A/II frequency versus decrease in AWA during drying for formulations containing 5% sucrose, 10% PVP, and no lyoprotectant. All formulations were in 100 mM acetate buffer pH 4.0, used the same process conditions (cycle 1 and 100  $\mu$ bar), and rendered native-like freeze-dried IgG. The corresponding shelf temperatures are added to indicate the process phases.

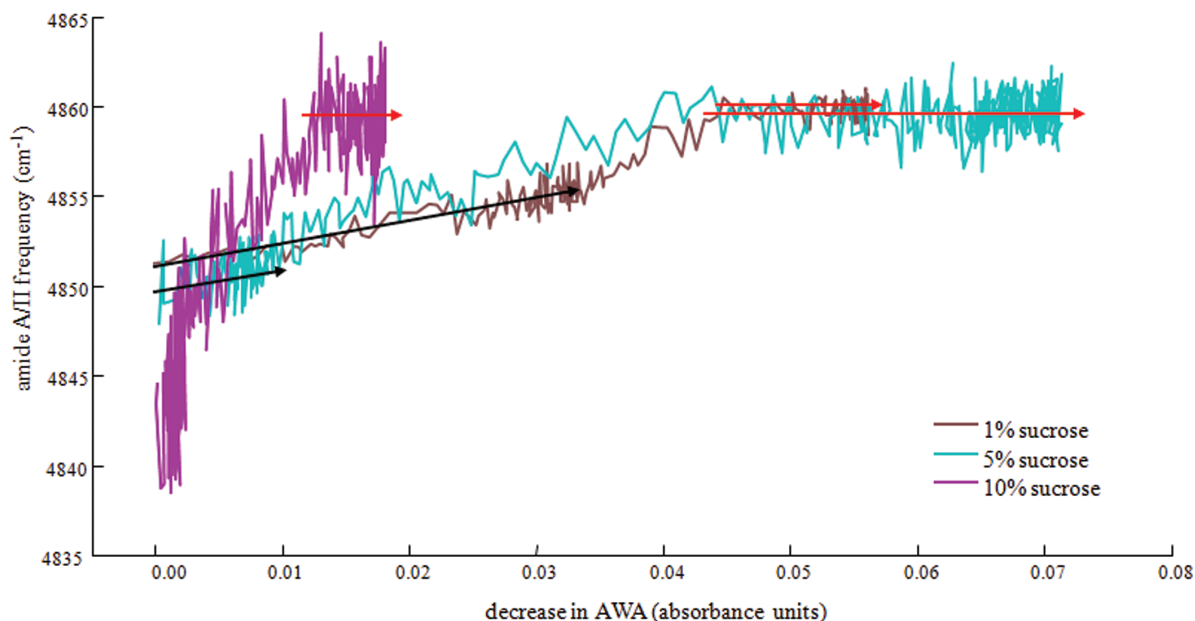


**Figure 7.** Amide A/II frequency versus decrease in AWA monitored during drying for experiments with different sucrose content. All formulations were in 100 mM acetate buffer pH 4.0, used the same process conditions (cycle 1 and 100  $\mu$ bar), and rendered native-like freeze-dried IgG. The black arrows indicate the trends when drying at  $-20\text{ }^{\circ}\text{C}$ , whereas the red arrows indicate the trends at the end of drying at  $50\text{ }^{\circ}\text{C}$ .

During drying at  $-20\text{ }^{\circ}\text{C}$ , a good correlation between amide A/II frequency and water removal was obtained (e.g., black arrows in Figures 6 and 7), suggesting dehydration of the protein molecules. This would mean that sucrose is not substituting the lost water in this process phase. However, increasing sucrose concentrations showed relative less water removal (i.e., less AWA decrease) in this process phase (Figures 6 and 7). Systems with high sucrose content may possibly require more energy, i.e., higher temperatures, to remove water from the amorphous matrix and may therefore provide relatively lower dehydration stress to proteins during this process phase.

During the shelf temperature increase from  $-20$  to  $50\text{ }^{\circ}\text{C}$ , the process trajectory showed a stronger upward trend in formulations with sucrose compared to the others (Figure 6). This may be the result of thermal expansion effects on the sucrose-amide bond, as explained earlier. In formulations with increasing sucrose content (Figure 7), this effect was more pronounced, indicating that a relative higher extent of sucrose–protein interaction is present in these systems.

When the final shelf temperature is reached, one continues drying at this constant temperature until an acceptable residual water level is obtained. Because of heat transfer, the solid cake temperature will gradually adapt to this temperature. Continuation of secondary drying at  $50\text{ }^{\circ}\text{C}$  showed that, despite there was still apparent water loss from the amorphous matrix, i.e., a decrease in AWA, the frequency of the amide A/II band remained unchanged (Figure 6). This trend was seen for all tested formulations containing 1%, 5%, and 10% sucrose (red arrows in Figure 7). A possible explanation is that nearly all the external amide groups of the proteins are now hydrogen bonded to sucrose, i.e., sucrose is replacing or has replaced water that was bound to the protein. Indeed, less amide A/II frequency shifting with AWA decrease was also seen in formulations with 25 mM histidine that also can act as a water

substitute<sup>26</sup> (Figure 4) but was barely seen in formulations with PVP, a poor water substitute because of its large molecular size (Figure 6).

## CONCLUSIONS

This work has demonstrated that in-line monitoring of the amide A/II frequency as a function of water elimination enables detecting protein unfolding during dehydration of IgG in freeze-drying processes. In formulations with increasing sucrose concentrations, an increasing extent of hydrogen bond interaction between the protein's backbone and surrounding molecules, i.e., sucrose and water, was detected immediately after sublimation. At the end of drying, there was evidence of nearly complete water substitution for formulations with 1%, 5%, and 10% sucrose. The presented approach may have potential for early fault detection of protein unfolding and for providing mechanistic process knowledge on actions of lyoprotectants. The parameters characterizing the process trajectory, i.e., amide A/II frequency and water absorbance, can be easily obtained from the in-line measured spectra using a noncontact NIR probe. The approach may not only be applied to freeze-drying processes but can be easily transferred to other drying processes of proteins. A drawback is that only that part of the cake which is illuminated by the NIR probe is measured, which is small compared to the cake volume. Because of the dominating ice signals, the approach also lacks the possibility to be used during freezing and sublimation. Since ice is a weak Raman scatterer, Raman spectroscopy may potentially fill this gap. To the best of our knowledge, this paper introduced the first in-line approach for obtaining real-time process knowledge on protein conformational stability and lyoprotection during freeze-drying in real-life conditions. The next steps to making this concept applicable in an industrial setting involve the development of a robust multivariate calibration model for

## Chapter 3: NEAR-INFRARED SPECTROSCOPY FOR IN-LINE MEASURING PROTEIN UNFOLDING DURING FREEZE-DRYING

### Analytical Chemistry

### Article

in-line determination of the actual moisture content (instead of estimating the water elimination via AWA) and defining acceptability and alarm borders on the process trajectory.

### ■ ASSOCIATED CONTENT

#### ■ Supporting Information

Additional information as noted in text. This material is available free of charge via the Internet at <http://pubs.acs.org>.

### ■ AUTHOR INFORMATION

#### Corresponding Author

\*Phone: +32 2 477 47 34. Fax: +32 2 477 47 35. E-mail: [yvanvdh@vub.ac.be](mailto:yvanvdh@vub.ac.be).

### ■ ACKNOWLEDGMENTS

S.P. thanks the Research Foundation–Flanders (FWO) for financial support.

### ■ REFERENCES

- (1) Banga, A. K. *Therapeutic Peptides and Proteins: Formulation, Processing, and Delivery Systems*, 2nd ed.; CRC Press: Boca Raton, FL, 2006.
- (2) Hill, J. J.; Shalae, E. Y.; Zografi, G. *J. Pharm. Sci.* **2005**, *94*, 1636–1667.
- (3) Luthra, S.; Obert, J. P.; Kalonia, D. S.; Pikal, M. J. *J. Pharm. Sci.* **2007**, *96*, 2242–2250.
- (4) Luthra, S.; Obert, J. P.; Kalonia, D. S.; Pikal, M. J. *J. Pharm. Sci.* **2007**, *96*, 61–70.
- (5) Kasper, J. C.; Friess, W. *Eur. J. Pharm. Biopharm.* **2011**, *78*, 248–263.
- (6) Carpenter, J. F.; Pikal, M. J.; Chang, B. S.; Randolph, T. W. *Pharm. Res.* **1997**, *14*, 969–975.
- (7) Dong, A.; Prestrelski, S. J.; Allison, S. D.; Carpenter, J. F. *J. Pharm. Sci.* **1995**, *84*, 415–424.
- (8) Schwegman, J. J.; Carpenter, J. F.; Nail, S. L. *J. Pharm. Sci.* **2007**, *96*, 179–195.
- (9) Remmele, R. L.; Stushnoff, C.; Carpenter, J. F. *Pharm. Res.* **1997**, *14*, 1548–1555.
- (10) Luyypaert, J.; Massart, D. L.; Vander Heyden, Y. *Talanta* **2007**, *72*, 865–883.
- (11) De Beer, T.; Burggraave, A.; Fonteyne, M.; Saerens, L.; Remon, J. P.; Vervaet, C. *Int. J. Pharm.* **2011**, *417*, 32–47.
- (12) Bogomolov, A. *Chemom. Intell. Lab. Syst.* **2011**, *108*, 49–63.
- (13) De Beer, T. R. M.; Wiggenghorn, M.; Veillon, R.; Debaq, C.; Mayeresse, Y.; Moreau, B.; Burggraave, A.; Quinten, T.; Friess, W.; Winter, G.; Vervaet, C.; Remon, J. P.; Baeyens, W. R. G. *Anal. Chem.* **2009**, *81*, 7639–7649.
- (14) De Beer, T. R. M.; Vercruyssen, P.; Burggraave, A.; Quinten, T.; Ouyang, J.; Zhang, X.; Vervaet, C.; Remon, J. P.; Baeyens, W. R. G. *J. Pharm. Sci.* **2009**, *98*, 3430–3445.
- (15) De Beer, T. R. M.; Wiggenghorn, M.; Hawe, A.; Kasper, J. C.; Almeida, A.; Quinten, T.; Friess, W.; Winter, G.; Vervaet, C.; Remon, J. P. *Talanta* **2011**, *83*, 1623–1633.
- (16) Liu, Y.; Cho, R. K.; Sakuri, K.; Miura, T.; Ozaki, Y. *Appl. Spectrosc.* **1994**, *48*, 1249–1254.
- (17) Tantipolphan, R.; Rades, T.; Medlicott, N. J. *Curr. Pharm. Anal.* **2008**, *4*, 53–68.
- (18) Murayama, K.; Ozaki, Y. *Biopolymers* **2002**, *67*, 394–405.
- (19) Barth, A.; Zscherp, C. *Q. Rev. Biophys.* **2002**, *35*, 369–430.
- (20) Katayama, D. S.; Carpenter, J. F.; Menard, K. P.; Manning, M. C.; Randolph, T. W. *J. Pharm. Sci.* **2009**, *98*, 2954–2969.
- (21) Cooper, A. *Biophys. Chem.* **2000**, *85*, 25–39.
- (22) Ragoonanan, V.; Aksan, A. *Transfus. Med. Hemother.* **2007**, *34*, 246–252.
- (23) Randolph, T. W. *J. Pharm. Sci.* **1997**, *86*, 1198–1203.
- (24) Perez-Moral, N.; Adnet, C.; Noel, T. R.; Parker, R. *Eur. J. Pharm. Biopharm.* **2011**, *78*, 264–270.
- (25) Allison, S. D.; Chang, B.; Randolph, T. W.; Carpenter, J. F. *Arch. Biochem. Biophys.* **1999**, *365*, 289–298.
- (26) Chang, L.; Pikal, M. J. *J. Pharm. Sci.* **2009**, *98*, 2886–2908.
- (27) Wang, B.; Tchessalov, S.; Warne, N. W.; Pikal, M. J. *Pharm. Sci.* **2009**, *98*, 3131–3144.
- (28) <http://www.mathworks.nl/help/techdoc/ref/spline.html> (accessed on October 10, 2011).
- (29) Räsänen, E.; Rantanen, J.; Mannermaa, J. P.; Yliruusi, J.; Vuorela, H. *J. Pharm. Sci.* **2003**, *92*, 2074–2081.
- (30) Rantanen, J.; Räsänen, E.; Antikainen, O.; Mannermaa, J. P.; Yliruusi, J. *Chemom. Intell. Lab. Syst.* **2001**, *56*, 51–58.
- (31) Rantanen, J.; Räsänen, E.; Tenhunen, J.; Käsäkoski, M.; Mannermaa, J. P.; Yliruusi, J. *Eur. J. Pharm. Biopharm.* **2000**, *50*, 271–276.
- (32) Matheus, S.; Friess, W.; Mahler, H. C. *Pharm. Res.* **2006**, *23*, 1350–1363.
- (33) Berg, J. M.; Tymoczko, J. L.; Stryer, L. *Biochemistry*, 5th ed.; W.H. Freeman: New York, 2002.
- (34) Walsh, S. T. R.; Cheng, R. P.; Wright, W. W.; Alonso, D. O. V.; Daggett, V.; Vanderkooi, J. M.; Degrad, W. F. *Protein Sci.* **2003**, *12*, 520–531.
- (35) Dong, A.; Kendrick, B.; Kreilgard, L.; Matsuura, J.; Manning, M. C.; Carpenter, J. F. *Arch. Biochem. Biophys.* **1997**, *347*, 213–220.
- (36) Allison, S. D.; Randolph, T. D.; Manning, M. C.; Middleton, K.; Davis, A.; Carpenter, J. F. *Arch. Biochem. Biophys.* **1998**, *358*, 171–181.
- (37) Bogomolov, A.; Engler, M.; Melichar, M.; Wigmore, A. *J. Chemom.* **2010**, *24*, 544–557.
- (38) Tang, X. C.; Pikal, M. J.; Taylor, L. S. *Pharm. Res.* **2002**, *19*, 484–490.
- (39) Levitt, M.; Park, B. H. *Curr. Biol.* **15**, 223–226.
- (40) Pikal, J. M.; Shah, S. *PDA J. Pharm. Sci. Technol.* **1997**, *51*, 17–24.
- (41) Demmel, F.; Doster, W.; Petry, W.; Schulte, A. *Eur. Biophys. J.* **1997**, *26*, 327–33.
- (42) Osterberg, T.; Wadsten, T. *Eur. J. Pharm. Sci.* **1999**, *8*, 301–308.



**Near-infrared spectroscopy for in-line monitoring of protein unfolding and its  
interactions with lyoprotectants during freeze-drying**

Sigrid Pieters<sup>1</sup>, Thomas De Beer<sup>2</sup>, Julia Christina Kasper<sup>3</sup>, Dorien Boulpaep<sup>1</sup>, Oliwia  
Waszkiewicz<sup>1</sup>, Mohammad Goodarzi<sup>1</sup>, Christophe Tistaert<sup>1</sup>, Wolfgang Friess<sup>3</sup>, Jean-Paul  
Remon<sup>4</sup>, Chris Vervaet<sup>4</sup>, Yvan Vander Heyden<sup>1</sup>

**SUPPORTING INFORMATION**

<sup>1</sup> Department of Analytical Chemistry and Pharmaceutical Technology, Center for  
Pharmaceutical Research, Vrije Universiteit Brussel - VUB, Laarbeeklaan 103, 1090  
Brussels, Belgium

<sup>2</sup> Laboratory of Pharmaceutical Process Analytical Technology, Universiteit Gent,  
Harelbekestraat 72, 9000 Ghent, Belgium

<sup>3</sup> Department of Pharmacy, Pharmaceutical Technology and Biopharmaceutics, Ludwig-  
Maximilians-University, Butenandtstr. 5, 81377 Munich, Germany

<sup>4</sup> Laboratory of Pharmaceutical Technology, Department of Pharmaceutics, Ghent University,  
Harelbekestraat 72, B-9000 Ghent, Belgium

Correspondence to: [yvanvdh@vub.ac.be](mailto:yvanvdh@vub.ac.be)

**Supporting Information Figures: 4 (figure S-1 to figure S-4)**

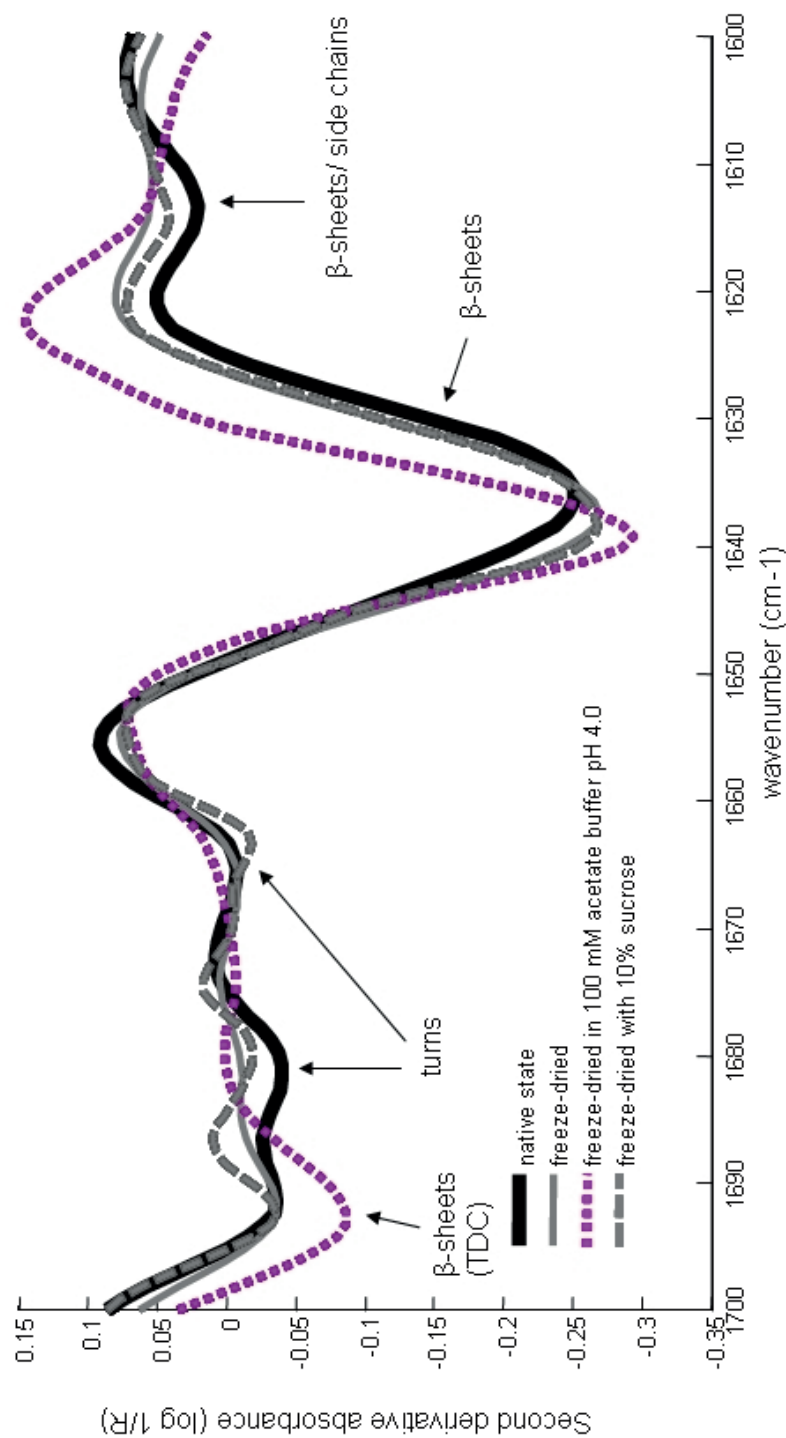


**Figure S-1.** Second derivative of the amide I band of IgG (in 25mM histidine buffer pH 6.2): native in solution, freeze-dried with and without 10% sucrose, and freeze-dried in 100 mM acetate buffer pH 4.0

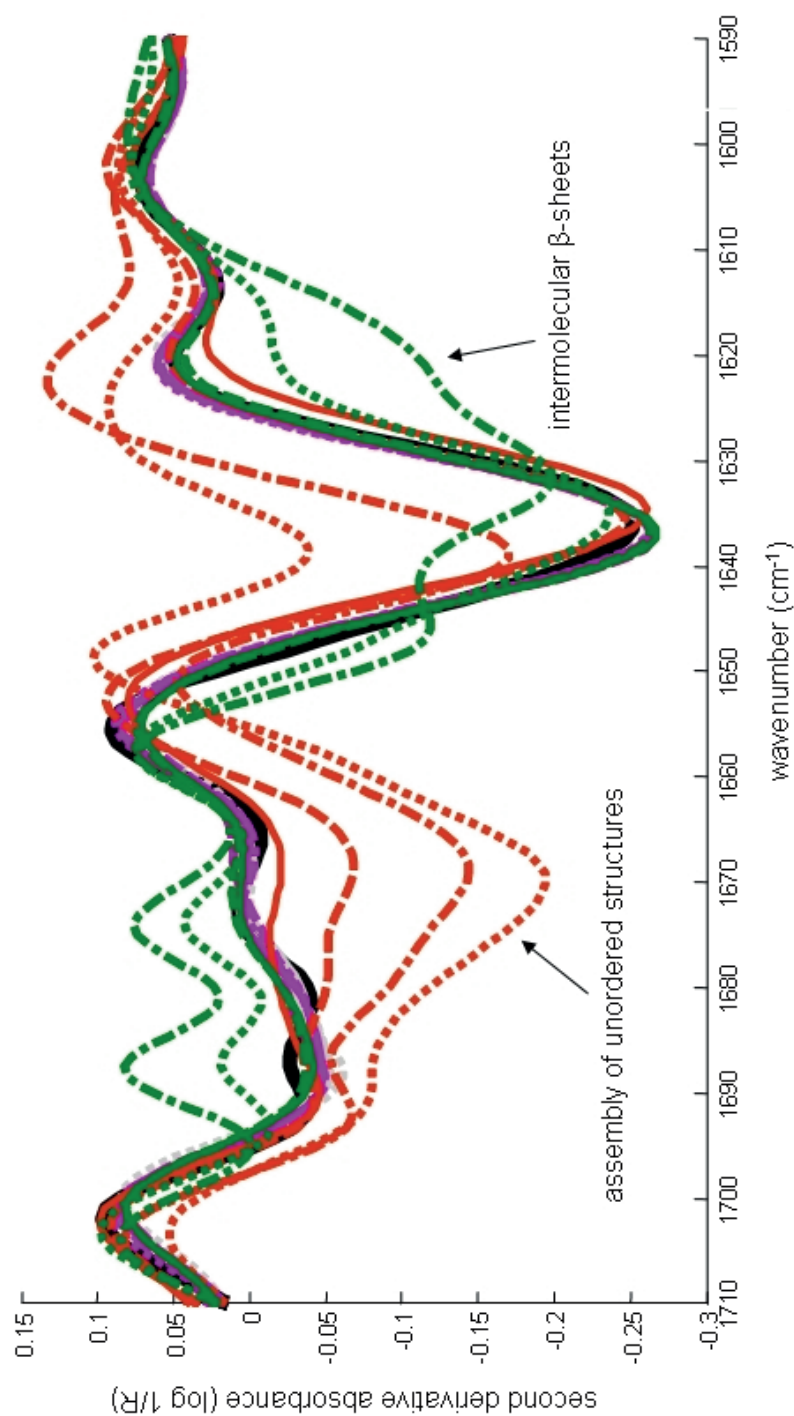


**Figure S-2.** Second derivative of amide I band of IgG in formulations containing 50 (—), 150 (-----), 300 (.....) and 600 mM (---) NaSCN in fresh solution (light grey), in solution after 6 weeks (purple), freeze-dried (red) and reconstituted (green). For comparison, the native state amide I band in a 25mM histidine buffer pH 6.2 solution is added (full black line)

S-3

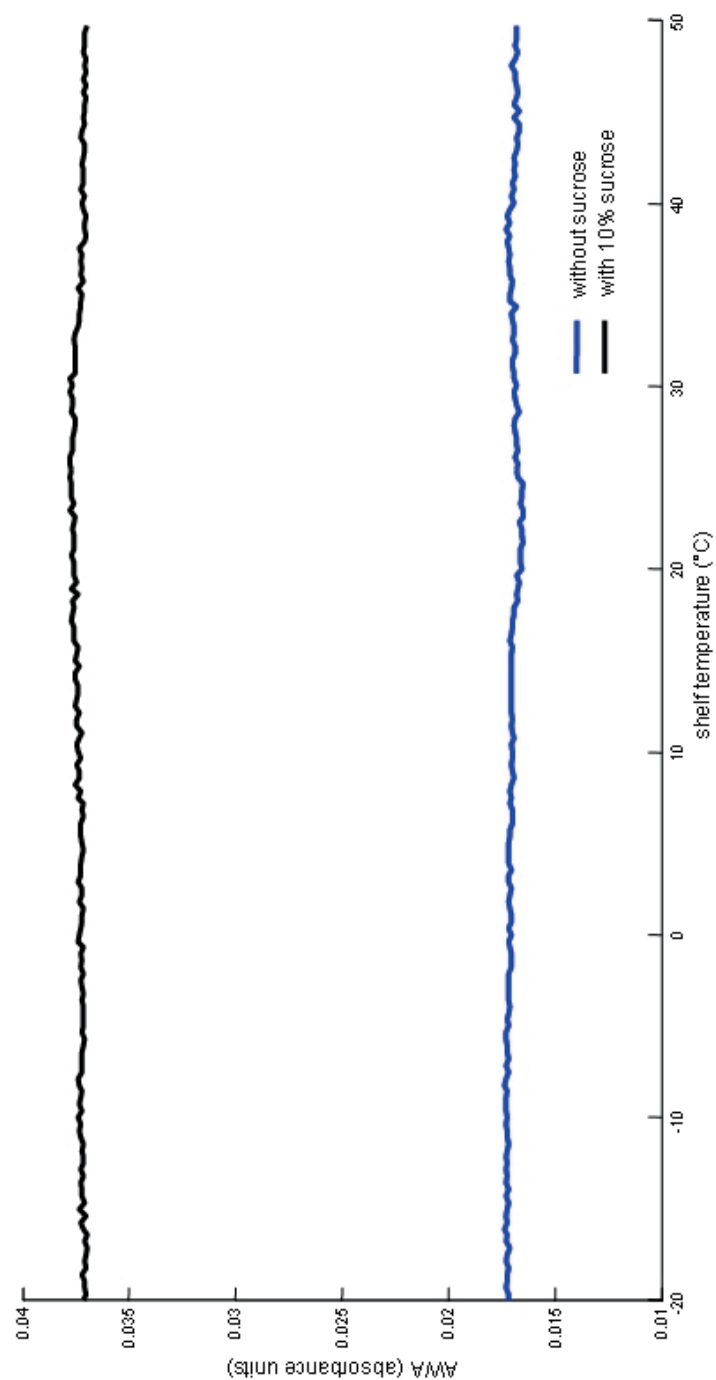


**Figure S-3.** Effect of the shelf temperature increase from -20°C to 50°C on the AWA for freeze-dried IgG formulations in 100 mM acetate pH 4.0 with and without 10% sucrose

S-4

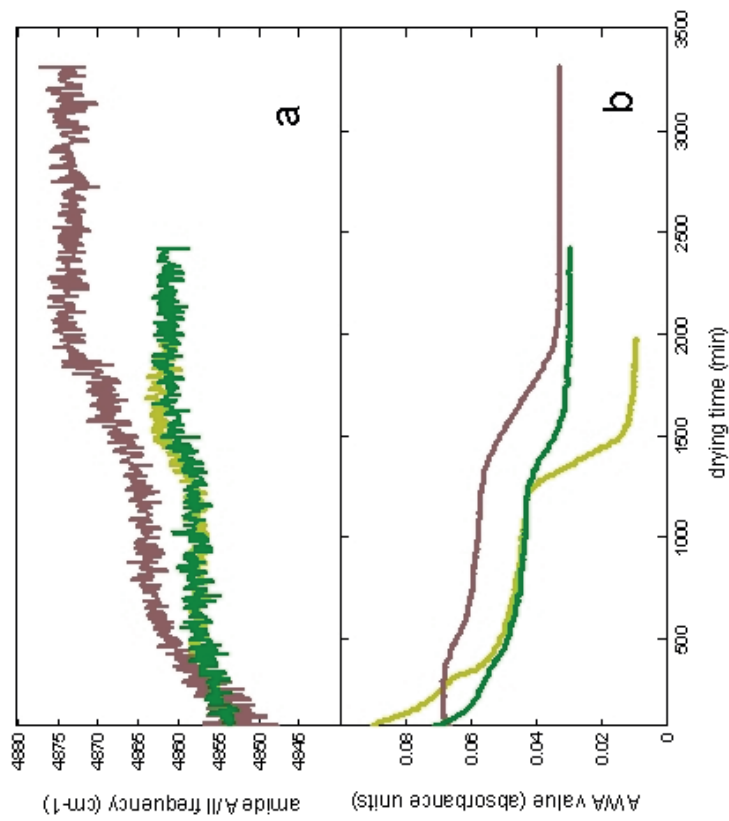


**Figure S-4.** Time series of the amide A/II frequency (a) and AWA (b) during drying of experiments E (yellow trace), G (green trace) and J (brown trace) producing native-like, moderately and strongly denaturated freeze-dried IgG, respectively

### 3.4. References

- [1] M. Miyazawa, M. Sonoyama, Second derivative near infrared studies on the structural characterisation of proteins, *J. Near Infrared Spec.* 6 (1998) 253-257.
- [2] Y. Liu, R.K. Cho, K. Sakuri, T. Miura, Y. Ozaki, Studies on spectra/structure correlations in near-infrared spectra of proteins and polypeptides. Part I: A marker band for hydrogen bonds, *Appl. Spectrosc.* 48 (1994) 1249-1254.
- [3] S. Bai, R. Nayar, J.F. Carpenter, M.C. Manning, Noninvasive determination of protein conformation in the solid state using near infrared (NIR) spectroscopy, *J. Pharm. Sci.* 94 (2005) 2030-2038.
- [4] K.I. Izutsu, Y. Fujimaki, A. Kuwabara, Y. Hiyama, C. Yomota, N. Aoyagi, Near-infrared analysis of protein secondary structure in aqueous solutions and freeze-dried solids, *J. Pharm. Sci.* 95 (2006) 781-789.
- [5] S.W. Bruun, PhD thesis: Protein-lipid-carbohydrate interactions and importance to food quality - Spectroscopic detection of macromolecular interactions, Technical University of Denmark, 2006.
- [6] R. Tantipolphan, T. Rades, N.J. Medlicott, Insights into the structure of protein by vibrational spectroscopy, *Curr. Pharm. Anal.* 4 (2008) 53-68.
- [7] K. Murayama, Y. Ozaki, Two-dimensional near-IR correlation spectroscopy study of molten globule-like state of ovalbumin in acidic pH region: simultaneous changes in hydration and secondary structure, *Biopolymers* 67 (2002) 394-405.
- [8] Y. Wang, K. Murayama, Y. Myojo, R. Tsenkova, N. Hayashi, Y. Ozaki, Two-dimensional fourier transform near-infrared spectroscopy study of heat denaturation of ovalbumin in aqueous solutions, *J. Phys. Chem. B* 102 (1998) 6655-6662.
- [9] Y.Q. Wu, B. Czarnik-Matusewicz, K. Murayama, Y. Ozaki, Two-dimensional near-infrared spectroscopy study of human serum albumin in aqueous solutions: using overtones and combination modes to monitor temperature-dependent changes in the secondary structure, *J. Phys. Chem. B* 104 (2000) 5840-5847.
- [10] D.S. Katayama, J.F. Carpenter, K.P. Menard, M.C. Manning, T.W. Randolph, Mixing properties of lyophilized protein systems: a spectroscopic and calorimetric study, *J. Pharm. Sci.* 98 (2009) 2954-2969.
- [11] S.W. Bruun, I. Sondergaard, S. Jacobsen, Analysis of protein structures and interactions in complex food by near-infrared spectroscopy. 1. Gluten powder, *J. Agric. Food Chem.* 55 (2007) 7234-7243.
- [12] Y. Ozaki, K. Murayama, Y. Wang, Application of two-dimensional near-infrared correlation spectroscopy to protein research, *Vibrational spectroscopy* 20 (1999) 127-132.
- [13] A. Cooper, Heat capacity of hydrogen-bonded networks: an alternative view of protein folding thermodynamics, *Biophys. Chem.* 85 (2000) 25-39.
- [14] J.K. Towns, Moisture content in proteins: its effects and measurement, *J. Chromatogr. A* 705 (1995) 115-127.
- [15] T. De Beer, A. Burggraef, M. Fonteyne, L. Saelens, J.P. Remon, C. Vervaet, Near infrared and Raman spectroscopy for the in-process monitoring of pharmaceutical production processes, *Int. J. Pharm.* 417 (2011) 32-47.

### Chapter 3: NEAR-INFRARED SPECTROSCOPY FOR IN-LINE MEASURING PROTEIN UNFOLDING DURING FREEZE-DRYING

---

- [16] Y. Zheng, X. Lai, S.W. Bruun, H. Ipsen, J.N. Larsen, H. Lowenstein, Determination of moisture content of lyophilized allergen vaccines by NIR spectroscopy, *J. Pharm. Biomed. Anal.* 46 (2008) 592-596.
- [17] H. Grohgan, D. Gildmyn, E. Skibsted, J.M. Flink, J. Rantanen, Towards a robust water content determination of freeze-dried samples by near-infrared spectroscopy, *Anal. Chim. Acta* 676 (2010) 34-40.
- [18] A. Kauppinen, M. Toiviainen, O. Korhonen, J. Aaltonen, K. Jarvinen, J. Paaso, M. Juuti, J. Ketolainen, In-line multipoint near-infrared spectroscopy for moisture content quantification during freeze-drying, *Anal. Chem.* 85 (2013) 2377-2384.
- [19] E. Rasanen, J. Rantanen, J.P. Mannermaa, J. Yliruusi, H. Vuorela, Dehydration studies using a novel multichamber microscale fluid bed dryer with in-line near-infrared measurement, *J. Pharm. Sci.* 92 (2003) 2074-2081.
- [20] M. Brulls, S. Folestad, A. Sparen, A. Rasmuson, J. Salomonsson, Applying spectral peak area analysis in near-infrared spectroscopy moisture assays, *J. Pharm. Biomed. Anal.* 44 (2007) 127-136.
- [21] M. Brulls, S. Folestad, A. Sparen, A. Rasmuson, In-situ near-infrared spectroscopy monitoring of the lyophilization process, *Pharm. Res.* 20 (2003) 494-499.





---

## Chapter 4: RAMAN SPECTROSCOPY FOR MEASURING PROTEIN UNFOLDING

---

### 4.1. Raman spectroscopy for detecting protein unfolding

Raman spectroscopy is a complementary technique to FTIR spectroscopy, as it uses the same region of the electromagnetic spectrum (i.e. the energies of fundamental molecular vibrations), but differs fundamentally in mechanism (i.e. light scattering versus absorption) and selection rules. In Raman spectra protein signals occur due to various backbone (amide), side chain and sulfur bridge vibrations. Among them, the amide I ( $1600\text{--}1700\text{ cm}^{-1}$ ) and III ( $1200\text{--}1320\text{ cm}^{-1}$ ) are the most prominent bands providing information on the protein secondary structure [1-4]. Different from FTIR spectroscopy is that the amide II Raman band has poorer structural sensitivity, because of its associated smaller change in polarizability [5-6]. Just as with FTIR, correlations between Raman frequencies and different secondary structures (i.e. assignments are based on model compounds) have been established (Table 4.1) [3, 5].

**Table 4.1. Assignments of secondary structures to the amide I and amide III bands in Raman spectra.**

Band	Approximate wave number ( $\text{cm}^{-1}$ )	Assignment
Amide I	1655	$\alpha$ -helix
	1670	$\beta$ -sheet
	1665	unordered structures
Amide III	> 1275	$\alpha$ -helix
	1235	$\beta$ -sheet
	1245	unordered structures

The secondary structures in the amide I and III bands have been specifically assigned (i.e. by curve fitting procedures and quantified [5, 7-10]. The latter has also been done by regression [11-12]. However, protein unfolding is in comparability studies generally detected by a distorted shape or shift of the unresolved amide I and III bands [5, 13-16]. Additionally, protein unfolding has also been detected by spectral intensity differences related to amino acid side chain vibrations, because alterations in the local environment polarity (buried versus exposed) of amino acids may influence their Raman features [2, 5-7, 16]. Besides the tryptophan (near  $760\text{ cm}^{-1}$ ) and tyrosine doublet ( $850/830\text{ cm}^{-1}$ )

vibrations, the  $\text{CH}_n$  bending and stretching vibrations (e.g. near 1450 and 2930  $\text{cm}^{-1}$ , respectively) have been frequently used for this [2, 6, 14]. Intensity changes in the  $\text{CH}_n$  vibrational bands have been attributed to a change in the exposure (local polarity) of the aliphatic hydrocarbon chains present in hydrophobic amino acids.

Recently, Brewster et al. [13] monitored the unfolding of ribonuclease (RNase A and B) when being stressed by increasing guanidine hydrochloride (Gu.HCl) concentrations in aqueous solutions. From the frequency shifts of the blank subtracted amide I Raman spectra (i.e. for each monitored Gu.HCl concentration), it was possible to develop stability curves that showed similar profiles to those developed with fluorescence spectroscopy. Based on spectral changes in the amide I, III,  $\text{CH}_3$  stretching and OH-stretching Raman bands, Gniadecka et al. [14] were able to distinguish between a young, chronologically aged, and photo aged skin, as these were the results of changes in structural proteins and hydration. Interestingly, the absence of a band near 180  $\text{cm}^{-1}$  (tetrahedron water) may indicate that most of the water molecules are bound to other macromolecules, whereas the total water content can be estimated by the OH stretching vibration band near 3250  $\text{cm}^{-1}$  [14]. Other studies also used univariate methods (i.e. monitoring intensity and/or frequency shifts) during thermal protein denaturation [2, 4, 17], during frozen storage [18], and denaturation caused by salts and extreme pH's [4].

Just as with FTIR spectroscopy, Raman analysis is possible in different physical states of the sample (e.g. aqueous, dried solid, frozen...). Because of the inherently weak scattering effect, Raman spectroscopy requires relatively high protein concentrations (e.g. > 5 mg/ml) to obtain good quality spectra. Selecting the proper feature(s) to obtain the information of interest from the spectra is essential for any spectral analysis. In univariate analysis, one should select a spectral response that is assumed to be highly selective for the quality attribute of interest. To ensure the assumption that the chosen spectral response is not biased by contributions from other sources, selectivity of the method should be carefully assessed before the univariate method can be used to predict the property in new samples [19-20]. Usually, spectral blank and background corrections are applied to remove possible interfering signals from other sources than the one of interest. Although the Raman signals of water and ice are not intense, a

subtraction of solvent and buffer components to minimize their interference prior to analysis is a common practice in Raman spectroscopic analysis of proteins [1, 10, 13]. Non-Raman effects, such as fluorescence (e.g. originating from fluorescent groups in amino acid side chains of proteins), may produce a (sometimes significant) spectral background on which the Raman signals are superimposed. A background correction can be performed [4, 21-22], though it can be time-consuming and a user-dependent bias (e.g. interpolation methods require an estimation of the background) might be introduced. Background corrections performed by mathematical procedures might also introduce artifacts, e.g. second derivative spectra might enhance the noise in the spectra.

Because of their strong but complex (i.e. many bands are involved) correlation to the folded protein structure, it can be more beneficial to treat the Raman spectra in a multivariate way. MVA methods have the advantage to simultaneously extract valuable information from multiple predictor variables constituting the whole (or relevant parts of the) spectra [19-20]. Thus, the spectra can be used in a more efficient way. Where the signal-to-noise ratio in one variable can be too low to detect a response, a noise reduction is generally obtained with MVA because multiple measurements of the same phenomenon are used (e.g. latent variable methods such as PCA and PLS use weighted averages of all the predictor variables). Moreover, MVA methods can cope with non-selectivity in the measured spectral signals [19-20]. Provided that the interfering signals are sufficiently incorporated into the calibration, the quality attribute of interest can be predicted for new samples by using an MVC model. Thus, MVA has the interesting characteristic to allow efficient extraction of selective information from highly unselective data. This makes MVA attractive to analyze quality attributes in complex matrices, as well as for process monitoring, where a lot of potentially varying interferences may influence the spectra. Moreover, when selectivity is less an issue, blank and background corrections (being unpractical for process monitoring) might become superfluous. Hence, a first aim was to investigate whether the use of MVA may allow the extraction of information related to protein unfolding from the experimentally obtained Raman spectra.

So far, Raman spectroscopy combined with MVA has been successfully used in a number of biomedical and bio-manufacturing applications. For instance, it was possible to distinguish accurately between glycated and non-glycated hemoglobin (i.e. glycation induced a decrease in  $\alpha$ -helix content and a weakening of the heme-globin interaction) in low concentrated aqueous solutions ( $\mu\text{M}$  range). However, the origin of the spectral changes in the Raman spectra was difficult to determine, probably because of the low protein concentrations. Yet a test for chance correlation showed that the differentiation was not based on random correlations [23]. The identification and quality assessment of five different components in mammalian cell culture media was also possible. The developed MVC classification models from Raman spectra allowed predicting whether an incoming media batch will generate either an acceptable or unacceptable product yield [24]. In another study, the early diagnosis and typing of adenocarcinoma in the stomach was allowed by combining Raman spectroscopy and MVA. Multiple marker bands in the Raman spectra were used simultaneously and originated from protein, nucleic acid and lipid signals [25].

#### **4.2. Raman spectroscopy and multivariate analysis for the rapid discrimination between native-like and non-native states in freeze-dried protein formulations**

In the following paper (S. Pieters, Y. Vander Heyden, J.M. Roger, M. D'Hondt, L. Hansen, B. De Spiegeleer, C. Vervaet, J.P. Remon, T. De Beer, Raman spectroscopy and multivariate analysis for the rapid discrimination between native-like and non-native conformational states in freeze-dried protein formulations, *European Journal of Pharmaceutics and Biopharmaceutics*, in press), it was evaluated whether the use of MVA allows obtaining information on protein unfolding directly from the experimentally obtained Raman spectra. Exploratory analysis (i.e. PCA) and supervised classification (i.e. Partial Least Squares - Linear Discriminant Analysis or PLS-LDA) were applied to discriminate between the NL and DEN classes of a model protein LDH (Fig. 4.1).

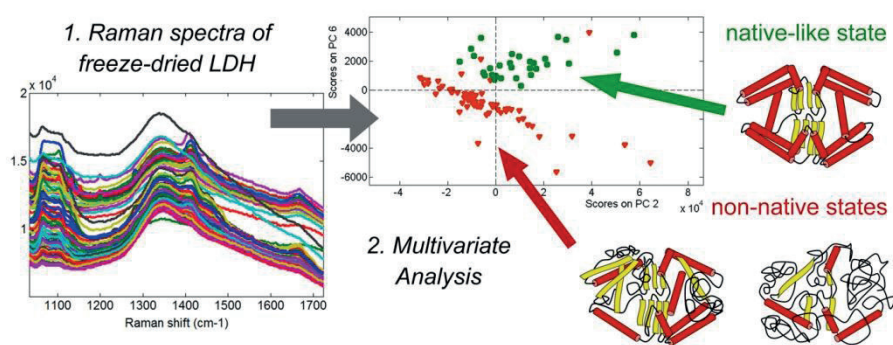


Fig. 4.1. Graphical abstract showing the idea of the study.

## ARTICLE IN PRESS

European Journal of Pharmaceutics and Biopharmaceutics xxx (2013) xxx–xxx



Contents lists available at SciVerse ScienceDirect

European Journal of Pharmaceutics and Biopharmaceutics

journal homepage: [www.elsevier.com/locate/ejpb](http://www.elsevier.com/locate/ejpb)

## Research paper

# Raman spectroscopy and multivariate analysis for the rapid discrimination between native-like and non-native states in freeze-dried protein formulations

Sigrid Pieters<sup>a</sup>, Yvan Vander Heyden<sup>a,\*</sup>, Jean-Michel Roger<sup>b</sup>, Matthias D'Hondt<sup>c</sup>, Laurent Hansen<sup>d</sup>, Bernard Palagos<sup>b</sup>, Bart De Spiegeleer<sup>c</sup>, Jean-Paul Remon<sup>e</sup>, Chris Vervaet<sup>e</sup>, Thomas De Beer<sup>d</sup>

<sup>a</sup> Department of Analytical Chemistry and Pharmaceutical Technology, Vrije Universiteit Brussel – VUB, Brussels, Belgium

<sup>b</sup> Irstea, UMR1201, Montpellier, France

<sup>c</sup> Laboratory of Drug Quality & Registration (DruQuaR), Universiteit Gent, Ghent, Belgium

<sup>d</sup> Laboratory of Pharmaceutical Process Analytical Technology, Universiteit Gent, Ghent, Belgium

<sup>e</sup> Department of Pharmaceutics, Universiteit Gent, Ghent, Belgium

## ARTICLE INFO

Article history:  
Available online xxxx

Keywords:  
Raman spectroscopy  
Multivariate analysis  
Freeze-drying  
Lactate dehydrogenase  
PAT  
Conformational state

## ABSTRACT

This study investigates whether Raman spectroscopy combined with multivariate analysis (MVA) enables a rapid and direct differentiation between two classes of conformational states, i.e., native-like and non-native proteins, in freeze-dried formulations. A data set comprising of 99 spectra, both from native-like and various types of non-native freeze-dried protein formulations, was obtained by freeze-drying lactate dehydrogenase (LDH) as model protein under various conditions. Changes in the secondary structure in the solid freeze-dried proteins were determined through visual interpretation of the blank corrected second derivative amide I band in the ATR-FTIR spectra (further called FTIR spectra) and served as an independent reference to assign class labels. Exploratory analysis and supervised classification, using Principal Components Analysis (PCA) and Partial Least Squares – Linear Discriminant Analysis (PLS-LDA), respectively, revealed that Raman spectroscopy is with 95% accuracy able to correctly discriminate between native-like and non-native states in the tested freeze-dried LDH formulations. Backbone (i.e., amide III) and side chain sensitive spectral regions proved important for making the discrimination between both classes. As discrimination was not influenced by the spectral signals from the tested excipients, there was no need for blank corrections. The Raman model may allow direct and automated analysis of the investigated quality attribute, opening possibilities for a real time and in-line quality indication as a future step. However, the sensitivity of the method should be further investigated and where possible improved.

© 2013 Elsevier B.V. All rights reserved.

## 1. Introduction

The FDA's process analytical technology (PAT) initiative [1] is one of the concepts encouraging the (bio-) pharmaceutical industry to invest in analytical methods that provide ultra-fast (i.e., real time) analysis results, while being information-rich and robust in the presence of interferents. Most of them rely on spectroscopic techniques combined with multivariate analysis (MVA) [2–4]. As they usually lack the conventional delay inherent to the standard analytical techniques for sampling, sample preparation, analysis, data extraction, and interpretation, not only the laboratory work,

time, and costs may be reduced, but also they may allow decision making in real time. This is essential for using these techniques as *in situ* diagnostic tools during manufacturing processes when the quality attribute of interest has to be assessed within a few seconds to make important decisions that ensure overall product and process quality.

The 3D folded structure of a native protein is required to properly exert its biological action. The most important bonds that make up the secondary to quaternary structure are hydrophobic interactions (e.g., between the side chains of the amino acids) and hydrogen bonds (e.g., for constituting the secondary structural elements such as  $\alpha$ -helix and  $\beta$ -sheets). However, these structures are fragile, since exposure to even mildly denaturing conditions may make them lose partially their natively folded structure. These conditions can be numerous, and freeze-drying is well known to be one of them [5–7]. When the protein does not refold back to its native state after reconstitution, its activity might be reduced or

\* Corresponding author. Department of Analytical Chemistry and Pharmaceutical Technology, Center for Pharmaceutical Research, Vrije Universiteit Brussel – VUB, Laarbeeklaan 103, B-1090 Brussels, Belgium. Tel.: +32 2 477 47 34; fax: +32 2 477 47 35.

E-mail address: [yvavndh@vub.ac.be](mailto:yvavndh@vub.ac.be) (Y. Vander Heyden).

absent. Partial unfolding can also result in the exposure of buried hydrophobic amino acid residues. This may favor aggregation when reconstituting the freeze-dried product with typically an up-concentrated protein fraction [8]. To avoid excessive unfolding and subsequent exposure of the hydrophobic sites, it is thus necessary to take preventive actions, conserving the native conformation of the proteins as much as possible during the whole manufacturing process and storage. The potential risk for reduced or absent activity of the non-native proteins, and immune responses of the aggregates, makes them important considerations in formulation and process development of protein drug products.

Among the many available techniques that may provide information on a protein's 3D-structural conformation (e.g., fluorescence spectroscopy, far-UV circular dichroism, NMR, and FTIR, etc.), Raman spectroscopy may have the potential to become an ultra-fast diagnostic tool in detecting real-time protein conformational changes during the freeze-drying process. Whereas other techniques require the protein to be in solution and/or are invasive (i.e., FTIR would affect the freeze-drying process), Raman spectroscopy is a noninvasive technique which is practically transparent for water and ice and requires minimal or no sample preparation. Near-infrared (NIR) spectroscopy can also detect protein unfolding during freeze-drying; however, due to its strong water and ice signals, it could only be used for monitoring a sample after sublimation in the illuminated sample spot [9].

Infrared (IR) and Raman spectroscopy have been extensively used in protein structural characterization, especially for determining changes in the secondary and/or tertiary structure of proteins in different matrices. Identification of specific bands associated with the secondary structure has been achieved using homopolypeptides and proteins with known  $\alpha$ -helix and  $\beta$ -sheet elements [10]. As these methods require a thorough peak-by-peak investigation to obtain the necessary information from the spectra of the protein formulations, they usually demand blank corrections, resolution enhancement techniques, and expert knowledge. Visual interpretation of the amide I FTIR spectral band ( $1700$ – $1600\text{ cm}^{-1}$ ) is by far the most established technique for determining secondary structure of proteins in the solid state [10]. As the original amide I spectrum is usually featureless and can be overlapped by the signals of other components, the visualization of the underlying secondary structure components is hampered. Therefore, prior to visual inspection, blank corrections and decomposition methods, such as Fourier deconvolution or second derivation of the spectra, have become popular to delineate overlapping secondary structures in the original spectrum [10]. As delineating is more complex in the blank corrected Raman spectra, the interpretation is frequently based on changes in peak shape rather than on individual band assignments [11–13]. Usually, the focus is on the visual interpretation of the well-known amide I and amide III bands.

Although aforementioned methods are very informative, they have the drawback of being time consuming and impractical for a rapid quality assessment, which is essential for in-line monitoring of the protein conformational state during freeze-drying processes. The proposed MVA method uses the Raman spectrum more efficiently, by extracting the relevant information directly from the sample spectrum, without the need for blank corrections, resolution enhancement, or subjective interpretations. Multivariate calibration methods can cope with non-selectivity in the obtained spectral signals, provided that the interferent signals are sufficiently incorporated into the calibration, and their shape is not completely identical to the signal of the analyte [14]. Additionally, MVA may actually point out these spectroscopic marker bands differentiating between native and non-native proteins, thus offering insights into the biochemical origin of the discrimination. Mathematical approaches may also allow detecting more subtle, but consistent, spectral changes that are visually undetectable [3].

In the present paper, we investigate whether Raman spectroscopy combined with MVA enables the discrimination between native-like and non-native conformational states of proteins in freeze-dried formulations in a rapid (i.e., a few seconds) and direct way. The aims are as follows: (1) to investigate whether Raman spectroscopy is able to rapidly and accurately differentiate between native-like and non-native freeze-dried proteins, (2) to develop and validate a calibration model to classify freeze-dried protein samples, (3) to study the influence of formulation interferents (i.e., excipient signals) on the discrimination, (4) to examine which part(s) of the Raman spectra are necessary to make this discrimination, and whether they can be linked to sound biochemical knowledge. Given its known instability during freeze-drying, lactate dehydrogenase (LDH) was selected as a model protein [15].

## 2. Methods and materials

### 2.1. Materials

L-Lactic Dehydrogenase (LDH) from rabbit muscle – Type II in ammonium sulfate – was obtained from Sigma–Aldrich (Saint Louis, MO, USA). Prior to freeze-drying, 2 mL type I vials (Nipro, Authon-du-Perche, France) were filled with 720  $\mu\text{L}$  formulation containing approximately 9 mg/mL LDH. Table 1 shows the different LDH formulations that were prepared in this study. Formulations 1–12 were used in the design of experiments (DoE) and contained a 40 mM buffer pH 7.4, either sodium phosphate (Sigma–Aldrich, Steinheim, Germany) (PHOS), L-histidine (HIS) or TRIS (Merck, Darmstadt, Germany). Some formulations contained a lyoprotectant, i.e., 5% sucrose (Suedzucker, Mannheim, Germany) and/or a cryoprotectant, i.e., 1% PEG 4000 (Fagron, Barsbüttel, Germany). Besides the DoE formulations, others (formulations 13–19) contained NaSCN, NaCl, or ethanol (Sigma–Aldrich, Steinheim, Germany) or were formulated in water.

### 2.2. Freeze-drying

Freeze-drying was performed using an Amsco FINN-AQUA GT4 freeze-dryer (GEA, Koeln, Germany). Eight batches were produced

**Table 1**  
Different LDH formulations (approximately 9 mg/mL LDH) prepared in this study.

Formulation number	Excipient composition
1	HIS
2	HIS, sucrose
3	HIS, PEG
4	HIS, sucrose, PEG
5	PHOS
6	PHOS, sucrose
7	PHOS, PEG
8	PHOS, sucrose, PEG
9	TRIS
10	TRIS, sucrose
11	TRIS, PEG
12	TRIS, sucrose, PEG
13	50 mM NaSCN
14	150 mM NaSCN
15	300 mM NaSCN
16	600 mM NaSCN
17	0.9% NaCl
18	1.0% ethanol
19	Water

Abbreviations: HIS = histidine buffer, PHOS = phosphate buffer, TRIS = TRIS buffer, all 40 mM at pH 7.4.

Please cite this article in press as: S. Pieters et al., Raman spectroscopy and multivariate analysis for the rapid discrimination between native-like and non-native states in freeze-dried protein formulations, Eur. J. Pharm. Biopharm. (2013), <http://dx.doi.org/10.1016/j.ejpb.2013.03.035>



**Table 2**

Design of the freeze-drying runs performed.

Batch	Freezing method	Secondary drying temperature (°C)	Formulations <sup>a</sup>
1	SL	40	1–19
2	ANN	40	1–19
3	CH	5	1–12
4	ANN	5	1–12
5	FA	40	1–12
6	FA	5	1–12
7	CH	40	1–12
8	SL	5	1–12

Abbreviations: SL = slow cooling, FA = fast cooling, ANN = annealing, CH = cooling hold.

<sup>a</sup> See Table 1.

with different cooling methods and secondary drying temperatures (Table 2). The cooling methods included the following: (1) slow cooling at a rate of 0.2 °C/min (SL), (2) fast cooling with pre-cooled shelf at –45 °C (FA), (3) cooling at 1 °C/min and after freezing an annealing step of 10 h at –7 °C (ANN), (4) cooling at 1 °C/min with cooling stop for 60 min at –10 °C (CH). Freezing was always performed for 2 h at –45 °C, primary drying for 20 h at –20 °C and 100 µbar and secondary drying for 6 h at 100 µbar with temperature ramps of 0.2 °C/min in between.

The full factorial experimental design led to 96 freeze-dried samples (8 runs × 12 formulations) (Tables 1 and 2). Seven additional samples (formulations 13–19) were added to runs 1 and 2 to produce more extremely denatured LDH. This resulted in a total of 110 freeze-dried samples that were analyzed with both FTIR and Raman spectroscopy. After reconstituting the samples, they were analyzed using the LDH activity assay. However, since the amide I bands in the FTIR spectra of some freeze-dried samples could not be interpreted, those were omitted and the data set for developing and validating the model comprised 99 freeze-dried samples.

### 2.3. LDH activity assay

The enzymatic activity of LDH after reconstitution of the freeze-dried samples in 720 µl water was determined with a UV-2401PC spectrophotometer (Shimadzu, Kyoto, Japan) by monitoring the rate of absorbance decrease per minute of NADH at 340 nm as a result of the reduction in pyruvate to lactate at 37 °C. The Sigma–Aldrich (Steinheim, Germany) experimental procedure was followed [16], using all their necessary chemicals (i.e., NADH, sodium pyruvate, and BSA). The remaining activity of the reconstituted freeze-dried samples was compared to that of native (not freeze-dried) LDH and expressed as % LDH activity recovery after freeze-drying. Each sample was measured in triplicate and averaged. The assay had a coefficient of variation of 4.1% for repeatability and 11.0% for day-to-day intermediate precision.

### 2.4. Spectroscopic conditions and spectral pre-processing

#### 2.4.1. Raman spectroscopy

A Raman Rxn1 spectrometer (Kaiser Optical systems, Ann Arbor, MI), equipped with an air-cooled CCD detector (back-illuminated deep depletion design), was used in combination with a fiber-optic non-contact MR probe. The Invictus NIR diode laser used a wavelength of 785 nm. Spectra were recorded with a resolution of 4 cm<sup>–1</sup> and an exposure time of 40 s, using a laser power of 400 mW. For MVA, the Raman spectra of the freeze-dried solids were used without any pre-processing. For visual comparison of the Raman spectra, the corresponding blank spectrum of each

formulation was subtracted, and the spectra were scaled and Savitzky–Golay smoothed.

#### 2.4.2. FTIR spectroscopy

FTIR spectroscopy functioned as a reference technique to evaluate potential changes in protein secondary structure in the freeze-dried solid. FTIR spectroscopy measurements were conducted on a Varian Scimitar 800 FTIR spectrometer, equipped with a Specac Golden Gate diamond ATR module (Varian Scimitar, Middelburg, the Netherlands). The spectra were recorded from 4000 to 500 cm<sup>–1</sup> in ATR mode at a resolution of 2 cm<sup>–1</sup>. Each measurement was the average of 100 scans. The FTIR spectra of the same freeze-dried samples and the corresponding blanks were first background (air) corrected and converted to absorbance format. The resulting FTIR absorbance spectra were subsequently corrected for the spectral contributions of the blank formulations. Finally, the second derivative with 17-point Savitzky–Golay smoothing was performed, and the FTIR spectra were area normalized over the amide I region (1700–1600 cm<sup>–1</sup>) for direct comparison. Individual peak positions were identified and assigned according to the literature [10].

### 2.5. Data handling and MVA

All data handling was performed with Matlab 7.1 (The Mathworks, Natick, MA) and the PLS toolbox 6.2 (Eigenvector Research, Wenatchee, WA). For PLS–LDA and orthogonal projections, in-house Matlab routines were used. Statistical data analysis was performed with Minitab 16 (Minitab, PA).

#### 2.5.1. Principal Component Analysis (PCA)

Principal Component Analysis (PCA) is an unsupervised MVA technique that allows seeing trends and structures in data sets. It reduces the number of variables to a new set of latent variables (LVs) that describe the data variability more efficiently. These LVs, called principal components, are linear combinations of the original ones. They are defined in such a way that they explain most the (remaining) variability in the data and are orthogonal to each other. They can be decomposed into loadings and scores. The loading vector gives qualitative information about the samples by describing what type of information characterizes them, i.e., which variables are important. The associated weighted averages of the original variables are the scores, providing quantitative information, i.e., the amount of each loading vector in each sample [14,17].

#### 2.5.2. Partial Least Squares – Linear Discriminant Analysis (PLS–LDA)

PLS–LDA is a supervised classification algorithm that combines PLS for dimension reduction with LDA for obtaining a classification outcome. LDA seeks an optimal low-dimensional space in which the projected data points are linearly well-separated into different classes [18]. It aims to maximize the ratio of between-class variance to within-class variance. The Mahalanobis distance, taking the shape of the considered cluster into account, is used to calculate the probability that a new object belongs to a certain class. As the number of variables (i.e., wavenumbers) in the Raman and FTIR spectral data is much higher than the number of objects (i.e., samples), LDA cannot directly be applied to the spectra. Therefore, PLS first compresses the data dimensionality [19]. PLS is performed on a set of dummy responses (0 and 1) encoded to represent the two classes and maximizes the co-variance between the measured signals (e.g., spectra) and the response [17].

For building the PLS–LDA models, the data set of 99 samples was randomly split into a training (75 freeze-dried LDH formulations) and a test set (24 freeze-dried LDH formulations for validation of the model), but it was made sure that all possible variation



in  $\mathbf{y}$  (i.e., containing native-like, mildly stressed (i.e., mainly altered ratio in  $\alpha$ -helix and  $\beta$ -sheet structures, further called  $\alpha/\beta$  ratio) and more strongly stressed (i.e., with the clear presence of non-native structures) LDH with % activity preservations ranging from <10% to >100%) was covered by both data sets. Both training and test set contained formulations with similar excipients originating from the eight freeze-drying runs. The optimal model complexity was determined with cross-validation (CV) on the training set. A permutation test was also a part of the validation procedure [20]. This can assess whether the classification of the samples in the two designed groups performs significantly better than any other random classification in two arbitrary groups. This test should exclude the possibility of chance correlation in the model. For every permutation test, the class labels were randomly assigned to different samples. The permutation test was repeated hundred times to obtain a distribution of classification expected to be non-significant.

### 2.5.3. Orthogonal projections to study the influence of the excipients

Protein formulations usually require excipients, such as buffers (here histidine, phosphate, or TRIS), lyo-, and/or cryoprotectants (here, sucrose and PEG), because of their delicate physical stability. As we directly use the unprocessed Raman spectra of a freeze-dried formulation (without the usual blank subtraction), we have to investigate the influence of the excipient signals on the discriminating power of the model. Therefore, we applied an orthogonal projection approach [21–24]. The contributions within the variable space of the calibration matrix  $\mathbf{X}$  (containing the spectra of the protein formulations) are originating from the pure protein signals ( $\mathbf{X}_p$ ), interferences such as the excipient signals ( $\mathbf{X}_b$ ) and other undefined spectral variance ( $\varepsilon$ ) (Eq. (1))

$$\mathbf{X} = \mathbf{X}_p + \mathbf{X}_b + \varepsilon \quad (1)$$

In practice, the interference space  $\mathbf{X}_b$  was estimated via an external data set containing only the Raman spectra of the freeze-dried blanks ( $\mathbf{B}$ ) of all possible formulations used in the data set (Table 1 and Fig. 1) [21]. The column vectors of the so obtained matrix  $\mathbf{B}$  form a basis of the detrimental subspace. To remove those variations in  $\mathbf{X}$  originating purely from excipients signals, an orthogonal projector to  $\mathbf{B}$ , i.e.,  $\mathbf{P}_B^\perp$ , can be calculated. This corrects  $\mathbf{X}$  as follows (Eq. (2)) to obtain  $\mathbf{X}^*$

$$\mathbf{X}^* = \mathbf{X}\mathbf{P}_B^\perp = \mathbf{X}(\mathbf{I} - \mathbf{B}(\mathbf{B}^T\mathbf{B})^{-1}\mathbf{B}^T) \quad (2)$$

where  $\mathbf{I}$  is the identity matrix.

Thus, the algorithm finds the dimensions of the spectral space which are affected by the studied excipients and projects the spectra orthogonal to this variation. After the orthogonalization

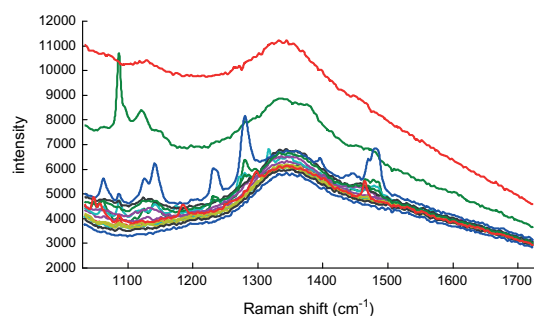


**Fig. 1.** Raman spectra of the blanks of the investigated formulations. (For interpretation of the references to color in this figure legend, the reader is referred to the web version of this article.)

procedure, it can be assessed whether the discrimination and the classification between freeze-dried formulations with native-like and non-native proteins are affected, this way revealing the influence of the removed factor [22].

## 3. Results and discussion

### 3.1. Generation of a relevant data set

Whether and to which extent a protein will lose its native conformation depends upon the environmental conditions it is exposed to and can be very erratic. Therefore, a relevant data set to study whether there can be discriminated between native-like and non-native states of proteins in freeze-dried formulations should cover sufficient native-like samples, as well as a distribution of denatured types (i.e., from mildly to more strongly stressed) obtained by freeze-drying. Therefore, the freezing method, secondary drying temperature, and formulation composition were varied to yield different relevant examples of native-like (further called NL) and non-native or denatured (further called DEN) LDH in freeze-dried formulations (Tables 1 and 2). An ANOVA was performed on the % LDH activity recovery of the 96 DoE samples, to investigate the influence of five process and formulation parameters on the preservation of the native protein conformation after reconstitution of the freeze-dried product (Table 3). Three factors, i.e., freezing method, buffer type, and sucrose addition, showed statistically significant effects ( $\alpha = 0.05$ ) on the % LDH activity recovery. Slow cooling showed a negative effect (i.e., it showed the lowest activities) on the % LDH activity recovery compared to the other tested cooling methods. The use of phosphate buffer showed a negative effect compared to the others, and the addition of 5% sucrose as a protectant to the formulation positively affected the LDH activity preservation.

### 3.2. FTIR as a reference technique to assign class labels

Since FTIR easily allows analysis in the solid freeze-dried state, is well known and frequently used, and is complementary to Raman spectroscopy, this technique was chosen as a reference for obtaining information on the protein conformation in the freeze-dried samples. To assign class membership labels (i.e., NL and DEN) to the samples, a two-step approach was used. First, we

**Table 3**

Factor level space of the studied process and formulation variables, their mean response per factor level and their significance on the % LDH activity preservation.

Factor	Unit	Levels	Mean response	p Value
Freezing method (A)	–	SL	78.89	0.003 <sup>*</sup>
		FA	88.94	
		ANN	90.16	
		CH	89.28	
Secondary drying temperature (B)	°C	5	85.19	0.174
		40	88.44	
Buffer type (C)	–	HIS	91.34	<0.001 <sup>*</sup>
		PHOS	79.63	
		TRIS	89.48	
Sucrose addition (D)	%	0	78.24	<0.001 <sup>*</sup>
		5	95.40	
PEG addition (E)	%	0	86.68	0.908
		1	86.96	

Abbreviations: SL = slow cooling, FA = fast cooling, ANN = annealing, CH = cooling hold, HIS = histidine buffer, PHOS = phosphate buffer, TRIS = TRIS buffer.

<sup>\*</sup> Significant effect ( $\alpha = 0.05$ ).

visually compared the experimental versus the native reference amide I FTIR spectrum to assign each sample to a class. Next, we performed a PCA on the spectra of the complete labeled sample set to independently confirm the correctness of the initial class labeling.

Changes in the distribution of secondary structures of freeze-dried proteins are most commonly assessed by visual comparison of the second derivative of the amide I band ( $1700\text{--}1600\text{ cm}^{-1}$ ) in the blank corrected FTIR spectra of the sample with a native reference spectrum [10,15,25–30]. Freeze-dried formulations were designated as NL if the amide I spectrum was similar (in secondary structural elements distribution) to that of the native LDH before freeze-drying (Fig. 2). The amide I region of native LDH indicated primarily alpha helix structures (near  $1658\text{ cm}^{-1}$ ), to a lesser extent beta-sheets (near  $1636\text{ cm}^{-1}$ ), and also a very small portion of intermolecular beta-sheets (near  $1620\text{ cm}^{-1}$ ), which is consistent with the literature [15]. The small frequency and intensity shifts of the main bands in their freeze-dried versus liquid form can be related to the altered hydration state of the protein molecules [10,31]. Since it was not possible to preserve the native state in the freeze-dried product without sucrose, the NL formulations contained sucrose. Membership to the NL class was defined by two criteria: (1) no clear changes in the distribution of the native secondary structural elements and (2) no clear formation of non-native structures, compared to the native state spectrum.

Freeze-dried samples showing signs of not preserving the fully native structure were designated as DEN. As protein denaturation in the freeze-dried product was diverse, some examples of the amide I FTIR spectra of DEN proteins are shown in Fig. 3. They are compared to the average of five native-like freeze-dried LDH formulations (bold dotted black line). Non-native LDH in the freeze-dried state was the result of an altered  $\alpha/\beta$  ratio (i.e., clear changes in the peak intensities near  $1658$  and  $1636\text{ cm}^{-1}$ ) or a decrease in these structures with the formation of non-native structures (i.e., clearly appearing peaks near  $1620\text{ cm}^{-1}$  and in the region  $1660\text{--}1680\text{ cm}^{-1}$ ) [10]. The samples, where the former phenomenon was mainly present, can be seen as mildly stressed since they still comprise largely of native secondary structures. Some examples are shown in Fig. 3A. The remaining LDH activity after reconstitution of these samples ranged between 90.3% and 108.9%, which may reflect their stronger tendency to refold back to the native conformation during reconstitution. Hence, they may provide a lower quality risk. Some of them had sucrose in their formulation, which probably helped preventing more excessive unfolding. Several DEN freeze-dried samples also showed clearly the presence of non-native structures in their amide I FTIR spectrum. Some examples with various % LDH activity recoveries in their reconstituted product are shown in Fig. 3B. Signals of non-na-

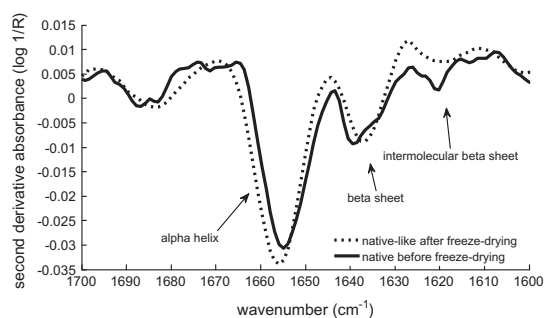


Fig. 2. Second derivative amide I FTIR spectrum of native LDH (in liquid) before freeze-drying (full line) and of native-like freeze-dried LDH (dotted line).

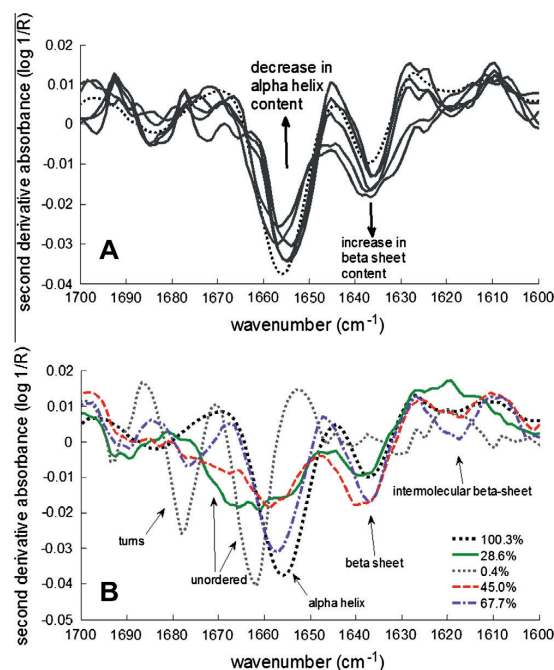
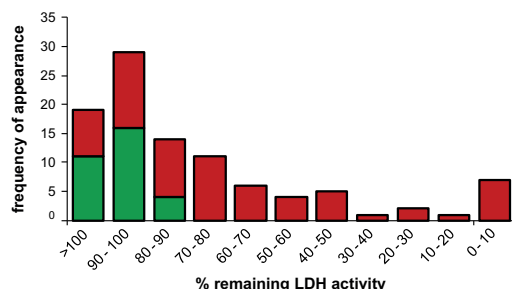


Fig. 3. Second derivative spectra of the amide I band (FTIR) of freeze-dried LDH formulations with different amounts of denaturation/unfolding. The black bold dotted line corresponds to native-like freeze-dried LDH. (A) Examples of mildly denatured freeze-dried LDH samples, having remaining LDH activities between 90.3% and 108.9% after reconstitution. (B) Examples of more denatured freeze-dried LDH samples, with formation of non-native secondary structures. Legend: % remaining LDH activity after reconstitution. (For interpretation of the references to color in this figure legend, the reader is referred to the web version of this article.)

tive structures appeared in the amide I FTIR spectra around  $1660\text{--}1680\text{ cm}^{-1}$  (turns and different unordered structures) and around  $1620\text{ cm}^{-1}$  (intermolecular  $\beta$ -sheets). Protein unfolding was also indicated by band broadening in these regions, where clear absorbance signals at particular wavenumbers are lost due to a fading of structural homogeneity among the protein population [32]. These samples will provide most likely the highest quality risk at the time of reconstitution, since the refolding of the protein to its native state may be more hampered or impossible [8]. This was also seen by their generally lower % LDH activity recovery after reconstitution.

The data set of 99 samples that was used for the exploratory analysis, model development, and model validation, comprised 31 NL and 68 DEN samples. Overall, the 99 freeze-dried formulations comprised a wide distribution of % LDH activity recoveries (Fig. 4). It can be seen that the reconstituted NL samples always had high % LDH activity recoveries (ranging from 88.1% to 109.3%), while those of DEN samples varied between 0.4% and 109.6%. The latter is the consequence of having different kinds of protein denaturation in the freeze-dried state, i.e., reversible and irreversible denaturation upon reconstitution. Both NL and DEN groups contained formulations with similar excipients (except samples formulated with NaSCN, NaCl, ethanol, and pure water that were always DEN), originating from the eight freeze-drying runs.

To independently confirm the visual assignment of the class labels to the samples, a PCA was performed on the full sample set constituting the same labeled amide I FTIR spectra as used for



**Fig. 4.** Histogram of the distribution of the 99 freeze-dried LDH samples in the data set according to their % remaining LDH activity after reconstitution. The divided bars display the conformational state of these samples in the freeze-dried cake, i.e., NL (green) or DEN (red). (For interpretation of the references to color in this figure legend, the reader is referred to the web version of this article.)

the visual interpretation. As spectral changes due to altered protein conformation largely exist in this set of samples, this type of systematic variation must be represented in the primary PCs. The separation among the scores of the NL and DEN samples in the PC1–PC2 scores plot (Fig. 5) was an independent justification for the correctness of the class labeling.

### 3.3. Raman spectroscopy: exploratory analysis and classification

To explore trends in the Raman spectra related to the conformational state of the LDH, PCA was performed on the Raman spectra of the data set of 99 samples. No pre-processing of the spectra was applied since different methods (i.e., standard normal variates, normalization, multiplicative scatter correction, Savitzky–Golay smoothing, and derivatives) did not improve the discrimination performance (data not shown). Different parts of the spectra within the 800–1800  $\text{cm}^{-1}$  range were assessed, since the range below 800  $\text{cm}^{-1}$  is known to be less sensitive for protein conformation [33]. The PC2–PC6 score plot of the Raman spectra in the range 1033–1725  $\text{cm}^{-1}$  showed for the majority of the samples, a discrimination between both NL and DEN states, but the scores of 5 DEN samples could not be differentiated from the NL group (Fig. 6).

The PLS–LDA model built from Raman spectra required 6 LVs and showed 5% (four samples) misclassifications in CV, while one sample of the 24 test set samples was classified wrongly. The discrimination performance of the PLS–LDA model before and after orthogonal projection of the matrix of blank spectra (**B**) to the 75 spectra of the calibration matrix (**X**) was unchanged (Table 4), which indicates that the model is able to predict the protein's con-

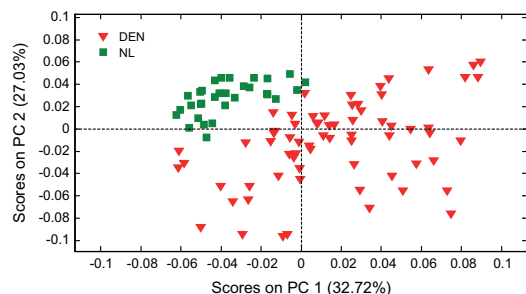


**Fig. 5.** PCA score plot (PC1–PC2) of the second derivative amide I FTIR spectra of the data set (99 samples) of freeze-dried LDH formulations. The spectra were mean centered before PCA. The spectra are independently labeled based on the visual interpretation of the amide I band (FTIR) as either NL (in green squares) or DEN (in red triangles). (For interpretation of the references to color in this figure legend, the reader is referred to the web version of this article.)

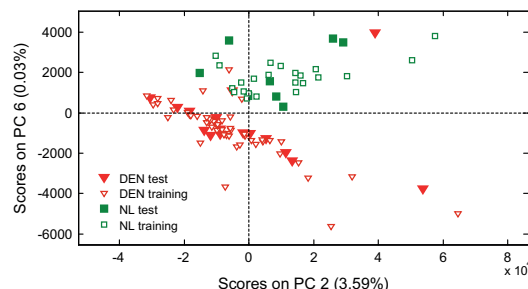


**Fig. 6.** PCA score plot (PC2–PC6) of the Raman spectra of the data set (99 samples) of the freeze-dried LDH formulations. The spectra were mean centered before PCA. The spectra are independently labeled based on the visual interpretation of the amide I band (FTIR) as either NL (in green squares) or DEN (in red triangles). The division of the samples in training and test set is visualized through filled and unfilled markers. (For interpretation of the references to color in this figure legend, the reader is referred to the web version of this article.)

**Table 4**

Performance of the PLS–LDA models built from Raman spectra.

Technique	Spectral region ( $\text{cm}^{-1}$ )	Number of PLS components	% Misclassifications in CV	% Misclassifications in test set
Raman	1033–1725	6	5	1/24
Raman blank corrected <sup>a</sup>	1033–1725	4	5	1/24

<sup>a</sup> After orthogonal projection to the blank matrix.

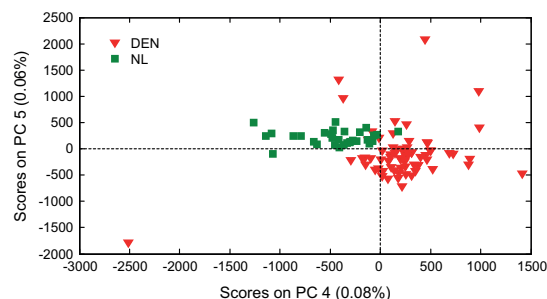


**Fig. 7.** PCA score plot of the Raman spectra after orthogonal projection to the blank matrix. (For interpretation of the references to color in this figure legend, the reader is referred to the web version of this article.)

formational state in the presence of this variation, while not being influenced by this variation. Hence, the signals of the tested excipients are not a confounding factor toward discrimination, neither positively nor negatively. Fig. 7 also shows that one is still able to discriminate for most of the samples between both NL and DEN states in a PCA score plot. This finding is of importance from a practical point of view. It implies that all the necessary information can be extracted from a single Raman spectrum of the sample and that no corresponding blanks (at least for the tested excipients) should be freeze-dried nor measured, while a blank correction is required for visual interpretation of Raman (and FTIR) spectra.

The wrongly classified samples were always mildly denatured LDH (see their amide I FTIR spectra in Fig. 3A). These samples were assigned as DEN by the reference technique, but were predicted by the model as NL samples. In these samples, it was mainly the  $\alpha/\beta$

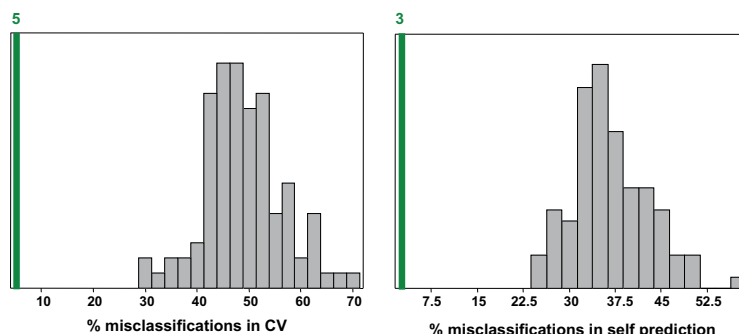


**Fig. 8.** Class prediction results (expressed as the % misclassifications) based on cross-validation (left) and self-prediction (right) of the training set with the original labeling (in green bold line) compared to the permuted data (gray histograms). (For interpretation of the references to color in this figure legend, the reader is referred to the web version of this article.)

ratio that was slightly changed, and almost no non-native structures were formed in the freeze-dried product. Their remaining LDH activities after reconstitution ranged between 90.3% and 108.9%. This is similar with those from NL samples, which implies that the denaturation is reversible upon reconstitution. These results suggest that the Raman model has lower sensitivity in detecting mildly denatured freeze-dried samples than the reference technique. It is indeed expected that when there is a continuum of states from NL to various kinds of DEN, there will be a limit for detecting first signs of protein denaturation. These results suggest that this limit is higher for the Raman model than for the visual interpretation of the FTIR spectra.

When comparing the number of misclassifications for the Raman model (in green) to the predictions of the models generated by the random permutations of the class labels, we noticed a clear distinction between the permutation distribution and the original classification (Fig. 8). When comparing the original classification with all the permutations, a  $p$  value of  $<0.001$  could be obtained at the 0.01 significance level, both for CV and self-prediction. This confirms that the classification is not based on spurious correlations but rather on consistent differences in spectral features between NL and DEN samples. It was studied whether these correlations could be linked to biochemical knowledge.

#### 3.4. Spectral regions responsible for discrimination

From Fig. 9, it was seen that the loading vector of PC6 and the discriminant vector of the PLS-LDA model had very similar shapes. PC6 described only 0.03% of the variation in the spectra, which means that there is a lot of other variation in the Raman spectra, not responsible for the discrimination between both classes (e.g., light scattering, physical and environmental effects, instrumental effects, etc.) [23,34]. Yet the loading vector of PC6 or the discriminant vector can be informative for studying the most important variables responsible for the discrimination. They indicated that the NL and DEN samples have maximum differences in the following regions of the Raman spectrum: (i) near  $1070\text{ cm}^{-1}$  (C–N stretch), (ii) near  $1130\text{ cm}^{-1}$  ( $\text{NH}_3$  deformation), (iii)  $1200\text{--}1320\text{ cm}^{-1}$  (amide III), and (iv)  $1320\text{--}1500\text{ cm}^{-1}$  (mainly  $\text{CH}_n$  non-stretching with possible participations of CN and CC stretching). Surprisingly, the amide I band ( $1600\text{--}1700\text{ cm}^{-1}$ ) was only slightly indicated. As the indicated bands comprised both backbone (i.e., amide III) and side chain sensitive regions, we tried to link them with biochemical knowledge. Therefore, we also visually inspected the blank corrected Raman spectra and the corresponding amide I FTIR spectra of some relevant NL and DEN samples (Fig. 10). When visually comparing the Raman spectra of those samples, we see that major spectral

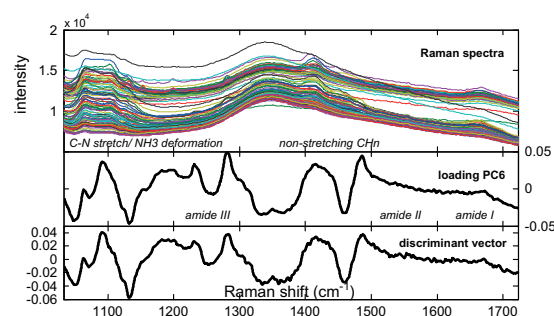


**Fig. 9.** Unprocessed Raman spectra of the data set (99 samples), the loading vector of the PC6 (0.03%) of the PCA, and the discriminant vector of the PLS-LDA model. (For interpretation of the references to color in this figure legend, the reader is referred to the web version of this article.)

differences between NL and DEN samples are manifested in similar spectral regions as indicated by the loading and discriminant vectors. To study more in depth the influence of the different regions (linked to certain biochemical knowledge) of the Raman spectrum, different PLS-LDA models were built using each of these spectral regions separately or combined.

##### 3.4.1. Backbone sensitive spectral regions

The amide I (peak with maximum near  $1665\text{ cm}^{-1}$ ) and III ( $1200\text{--}1320\text{ cm}^{-1}$ ) Raman bands are well known to be related to the protein's backbone conformations (secondary structural elements) [35,36]. Their shapes are the result of overlapping components corresponding to  $\alpha$ -helices,  $\beta$ -sheets, turns, and random structures. Therefore, broadening of the peak width and/or differences in shape of the amide I and III bands suggest an altered distribution of secondary structures (native and/or non-native) [35–38]. However, among the PLS-LDA models built from different separate amide ranges (Table 5), the ones using the amide I and II bands showed a very high number of misclassifications, both for CV and for test set prediction. It confirms the knowledge that the amide II Raman band has little sensitivity for protein secondary structure determination [35,39]. This was also seen in Fig. 10A when visually inspecting the amide II band. Despite its very well-known sensitivity for protein secondary structures, the poor performance of the PLS-LDA model built from the amide I band indicates that this band is little suitable for differentiation between NL and DEN in the studied formulations. This is also noticed when visually inspecting the amide I bands in the blank corrected Raman



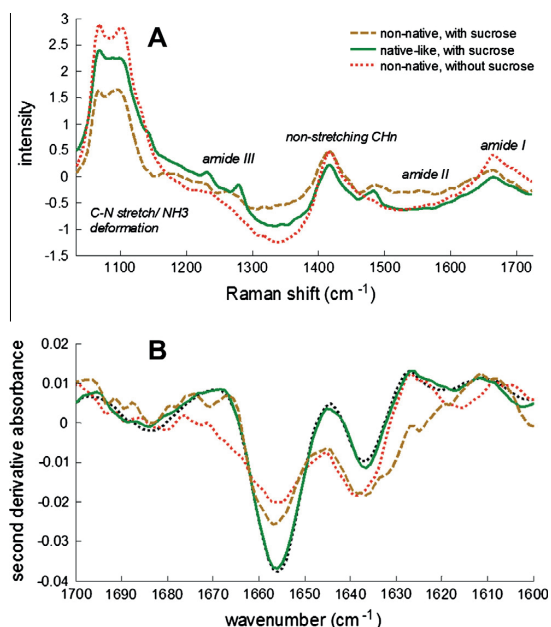


**Fig. 10.** Raman (A) and amide I FTIR (B) spectra of NL and DEN freeze-dried LDH samples. The Raman spectra were the result of the difference between the sample and corresponding blank spectra, and were subsequently Savitzky–Golay smoothed and normalized. The FTIR spectra were pre-processed as described in Methods and Materials. The black dotted line in (B) corresponds to the average spectrum of 5 NL freeze-dried LDH formulations. (For interpretation of the references to color in this figure legend, the reader is referred to the web version of this article.)

spectra (Fig. 10A). The amide I band of a DEN sample in a sucrose containing formulation resembles more that of a NL sample with sucrose than that of a DEN sample without sucrose. It is well known that co-lyophilized mixtures of sucrose and polymers (e.g., proteins) interact at a molecular level through hydrogen bonding, forming miscible amorphous molecular dispersions [40–42]. As there is evidence that the C=O stretching vibration is strongly influenced by the polymer–sucrose hydrogen bond [40], it is expected that this will notably influence the amide I band, typically dominated by signals of the backbone C=O stretching vibrations. Thus, the strong influence of the extent of hydrogen bonding of the protein with the environment (i.e., hydration state) on the amide I Raman band is here possibly the reason for the modest discrimination between NL and DEN when only considering this band. Among the tested backbone sensitive regions, the amide III band clearly showed being the most suitable for building the model.

**Table 5**

Performance of the PLS–LDA models built from smaller spectral (or fused) regions of the Raman spectra assigned to certain protein information.

Spectral region		Number of PLS components	% Misclassifications in CV	% Misclassifications in test set
Band assignment	Wavenumber (cm <sup>-1</sup> )			
Amide I	1600–1700	5	33	7/24
Amide II	1500–1600	8	23	12/24
Amide III	1200–1320	6	7	2/24
Backbone sensitive regions fused <sup>a</sup>		6	5	2/24
CH <sub>n</sub> non-stretch	1320–1500	5	7	2/24
C–N stretch + NH <sub>3</sub> deformation	1033–1200	4	5	3/24
Side chain sensitive regions fused <sup>b</sup>		6	5	1/24

<sup>a</sup> Fusion of the amide I–III regions.

<sup>b</sup> Fusion of the CH<sub>n</sub> non-stretch, C–N stretch and NH<sub>3</sub> deformation regions.

### 3.4.2. Side chain sensitive spectral regions

In Fig. 10A, there were also significant differences between NL and DEN samples in the spectral regions related to some amino acid side chains, i.e., the bands 1320–1500 cm<sup>-1</sup>, and near 1130 cm<sup>-1</sup> and 1070 cm<sup>-1</sup> [35,43]. This matches again with the variables indicated by the loading and discriminant vectors. The performances of the PLS–LDA models built from these separate side chain sensitive regions are shown in Table 5 and could further improve when combining the different regions. Major changes in the CH<sub>n</sub> non-stretching region (1320–1500 cm<sup>-1</sup>) were linked to a change in “exposure” of the hydrophobic amino acid residues to the outer surface, i.e., buried versus exposed to the environment, as they were likewise assigned for heat-denatured proteins [35]. This can be considered as an indication of protein unfolding, since hydrophobic residues will be buried in a natively folded protein, yet a larger fraction of them will be exposed in the partially unfolded states. Wang et al. [44] also found drastic changes in the 1050–1200 cm<sup>-1</sup> region of heat-denatured insulin and attributed this to protein unfolding.

### 3.4.3. Combined spectral regions

The classification performance of the PLS–LDA models built from fused backbone or side chain sensitive spectral regions surpassed those from single isolated bands (Table 5). Overall, the models considering the fused side chain sensitive regions and the full range (1033–1725 cm<sup>-1</sup>) (Table 4) showed the highest accuracy. The latter model was preferred because it combines information from complementary sources, i.e., backbone (i.e., amide III) and side chain sensitive regions.

## 4. Conclusions

This study, performed on a data set containing NL and a wide distribution of DEN states, demonstrated that Raman spectroscopy with 95% accuracy is able to rapidly and directly discriminate between NL and DEN states of LDH in various freeze-dried formulations. Misclassifications were always the result of assigning mildly (and reversible) DEN samples (with minimal changes in secondary structure detected by the reference technique) to the NL class. Hence, the sensitivity to detect minimal signs of protein denaturation is lower than the chosen reference approach. Therefore, the sensitivity of the Raman model should be further investigated with appropriate data sets. For instance, further research should include the following: (1) What is the limit for detecting first signs of protein denaturation by the Raman model? (2) How can sensitivity be improved? and (3) What is an acceptable criterion for this limit considering the intended (i.e., future in-line) use of the model? Also, further testing of the model performance on samples from novel batches is still required. This feasibility study suggests positive outlooks for Raman spectroscopy for the direct and automated analysis of the investigated quality attribute.

However, as one analytical method can never fully characterize the conformational state of proteins, the proposed method rather aims giving a *quality indication*. The speed and automatic nature of the method advocate that a transfer of the Raman model to in-line and real-time diagnostic use during freeze-drying processes may be a possible future step.

### Acknowledgements

SP is funded as an aspirant of the Research Foundation-Flanders (FWO). She would also like to thank the same institution and Irstea for the funding and hosting, respectively, of a research stay. MD and LH thank the Agency for Innovation by Science and Technology (IWT) for financial support.

### References

- [1] <www.fda.gov/downloads/Drugs/.../Guidances/ucm070305.pdf> (accessed 26.10.12).
- [2] T. De Beer, A. Burggraef, M. Fonteyne, L. Saerens, J.P. Remon, C. Vervaet, Near-infrared and Raman spectroscopy for the in-process monitoring of pharmaceutical production processes, *Int. J. Pharm.* 417 (2011) 32–47.
- [3] N.C. Dingari, G.L. Horowitz, J.W. Kang, R.R. Dasari, I. Barman, Raman spectroscopy provides a powerful diagnostic tool for accurate determination of albumin glycation, *PLoS One* 7 (2012) 1–11.
- [4] B. Li, P.W. Ryan, B.H. Ray, K.J. Leister, N.M.S. Sirimuthu, A.G. Ryder, Rapid characterization and quality control of complex cell culture media solutions using Raman spectroscopy and chemometrics, *Biotechnol. Bioengin.* 107 (2010) 290–301.
- [5] J.J. Hill, E.Y. Shalae, G. Zografi, Thermodynamic and dynamic factors involved in the stability of native protein structure in amorphous solids in relation to levels of hydration, *J. Pharm. Sci.* 94 (2005) 1636–1667.
- [6] J.C. Kasper, W. Friess, The freezing step in lyophilization: physico-chemical fundamentals, freezing methods and consequences on process performance and quality attributes of biopharmaceuticals, *Eur. J. Pharm. Biopharm.* 78 (2011) 248–263.
- [7] J.F. Carpenter, M.J. Pikal, B.S. Chang, T.W. Randolph, Rational design of stable lyophilized protein formulations: some practical advice, *Pharm. Res.* 14 (1997) 969–975.
- [8] S.K. Niazi, Handbook of Biogeneric Therapeutic Proteins: Regulatory, Manufacturing, Testing, and Patent Issues, Informa Healthcare, St Helier, Jersey, 2005, pp. 265–289.
- [9] S. Pieters, T. De Beer, J.C. Kasper, D. Boulpaep, O. Waszkiewicz, M. Goodarzi, C. Tistaert, W. Friess, J.P. Remon, C. Vervaet, Y. Vander Heyden, Near-infrared spectroscopy for in-line monitoring of protein unfolding and its interactions with lyoprotectants during freeze-drying, *Anal. Chem.* 84 (2012) 947–955.
- [10] A. Barth, C. Zscherp, What vibrations tell us about proteins, *Q. Rev. Biophys.* 35 (2002) 369–430.
- [11] S. Mangialardo, F. Piccirilli, A. Perucchi, P. Dore, P. Postorino, Raman analysis of insulin denaturation induced by high-pressure and thermal treatments, *J. Raman Spectrosc.* 43 (2012) 692–700.
- [12] A.A. Elkordy, R.T. Forbes, B.W. Barry, Study of protein conformational stability and integrity using calorimetry and FT-Raman spectroscopy correlated with enzymatic activity, *Eur. J. Pharm. Sci.* 33 (2008) 177–190.
- [13] R. Tuma, Raman spectroscopy of proteins: from peptides to large assemblies, *J. Raman Spectrosc.* 36 (2005) 307–319.
- [14] R. Bro, Multivariate calibration: what is in chemometrics for the analytical chemist?, *Anal. Chim. Acta* 500 (2003) 185–194.
- [15] A. Al-Hussein, H. Gieseler, The effect of mannitol crystallization in mannitol-sucrose systems on LDH stability during freeze-drying, *J. Pharm. Sci.* 101 (2012) 2534–2544.
- [16] www.sigmaaldrich.com/etc/medialib/docs/Sigma/Enzyme\_Assay/I2500enz.Par.0001.File.tmp/I2500enz.pdf.
- [17] B.G.M. Vandeginste, D.L. Massart, L.C.M. Buydens, S. De Jong, P.J. Lewi, J. Smeyers-Verbeke, Handbook of Chemometrics and Qualimetrics: Part B, Elsevier Science, Amsterdam, 1998, pp. 87–160.
- [18] R.A. Fisher, The use of multiple measurement in taxonomic problems, *Ann. Eugen.* 7 (1936) 179–188.
- [19] M. Barker, W. Rayens, Partial least squares for discrimination, *J. Chemom.* 17 (2003) 166–173.
- [20] J.A. Westerhuis, H.C.J. Hoefsloot, S. Smit, D.J. Vis, A.K. Smilde, E.J.J. van Velzen, J.P.M. van Duijnhoven, F.A. van Dorsten, Assessment of PLS-DA cross validation, *Metabolomics* 4 (2008) 81–89.
- [21] E.T.S. Skibsted, H.F.M. Boelens, J.A. Westerhuis, A.K. Smilde, N.W. Broad, D.R. Rees, D.T. Witte, Net analyte signal based statistical quality control, *Anal. Chem.* 77 (2005) 7103–7114.
- [22] C.L. Hansen, F. van den Berg, M.A. Rasmussen, S.B. Engelsen, S. Holroyd, Detecting variation in ultrafiltrated milk permeates – infrared spectroscopy signatures and external factor orthogonalization, *Chemom. Intell. Lab. Syst.* 104 (2010) 243–248.
- [23] R.C. Pinto, J. Trygg, J. Gottfries, Advantages of orthogonal inspection in chemometrics, *J. Chemom.* 26 (2011) 231–235.
- [24] J.C. Boulet, J.M. Roger, Pretreatments by means of orthogonal projections, *Chemom. Intell. Lab. Syst.* 117 (2012) 61–69.
- [25] J.T. Peltton, L.R. McLean, Spectroscopic methods for analysis of protein secondary structure, *Anal. Biochem.* 277 (2000) 167–176.
- [26] P.I. Harris, F. Severcan, FTIR spectroscopic characterization of protein structure in aqueous and non-aqueous media, *J. Mol. Catal. B: Enzymatic* 7 (1999) 207–221.
- [27] J. Kong, S. Yu, Fourier transform infrared spectroscopic analysis of protein secondary structures, *Acta Biochim. Biophys. Sinica* 39 (2007) 549–559.
- [28] A. Dong, S.J. Pestrelski, S.D. Allison, J.F. Carpenter, Infrared spectroscopic studies on lyophilization- and temperature-induced protein aggregation, *J. Pharm. Sci.* 84 (1995) 415–424.
- [29] K. Izutsu, N. Aoyagi, S. Kojima, Protection of protein secondary structure by saccharides of different molecular weights during freeze-drying, *Chem. Pharm. Bull.* 52 (2004) 199–203.
- [30] M. Jackson, H.H. Mantsch, The use and misuse of FTIR spectroscopy in the determination of protein structure, *Crit. Rev. Biochem. Mol. Biol.* 30 (1995) 95–120.
- [31] S.T.R. Walsh, R.P. Cheng, W.W. Wright, D.O.V. Alonso, V. Daggett, J.M. Vanderkooi, W.F. Degrad, The hydration of amides in helices: a comprehensive picture from molecular dynamics, IR, and NMR, *Protein Sci.* 12 (2003) 520–531.
- [32] S.D. Allison, T.D. Randolph, M.C. Manning, K. Middleton, A. Davis, J.F. Carpenter, Effects of drying methods and additives on structure and function of Actin: mechanisms of dehydration-induced damage and its inhibition, *Arch. Biochem. Biophys.* 358 (1998) 171–181.
- [33] A.M. Herrero, Raman spectroscopy for monitoring protein structure in muscle food systems, *Crit. Rev. Food Sci. Nutr.* 48 (2008) 512–523.
- [34] K. Kjeldahl, R. Bro, Some common misunderstandings in chemometrics, *J. Chemom.* 24 (2010) 558–564.
- [35] A.M. Herrero, F. Jiménez-Colmenero, P. Carmona, Elucidation of structural changes in soy protein isolate upon heating by Raman spectroscopy, *Int. J. Food Sci. Technol.* 44 (2009) 711–717.
- [36] N.C. Maiti, M.M. Apetri, M.G. Zagorski, P.R. Carey, V.E. Anderson, Raman spectroscopic characterization of secondary structure in natively unfolded proteins:  $\alpha$ -synuclein, *J. Am. Chem. Soc.* 126 (2004) 2399–2408.
- [37] A. Hédoux, L. Paccou, S. Achir, Y. Guinet, In situ monitoring of proteins during lyophilization using micro-Raman spectroscopy: a description of structural changes induced by dehydration, *J. Pharm. Sci.* 101 (2012) 2316–2326.
- [38] N.C. Maiti, M.M. Apetri, M.G. Zagorski, P.R. Carey, V.E. Anderson, Raman spectroscopic characterization of secondary structure in natively unfolded proteins:  $\alpha$ -synuclein, *J. Am. Chem. Soc.* 126 (2004) 2399–2408.
- [39] R. Tantipolphan, T. Rades, N.J. Medlicott, Insights into the structure of proteins by vibrational spectroscopy, *Curr. Pharm. Anal.* 4 (2008) 53–68.
- [40] L.S. Taylor, G. Zografi, Sugar-polymer hydrogen bond interactions in lyophilized amorphous mixtures, *J. Pharm. Sci.* 87 (1998) 1615–1621.
- [41] T.W. Randolph, Phase separation of excipients during lyophilization: effects on protein stability, *J. Pharm. Sci.* 86 (1997) 1198–1203.
- [42] S.D. Allison, B. Chang, T.W. Randolph, J.F. Carpenter, Hydrogen bonding between sugar and protein is responsible for inhibition of dehydration induced protein unfolding, *Arch. Biochem. Biophys.* 365 (1999) 289–298.
- [43] D. Ostrovskii, P. Jacobsson, B. Nystrom, O. Marstokk, H.B.M. Kopperud, Raman spectroscopic characterization of association and thermoreversible gelation in aqueous systems of poly(N-acetamidoacrylamide), *Macromolecules* 32 (1999) 5552–5560.
- [44] M. Wang, M. Benford, N. Jing, G. Coté, J. Kameoka, Optofluidic device for ultra-sensitive detection of proteins using surface-enhanced Raman spectroscopy, *Microfluid. Nanofluid.* 6 (2009) 411–417.

### 4.3. References

- [1] J.T. Pelton, L.R. McLean, Spectroscopic methods for analysis of protein secondary structure, *Anal. Biochem.* 277 (2000) 167-176.
- [2] A.M. Herrero, F. Jiménez-Colmenero, P. Carmona, Elucidation of structural changes in soy protein isolate upon heating by Raman spectroscopy, *Int. J. Food Sci. Technol.* 44 (2009) 711-717.
- [3] Z.Q. Wen, Raman spectroscopy of protein pharmaceuticals, *J. Pharm. Sci.* 96 (2007) 2861-2878.
- [4] S.M. Choi, C.Y. Ma, Structural characterization of globulin from common buckwheat (*Fagopyrum esculentum* Moench) using circular dichroism and Raman spectroscopy, *Food Chem.* 102 (2007) 150-160.
- [5] R. Tantipolphan, T. Rades, N.J. Medlicott, Insights into the structure of protein by vibrational spectroscopy, *Curr. Pharm. Anal.* 4 (2008) 53-68.
- [6] A.M. Herrero, Raman spectroscopy for monitoring protein structure in muscle food systems, *Crit. Rev. Food Sci. Nutr.* 48 (2008) 512-523.
- [7] E.G. Ferrer, A.V. Gomez, M.C. Anon, M.C. Puppo, Structural changes in gluten protein structure after addition of emulsifier. A Raman spectroscopy study, *Spectrochim. Acta A* 79 (2011) 278-281.
- [8] N.C. Maiti, M.M. Apetri, M.G. Zagorski, P.R. Carey, V.E. Anderson, Raman spectroscopic characterization of secondary structure in natively unfolded proteins:  $\alpha$ -synuclein, *J. Am. Chem. Soc.* 126 (2004) 2399-2408.
- [9] G.J. Thomas Jr., D.A. Agard, Quantitative analysis of nucleic acids, proteins, and viruses by Raman band deconvolution, *Biophys. J.* 46 (1984) 763-768.
- [10] S.D. Yeo, P.G. Debenedetti, S.Y. Patro, T.D. Przybycien, Secondary structure characterization of microparticulate insulin powders, *J. Pharm. Sci.* 83 (1994) 1651-1656.
- [11] M.N. Kinalwa, E.W. Blanch, A.J. Doig, Accurate determination of protein secondary structure content from Raman and Raman optical activity spectra, *Anal. Chem.* 82 (2010) 6347-6349.
- [12] S.U. Sane, R. Wong, C.C. Hsu, Raman spectroscopic characterization of drying-induced structural changes in a therapeutic antibody: correlating structural changes with long-term stability, *J. Pharm. Sci.* 93 (2004) 1005-1018.
- [13] V.L. Brewster, L. Ashton, R. Goodacre, Monitoring guanidinium-induced structural changes in ribonuclease proteins using Raman spectroscopy and 2D correlation analysis, *Anal. Chem.* 85 (2013) 3570-3575.
- [14] M. Gniadecka, O. F. Nielsen, S. Wessel, M. Heidenheim, D.H. Christensen, H.C. Wulf, Water and protein structure in photoaged and chronically aged skin, *The journal of investigative dermatology* 111 (1998) 1129-1133.
- [15] J. Fontecha, J. Bellanato, M. Juarez, Infrared and Raman spectroscopic study of casein in cheese: Effect of freezing and frozen storage, *J. Dairy Sci.* 76 (1993) 3303-3309.
- [16] S. Mangialardo, F. Piccirilli, A. Perucchi, P. Dore, P. Postorino, Raman analysis of insuline denaturation induced by high-pressure and thermal treatments, *J. Raman Spectrosc.* 43 (2012) 692-700.

- [17] J.A. Seo, A. Hédoux, Y. Guinet, L. Paccou, F. Affouard, A. Lerbret, M. Descamps, Thermal denaturation of beta-lactoglobulin and stabilization mechanism by trehalose analyzed from Raman spectroscopy investigations, *J. Phys. Chem. B* 114 (2010) 6675-6684.
- [18] A.M. Herrero, P. Carmona, M. Careche, Raman spectroscopic study of structural changes in Hake (*Merluccius merluccius* L.) Muscle Proteins during frozen storage, *J. Agric. Food Chem.* 52 (2004) 2147-2153.
- [19] R. Bro, Multivariate calibration: What is in chemometrics for the analytical chemist?, *Anal. Chim. Acta* 500 (2003) 185-194.
- [20] A.C. Olivieri, N.M. Faber, J. Ferré, R. Boqué, J.H. Kalivas, H. Mark, Uncertainty estimation and figures of merit for multivariate calibration, *Pure Appl. Chem.* 78 (2006) 633-661.
- [21] T.M. Przybycien, J.P. Dunn, P. Valax, G. Georgiou, Secondary structure characterization of  $\beta$ -lactamase inclusion bodies, *Protein Eng.* 7 (1994) 131-136.
- [22] R. Tuma, Raman spectroscopy of proteins: from peptides to large assemblies, *J. Raman Spectrosc.* 36 (2005) 307-319.
- [23] I. Barman, N.C. Dingari, J. W. Kang, G.L. Horowitz, R.R. Dasari, M.S. Feld, Raman spectroscopy-based sensitive and specific detection of glycated hemoglobin, *Anal. Chem.* 84 (2012) 2474-2482.
- [24] B. Li, P.W. Ryan, B.H. Ray, K.J. Leister, N.M.S. Sirimuthu, A.G. Ryder, Rapid characterization and quality control of complex cell culture media solutions using Raman spectroscopy and chemometrics, *Biotechnol. Bioengin.* 107 (2010) 290-301.
- [25] S.K. Teh, W. Zheng, K.Y. Ho, M. Teh, K.G. Yeoh, Z. Huang, Near-infrared Raman spectroscopy for early diagnosis and typing of adenocarcinoma in the stomach, *British J. Surgery* 97 (2010) 550-557.



---

## Chapter 5: MEASURING PROTEIN UNFOLDING IN RAMAN SPECTRA IN THE PRESENCE OF INTERFERENCES

---

### 5.1. Introduction

In the previous chapter, PCA and the high accuracy of the initial Partial Least Squares - Linear Discriminant Analysis (PLS-LDA) classification model confirmed that Raman spectroscopy can supply multivariate predictive spectral variation to discriminate between NL and DEN conformational states of the model protein LDH in freeze-dried formulations. The MVA allowed obtaining the information of interest directly and automatically from the experimentally obtained spectra. This is an absolute requirement for enabling the further use of the technique as an in-line and real-time monitoring tool during the freeze-drying process. However, during the intended usage of the Raman model (i.e. when the CQA needs to be predicted in new specimens, regardless whether this is in-line or off-line), new spectral variations may arise in the acquired Raman spectra. Such spectral variations can be the result of varying physical, chemical, instrumental, experimental or process factors. For instance, the experimental Raman spectra from the model protein exhibited a large background, originating from non-Raman effects. To ensure reliable classification for all future samples (where such variations are prone to happen), it should be investigated whether, in such circumstances, one is still able to classify the protein conformational state correctly, thus without compromised accuracy. In other words, to develop a robust multivariate model, one must anticipate all expected future variations and consider them when developing and validating the model [1].

### 5.2. The robustness of multivariate calibration (MVC) models

The linear MVC, including PLS and other inverse linear MVC methods, can be generally written as follows (eq. 5.1).

$$\mathbf{y} = b_0 + \mathbf{Xb} + \mathbf{E} \quad (5.1)$$

where  $\mathbf{E}$  is the matrix of residuals to the model.

Using Eq. 5.1, one estimates the regression parameters of the model, i.e.  $b_0$  (intercept, which is 0 when data are mean centered) and  $\mathbf{b}$  by relating  $\mathbf{y}$  ( $n$  quality responses) to  $\mathbf{X}$  ( $n$  calibration spectra). This implies that any correlation between  $\mathbf{X}$  and  $\mathbf{y}$  will be picked up, regardless the origin. Therefore, it is important to ensure that all possible future variations are fully (i.e. every type of variation and its full expected range of variation) considered when developing a robust MVC model [1-2].

Variations in factors (other than the one of interest) that influence the spectral response may add a perturbation, i.e.  $\delta\mathbf{x}$ , to a sample spectrum. This will yield an error in its predicted response (eq. 5.2).

$$\delta\hat{y} = \delta\mathbf{x}^T \mathbf{b} \quad (5.2)$$

Geometrically, the robustness problem in linear MVC can be represented as follows (eq. 5.3 and Fig. 5.1).

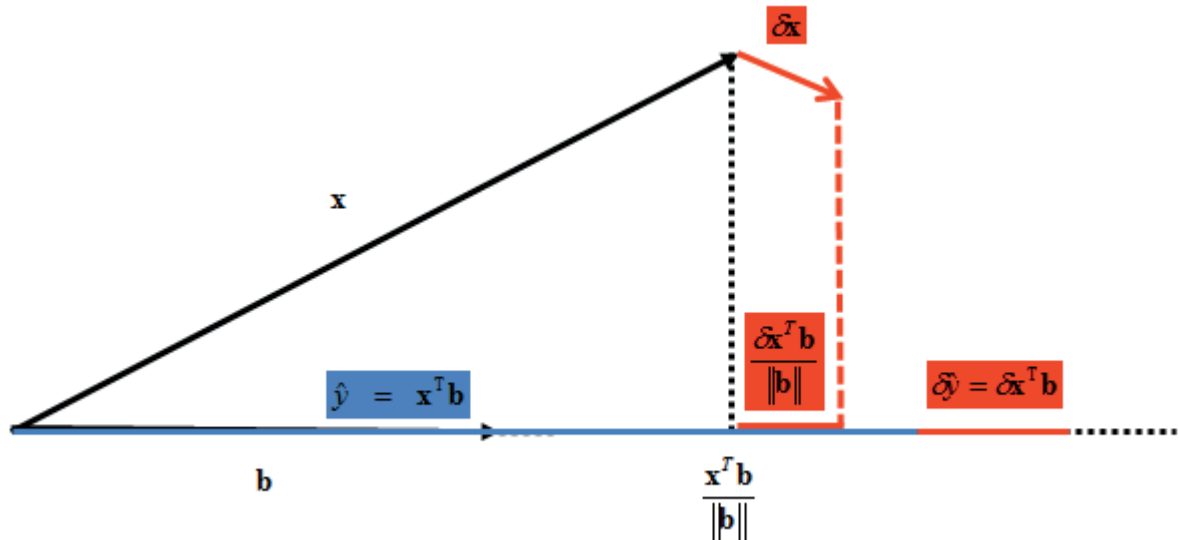


Fig. 5.1. Geometrical representation of inverse MVC and its robustness problem.

$$|\delta\hat{y}| = \|\delta\mathbf{x}\| \|\mathbf{b}\| |\cos(\delta\mathbf{x}, \mathbf{b})| \quad (5.3)$$

Thus,  $|\delta\mathbf{y}|$  can be reduced by minimization of one or more of the three terms of the right hand side of eq. 5.3. In other words, to increase robustness of MVC models one might (1) a priori remove known interfering perturbations from the spectra (i.e. spectral pre-processing to reduce the  $\|\delta\mathbf{x}\|$  term), (2) fully consider the perturbations in the calibration spectra (i.e. to reduce the  $\|\mathbf{b}\|$  term), or (3) project the calibration spectra, holding the informative features, onto a subspace being orthogonal to a basis containing an estimation of  $\delta\mathbf{x}$  (i.e.  $|\cos(\delta\mathbf{x}, \mathbf{b})|$  is reduced and is ideally  $\cos 90^\circ=0$ ) [3].

Thus, one possibility to make MVC models more robust is by removing a priori known spectral variations from  $\mathbf{X}$  that might interfere with the desired prediction (e.g. by background correction, blank correction, scatter correction). In the literature, the removal or standardization of background contributions in the experimentally obtained Raman spectra prior to modeling has been proposed by various spectral pre-processing methods (e.g. using interpolation baseline correction methods, (Extended) Multiplicative Scatter Correction or (E)MSC, Standard Normal Variates or SNV, ...) [4]. Several spectral pre-processing methods (SNV, MSC, normalization, derivatives, smoothing) were tested in **chapter 4** but did not improve the model performance (they rather decreased it). Interpolation methods estimate the baseline prior to subtraction from the spectrum. However, such baseline removal may introduce artifacts when estimating the baseline. Among different baseline correction methods, the lowest prediction errors in MVC models were obtained when using singular value decomposition (SVD)-based linear interpolation [4]. This method estimates the non-Raman background by performing an SVD on the raw data. The PC loadings that exhibit a significant background are visually identified based on relative band widths. Linear interpolation is then used on the selected loadings to estimate the non-Raman background, using 25-30 points defined for each loading. The estimated backgrounds are then scaled using the PCA scores and summed before subtraction from the original spectra [5].

When fully considering each type of interfering spectral variation in the calibration, a robust model can generally be obtained, as PLS (and other inverse) MVC methods can selectively model the variation of interest in the presence of multiple interferences [2, 6]. However, exhaustive calibration can increase the model development time and costs significantly, as more time and resources (e.g. reference analyses) have to be invested to model the interfering sources of variation. When there are a lot of different sources leading to spectral variations the model complexity may also increase.

Orthogonal projection methods can increase the model robustness by reducing the dimensions of the spectral variable space in  $\mathbf{X}$ . The aim is to find the subspace mainly containing variations related to  $\mathbf{y}$ . These methods rely on the fact that the spectral variable space contains a useful part (i.e. the Net Analyte Signal or is that part of the raw signal used for prediction of the attribute of interest) and a detrimental part (i.e. spanned by systematic variations of all interferences), being orthogonal to each other (Fig. 5.2.) [2-3, 7].

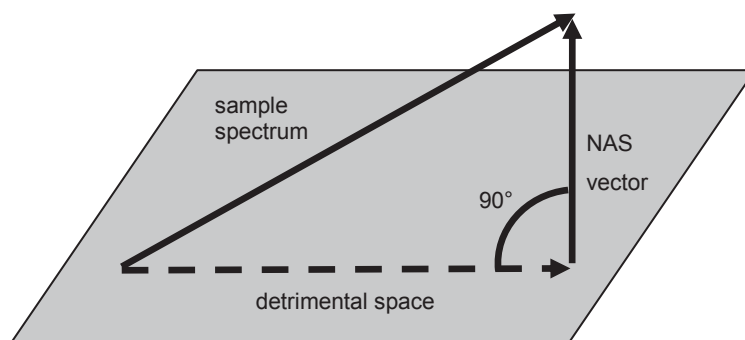


**Fig. 5.2.** Geometrical representation of the contributions of a sample spectrum, being the NAS vector and the space spanned by the interferences (Adapted from [2]).

In practice, the basis of the detrimental subspace is being estimated. This can be done, for instance, by using pure interferent spectra or information from an experimental design. The column vectors of the obtained matrix  $\mathbf{S}$ , containing the undesired signatures, estimate the basis of the detrimental subspace. In a next step, the calibration space  $\mathbf{X}$  is projected orthogonally to this subspace, in order to obtain a calibration set  $\mathbf{X}^*$  being "cleaned" from the identified interferent(s) [7].

$$\mathbf{X}^* = \mathbf{X}P_S^\perp = \mathbf{X}(\mathbf{I} - \mathbf{S}(\mathbf{S}^T\mathbf{S})^{-1}\mathbf{S}^T) \quad (5.4)$$

Using this new calibration space, a model is calibrated. As the correction is embedded into the model, the model becomes independent from the perturbation factor. Hence, prediction does not compromise accuracy when the external influence appears or disappears. As several influences can be filtered, also without the need for extra reference analyses, this approach also offers a simple means to make an existing calibration model more robust. Generally, these methods also reduce the complexity of the model, helping to reduce  $\|\mathbf{b}\|$  as well [3, 7].

In all of the above approaches, the success of the robustness improvement of the model strongly relies on how well the possible spectral variations can be identified [7]. However, deciding whether and when the calibration samples are representative is a complex task, especially if there are many potentially interfering factors. Therefore, the paper in the **Annex** (S. Pieters, W. Saeys, T. Van den Kerkhof, M. Goodarzi, M. Hellings, T. De Beer, Y. Vander Heyden, Robust calibrations on reduced sample sets for API content prediction in tablets: definition of a cost-effective NIR model development strategy, *Analytica Chimica Acta* 761, 2013, 62-70) proposes a strategy for the cost-effective development of a PLSR model to predict the API content in tablets. The proposed strategy did neither require exact knowledge of the perturbation levels (only controlled variability of the general perturbations was necessary), nor needed extra reference analyses, to make the PLSR model more robust for intra-and inter-batch variations.

In the following paper (S. Pieters, J.M. Roger, T. De Beer, M. D'Hondt, B. De Spiegeleer, Y. Vander Heyden, Increasing robustness against spectral background variability of a Raman model for the protein conformational state classification in freeze-dried formulations, submitted), it was aimed at making the preliminary off-line PLS-LDA Raman classification model more robust for spectral variations originating from different formulation types and freeze-drying batches.

**Increasing robustness against spectral background variability of a  
Raman model for the protein conformational state classification in  
freeze-dried formulations**

Sigrid Pieters<sup>1</sup>, Jean-Michel Roger<sup>2</sup>, Thomas De Beer<sup>3</sup>, Matthias D'Hondt<sup>4</sup>, Bart  
De Spiegeleer<sup>4</sup>, Yvan Vander Heyden<sup>1\*</sup>

<sup>1</sup> Department of Analytical Chemistry and Pharmaceutical Technology, Center for  
Pharmaceutical Research, Vrije Universiteit Brussel - VUB, Laarbeeklaan 103, B-1090  
Brussels, Belgium

<sup>2</sup> Irstea, UMR1201 ITAP, Rue J.F. Breton 361, 34191 Montpellier, France

<sup>3</sup> Laboratory of Pharmaceutical Process Analytical Technology, Ghent University,  
Harelbekestraat 72, B-9000 Ghent, Belgium

<sup>4</sup> Laboratory of Drug Quality & Registration (DruQuaR), Ghent University,  
Harelbekestraat 72, B-9000 Ghent, Belgium

\* Corresponding author: Tel.: +32 2 477 47 34

Fax: +32 2 477 47 35

Email: yvanvdh@vub.ac.be (Y. Vander Heyden)

**Key words**

Raman spectroscopy, multivariate calibration; spectral background  
variability, robustness, external parameter orthogonalization

**Abstract**

Raman spectra may suffer from variations in the spectral background (i.e. caused by non-Raman effects such as fluorescence). When not sufficiently considering such variations in the calibration, or properly removing them, they may compromise the robustness of multivariate calibration (MVC) models. In an earlier feasibility study, the high accuracy of a PLS-LDA classification model confirmed that Raman spectroscopy can supply predictive spectral variation to discriminate between native-like (NL) and non-native (DEN) conformational states of the model protein lactate dehydrogenase (LDH) in freeze-dried formulations. The present study aims investigating whether or not classification accuracy is compromised for certain formulation types or new production batches (i.e. model robustness). A variance analysis within the Raman spectral data space identified significant spectral background variations among certain batches and formulation types in the studied samples. We demonstrate the successful use of both exhaustive calibration and External Parameter Orthogonalization (EPO) pre-processing to make the Raman classification model more robust for the expected spectral background variations.

## 1. Introduction

Multivariate calibration (MVC) models to predict quality attributes from spectroscopic (e.g. Near-infrared, Raman) measurements of samples are gaining popularity in the (bio) pharmaceutical field [1-2]. The typical procedure for building an MVC model is obtaining a number of representative calibration samples and collect a spectrum for each of them as well as determining the quality attribute of interest through a reference method. It is then aimed to describe the quality attribute ( $\mathbf{y}$ ), expressed as a numerical value or as a dummy variable related to its class membership, as a function of the measured spectral signals ( $\mathbf{X}$ ). The Partial Least Squares (PLS) algorithm that captures efficiently the covariance between  $\mathbf{X}$  and  $\mathbf{y}$  has become the most popular means for developing multivariate regression models [3]. It is also frequently used as a dimensionality reduction technique in conjunction with classification algorithms, such as discriminant analysis (DA) [4].

In most cases, only a fraction of the spectral variation in  $\mathbf{X}$  is correlated to  $\mathbf{y}$ . This is the predictive (or correlated) spectral variation. The Net Analyte Signal (NAS) is defined as the useful part of the raw signal for the prediction of the quality attribute of interest (Fig. 1).

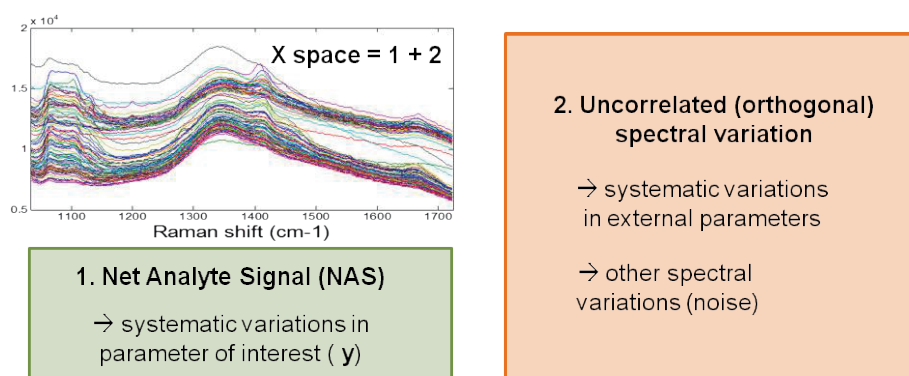


**Fig.1. Scheme representing the spectral variations within the  $\mathbf{X}$  variable space (Raman spectra).**

Therefore it theoretically corresponds to 100% predictive variation, while being orthogonal to the variation of all other spectral contributors [5-6]. The other variations within the  $\mathbf{X}$  variable space constitute of orthogonal (or uncorrelated) spectral variability [7-9]. This variability may find its origin in



all other spectrally contributing factors, including spectral noise and systematic variations caused by external factors. The complexity of this orthogonal variation will largely depend on the type of spectroscopic technique and the application. For instance, spectral variations can be the result of varying physical, chemical, instrumental or process factors. One example is spectral background variation. In Raman spectra this may arise from non-Raman effects (such as fluorescence) [10-11], while in diffuse reflectance NIR spectra light scattering effects of particles and a variable path length may produce a spectral background.

As PLS is an efficient tool to recognize most of the predictive variation, it may enable selective and accurate analysis in the presence of strong interferences, such as in complex matrices or processes [12]. However, PLS-based calibration models will pick up any correlation that can be found between  $\mathbf{X}$  and  $\mathbf{y}$ , regardless the origin of the spectral changes. As a result, conditions changing the orthogonal spectral variation, can make the calibration model lose its prediction accuracy for the quality attribute when that type of orthogonal variation was not adequately considered in the calibration set [13]. This necessitates a calibration set being representative for future specimens and therefore also requires the identification of factors contributing to the orthogonal systematic spectral variation. Calibration samples should be selected in such a way that not only the variation related to the quality attribute of interest, but also the expected orthogonal variation, varies over a range that is expected to be present in future specimens (i.e. exhaustive calibration) [14]. Composing a representative calibration set can therefore become a challenging and costly task, especially if there are many potential sources of spectral variability.

Pre-processing of the spectra in  $\mathbf{X}$  is another way to diminish the effects of known external factors hampering the model robustness. For instance, background corrections (e.g. (linear) interpolation baseline correction methods, (E)MSC, SNV...) have been applied to remove the background contributions of the experimentally obtained Raman spectra prior to interpretation or modeling [10-11]. Another alternative for making the

calibration set representative is using the existing calibration base after filtering the orthogonal space containing the identified harmful variability. External Parameter Orthogonalization (EPO) has been used for this purpose in order to make NIR models more robust [8, 15-17]. Considering the contributions within the calibration matrix  $\mathbf{X}$ , i.e. predictive variation for the analyte  $k$  ( $\mathbf{X}_k$ ), orthogonal variation from all other sources ( $\mathbf{X}_{-k}$ ), and the random spectral variation ( $\mathbf{E}$ ), Eq.1 can be written.

$$\mathbf{X} = \mathbf{X}_k + \mathbf{X}_{-k} + \mathbf{E} \quad (1)$$

EPO uses the spectra from a small experimental design to define a basis of the space spanned by the 'interfering' external factor(s), this way estimating the parasitic subspace  $\mathbf{X}_{-k}$ . Hereby, the external factor is varying while the quality attribute of interest stays constant. In other words, for a set of  $n$  samples,  $n$  spectra are acquired at  $k$  levels of the external factor. Mean centering each set of  $k$  spectra removes the information of the quality attribute of interest, hence only the spectral variations due to the external factor remain. Then the matrix  $\mathbf{D}$  is composed by merging the  $k$  mean-centered spectra from each of the  $n$  samples. Principal Component Analysis (PCA) is then applied to  $\mathbf{D}$ . Retaining only the first  $g$  principal components (PC's), the column vectors of the matrix of eigenvectors  $\mathbf{G}$  will represent an orthonormal basis of the subspace to be removed. Finally, an orthogonal projection is defined to filter the calibration spectra  $\mathbf{X}$  in order to obtain the 'corrected' ones ( $\mathbf{X}^*$ ).

$$\mathbf{X}^* = \mathbf{X}(\mathbf{I} - \mathbf{G}\mathbf{G}^T) \quad (2)$$

where  $\mathbf{G}$  is a matrix comprising the  $g$  first eigenvectors of the square matrix  $[\mathbf{D}^T\mathbf{D}]$ , and  $\mathbf{I}$  is the identity matrix.

A previous study [18] evaluated the feasibility of Raman spectroscopy for discriminating between native-like (NL) and non-native (DEN) conformational states of a model protein LDH in freeze-dried formulations. Therefore, a preliminary PLS-LDA classification model was developed to evaluate whether Raman spectroscopy allows sufficient predictive variation in the spectra. With

cross-validation and test set validation, a classification accuracy of 95% was obtained, and a permutation test showed that the model is not based on random correlations. However, misclassified samples were always samples with mildly denatured proteins in mainly two types of formulations, i.e. formulations 2 and 4 containing histidine and sucrose together (Table 1).

The performance of MVC models for future predictions strongly depends on how well the calibration set represents the composition of new specimens. Therefore robust MVC model development requires the knowledge of the external factors that systematically may influence the spectral variability [13, 19]. Therefore, in the present study, a first aim was to identify the factors influencing significantly the class-orthogonal spectral variability and being potentially present in a routine use of the model. 'Formulation type' was chosen as the first factor because the model should be able to predict the conformational state of the proteins in various model formulations. Moreover, the high probability for misclassifications in certain formulation types (i.e. those containing histidine and sucrose together) by the initial model suggested that not all types of formulations behaved similar. 'Batch' was the second factor because the MVC model should allow the correct classification of samples from new production batches. In a second part of this paper the robustness of the PLS-LDA model for these factors (they caused spectral background variability) was evaluated with external test sets. Both exhaustive calibration and EPO were evaluated for making the initial PLS-LDA model more robust.

## **2. Methods and materials**

### *2.1. Materials and equipment*

Two batches of Lactic-dehydrogenase from rabbit muscle - Type II in ammonium sulfate were obtained from Sigma-Aldrich (Saint Louis, MO, USA). Due to a shortage of the type of LDH used, it was not possible to obtain more LDH raw material batches from the supplier. From this raw material, different LDH formulations were prepared as described in ref. [18]. Freeze-dried samples were analyzed with both dispersive Raman (Kaiser Optical Systems, MR probe, 785 nm laser), and ATR-FTIR spectroscopy (Varian Scimitar 800),

as described in ref. [18]. The latter technique was used as a reference to assign class membership labels by evaluating changes in the protein secondary structure in the freeze-dried samples. The Raman spectra of the 96 experiments (8 batches x 12 formulations) balanced full factorial design from ref. [18] were used to perform a variance analysis. In total, nineteen production batches were manufactured with all freeze-drying conditions within the experimental space used in ref. [18]. They were used to calibrate, update and validate the initial PLS-LDA model.

### *2.2. Data handling*

All data handling was performed in Matlab 7.1. (The Mathworks, Natick, MA) using in-house routines, Minitab 16 (Minitab, PA) and excel.

#### *2.2.1. Statistical analysis of variance*

Tables 1 and 2 show the formulation types and freeze-drying runs (production batches), respectively, used for the statistical analysis of the spectral variability in the Raman spectra of the 96 samples (8 batches x 12 formulations). They correspond to the same samples used in the experimental design in ref. [18] and contained both NL (appr. 1/3) and DEN (appr. 2/3) samples. To study the effects of the two factors 'batch' and 'formulation type' on the variability in the Raman spectra, we first performed PCA on the spectra. A balanced two-way ANOVA was then performed by fitting a General Linear Model (GLM) on the scores of each of the first 6 PC's. To find information on the origin of the variation, post-hoc tests were performed by one-way ANOVA within each factor with Bonferroni adjustment for multiple comparisons.

The factor 'batch' (first way) had 8 levels to estimate the spectral variability caused by production variability (i.e. by the freeze-drying process and raw material batch variability). The first two production batches used LDH raw material originating from a different Sigma-Aldrich batch (Table 2). The factor 'formulation type' (second way) comprised variability from 12 levels, i.e. different formulation compositions (Table 1). It is supposed that these different formulations will result in different sample matrices (e.g. cake structure, protein-excipient volume ratio, different residual water content...).

## Chapter 5: MEASURING PROTEIN UNFOLDING IN RAMAN SPECTRA IN THE PRESENCE OF INTERFERENCES

It was earlier shown that the spectral signals from the different excipients in the formulations did not influence the discrimination between NL and DEN samples [18].

**Table 1. LDH formulations prepared to study the effect of formulation type on the Raman spectral variability. Formulations contained  $\pm 9$  mg/ml LDH in a 40 mM buffer pH 7.4 and/or 5% sucrose or 1% polyethyleneglycol (PEG).**

Formulation number	Matrix composition
1	HIS
2	HIS, sucrose
3	HIS, PEG
4	HIS, sucrose, PEG
5	PHOS
6	PHOS, sucrose
7	PHOS, PEG
8	PHOS, sucrose, PEG
9	TRIS
10	TRIS, sucrose
11	TRIS, PEG
12	TRIS, sucrose, PEG

Abbreviations: HIS= histidine buffer, PHOS = phosphate buffer, TRIS = TRIS buffer

### 2.2.2. Data sets for model calibration and validation

Three data sets, i.e.  $S_0$ ,  $S_1$  and  $S_2$ , were used for developing and validating the (updated) PLS-LDA models (Table 3). In ref. [18] the initial pool of 99 samples, originating from 8 freeze-drying batches and covering all formulation types, was split into a calibration set and a test set, here called  $S_0$  and Test set 1. As there was in ref. [18] no knowledge on the class-orthogonal spectral variation, the samples were merely selected to cover the full variability of the quality attribute, i.e. different types of conformational states. Formulations 2 and 4 were modestly represented, and most misclassifications occurred from these formulations. The knowledge obtained in section 3.1. of this paper learned us that the Maillard reaction in formulations containing sucrose together with histidine, i.e. in formulations 2 and 4, can induce increased Raman spectral background variability. Therefore,  $S_1$  was a separate data set designed to estimate the Raman spectral background subspace possibly present in the studied formulations.

## Chapter 5: MEASURING PROTEIN UNFOLDING IN RAMAN SPECTRA IN THE PRESENCE OF INTERFERENCES

**Table 2. Freeze-drying runs (production batches) performed to study the batch effect on the Raman spectral variability.**

Production batch	Formulations*	Raw LDH material batch
1	1-12	1
2	1-12	1
3	1-12	2
4	1-12	2
5	1-12	2
6	1-12	2
7	1-12	2
8	1-12	2

\* See table 1.

It was supposed to capture the full range of possible varying Raman spectral background for all types of formulations, i.e. those with normal (e.g. form 2), decelerated (e.g. form 4) and no Maillard reaction (e.g. form 9) (for explanation see results and discussion).  $S_1$  contained 24 Raman spectra from  $n=8$  samples obtained over  $k=3$  different storage times (months), since the background effects in the Raman spectra increased gradually with storage time when a Maillard reaction was present. The conformational state (physical stability) of the proteins did not change over storage time in the dried solid.

**Table 3. Details on the data sets used in this study for PLS-LDA model development and validation.**

Data set	Purpose	n° Raman spectra	n° NL	n° DEN	Formulation types	From pool of batches
$S_0$	Initial calibration	75	23	52	all	1-8
$S_1$	Estimate background subspace	24*	3	21	2,4,9	1-8
$S_2$	Validation	110	39	71	all	1-19
Test set 1	- initial test set validation	24	8	16	all	1-8
Test set 2	- stronger background, new batches	45*	9	36	2,4	9-19
Test set 3	- normal background, new batches	41	22	19	all except 2 and 4	9-19

\* all samples were measured at 3 different storage times

$S_2$  was a data set to validate the model. It was divided into 3 separate test sets to evaluate the model robustness for different perturbation factors individually (Table 3). The samples from Test set 1 originated from the same pool (same batches, same formulation types) as the calibration samples. Samples from Test sets 2 and 3 originated from different production batches,

but were produced with the same LDH raw material batches as the calibration samples. Test set 2 contained explicitly samples from formulations 2 and 4, where a Maillard reaction, and thus a stronger background effect in the Raman spectra, is possible. Just as in  $S_1$ , all samples were measured over 3 different storage times (months). The samples in Test set 3 originated from formulation types having no Maillard reaction in the freeze-dried cakes.

Two approaches were used for making the initial PLS-LDA model more robust. The first approach was exhaustive calibration of the spectral background. The second approach was EPO to filter the identified harmful effects from the spectral space holding the informative features. This method has the advantage that there is no need for corresponding  $y$  values (here class memberships) [15-17, 20]. The original model and the EPO model used  $S_0$  for calibration, while exhaustive calibration was performed with  $S_0 + S_1$ . For EPO, the Raman spectra from  $S_1$  were mean-centered for each sample, this way leaving only the background contributions. The obtained data matrix  $\mathbf{D}$  was then used to estimate the subspace spanned by the Raman spectral background effects (Fig. 2).

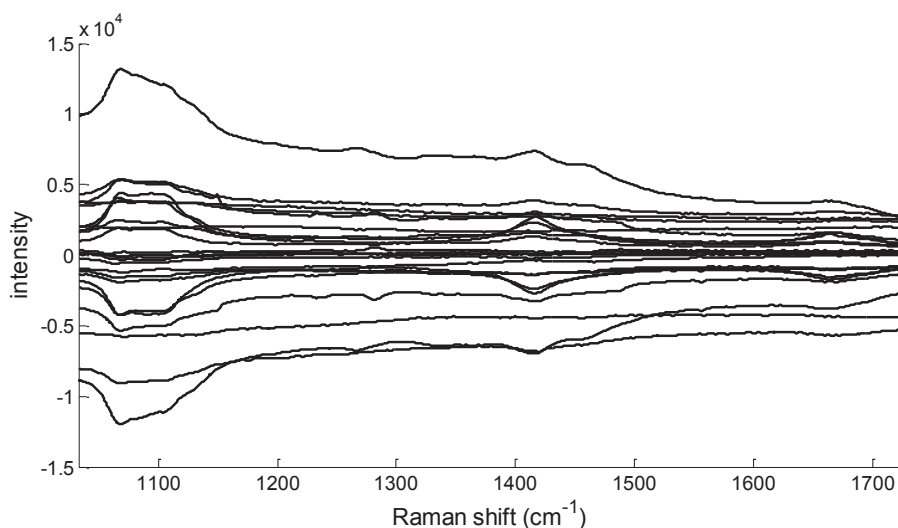


**Fig. 2.** Plot of  $\mathbf{D}$ , composed by merging the 3 mean-centered spectra (measured repeatedly over time) from each of the 8 samples from  $S_1$ . This matrix is used to estimate the harmful subspace within the  $\mathbf{X}$ -space, containing the spectral background effects possibly present in the studied formulations.

### 2.2.3. Evaluation of the model performance

The performances of the classification models were evaluated by the absolute number of misclassifications in cross validation and for Test sets 1-3, as well as by the overall % classification accuracy, % sensitivity and % specificity. The number of true positives (TP), true negatives (TN), false positives (FP) and false negatives (FN) were determined from the confusion matrices of every test set. Percent classification accuracy, sensitivity and specificity were calculated according to Eqs. 1-3, using an equal weight for every test set.

$$\% \text{ Accuracy} = ((\text{TN} + \text{TP}) / (\text{TN} + \text{TP} + \text{FN} + \text{FP}))100 \quad (1)$$

$$\% \text{ Sensitivity} = (\text{TP} / (\text{TP} + \text{FN}))100 \quad (2)$$

$$\% \text{ Specificity} = (\text{TN} / (\text{TN} + \text{FP}))100 \quad (3)$$

Sensitivity indicates how good the PLS-LDA model is at detecting DEN samples, while specificity indicates how good the PLS-LDA model is at identifying the negative (here NL) condition. To compare different models their performances were plotted in a Receiver Operating Characteristics (ROC) space [21].

## 3. Results and discussion

### 3.1. Study of the irrelevant spectral effects

A PCA on the Raman spectra of the freeze-dried LDH samples from the studied formulations and production batches revealed that the separation between NL and DEN classes is largely represented in PC6 [18]. The shape of the PC6 loading vector was also very similar to the shape of the discriminant vector of the PLS-LDA model [18]. Hence, PC6 describes a large portion of the spectral variation related to the quality attribute. To study the orthogonal variation described by PC1-PC6, we performed a variance analysis. Hereby, for each PC the factors 'formulation type' and 'batch' were studied on the principal component scores of the 96 Raman spectra of an experimental design (12 formulations x 8 batches). The PC1 described 99,58% of the total spectral variation. Its reversed loading vector had a shape similar to the mean spectrum of the data set (Fig. 3).



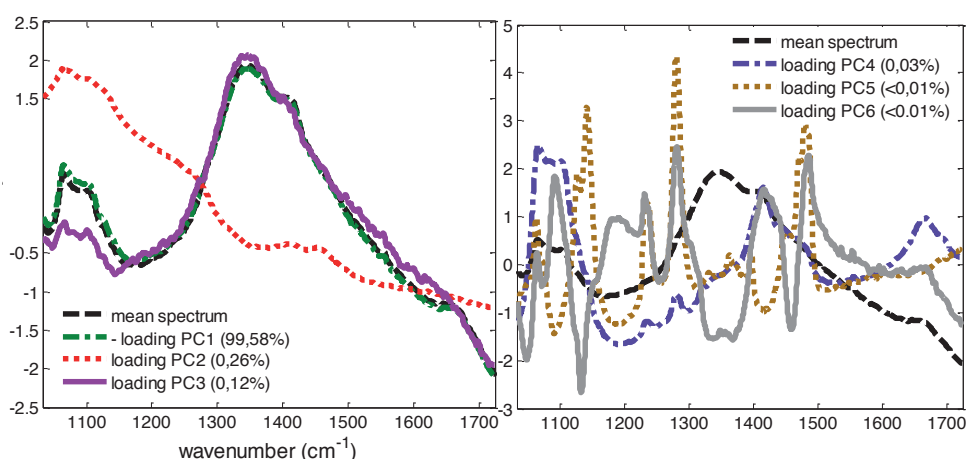


**Fig. 3.** Loading vectors of the first 6 PC's of a PCA on the 96 Raman spectra used in the spectral variance analysis. Comparison is made to the mean Raman spectrum of the data set (the loadings were SNV preprocessed for direct comparison).

By mean centering, removing this effect, we found that PC1 mainly describes an additive effect, shifting the whole spectrum up and down. Both factors, i.e. batch and formulation type, had significant effects on the scores of PC1 (Table 4 and Fig. 4). From the effects plot (Fig. 5A) it could be observed that the batch effect was different for freeze-drying runs 1 and 2, while the formulation type effect was different for formulation 2.

**Table 4.** Two-way ANOVA on the PC1-PC6 scores of the 96 Raman spectra from an experimental design with 'batch' effect being the first way, and 'formulation' effect being the second.

Response	Variance source	<i>p</i> value
Scores on PC1	Batch	<0,001*
	Formulation	<0,001*
Scores on PC2	Batch	0,140
	Formulation	<0,001*
Scores on PC3	Batch	<0,001*
	Formulation	<0,001*
Scores on PC4	Batch	0,768
	Formulation	0,008*
Scores on PC5	Batch	0,834
	Formulation	<0,001*
Scores on PC6	Batch	0.421
	Formulation	<0,001*

\*Significant effect ( $\alpha=0,05$ )

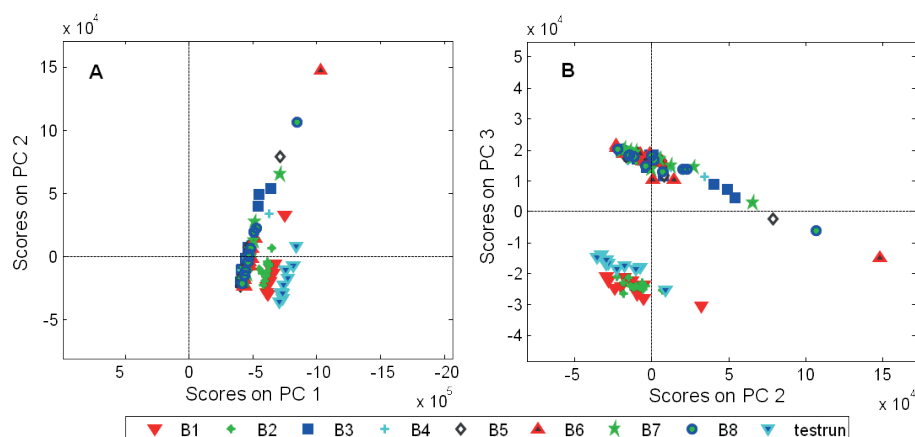


**Fig. 4. PCA score plots (A) PC1 versus PC2 and (B) PC2 versus PC3 of the 96 Raman spectra used in the spectral variance analysis and the ten samples from a test run. Samples originating from different production batches (B1-B8, test run) are marked by different signs and colors.**

Post hoc testing confirmed that these factor levels were significantly different. The PC2 described 0,26% of the total spectral variation, and only the factor formulation type had a significant effect on the PC2 scores. Again only formulation 2 behaved differently (Fig. 5B), which was confirmed by post hoc testing. The corresponding loading vector (Fig. 3) revealed a slope in the background. Both factors batch and formulation type significantly affected the scores of PC3, describing 0,12% of the total spectral variability (Table 4). Post hoc testing again confirmed that the effect of the first 2 batches was significantly different from that of the other batches (Fig. 5C). The loading vector of PC3 resembled closely the shape of the mean spectrum of the data set. The PC3 scores of formulation 2 were significantly different from those from the other formulations, but the effect was much smaller compared to the batch effect. PC4 showed to be significantly influenced by the formulation type factor, but not by the batch factor (Table 4). By inspecting the effects plot (Fig. 5D) and performing multiple comparisons, we found that the PC4 scores from formulations 2 were again significantly different from those from other formulations. For PC5 and PC6 the batch effect proved neither significant, while the formulation effect was significant (Table 4). Post hoc tests revealed differences on the effects of the PC5 scores among formulation types, they were generally related to the addition of sucrose and/or PEG (Fig. 5E). This may be the result of different ratios between protein and excipient (and residual water) fractions among the formulations, but should be further

## Chapter 5: MEASURING PROTEIN UNFOLDING IN RAMAN SPECTRA IN THE PRESENCE OF INTERFERENCES

confirmed with appropriate tests. The scores on PC6 showed strong differences between formulation types (Fig. 5F). Given the large influence of protein conformation on PC6, this may possibly be the result of the diverse probabilities in different formulations to obtain a NL (or DEN) protein state.

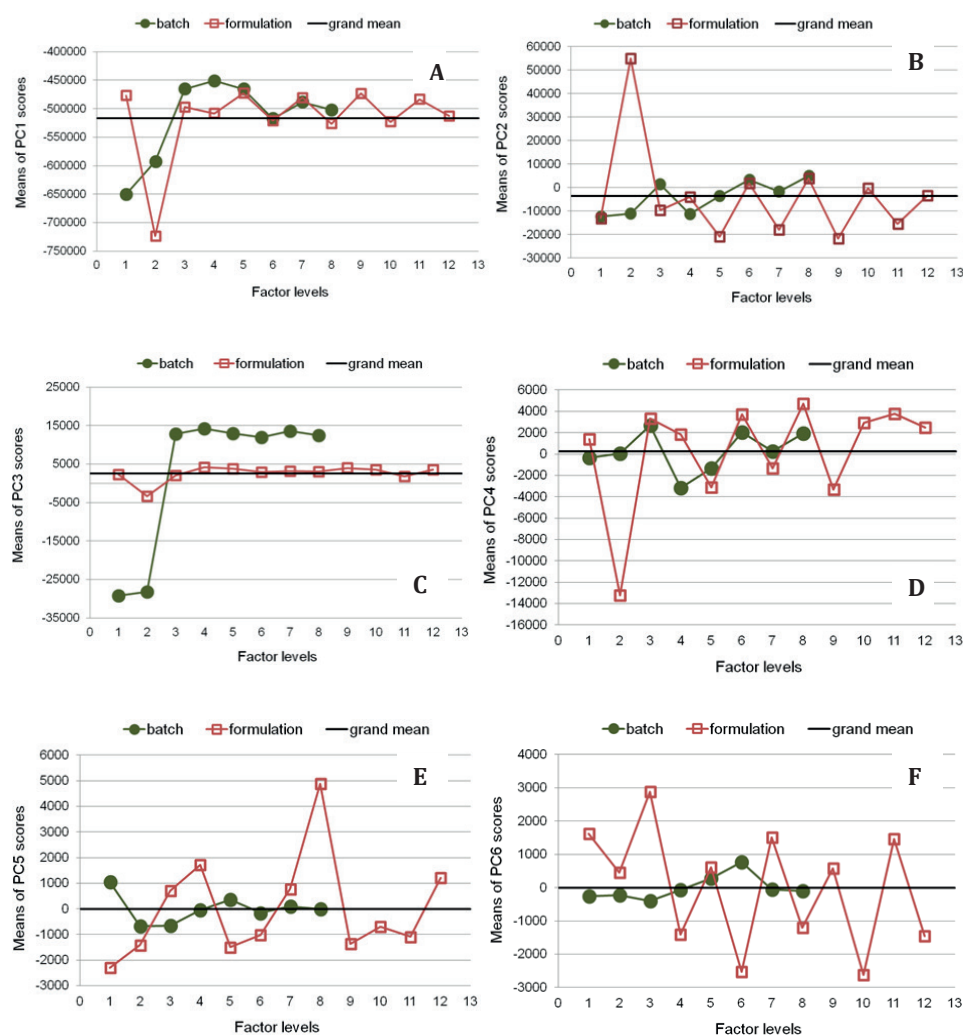


**Fig. 5.** Plot showing the means of the PC1 (A), PC2 (B), PC3 (C), PC4 (D), PC5 (E), PC6 (F) scores for each level of the factors 'batch' and 'formulation type'. The black horizontal line corresponds to the grand mean. The effects are the differences between the individual means and the grand mean.

The loadings revealed that the spectral variability described by PC1 to PC4 (together 99.99%) was found to be dominated by irrelevant changes in the spectral background. These were visually identified based on the relative bandwidths of their features (i.e. features with bandwidths of  $> 100 \text{ cm}^{-1}$  were assumed to be non-Raman in origin [10]). Background variability in Raman

spectra originates from non-Raman effects (e.g. the presence of luminescence from sample components and the analyte itself) and is influenced by the laser intensity [22-24]. As proteins also contain fluorescent amino acids, i.e. tryptophane, tyrosine and phenylalanine [25], a fluorescence contribution is likely to be present in the background of the Raman spectrum of a protein sample. Also, the sample-probe distance is slightly varied with each measurement. Since the fluorescence contribution in the spectral background is dependent on the sample-probe distance [22], this variation is supposed to be equally represented over all samples, regardless their batch or formulation origin. Repeated measurements indeed showed some variability in the spectral background (Fig. 6).

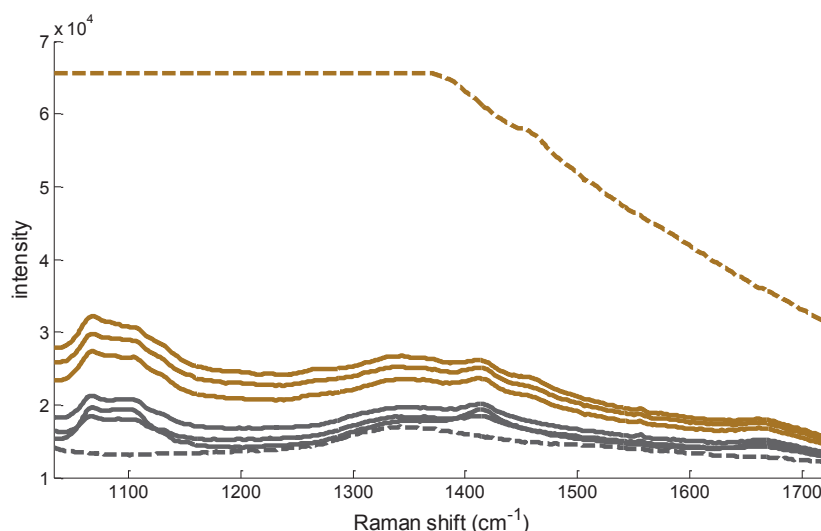


**Fig. 6. Repeated measurements (with varying sample-probe distance) of the Raman spectra of stored (months) freeze-dried LDH samples with formulation 2 (with Maillard reaction) and formulation 9 (without Maillard reaction), respectively in yellow and grey. The dotted lines represent their respective blanks. The samples originated from the same production batch.**

For the factor batch, the first 2 production batches had significantly different scores on PC1 and PC3. These batches used LDH raw material from a different batch. Thus, production batch variability did not affect the spectral variation significantly, unless the batches use different LDH raw material. The samples from another production batch (test run) using the same LDH raw material as batches 1 and 2 indeed confirmed the same variation in the PCA score plot

(Fig. 4). A possible explanation for this may be that the variations in LDH protein purification process have an effect on the spectral background.

For the factor formulation, formulation 2 had significantly different scores on PC's 1-4 compared to the other formulation types. Formulation 2 contains the combination of sucrose and histidine (Table 1). A further inspection of the samples after storage revealed that the color of the cakes of formulation 2 was visibly changed from white to yellowish. In other formulations there was no visible color change. The color may be the result of the Maillard reaction, also called sugar browning. This is a chemical reaction between reducing sugars and basic amino acids (i.e. histidine), leading to this 'browning' [26-27]. It involves different stages. In a first stage there is the aminocarbonyl condensation between the carbonyl of a reducing sugar and an amino group to form a Schiff base and a water molecule. Although sucrose itself is no reducing sugar, it may hydrolyze into reducing sugars [28]. In the advanced stages, several Maillard reaction products (MRP's) are formed, with different fluorescent and browning properties [29-30]. In some conditions the fluorescent MRP's have been proposed as precursors of the colored MRP's [30]. The presence of the fluorescent MRP's may thus be responsible for the different Raman spectral background compared to those where no such a reaction occurs. As the Maillard reaction continues during storage, the color became more intense, and so did the background contribution in the Raman spectra. Fig. 6 shows the repeated measurements of two samples, i.e. one stored sample with Maillard reaction versus one of the same age without Maillard reaction. The sample with the Maillard reaction shows visibly stronger effects in its background resulting in the loadings of the first PC's.

Although a Maillard reaction can also occur between reducing sugars and amino acids from exposed protein side chains (possibly affecting the chemical stability of the protein [27, 31]), this was not detectable in the Raman spectra. Formulation 2 was the only formulation where this effect was significantly observed while it was not in formulations 6 and 10 that also contained sucrose, but with other buffers (Table 1). In the variance analysis, formulation 4 (histidine + sucrose + PEG) did not behave significantly different from the

others. However, the samples for the variance analysis were analyzed directly after freeze-drying. When analyzing stored formulations we saw similar effects appearing in the background as in formulations 2 (data not shown). We suppose that polymers may physically hamper the contact between histidine and sucrose, possibly decelerating the Maillard reaction. This was also confirmed by the darker yellow color of the blank of formulation 2 (proteins are polymers as well), having an intense spectral background (probably due to increased fluorescent MRP's) after storage (Fig. 6).

### *3.2. PLS-LDA model performance*

From the variance analysis production batch variability is not found to be significant, unless batches are produced with different LDH raw material. In this study, the original model calibration base  $S_0$  was built from 8 production batches, manufactured from two LDH raw material batches. The test set samples ( $S_2$ ) also originated from the same LDH raw material batches. Due to a shortage of the type of LDH used, it was not possible to obtain more LDH raw material batches from the supplier. Hence, the PLS-LDA model robustness for this factor could not be fully investigated and is still required as a future work.

In our previous study [18] we concluded that the model has reduced sensitivity for correctly classifying slightly denatured proteins, as the visual interpretation of reference FTIR spectra of the misclassified samples in cross (4/75) and Test set 1 (1/24) validation indicated slight signs of protein denaturation. Since four out of five misclassified samples contained formulations 2 or 4, we are now aware that the stronger Raman spectral background in these samples might have contributed to this result. Moreover, in this type of formulation the protective action of sucrose will normally lead to less protein unfolding in DEN samples. Thus formulations with non-native LDH, having large interfering backgrounds and low signs of protein denaturation, represent the highest challenge for the model. They were much represented in Test set 2, evaluating the robustness of the PLS-LDA model for the background effect due to the Maillard reaction. In Table 5 it can be seen that the original PLS-LDA model calibrated on  $S_0$  needed 6 latent variables (LV's) and had a large number of misclassifications for Test set 2 (21/45). The

misclassified samples in Test set 2 were indeed DEN samples containing mildly denatured LDH with stronger fluorescent backgrounds in their Raman spectra. All samples of Test set 3 (novel production batches from samples without Maillard reaction) were correctly classified. This was not unexpected given the insignificant effects of production variability (with LDH from the same raw material batches) obtained by the variance analysis. Thus the performance of a model not explicitly considering the orthogonal variation led to a classification accuracy of only 82.8% with excellent specificity (100.0%) while suffering from poor sensitivity (78.1%).

Exhaustive calibration, using  $S_0 + S_1$ , explicitly considered the background interference due to the Maillard reaction in the calibration base. This resulted in the need for 1 extra LV (7 instead of 6). A much lower number of misclassifications (6/45) for samples of Test set 2 was obtained, however classification performance was a bit compromised in Test set 1. Just as with the original model calibrated on  $S_0$ , Test set 3 could be perfectly classified. This indicates that samples without a Maillard reaction still could be classified correctly. The overall model accuracy was increased from 82.8% to 91.4%, with 90.3% sensitivity and 95.8% specificity.

The performances of the PLS-LDA models with EPO correction of  $S_0$  are shown in Table 5, and plotted in the ROC space (Fig. 7). Among these models, the PLS-LDA model with EPO preprocessing with  $g=8$  showed the highest overall classification accuracy (91.3%). It maximizes the true positive rate (sensitivity) and minimizes the false positive rate (1-specificity), i.e. its point in the ROC space is the closest to the ideal coordinate (0,100) in the upper left hand side of the plot (Fig. 7) [21]. This model, using 4 LV's, was more parsimonious than the original or exhaustive calibrations, and nearly had the same classification accuracy as the model using exhaustive calibration (91.3% versus 91.4%). Sensitivity was increased from 78.1% to 89.6%, while specificity was compromised from 100.0% to 96.3% (Fig. 7). Its classification performance (10/45 misclassifications) for Test set 2 was better than the original model, but worse than the model that used exhaustive calibration.

## Chapter 5: MEASURING PROTEIN UNFOLDING IN RAMAN SPECTRA IN THE PRESENCE OF INTERFERENCES

**Table 5. Performance of PLS-LDA models for classification of the conformational state of freeze-dried protein formulations, expressed as the absolute number of misclassifications in cross validation (CV) and in the test sets, % accuracy, % sensitivity and % specificity. Every model used  $S_0$  as the calibration set, except exhaustive calibration which was performed with  $S_0+S_1$ . EPO preprocessing used  $S_1$  to calculate the basis of the subspace to be removed. Test set 1 contains samples originating from the same pool as the calibration samples. Test sets 2 and 3 consist of samples from new production batches with and without a Maillard reaction, respectively. % accuracy, % sensitivity and % specificity are calculated as described in Methods and materials.**

PLS-LDA calibration	Number of LV's	CV	Test set 1 (/24)	Test set 2 (/45)	Test set 3 (/41)	% accuracy	% sensitivity	% specificity
$S_0$	6	4/75	1	21	0	82.8	78.1	100.0
<b><math>S_0 + S_1</math></b>	<b>7</b>	<b>5/99</b>	<b>3</b>	<b>6</b>	<b>0</b>	<b>91.4</b>	<b>90.3</b>	<b>95.8</b>
$S_0$ EPO g=1	4	3/75	1	11	0	90.5	87.7	100.0
$S_0$ EPO g=2	3	3/75	1	13	22	71.2	92.4	40.7
$S_0$ EPO g=3	3	3/75	1	12	0	89.8	86.8	100.0
$S_0$ EPO g=4	3	3/75	3	9	22	71.3	87.5	62.5
$S_0$ EPO g=5	2	2/75	2	14	22	68.9	86.8	55.1
$S_0$ EPO g=6	3	2/75	2	13	0	87.6	89.6	81.1
$S_0$ EPO g=7	3	2/75	1	10	6	86.4	91.5	79.8
<b><math>S_0</math> EPO g=8</b>	<b>4</b>	<b>2/75</b>	<b>1</b>	<b>10</b>	<b>0</b>	<b>91.3</b>	<b>89.6</b>	<b>96.3</b>
$S_0$ EPO g=9	3	2/75	2	13	0	87.6	91.5	73.7
$S_0$ EPO g=10	3	2/75	3	14	0	85.5	89.4	69.9

The samples from Test set 1 were classified with the same accuracy as the original model, and the performance in CV was improved. Also, the samples from new production batches absent from a Maillard reaction (Test set 3) were all correctly classified.



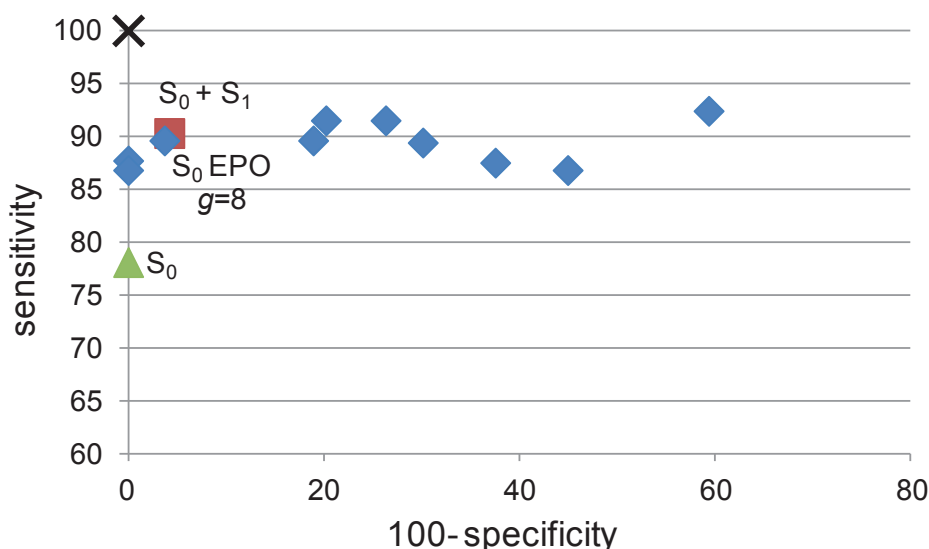


**Fig. 7. Classification performance of the different PLS-LDA models plotted in the Receiver Operating Characteristic (ROC) space. The green triangle corresponds to the model calibrated with  $S_0$ . The red square stands for the model using exhaustive calibration with  $S_0 + S_1$ . The blue diamonds match with models after EPO preprocessing of the calibration set  $S_0$  with different  $g$  used for the orthogonal projection. The black cross at (0,100) coordinates represents perfect classification.**

Both exhaustive calibration and EPO preprocessing increased the overall classification accuracy and sensitivity to nearly the same level (Table 5). They both varied the discrimination threshold of the PLS-LDA model for classifying the conformational state of the proteins in the freeze-dried formulations: the former by calibrating the full range of spectral background variation, the latter by filtering it. Advantages of EPO compared to exhaustive calibration were that there is no need for class memberships ( $y$  values) to estimate the harmful subspace, and that a more parsimonious PLS-LDA model could be developed. It is suggested that EPO increased the signal-to-noise ratio, being the ratio between the NAS and the background variability [12], by removing the part of the  $\mathbf{X}$  space mostly influenced by spectral background variations.

#### 4. Conclusion

In the present case study, a variance analysis on the PC scores of the Raman spectra of freeze-dried LDH formulations identified the factors most responsible for class-orthogonal systematic spectral variation. Most variation in the Raman spectra (PC1-PC4) was due to varying spectral background

effects. It is suggested that the different LDH raw material batches, and the fluorescent MRP's in formulations where a Maillard reaction occurs, are contributing the most to this. This knowledge was used to make a PLS-LDA model more robust for classifying proteins according to their conformational state (physical stability) in different types of freeze-dried formulations. Both explicitly calibrating (exhaustive calibration) and filtering (EPO preprocessing) the expected background variation in a PLS-LDA model resulted in a reduced number of misclassifications. Mildly denatured protein samples in formulations having a stronger background in their Raman spectra were now more frequently correctly classified. Both methods improved the PLS-LDA model performances in the presence of large background variation up to nearly the same levels, with a limited compromise in specificity. This study demonstrated that the spectral background variations, hampering the sensitivity of the model, lay in a subspace of the spectral space. This can either be taken into account by the calibration, if representative samples are present in the calibration database, or be explicitly filtered by means of an orthogonal projection.

### Acknowledgements

SP is funded as an aspirant of the Research Foundation-Flanders (FWO). She would also like to thank the same institution and Irstea for the funding and hosting, respectively, of a research stay. MD thanks the Agency for Innovation by Science and Technology (IWT 101529) for financial support.

### References

- [1] T. Rajalahti, O.M. Kvalheim, *Int. J. Pharm.* 417 (2011) 280-290.
- [2] T. De Beer, A. Burggraeve, M. Fonteyne, L. Saerens, J.P. Remon, C. Vervaet, *Int. J. Pharm.* 417 (2011) 32-47.
- [3] B.G.M. Vandeginste, D.L. Massart, L.C.M. Buydens, S. De Jong, P.J. Lewi, J. Smeyers-Verbeke, *Handbook of chemometrics and qualimetrics: Part B*, Elsevier Science, Amsterdam, 1998.
- [4] M. Barker, W. Rayens, *J. Chemom.* 17 (2003) 166-173.
- [5] A. Lorber, N.K.M. Faber, B.R. Kowalski, *Anal. Chem.* 69 (1997) 1620-1626.
- [6] J. Ferre, N.K.M. Faber, *Chemom. Intell. Lab. Syst.* 69 (2003) 123-136.

- [7] T. Fearn, *Chemom. Intell. Lab. Syst.* 50 (2000) 47-52.
- [8] J.C. Boulet, J.M. Roger, *Chemom. Intell. Lab. Syst.* 117 (2012) 61-69.
- [9] R. C. Pinto, J. Trygg, J. Gottfries, *J. Chemom.* 26 (2012) 231-235.
- [10] J.R. Beattie, J.J. McGarvey, *J. Raman spectrosc.* 44 (2013) 329-338.
- [11] A.E. Kandjani, M.J. Griffin, R. Ramanathan, S.J. Ippolito, S.K. Bhargava, V. Bansal, *J. Raman Spectrosc.* 44 (2013) 608-621.
- [12] A.C. Olivieri, N.M. Faber, J. Ferré, R. Boqué, J.H. Kalivas, H. Mark, *Pure Appl. Chem.* 78 (2006) 633-661.
- [13] M. Zeaiter, J.M. Roger, V. Bellon-Maurel, D.N. Rutledge, *TrAC* 23 (2004) 157-170.
- [14] [www.fda.gov/downloads/Drugs/.../Guidances/ucm070305.pdf](http://www.fda.gov/downloads/Drugs/.../Guidances/ucm070305.pdf) (accessed on 26/10/2012)
- [15] J.M. Roger, F. Chauchard, V. Bellon-Maurel, *Chemom. Intell. Lab. Syst.* 66 (2003) 191-204.
- [16] M. Zeaiter, J.M. Roger, V. Bellon-Maurel, *TrAC* 24 (2005) 437-445.
- [17] S. Pieters, W. Saeys, T. Van den Kerkhof, M. Goodarzi, M. Hellings, T. De Beer, Y. Vander Heyden, *Anal. Chim. Act.* 761 (2013) 62-70.
- [18] S. Pieters, Y. Vander Heyden, J.M. Roger, M. D'Hondt, L. Hansen, B. Palagos, B. De Spiegeleer, J.P. Remon, C. Vervaet, T. De Beer, *Eur. J. Pharm. Biopharm.*, in press (doi: 10.1016/j.ejpb.2013.03.035).
- [19] H. Swierenga, A.P. de Weijer, R.J. van Wijk, L.M.C. Buydens, *Chemom. Intell. Lab. Syst.* 49 (1999) 1-17.
- [20] T. Giordanengo, J.P. Charpentier, J.M. Roger, S. Roussel, L. Brancheriau, G. Chaix, H. Baillères, *Ann. For. Sci.* 65 (2008) 803.
- [21] T. Fawcett, *Pattern Recognition Letters* 27 (2006) 861-874.
- [22] B. Wang, S. Fan, L. Li, C. Wang, *Biomedical Engineering Online* 10 (2011) 95-103.
- [23] T. Vankeirsbilck, A. Vercauteren, W. Baeyens, G. Van der Weken, F. Verpoort, G. Vergote, J.P. Remon, *TrAC* 21 (2002) 869-877.
- [24] R.L. McCreery, *Raman spectroscopy for chemical analysis*, J.D. Winefordner (Ed.), John Wiley & Sons, 2000.
- [25] A.K. Banga, *Therapeutic peptides and proteins: formulation, processing and delivery systems* (2<sup>nd</sup> edition), Taylor and Francis group, Boca Raton, 2006.

- [26] L. Chang, M.J. Pikal, J. Pharm. Sci. 98 (2009) 2886-2908.
- [27] M. D'Hondt, W. Demaré, S. Van Dorpe, E. Wynendaele, C. Burvenich, K. Peremans, B. De Spiegeleer, Food Chemistry 128 (2011) 114-122.
- [28] W. Wang, Int. J. Pharm. 203 (2000) 1-60.
- [29] F.J. Morales, S. Jiménez-Pérez, Food chemistry 72 (2001) 119-125.
- [30] S.B. Matiacevich, M. Pilar Buera, Food chemistry 95 (2006) 423-430.
- [31] S. Li, T.W. Patapoff, D. Overcashier, C. Hsu, T.H. Nguyen, R.T. Borchardt, J. Pharm. Sci. 85 (1996) 873-877.

### **5.3. In-line monitoring protein unfolding during freeze-drying processes using Raman spectroscopy**

Freeze-drying is a batch process, having typically a finite duration, and consisting of three subsequent phases, i.e. freezing, primary and secondary drying. As a result of the inherently varying process conditions (e.g. changes in pressure and temperature settings) and variations in the sample (from liquid to ice to solid), there are many variables in the Raman process spectra that change differently due to the batch evolution (i.e. their trajectories mainly describe dynamic time dependencies). As these variations might interfere with the desired classification, it is aspired to make the classification between NL and DEN states robust for process interferences. Real-time process analysis is generally performed by multivariate calibration or statistical in-line models [8].

The necessity for reference sampling makes developing in-line MVC models complex and less practically appealing, sometimes even impossible. Compared to continuous processes, this is especially an issue for batch processes, where process settings are expected to change during the entire process course and thus may cause continuous spectral variations [8]. One possible way is to transfer the off-line calibration model to in-line use. Instead of adjusting the calibration, i.e. making a calibration with the same samples in- and off-line measured, methods adjusting the spectra without reference values (e.g. direct standardization [9], dynamic orthogonal projections [10]) can be a valuable alternative. However, to develop a robust model its validation with representative in-line acquired spectra and their corresponding reference values will remain necessary, and this for each type of process variation that may occur. In our case study, where spectral changes due to the varying process were eminent and where there was no sample thief to extract the samples from the process stream for off-line reference analysis, we did not choose to make an in-line calibration model.

A calibration-free alternative for in-line monitoring purposes are statistically based models. In multivariate statistical process control (MSPC), the huge process data space is usually collapsed into a lower dimensional space. Most popular methods for doing this

are PCA and PLS. By creating latent variables, more meaningful process trajectories can be visualized as typical patterns from their scores. The multivariate scores may not only provide a more simplified summary of the measured variables, they also have the advantage that they are mathematically orthogonal, and less noisy than original variables (since they are weighted averages). Thus, in MSPC the measured variables have been replaced by their abstract PCA or PLS projections, and the problem becomes basically a classification of process trajectories being acceptable or unacceptable. Based on historical data, that consistently showed an in-control situation for the parameter(s) of interest, one can establish a multivariate acceptability area in a statistical way. This way, one can assess from each process measurement whether the process is still in a state of statistical control, i.e. whether it is operating as it should be with respect to the CQA(s) of interest. Popular multivariate control charts are based on Hotelling  $T^2$  and  $Q$  residual statistics (Fig. 5.3) [8, 11-12].

The Hotelling  $T^2$  test indicates how far away the projection of a new observation (i.e. the scores of a sample spectrum described by the model) is situated from the center of the model (scores=0). The Hotelling  $T^2$  for scores is calculated as follows (eq. 5.4).

$$T_A^2 = \sum_{i=1}^A \frac{t_i^2}{s_{t_i}^2} \quad (5.4)$$

where  $s_{t_i}^2$  is the estimated variance of the corresponding latent variable  $t_i$ , and  $A$  being the number of latent variables in the model. The values represent thus a measure of the variation in each sample within the model (defined by  $A$  latent variables), and this chart checks if a new observation vector (having  $k$  variables) is within the limits when projected on the hyper-plane determined by the model reference data [11-12].

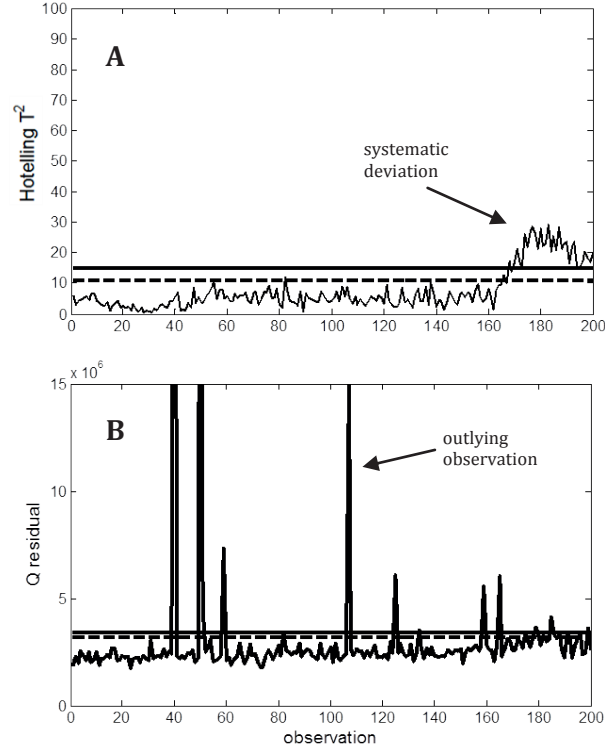


**Fig. 5.3.** Example of the Hotelling  $T^2$  and Q residual control charts. The horizontal dashed and full lines are the warning (95%) and action (99%) limits, respectively.

Conversely, the Q residuals test checks whether the unexplained variations in the system remain similar to those observed during model development. For every  $i^{\text{th}}$  of the  $k$  original variables the sum of squares of the differences (i.e. residuals) between a sample spectrum ( $x_{new}$ ) and its projection onto the hyper-plane of the model ( $\hat{x}_{new}$ ) is calculated to obtain the Squared Prediction Error (SPE) (eq. 5.5).

$$SPE_X = \sum_{i=1}^k (x_{new,i} - \hat{x}_{new,i})^2 \quad (5.5)$$

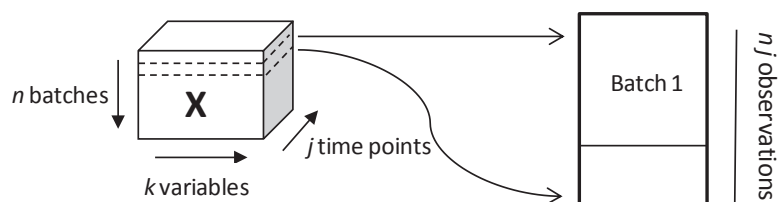
This statistic is also referred to as "distance to model", lack-of-fit or Q-statistic. When the process is in control the Q residual value should be small. Any new spectral observation with a type of variation (i.e. a new event happens) that is not covered by the model will render a high Q residual value [11-12].

Both complementary charts (Fig. 5.3) may give information on the magnitude of the (systematic or outlying) deviation. For each chart, statistical limits (e.g. warning and action limits) can be calculated. Additionally, monitoring certain individual score values as a function of process time, especially when it is known that certain LV's strongly correlate to the CQA of interest, can also be interesting to obtain an idea of the direction of the change. T and Q contribution plots, describing how individual variables contribute to the Hotelling  $T^2$  and Q residual values, can be of particular interest to diagnose the event that caused the deviation [11-12].

MSPC is generally used for continuous processes, whereas batch processes usually require batch statistical process control (BSPC). As batch processes yield a 3-way data structure (i.e.  $n$  batches,  $j$  time points,  $k$  variables), the idea is to either unfold the data structure or use a 3-way approach for data analysis. Unfolding of the 3-way data structure can be performed on the batch level ( $n, k$ ) or on the observation level ( $nj, k$ ) (Fig. 5.4). Using the batch level (Fig. 5.4B), one should wait until the entire batch is finished to draw conclusions, hence real-time monitoring is not possible. This approach will pass the process data through the model directly after completion of the batch, i.e. the scores of the entire batch are investigated prior to releasing the batch. This is not the case when the data matrix is unfolded as if it were individual observations (Fig. 5.4A). Here, the evolution of new batches can be real-time monitored. In BSPC, it is generally required that batches have an equal duration and are synchronized [11-12, 13]. Currently, there is a trend to predict the end points of primary and secondary drying from in-process measurements using PAT-tools, such as MTM or TDLAS [14]. Hence, the duration of the individual phases may not be predefined in modern freeze-drying processes.



**(A) unfolding to observation level**



**(B) unfolding to batch level**

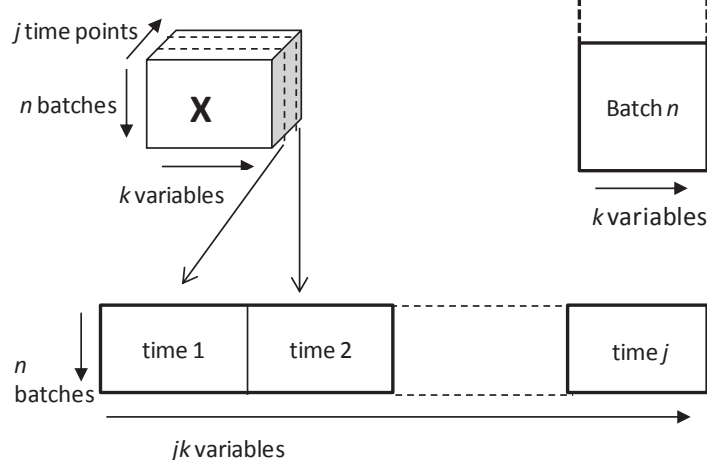


**Fig. 5.4. Unfolding of the 3-way data structure  $X$  to (A) observation level and (B) batch level.**

In the following manuscript (S. Pieters, Y. Vander Heyden, J.M. Roger, L. Hansen, M. D'Hondt, B. De Spiegeleer, C. Vervaet, J.P. Remon, T. De Beer, Raman spectroscopy for the in-line monitoring of protein unfolding during freeze-drying processes, in preparation) a strategy for the multivariate statistical in-line monitoring of protein unfolding with Raman spectroscopy is proposed and tested for the model protein LDH. Since the requirement for synchronous batches of equal length cannot be fulfilled in modern freeze-drying processes, the strategy proposes orthogonal projections to circumvent this problem.

**Multivariate statistical in-line monitoring of protein unfolding during  
freeze-drying using Raman spectroscopy**

Sigrid Pieters<sup>1</sup>, Yvan Vander Heyden<sup>1\*</sup>, Matthias D'Hondt<sup>2</sup>, Laurent Hansen<sup>3</sup>,  
Bart De Spiegeleer<sup>2</sup>, Jean-Paul Remon<sup>4</sup>, Chris Vervaet<sup>4</sup>, Thomas De Beer<sup>3</sup>

<sup>1</sup> Department of Analytical Chemistry and Pharmaceutical Technology, Center for  
Pharmaceutical Research, Vrije Universiteit Brussel - VUB, Laarbeeklaan 103, B-1090  
Brussels, Belgium

<sup>2</sup> Laboratory of Drug Quality & Registration (DruQuaR), Universiteit Gent,  
Harelbekestraat 72, B-9000 Ghent, Belgium

<sup>3</sup> Laboratory of Pharmaceutical Process Analytical Technology, Universiteit Gent,  
Harelbekestraat 72, B-9000 Ghent, Belgium

<sup>4</sup> Laboratory of Pharmaceutical Technology, Department of Pharmaceutics,  
Universiteit Gent, Harelbekestraat 72, B-9000 Ghent, Belgium

\* Corresponding author: Tel.: +32 2 477 47 34

Fax: +32 2 477 47 35

Email: [yvanvdh@vub.ac.be](mailto:yvanvdh@vub.ac.be) (Y. Vander Heyden)

**Key words**

Raman spectroscopy, in-line monitoring, freeze-drying, protein unfolding,  
multivariate statistical process control, orthogonal projection

**Abstract**

As protein unfolding should be minimized during freeze-drying to obtain protein pharmaceuticals with acceptable safety and efficacy, it is aspired to obtain this knowledge during the process itself. This work presents a strategy for continuously in-line monitoring of protein unfolding during freeze-drying processes using a fiber optic Raman probe. First, a detrimental spectral subspace containing only intra-batch process variability was defined from a set of Normal Operational Conditions (NOC) batches, i.e. batches leading to the desired native-like (NL) protein conformational state in the freeze-dried end product. To maximize the relevant-to-irrelevant spectral variance ratio, the process spectra of the NOC batches were, prior to building a statistical PCA model, orthogonally projected onto this subspace. Hence, the subspace used for building the PCA model was being practically transparent to experimental and process variations. This procedure made every process observation independent from the batch progress, just as if they were measurements over time. To distinguish at any process minute between the NL (in-control) and non-native (out-of-control) state of a model protein, lactate dehydrogenase (LDH), control charts based on Hotelling  $T^2$  and Q residuals were developed. As the same model could be used during the entire process, independent of the length of the successive freeze-drying phases (i.e. freezing, primary and secondary drying), this diagnostic tool may have potential to be implemented in flexible processes, e.g. during process development and combined with other PAT tools, determining the end points of primary and secondary drying of the batch. Using more NOC batches may eventually lead to more robust models.

### 1. Introduction

Freeze-drying is a low temperature drying process that is frequently used for drying pharmaceuticals, mostly proteins, to ensure their long term stability. It is a batch process where the starting material (solution) undergoes several transformations which finally lead to the end product (dry cake). It involves basically three different phases, i.e. freezing, primary and secondary drying, each characterized by different specific physical phenomena. The process starts with a freezing phase, where most of the water is converted into ice. The solutes are crystallized or transformed into a solid amorphous system. Next, during the primary drying step it is aimed to remove the ice crystals by sublimation. Finally, during the secondary drying step most of the unfrozen water is removed by desorption. During the entire freeze-drying process there are various large temperature changes (e.g. from -40° to +20°C) and during primary and secondary drying a vacuum (e.g. 150 µbar) is introduced [1-3]. Current Process Analytical Technology (PAT) tools, such as Tunable Diode Laser Absorption Spectroscopy (TDLAS), Manometric Temperature Measurement (MTM), allow determining the end points of primary and secondary drying of the batch. Hence, modern freeze-drying processes do not have fixed lengths for these process phases [4].

One important goal of the PAT concept is to transfer the off-line analyses of quality parameters (i.e. Critical Quality Attributes or CQA's) from the off-line laboratory to the process environment [5]. Consequently, one aspires improved quality assurance and process understanding, and ultimately, when all CQA's can be efficiently monitored and controlled, real-time release (RTR). Spectroscopic techniques have been proposed for the in-line monitoring of several CQA's of pharmaceutical formulations, such as moisture content by NIR [6-7], excipient solid state characterization by Raman and NIR [8-10], the crystallization of the active pharmaceutical ingredient fenofibrate by Raman [11], and protein unfolding and lyoprotection by NIR [12], during freeze-drying processes. NIR and Raman spectroscopy proved also being useful to determine process end points and physical phenomena happening during the different process phases [8-9].

Given its high sensitivity towards protein secondary structure, Raman spectroscopy has been proposed for monitoring ribonuclease unfolding in solutions when being stressed by guanidinium [13]. Unlike the univariate methodology that was used in the latter study, our previous study made use of the strong multivariate correlation between Raman spectra and protein unfolding to off-line classify native-like (NL, i.e. showing minimal changes in secondary structural element distribution) and non-native (DEN, i.e. showing significant changes in secondary structural element distribution) conformational states of the model protein lactate dehydrogenase (LDH) [14]. In this manuscript, we aimed evaluating whether Raman spectroscopy can be applied for obtaining *in-line* and *real-time* information on protein unfolding during the freeze-drying process itself. A serious drawback when transferring the supervised off-line classification model to in-line use would be the requirement for process reference sampling [15]. Direct standardization methods [16] and orthogonal projection methods, such as Transfer by Orthogonal Projection (TOP) [17] and Dynamic Orthogonal Projections (DOP) [18], may be helpful to keep the reference sampling for calibration transfer minimal. However, even then one would still require reference in-line sampling for method validation. This can be more complex in a batch process where strong dynamic time dependencies are expected, as the process Raman spectra may also be sensitive to some of these types of variation.

Multivariate Statistical Process control (MSPC) and Batch Statistical Process Control (BSPC) have become attractive alternatives to the in-line calibration problem [15, 19-20]. A statistical model compares the multivariate process observations to those from historical process data in Normal Operating Conditions (NOC), i.e. conditions providing products with an acceptable quality. Hence, the variation within the NOC samples provides a reference distribution, against which the new observations can be compared. Usually, to simplify the problem, the high-dimensional process data space is projected onto a much lower dimensional latent variable space. Principal Component Analysis (PCA) and Partial Least Squares (PLS) are commonly used for this. The statistical model is typically validated with in- and out-of-control batches.

Orthogonal pre-processing may allow separating the systematic variations in the spectra originating from the property of interest from those with other origins [21-22]. This can be advantageous to enhance the interpretability of multivariate models (i.e. projection-based latent variable models) [15, 22-23], which may not be straightforward because of the confounding of different systematic variations in the model components. A well-known example of this in MVC is o-PLS [24]. In MSPC, Net Analyte Signal-based statistical quality control has been developed to enhance the interpretability of the control charts for multivariate product quality monitoring [23].

MSPC is generally used for continuous processes, whereas batch processes usually require BSPC. As batch processes yield a 3-way data structure (i.e.  $n$  batches,  $j$  time points,  $k$  variables), the idea for data analysis is to either unfold the data structure or to use a 3-way approach. Unfolding can be performed on the batch level ( $n,k,j$ ) or on the observation level ( $nj,k$ ). Unfolding on the observation level makes in-line monitoring possible. However, a typical problem in BSPC is that it requires making a statistical model at any observation point during the batch evolution. This requires thus a number of synchronized NOC batches (enough to approximate a statistical distribution at any measurement point) of equal duration (or properly aligned) [19-20]. This can be a drawback, especially for batch processes consisting of different phases of an unfixed length, such as modern freeze-drying processes.

In this work, it was investigated whether the real-time discrimination (i.e. for every process minute) between the NL and the DEN conditions during freeze-drying processes is possible from the in-line acquired Raman spectra. In an earlier study [14], it was found that Raman spectra proved highly sensitive to make this classification, i.e. the NL state is desired and any deviation from this is regarded as non-native (DEN) and should be avoided. As the freeze-drying process Raman spectra are also influenced by dynamic time dependencies originating from the inherently varying process and experimental parameters, this may interfere with the classification. To circumvent the problem of having batch processes of unequal duration, the following strategy proposes making

the in-line classification independent from the process dynamics by orthogonal projections.

## 2. Proposed in-line monitoring strategy

### 2.1. Orthogonal spectral pre-processing to reduce the space dimensionality with regard to process dynamics and experimental parameters

The process Raman spectra of  $n$  NOC batches were acquired. The length of the processes, as well as the individual duration of the different process phases, was ignored. Hence, the obtained batch data structure consisted of  $n$  NOC batches,  $k$  variables, and  $j$  observations (where  $j$  can be variable for each batch). This 3-way data structure was unfolded to the observation level, hence a matrix  $\mathbf{X}$  ( $nj \times k$ ) is obtained.

Let  $U$  be the property to be predicted, and  $Z$  the external parameter(s) to be removed. In our case study, the variable vector space of the Raman spectral data matrix  $\mathbf{X}$ , i.e.  $\vec{X}$ , can be seen as the sum of three subspaces, namely  $\vec{U}$ ,  $\vec{Z}$  and  $\vec{R}$ .  $\vec{U}$  spans the predictive systematic spectral variation correlated to  $U$  (i.e. the class membership) and is independent from  $Z$ .  $\vec{Z}$  covers the systematic spectral variation generated by  $Z$  while being independent from  $U$  (i.e. the class-orthogonal variation).  $\vec{R}$  contains the residual spectral information, such as the measurement noise. The aim of the orthogonal projection method is to project  $\mathbf{X}$  in such a way that only the useful subspace  $\vec{U}$  is retained to develop the multivariate model. In other words, the subspace decomposition of  $\mathbf{X}$  can be written in matrix notations as follows (Eq. 1) [25].

$$\mathbf{X} = \mathbf{XM} + \mathbf{XQ} + \mathbf{R} \quad (1)$$

where  $\mathbf{M}$  and  $\mathbf{Q}$  are the matrices of the projection operators onto  $\vec{U}$  and  $\vec{Z}$ , respectively, and  $\mathbf{R}$  is the residual matrix.

In this case study, the detrimental subspace  $\vec{Z}$  is estimated from the within NL class process variation. The mean-centered process spectra of batches leading to a NL end product (i.e. these conditions represent the NOC) were

used for this. In other words, for such NOC batches all spectral variations happening during the process can be regarded as class-orthogonal spectral variations. As they typically originate from batch process dynamics and experimental variations, we can assume that such variations are equally present in the process spectra leading to DEN samples (as they will undergo the same influences of external process parameters).

In practice,  $\bar{Z}$  was estimated in the following way:

- (1) The process Raman spectra of each NOC batch are split into their respective phases i.e. freezing, primary and secondary drying. Thus, for each  $i^{\text{th}}$  NOC batch 3 matrices of process Raman spectra are obtained, namely  $\mathbf{A}_{i,fr}$ ,  $\mathbf{A}_{i,prim}$  and  $\mathbf{A}_{i,sec}$ . The number of rows of these matrices correspond to the respective number of process observations, and the number of columns match to the number of variables acquired in the Raman spectra.
- (2) Each of these matrices is mean centered to obtain the matrices  $\mathbf{A}_{i,fr,c}$ ,  $\mathbf{A}_{i,prim,c}$  and  $\mathbf{A}_{i,sec,c}$ , basically consisting of the process and experimental spectral variations typically for every process phase in each batch.
- (3) Three new matrices, i.e. one for every process phase, are composed by adding the individual matrices of the  $n$  batches for each process phase. Consequently,  $\mathbf{F}$  (freezing) consists of the  $n$  obtained  $\mathbf{A}_{i,fr,c}$  matrices,  $\mathbf{P}$  (primary drying) consists of the  $n$   $\mathbf{A}_{i,prim,c}$  matrices, and  $\mathbf{S}$  (secondary drying) consists of the  $n$   $\mathbf{A}_{i,sec,c}$  matrices.
- (4) With the aid of the minimal root mean square error of cross-validation (i.e. random subsets, 20 splits, 5 iterations) or root mean square error of cross validation (RMSECV), PCA models are developed for each of these matrices  $\mathbf{F}$ ,  $\mathbf{P}$  and  $\mathbf{S}$ , to separate the systematic variations from the noise. For  $\mathbf{F}$  the first  $f$  principal components (PC's) were selected, for  $\mathbf{P}$  the first  $p$  PC's, and for  $\mathbf{S}$  the first  $s$  PC's.
- (5) The  $f$ ,  $p$  and  $s$  PCA loadings for the freezing, primary and secondary drying step, respectively, are merged into a matrix  $\mathbf{Z}$ . Hence, this matrix contains the undesired process spectral signatures. The column vector space of this matrix  $\mathbf{Z}$ , defined by its full rank, estimates the basis of the detrimental subspace  $\bar{Z}$ . Hence, an estimation of  $\mathbf{Q}$  is obtained by Eq. 2.



$$\mathbf{Q} = \mathbf{Z}(\mathbf{Z}^T \mathbf{Z})^{-1} \mathbf{Z}^T \quad (2)$$

(6) Projection of the Raman process spectra  $\mathbf{X}$  onto the subspace orthogonal to the estimate of the detrimental subspace  $\vec{Z}$  renders  $\mathbf{X}^*$  (Eq. 3).

$$\mathbf{X}^* = \mathbf{X}\mathbf{M} = \mathbf{X}(\mathbf{I} - \mathbf{Q}) \quad (3)$$

Where  $\mathbf{I}$  is the identity matrix. Thus, it is aspired that the returned spectra in  $\mathbf{X}^*$  are now being cleaned from the systematic variations spanned by  $\vec{Z}$ .

Orthogonal preprocessing before building a multivariate model has the advantage that multiple external factors can be handled, and that the model remains robust even when the influence of the factor disappears [21]. Using this strategy, it is aspired to make the multivariate model built from  $\mathbf{X}^*$  robust for multiple interfering external factors (appearing and disappearing over process time) during the freeze-drying process. Of course, the success of this operation will strongly depend on how well  $\vec{Z}$  can be estimated. In this case study, it was aspired to make the process spectra basically transparent to the dynamic process and experimental spectral variations by estimating  $\vec{Z}$  via the within-NL class process variation of the set of NOC batches.

## 2.2. Model development

Based on historical data, that consistently showed an in-control situation for the parameter(s) of interest, one can establish a multivariate acceptability area in a statistical way. This way, one can assess from each process measurement whether the process is still in a state of statistical control, i.e. whether it is operating as it should be with respect to the quality attribute of interest. A PCA-based confidence domain was defined by developing a PCA model from the orthogonally pre-processed Raman process spectra ( $\mathbf{X}^*$ ) of the  $n$  NOC batches. The optimal dimension of the PCA model was found by the minimal RMSECV (random subsets, 20 splits, 5 iterations). Thus, the orthogonally pre-processed training spectra are projected onto a latent variable space of much lower dimension than the original variable space.

Multivariate control charts were developed based upon two complementary statistics, i.e. Hotelling  $T^2$  and Q residuals. In brief, the Hotelling  $T^2$  statistic monitors the variation within the established model, whereas the Q residuals measure the lack-of-fit to the model [19-20]. Warning and action limits were set at 95% and 99%, respectively.

### *2.3. Model validation*

Process Raman spectra from new batches leading to NL and DEN end products were acquired to validate the model. Hence, for any validation batch process spectrum  $\mathbf{v}$ , the orthogonal projection defined in step (6) of section 2.1 is applied, in order to render  $\mathbf{v}^*$ . Next,  $\mathbf{v}^*$  is projected onto the hyperplane defined by the PCA model developed from the NOC batches (see section 2.2). Hotelling  $T^2$  and Q residual values are calculated for the process observations of the validation batches to monitor the processes and compare the process trajectories with the statistical limits (defined in section 2.2). T and Q contributions are calculated to get an indication of the origin of the deviation [19-20]. For a given sample, T and Q contributions, respectively, describe how individual variables contribute to the Hotelling  $T^2$  and Q residual values.

## **3. Experimental section**

### *3.1. Materials*

L-Lactic Dehydrogenase from rabbit muscle - Type II in ammonium sulfate was obtained from Sigma-Aldrich (Saint Louis, MO, USA). From this raw material, LDH formulations were prepared (see Table 1) containing approximately 9 mg/ml LDH [14]. The formulations were either in water or in 40 mM buffer pH 7.4. Sodium phosphate (PHOS) and sodiumthiocyanate (NaSCN) were from Sigma-Aldrich (Steinheim, Germany). L-histidine (HIS) and TRIS were purchased from Merck (Darmstadt, Germany). Some formulations contained 5% sucrose from Suedzucker (Mannheim, Germany) and/or 1% polyethylene glycol (PEG 4000) from Fagron (Barsbüttel, Germany). Plastic cutted vials were filled with 2 mL formulation prior to freeze-drying.

### *3.2. Freeze-drying*

Freeze-drying was performed using an Amsco FINN-AQUA GT4 laboratory scale freeze-dryer (GEA, Koeln, Germany). Freezing was always performed at -40°C, primary drying at -20°C, and secondary drying at 20°C. Freezing was performed at atmospheric pressure, while primary and secondary drying were performed at 150 µbar. Temperature ramps between the process phases were always at a rate of 0.2°C/min. Processes with a longer freezing duration had slower cooling rates, while the actual freezing step at constant temperature (-40°C) always lasted 2h. From Table 1 it can be seen that the individual lengths of the different process phases, i.e. freezing, primary drying and secondary drying, of the batches produced for this study were not always equal. Yet all batches underwent the same necessary processing steps to obtain the end product and thus experienced the same external influences inherent to the freeze-drying process. Five out of ten in-line monitored freeze-drying batches led to a NL state of the proteins in the freeze-dried end product, whereas the proteins in the five other freeze-dried batches were being evaluated as non-native in the freeze-dried end product. Batches 2, 5, 6 and 7, which led to the NL condition in the end product, were considered as NOC batches. Hence, they were being used for the calculation of the orthogonal projection and for the statistical model development. The other batches, containing one labeled as NL, were used to validate the model.

### *3.3. Raman spectroscopic conditions and in-line set-up*

A Raman Rxn1 spectrometer (Kaiser Optical systems, Ann Arbor, MI), equipped with an air-cooled CCD detector (back-illuminated deep depletion design), was used in combination with a fiber-optic non-contact MR probe. The Invictus NIR diode laser used a wavelength of 785 nm. Spectra were recorded with a resolution of 4 cm<sup>-1</sup> and an exposure time of 50 s, using a laser power of 400 mW. The experimental Raman spectra were used without any pre-processing, as this gave the best classification result in reference [14].

Table 1. Experimental conditions of the in-line monitored freeze-drying runs (batches) used in this study.

batch	formulation type	duration freezing (min)	duration primary drying (min)	duration secondary drying (min)	total number of process observations	conformational state in the freeze-dried product	purpose
1	HIS, 5% sucrose	162	1270	225	1657	DEN	test
2	HIS, 5% sucrose, 1% PEG	300	1270	58	1628	NL	NOC
3	water	360	1270	669	2299	DEN	test
4	PHOS, 50 mM NaSCN	360	1230	2701	4291	DEN	test
5	TRIS, 5% sucrose	135	985	614	1734	NL	NOC
6	TRIS, 5% sucrose	135	985	1087	2207	NL	NOC
7	TRIS, 5% sucrose	135	985	603	1723	NL	NOC
8	TRIS, 5% sucrose	135	985	1324	2444	NL	test
9	water	135	985	599	1719	DEN	test
10	PHOS	135	985	2833	3953	DEN	test

Abbreviations: NL (native-like), DEN (non-native), NOC (Normal Operational Conditions, to calculate the orthogonal projection and to train the statistical model), test (test set, to validate the statistical model), HIS (40 mM histidine buffer pH 7.4), PHOS (4. mM phosphate buffer pH 7.4), TRIS (40 mM TRIS buffer pH 7.4).

The Raman probe was built into the freeze-dryer chamber via a modification of the laboratory scale freeze-dryer. The optical fiber cable entered the freeze-drier through a small channel made in the chamber wall. The probe head was placed above the open vial, so it could monitor a part of the top surface of the protein formulation, as in refs [8-9]. Every process minute, one Raman spectrum was acquired. Given the typical long duration of the freeze-drying process, one can claim that this set-up allows practically real-time monitoring of the product behavior.

### *3.4. FTIR spectroscopy*

FTIR spectroscopy functioned as a reference technique to evaluate whether or not the proteins in the freeze-dried product are NL [14]. FTIR spectroscopy measurements were conducted on a Varian Scimitar 800 FTIR spectrometer, equipped with a Specac Golden Gate diamond ATR module (Varian Scimitar, Middelburg, The Netherlands). The spectra were recorded from 4000 to 500  $\text{cm}^{-1}$  in ATR mode at a resolution of 2  $\text{cm}^{-1}$ . Each measurement was the average of 100 scans. The FTIR spectra of the same freeze-dried samples and the corresponding blanks were first background (air) corrected and converted to absorbance format. The resulting FTIR absorbance spectra were subsequently corrected for the spectral contributions of the blank formulations. Finally, the second derivative with 17-point Savitzky-Golay smoothing was performed and the FTIR spectra were area normalized over the amide I region (1700-1600  $\text{cm}^{-1}$ ) for direct comparison.

### *3.5. Data handling*

All data handling was performed in Matlab 7.1. (The Mathworks, Natick, MA) using in-house routines for the orthogonal projections and the PLS toolbox 6.2 (Eigenvector Research, Wenatchee, WA) for building the PCA models and developing the control charts.

## 4. Results and discussion

### 4.1. Influence of the Raman laser on the physical stability of the protein during in-line monitoring

The intense energy of the Raman laser may affect the stability of certain samples [26]. Therefore, it was first investigated whether the physical stability of the model protein was not affected when being continuously exposed to the Raman laser during the freeze-drying process. After in-line monitoring of batch 2 (see Table 1), the monitored sample spot was visible as a small cavity in the top section of the cake. This spot was specifically sampled for ATR-FTIR analysis. Fig. 1 shows that the amide I FTIR spectrum of this sample spot has minimal changes in terms of secondary structural element distribution compared to the native state spectrum. Therefore, it was concluded that the exposure to the Raman laser during a freeze-drying process did not negatively affect the physical stability (in terms of secondary structures) of the model protein LDH. In the DEN samples, obvious changes in secondary structures were observed. An example of a DEN sample from batch 4 is also shown in the Figure.

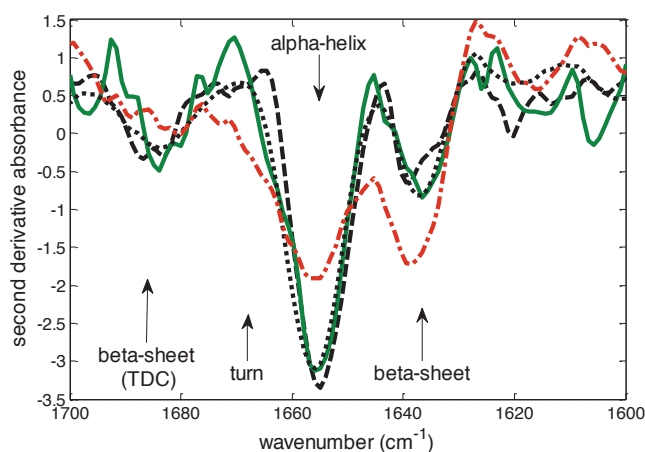


**Fig. 1.** The amide I FTIR spectrum of a freeze-dried sample of batch 2 (NL) that was continuously exposed to the Raman laser (full green line), that of the native state in solution (dashed black line), that of the average NL freeze-dried state (black dotted line), and that of a freeze-dried DEN sample (dotted red line) from batch 4.

### 4.2. Common cause variation in process Raman spectra

To get an idea of the common cause variation in process Raman spectra (i.e. the within NL class process variation), a PCA was performed on the process

spectra of the NOC batches. For simplicity, only one representative example (batch 5) is shown in Fig. 2. The PC1-PC2 scores plot of the mean-centered process spectra shows the process variation that can be considered for this batch. This plot clearly illustrates that the variations originating from process dynamics are dominant in the process Raman spectra. There are, compared to the drying phases with much longer duration, strong spectral changes during the relatively short freezing step. The latter variations could be related to the transformation of the liquid solution to ice. Other clearly observed systematic variations (not shown) in the process spectra were the result of the induction of the vacuum and temperature changes, being inherent to the freeze-drying process as well.

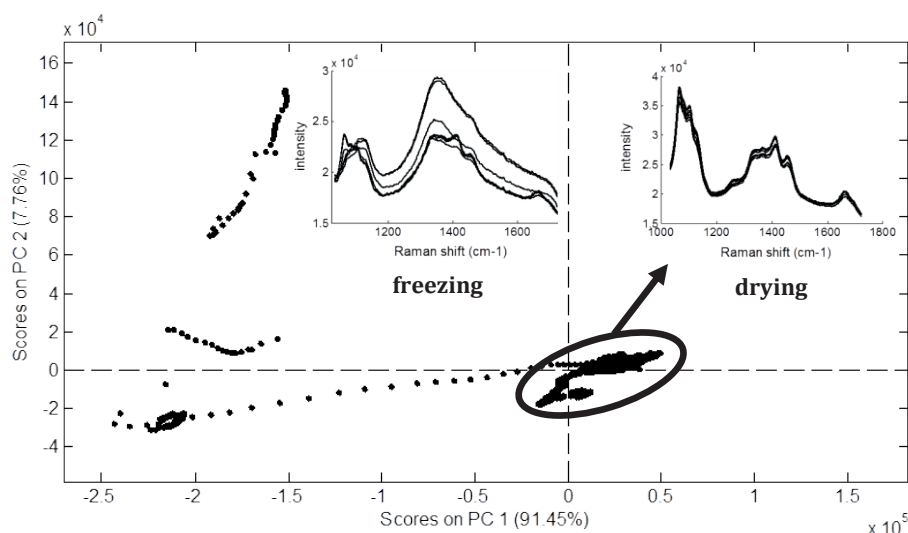


**Fig. 2.** PC1-PC2 scores plot of a PCA on the mean centered process spectra of batch 5. The freezing spectra shown are every 20' recorded during the freezing phase, the drying spectra shown are every 200' recorded during drying.

Between-batch variations were also detected in the process Raman spectra. An obvious example is shown in Fig. 3. The process Raman spectra of batch 7 showed intense systematic variations for the observations from 1400 to 1734, while these were not seen for batches that, according to the process settings, should experience exactly the same process influences (e.g. batch 5).

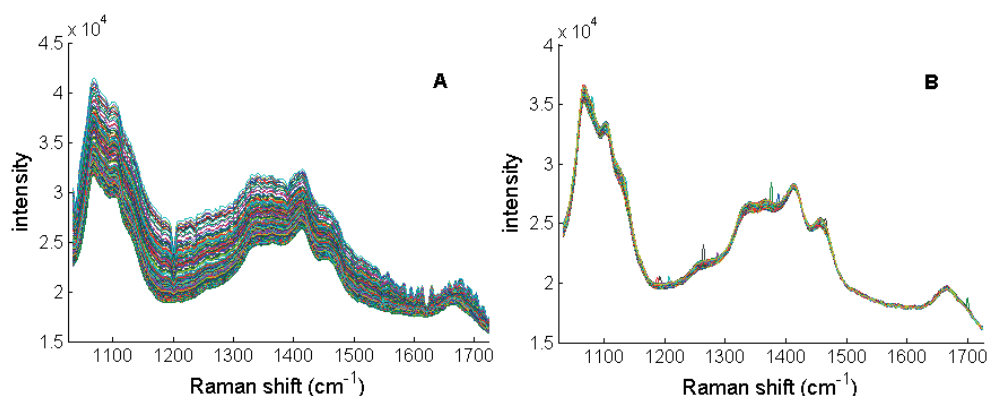


**Fig. 3.** Process Raman spectra 1400-1734 (secondary drying at constant 20°C at 150 µbar) are shown for batch 7 (A) and batch 5 (B).

As these variations were only present during this short time frame, and showed an additive background effect, it is believed that they might originate from changes in the sample-probe distance. This kind of experimental variability may occur when the vial moves a little as a result of the vacuum. It should also be noted that during the freeze-drying of proteins leading to a NL end product there may also happen some minimal changes in the protein conformation (i.e. a NL protein is never completely identical to the native state conformation in solution). However, these minimal changes (being inherent to the NL class), are 'allowed' as long as they do not exceed a certain limit (and then become members of the DEN class).

Thus, to obtain a good estimate of the within NL-class process variation, the process spectra of representative NOC batches should be considered. In a preliminary experiment, it was aspired to estimate the detrimental subspace from a PCA performed on the matrix (7292 observations  $\times$  2301 variables), containing all the process spectra of the 4 NOC batches (mean-centered per batch). However, because of the unequal weights of the spectral variations in this matrix, it was not possible to obtain this way a good estimate for the detrimental subspace (data not shown).

For instance, a problem was that the spectral variations of the freezing phase were insufficiently covered by the principal components. This is possibly the result of the fact that these spectral variations occur only during a relatively



short time frame, compared to those in the much longer drying phases. Therefore, estimates for the external factors to be removed were found by performing PCA on each individual process phase. For the freezing, primary drying and secondary drying, the first  $f=11$ ,  $k=3$  and  $s=3$  LV's were selected and merged into **T** (17 x 2301). They described 99.95%, 99.56% and 99.11% of the variances in **F**, **K**, and **S**, respectively. Afterwards, the 17 relevant loading vectors were merged into one matrix to calculate the orthogonal projection for the full process (as is explained in section 2.1).

#### *4.3. Effect of orthogonal preprocessing on the process spectra*

To investigate the effect of the orthogonal preprocessing on the process spectra, we performed an exploratory analysis (PCA) on the process spectra of 2 NL and 2 DEN batches, before and after orthogonal pre-processing (Figs. 4-5). In both figures, differences between the process trajectories of the NL and DEN samples can be observed. Without orthogonal pre-processing (Fig. 4), the process trajectories of all batches are strongly dominated by dynamic time dependencies inherent to the freeze-drying process. Conversely, in Fig. 5, it can be seen that the orthogonal pre-processing has basically removed these dynamic time dependencies from the batch process spectra, i.e. they have been returned just as if they were repeated observations. There was essentially random variability in the scores of the first 3 PC's (and also in the higher PC's) of the pre-processed process spectra of the NL batches. Compared to Figs. 4B-D, the Figs. 5B-D show more pronounced differences between the NL and DEN batches. We also see that the scores of the DEN batches start in the cluster of the scores of the NL batches and, as the process continues, move gradually away from it. Thus, this operation has increased the relevant-to-irrelevant data variance ratio's and improved the interpretability of the score plots.

#### *4.4. Statistical model development from orthogonally pre-processed NOC spectra*

As it is possible to 'clean' the process spectra from the expected process variations, a statistical model to distinguish between the NL and DEN conditions can be developed in a more straightforward way, i.e. not every process observation should be modeled (as is the standard for batch

processes), but one model can be made to monitor the whole process. This also eliminates the requirement that the processes (and their phases) need to have the same duration. A PCA model (5 LV's) has been developed from the orthogonally pre-processed process Raman spectra ( $\mathbf{X}^*$ ) of the 4 NOC batches. It described 90.55% of the variance of  $\mathbf{X}^*$ . The orthogonal preprocessing has basically removed the within-process variation from the process spectra of the NOC batches. However, the inter-batch variability remains and is modeled. This can, for instance, be seen in Fig. 6A, showing the PC2-PC4 scores plot of the PCA model built from the NOC batches. Interestingly, the first PC of the model described mainly the variation between the batches that were produced at different times (i.e. batches 1, 2, 3 and 4 were produced 7 months earlier) (Fig. 6B). As they were all produced from the same LDH raw material batch, the reason for this should be further investigated with appropriate experiments.

The PCA model is assumed to be static. This means that every process observation is compared to a settled mean vector and variance-covariance matrix, defined by the NOC conditions. The Hotelling  $T^2$  control chart relies on the assumption of multivariate normality of the variables constituting the model. The scores of PC1 behave in a discrete manner (Fig. 7A), while the scores of the other PC's behave in a continuous way and follow all a normal distribution (Fig. 7B-C). Since PC's are by definition orthogonal, the PC's with continuous score values are here thus multivariate normal. The Q residuals chart follows a weighted chi-square distribution ( $\sim g\chi^2$ ), since the Q residuals are squared prediction errors. Fig. 8 shows the two multivariate control charts with the statistical limits (i.e. 95% and 99%) that were developed from the PCA model (5 PC's) of the 4 NOC batches, and its residuals to the model.

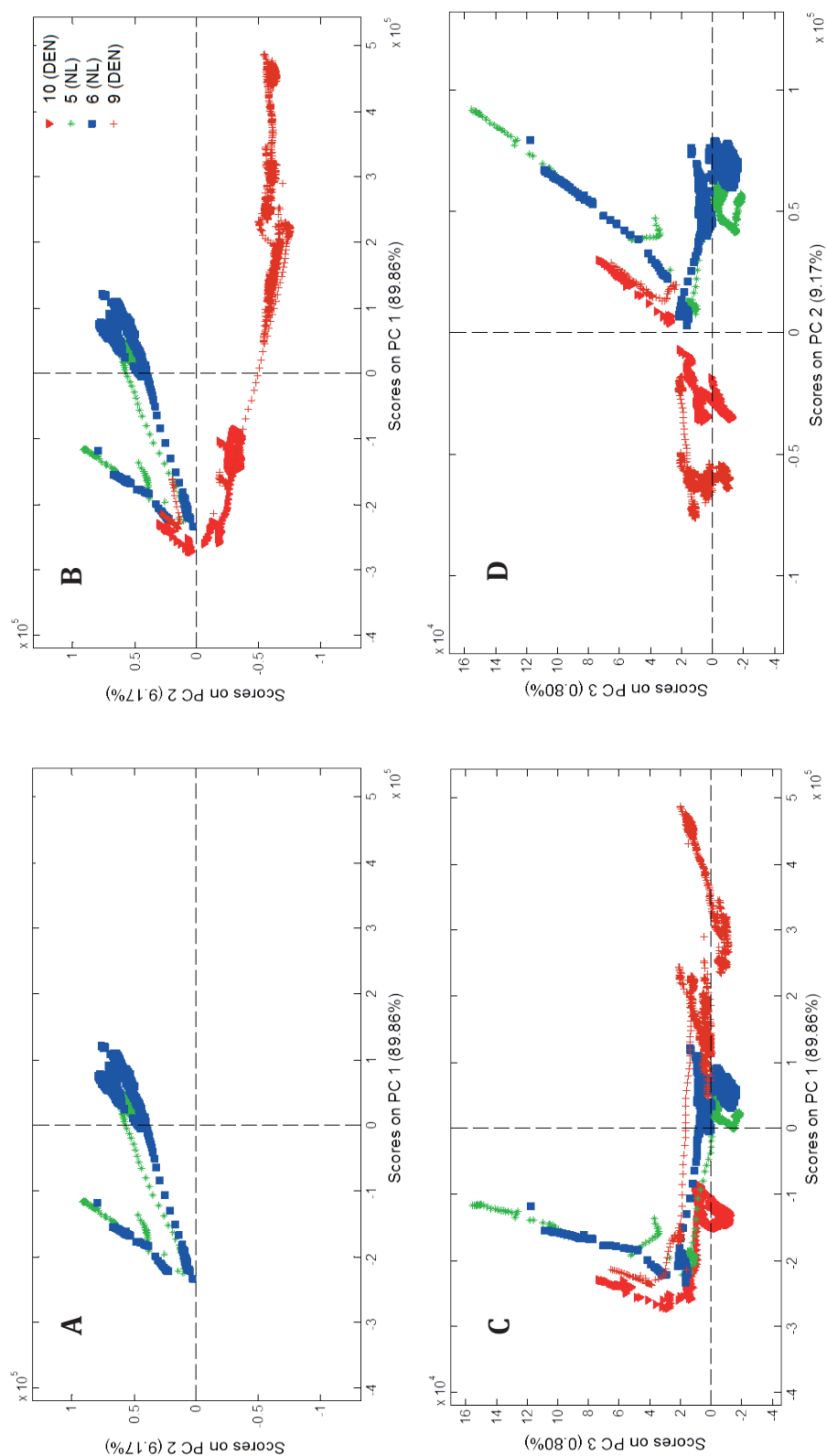


Fig. 4. Exploratory analysis (PCA) of the process spectra of 4 batches (2 NL and 2 DEN). (A) PC1-PC2 scores plot showing only the two NL batches 5 and 6, (B) PC1-PC2, (C) PC1-PC3, and (D) PC2-PC3 scores plots of the 4 batches.

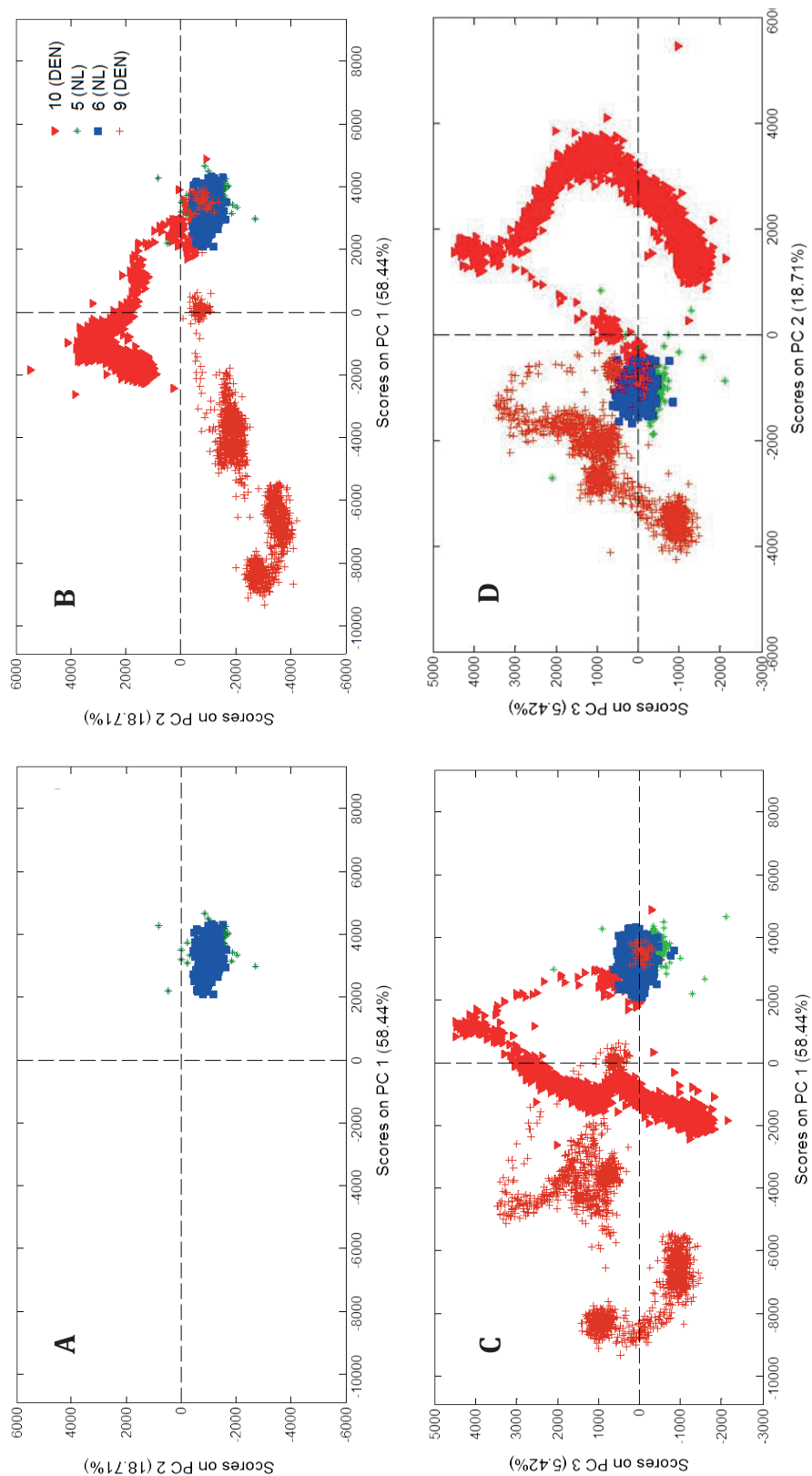


Fig. 5. Exploratory analysis (PCA) of the process spectra of 4 batches (2 NL and 2 DEN) after being orthogonally pre-processed. (A) PC1-PC2 scores plot showing only the two NL batches 5 and 6, (B) PC1-PC2, (C) PC1-PC3, and (D) PC2-PC3 scores plots of the 4 batches.

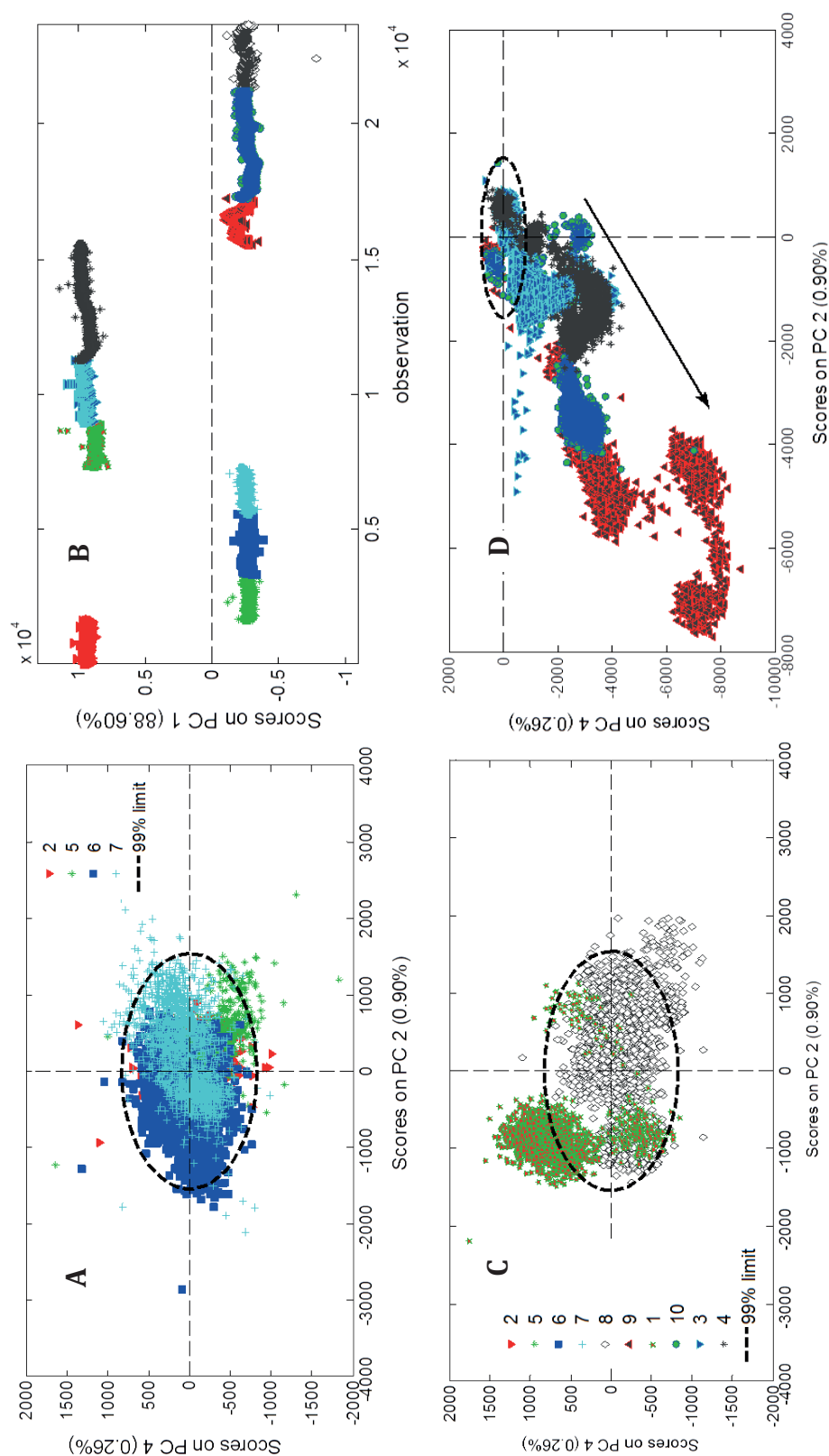
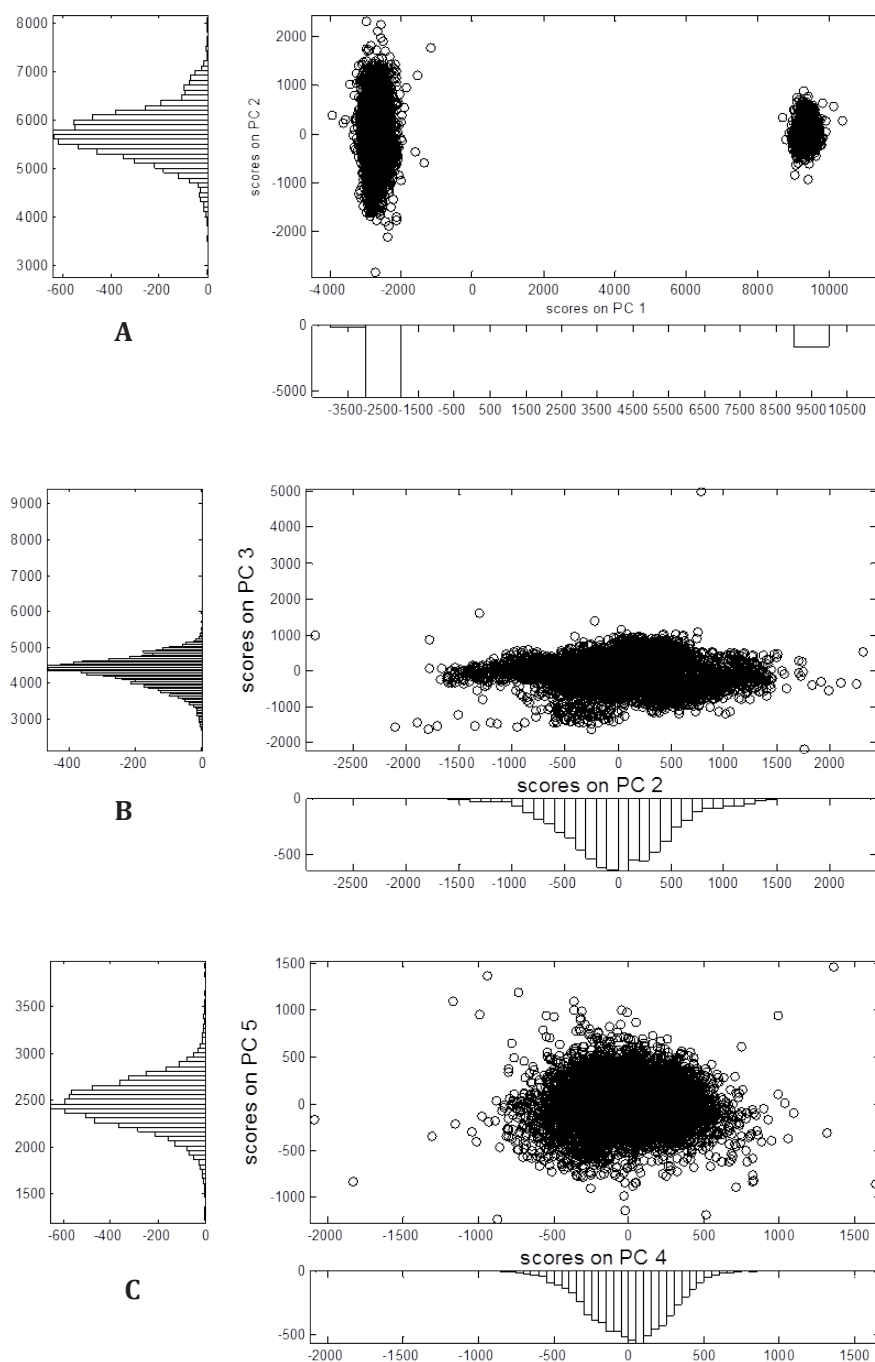
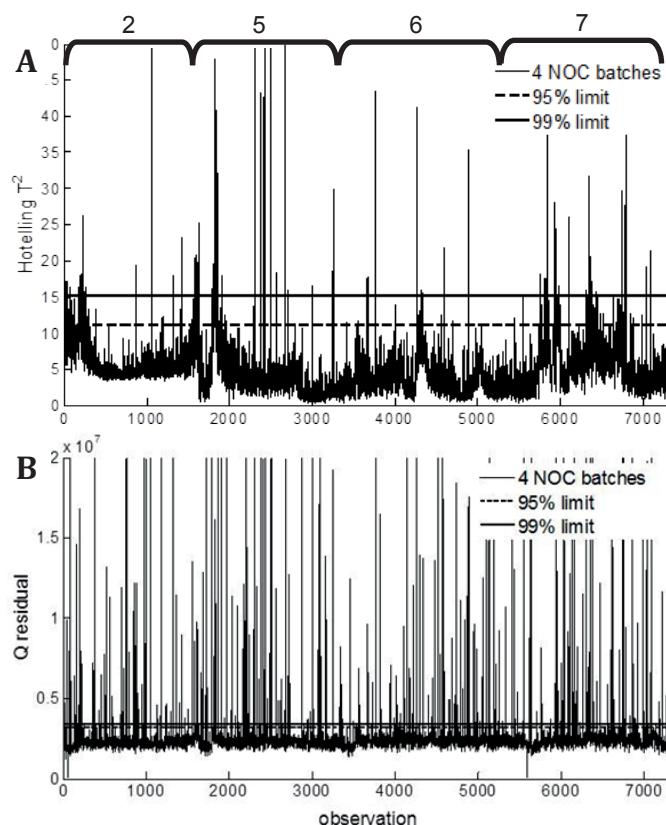


Fig. 6. Statistical PCA model developed from the 4 orthogonally pre-processed NOC batches. PC2-PC4 scores plot of (A) the 4 NOC batches, (C) test batches 1 (DEN) and 8 (NL), (D) test batches 3,4,9 and 10 (all DEN), (B) PC1 scores of all batches as a function of observation.

## Chapter 5: MEASURING PROTEIN UNFOLDING IN RAMAN SPECTRA IN THE PRESENCE OF SPECTRAL INTERFERENCES



**Fig.7.** Scatter plots of the scores of the 5 PC's constituting the PCA model used for MSPC. (A) PC1-PC2, (B) PC2-PC3, and (C) PC4-PC5 score plots. For each individual PC a histogram, showing the distribution of the scores, is shown as well.



**Fig. 8. (A) Hotelling  $T^2$  and (B) Q residuals control charts of the PCA model developed from the orthogonal preprocessed Raman spectra of 4 NOC batches used (i.e. batches 2, 5, 6 and 7) with statistical limits developed on the 95% and 99% confidence intervals.**

#### 4.5. Validation with in-line runs leading to NL and DEN samples

Figs. 9-14 show the control charts for monitoring the test batches 1, 3, 4, 8, 9, 10. For the NL batch 8 (Fig. 9), the Hotelling  $T^2$  chart was during the entire process generally within the limits, except for a short interval between 170 and 240 min (primary drying). The Q residuals did not systematically increase during the process time. However, they were sometimes slightly exceeding the limits, also during that same time interval. In Fig. 6C, the scores that fall systematically outside the ellipse being related to the 99% limit (defined by the NOC batches) are those observations 170-240. The others fall, except for some individual outliers, inside the limits. The reason for this deviation should be further investigated, but may possibly be related to the strong pressure differences at the beginning of primary drying (primary drying started at 136 min in this process) to reach the vacuum. Possibly, the spectral responses to this were stronger, or different, than those seen in the NOC batches.

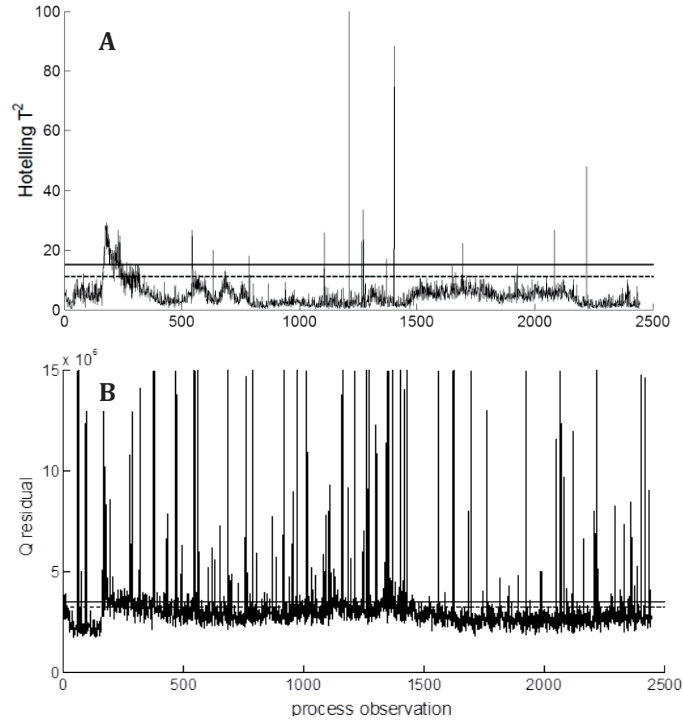


**Fig. 9. (A) Hotelling  $T^2$  and (B) Q residuals charts of the orthogonally pre-processed process spectra of test batch 8 (NL) when being projected onto the PCA model developed from the 4 NOC batches. The dashed and full lines represent the 95% and 99% limits, respectively.**

As it is very important to fully identify the detrimental information to be removed by orthogonal projection [21], considering more NOC batches (i.e. they should be representative for all the expected common cause process variability) in the model may potentially overcome this problem and increase the model robustness.

In Fig. 10, the control charts for monitoring test batch 1 (DEN) are shown. Around approximately 200 min (during freezing), there is a systematic increase in the Hotelling  $T^2$  and Q residual values. After this, they remain higher (generally outside the limits) until the end of the process. However, before this systematic change the Hotelling  $T^2$  values appeared already near or slightly above the statistical limits, whereas the Q residual values were already from the beginning much higher than the statistical limits, as if there was an offset. The latter indicates that the variation in this batch cannot be described by the developed model.



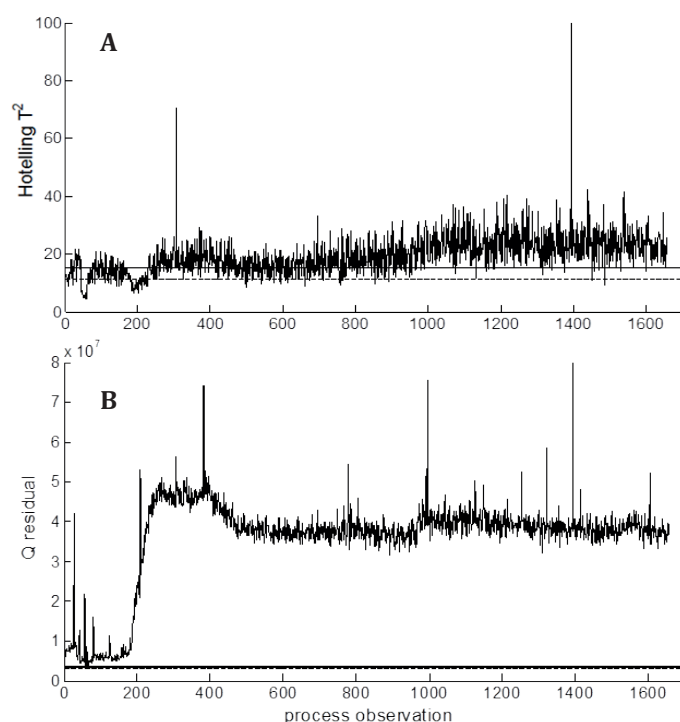


**Fig. 10. (A) Hotelling  $T^2$  and (B) Q residuals charts of the orthogonally pre-processed process spectra of test batch 1 (DEN) when being projected onto the PCA model developed from the 4 NOC batches. The dashed and full lines represent the 95% and 99% limits, respectively.**

In Fig. 6C, the scores went, as the process continued, out of the limit along PC4, while the other DEN batches (Fig. 6D) went out of the limit in a different direction. This batch contained, just as batch 2, histidine and sucrose, where possibly a Maillard reaction can occur [27]. It was also seen that all process spectra from batch 2 behaved differently than the other NOC batches (data not shown). Because of the higher distances to the model, this offset suggests that the spectra of batch 1 carry spectral variations that were not fully covered by the NOC batches used to develop the model. As the spectra of batch 1 differ from the training data, this might result in inaccurate predictions [15]. Hence, to allow reliable predictions for new batches the model should also cover all the expected inter-batch variation. Thus, for robust statistical model development, one should consider more NOC batches to fully represent the intra- and inter-batch variability. As a future work, more NOC batches will be produced for this reason. In Figs. 11-14, the control charts for monitoring the DEN batches 3, 4, 9 and 10, respectively, are shown. In all charts, the Hotelling  $T^2$  and Q residuals values start to systematically increase at a certain process

moment, mostly already during freezing. This was somehow expected given that freezing is a well-known stress factor for protein unfolding [28]. This was also seen in Fig. 6D, where the scores of the process spectra started within the 99% confidence ellipse, and gradually moved away, hereby following the same direction (indicated in Fig. 6D with an arrow). Fig. 15 shows the T and Q contribution plots of an out-of-control sample (i.e. sample 1832) of batch 4. They indicate the variables that contribute to the deviations in the respective charts. In the T contribution plot of this sample (Fig. 15A), the spectral regions that were earlier linked to protein unfolding [14] were clearly emphasized. These regions include the amide III (1200-1320  $\text{cm}^{-1}$ ) being related to the protein backbone, and the  $\text{CH}_n$  non-stretching (1320-1500  $\text{cm}^{-1}$ ), the C-N stretching and  $\text{NH}_3$  bending regions (1033-1200  $\text{cm}^{-1}$ ), being related to exposure of amino acid side chains. They indicate that protein unfolding is the major cause of this deviation in this sample.

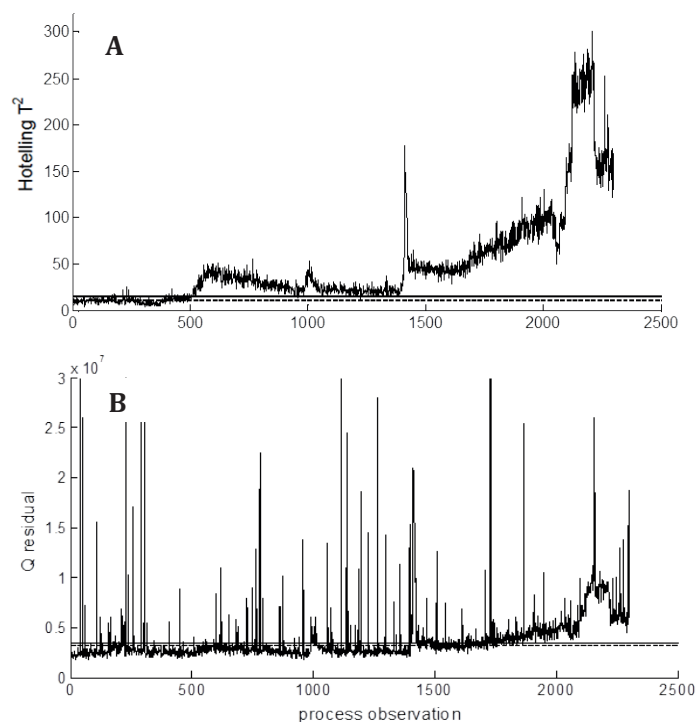


**Fig. 11. (A) Hotelling  $T^2$  and (B) Q residuals charts of the orthogonally pre-processed process spectra of test batch 3 (DEN) when being projected onto the PCA model developed from the 4 NOC batches. The dashed and full lines represent the 95% and 99% limits, respectively.**

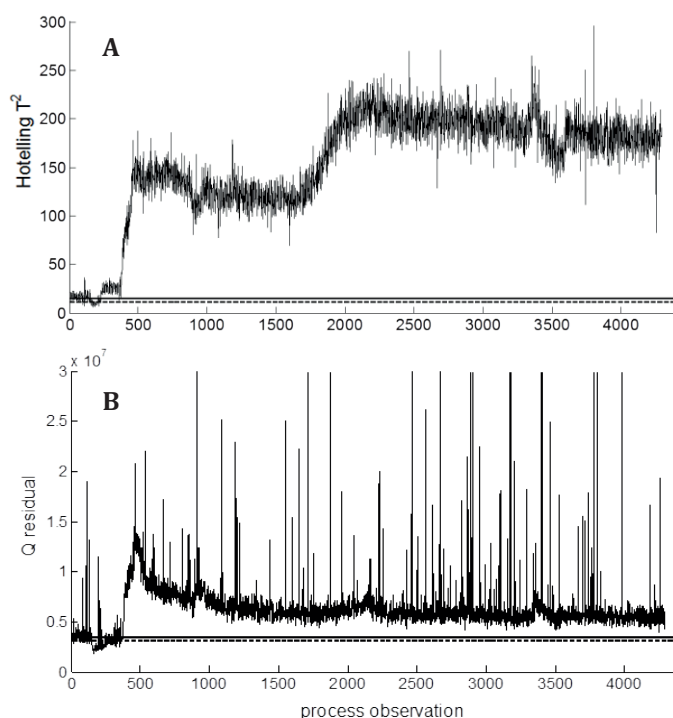


**Fig. 12. (A) Hotelling  $T^2$  and (B) Q residuals charts of the orthogonally pre-processed process spectra of test batch 4 (DEN) when being projected onto the PCA model developed from the 4 NOC batches. The dashed and full lines represent the 95% and 99% limits, respectively.**

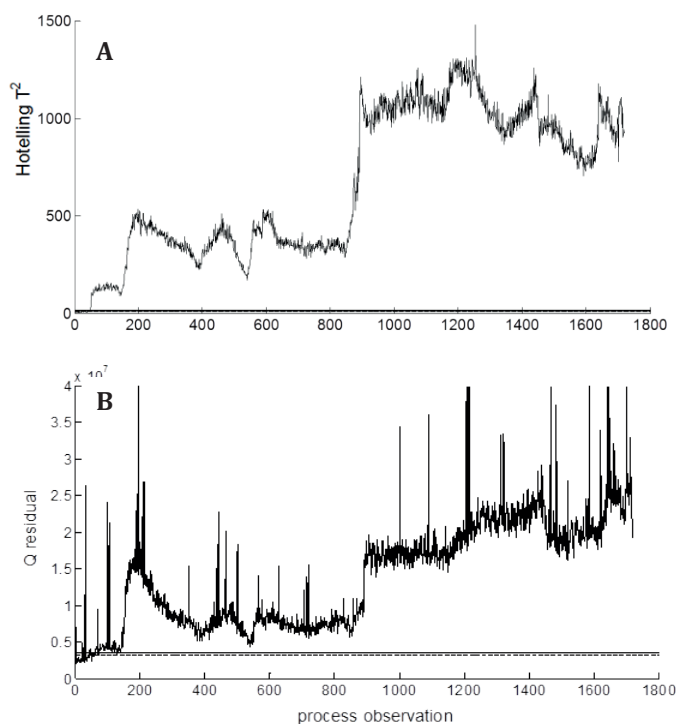


**Fig. 13. (A) Hotelling  $T^2$  and (B) Q residuals charts of the orthogonally pre-processed process spectra of test batch 9 (DEN) when being projected onto the PCA model developed from the 4 NOC batches. The dashed and full lines represent the 95% and 99% limits, respectively.**

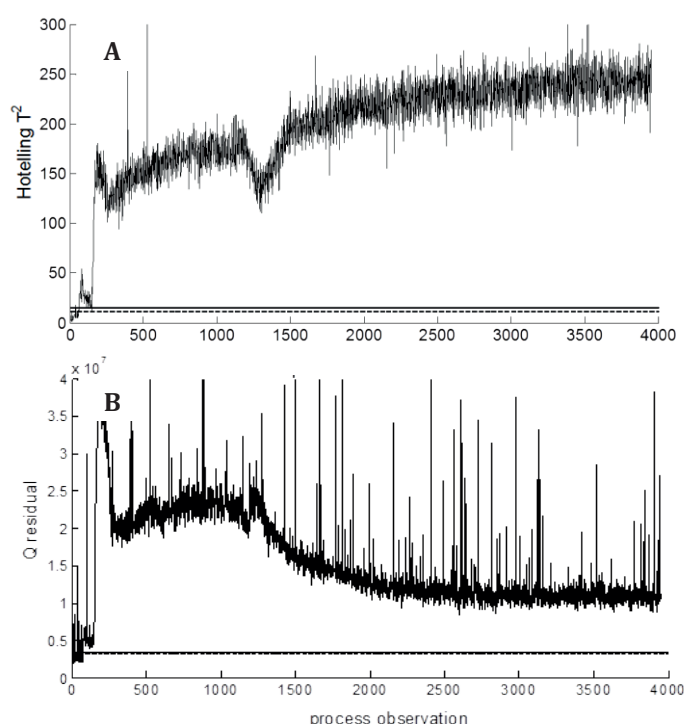


Fig. 14. (A) Hotelling  $T^2$  and (B) Q residuals charts of the orthogonally pre-processed process spectra of test batch 10 (DEN) when being projected onto the PCA model developed from the 4 NOC batches. The dashed and full lines represent the 95% and 99% limits, respectively.

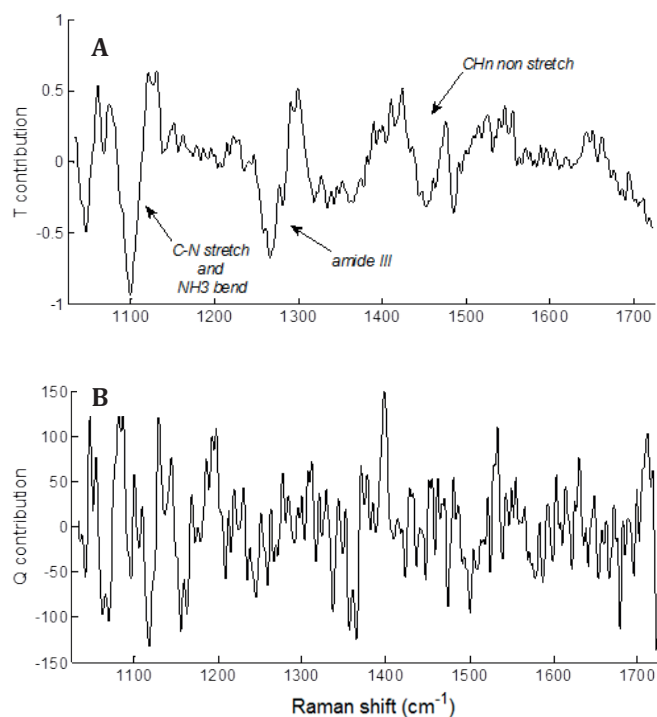


Fig. 15. T contribution (A) and Q contribution (B) plots of process observation number 1832 of batch 4 (being out-of-control).

## 5. Conclusions

This preliminary study shows that it is possible to detect protein unfolding during the freeze-drying process when in-line monitoring with Raman spectroscopy. Using the proposed approach, it was shown via monitoring of the Hotelling  $T^2$  and Q residuals that DEN batches from a certain process moment systematically deviated from the normal process course (NL batches). This deviation was then maintained until the end of the process, and was generally detected during the freezing step, which makes sense given the fact that freezing is a well-known stress factor to many proteins. Via the Hotelling  $T^2$  contribution plots, it could also be confirmed that protein unfolding was the main reason for the deviation.

However, this preliminary statistical model developed from only 4 NOC batches was a proof of principle to check whether the proposed strategy might work. Although the result is encouraging, it is obvious that the model should be further refined. Given the inter- and intra-batch variabilities, it would be beneficial to increase the number of NOC batches for model development, in order to cover more representatively the expected variations in future batches (i.e. to more efficiently filter the within-NL class process variations and to more efficiently model the inter-batch variability). This may possibly allow increasing the robustness of the statistical model, which will be considered as the next step, when more batches are available.

The orthogonalization step before statistical multivariate model development allows cleaning the spectral space from expected process variations. This can make the model transparent to variations from multiple external parameters, appearing and disappearing throughout the process. Hence, advantages of this approach are that no statistical PCA model needs to be developed at every process time point (as is the case in normal BSPC), and more importantly, that the model becomes insensitive to dynamic time variations. The latter is particularly interesting when the process consists of different phases of undefined duration, as is the case in most state-of-the-art freeze-drying processes using PAT tools to predict the end points of primary and secondary drying of the batch.

## References

- [1] X.C. Tang, M.J. Pikal, Design of freeze-drying processes for pharmaceuticals: practice advice, *Pharm. Res.* 21 (2004) 191-200.
- [2] F. Franks (Ed.), *Freeze-drying of pharmaceuticals and biopharmaceuticals*, 1<sup>st</sup> edition, The Royal Society of Chemistry, Cambridge, UK, 2007, pp. 206.
- [3] S.L. Nail, S. Jiang, S. Chongprasert, S.A. Knopp, *Fundamentals of freeze-drying*, *Pharm. Biotechnol.* 14 (2002) 281-360.
- [4] J.C. Kasper, G. Winter, W. Friess, Recent advances and further challenges in lyophilization, *Eur. J. Pharm. Biopharm.*, 2013, in press (doi: 10.1016/j.ejpb.2013.05.019).
- [5] U.S., Department of Health, Human Services, Food, Drug Administration, Center for Drug Evaluation Research, Center for Veterinary Medicine, Office of Regulatory Affairs, Guidance for industry: PAT - A framework for innovative pharmaceutical manufacturing and quality assurance, 2004.  
<http://www.fda.gov/downloads/Drugs/Guidances/ucm070305.pdf>  
(accessed on 15/04/2013).
- [6] A. Kauppinen, M. Toiviainen, O. Korhonen, J. Aaltonen, K. Jarvinen, J. Paaso, M. Juuti, J. Ketolainen, In-line multipoint near-infrared spectroscopy for moisture content quantification during freeze-drying, *Anal. Chem.* 85 (2013) 2377-2384.
- [7] M. Brulls, S. Folestad, A. Sparen, A. Rasmuson, J. Salomonsson, Applying spectral peak area analysis in near-infrared spectroscopy moisture assays, *J. Pharm. Biomed. Anal.* 44 (2007) 127-136.
- [8] T.R.M De Beer, P. Vercruysse, A. Burggraeve, T. Quinten, J. Ouyang, X. Zhang, C. Vervaet, J.P. Remon, W.R.G Baeyens, In-line and real-time process monitoring of a freeze-drying process using Raman and NIR spectroscopy as complementary process analytical technology (PAT) tools, *J. Pharm. Sci.* 98 (2009) 3430-3446.
- [9] T.R.M De Beer, M. Alleso, F. Goethals, A. Coppens, Y. Vander Heyden, H. Lopez De Diego, J. Rantanen, F. Verpoort, C. Vervaet, J.P. Remon, W.R.G. Baeyens, Implementation of a process analytical technology system in a freeze-drying process using Raman spectroscopy for in-line process monitoring, *Anal. Chem.* 79 (2007) 7992-8003.

- [10] A. Kauppinen, M. Toiviainen, J. Aaltonen, O. Korhonen, K. Jarvinen, M. Juuti, R. Pellinen, J. Ketolainen, Microscale freeze-drying with Raman spectroscopy as a tool for process development, *Anal. Chem.* 85 (2013) 2109-2116.
- [11] H. de Waard, T. De Beer, W.L. Hinrichs, C. Vervaet, J.P. Remon, H.W. Frijlink, Controlled crystallization of the lipophilic drug fenofibrate during freeze-drying: elucidation of the mechanism by in-line Raman spectroscopy, *AAPS J.* 12 (2010) 569-575.
- [12] S. Pieters, T. De Beer, J.C. Kasper, D. Boulpaep, O. Waszkiewicz, M. Goodarzi, C. Tistaert, W. Friess, J.P. Remon, C. Vervaet, Y. Vander Heyden, Near-infrared spectroscopy for in-line monitoring of protein unfolding and its interactions with lyoprotectants during freeze-drying, *Anal. Chem.* 84 (2012) 947-955.
- [13] V.L. Brewster, L. Ashton, R. Goodacre, Monitoring guanidinium-induced structural changes in ribonuclease proteins using Raman spectroscopy and 2D correlation analysis, *Anal. Chem.* 85 (2013) 3570-3575.
- [14] S. Pieters, Y. Vander Heyden, J.M. Roger, M. D'Hondt, L. Hansen, B. Palagos, B. De Spiegeleer, J.P. Remon, C. Vervaet, T. De Beer, *Eur. J. Pharm. Biopharm.*, in press (doi: 10.1016/j.ejpb.2013.03.035).
- [15] A. Bogomolov, Multivariate process trajectories: capture, resolution and analysis, *Chemom. Intell. Lab. Syst.* 108 (2011) 49-63.
- [16] T. Fearn, Standardisation and calibration transfer for near infrared instruments: a review, *J. Near infrared Spec.* 9 (2001) 229-244.
- [17] A. Andrew, T. Fearn, Transfer by orthogonal projection: making near-infrared calibrations robust to between-instrument variation, *Chemom. Intell. Lab. Syst.* 72, 2004, 51-56.
- [18] M. Zeaiter, J.M. Roger, V. Bellon-Maurel, Dynamic orthogonal projection. A new method to maintain the on-line robustness of multivariate calibrations. Application to NIR-based monitoring of wine fermentations, *Chemom. Intell. Lab. Syst.* 80 (2006) 227-235.
- [19] J.F. MacGregor, T. Kourti, Statistical process control of multivariate processes, *Control Eng. Practice* 3 (1995) 403-414.
- [20] T. Kourti, Process Analytical Technology: Beyond real-time analyzers: the role of multivariate analysis, *Crit. Rev. Anal. Chem.* 36 (2006) 257-278.

- [21] J.C. Boulet, J.M. Roger, Pretreatments by means of orthogonal projections, *Chemom. Intell. Lab. Syst.* 117 (2012) 61-69.
- [22] R.C. Pinto, J. Trygg, J. Gottfries, Advantages of orthogonal inspection in chemometrics, *J. Chemom.* 26 (2012) 231-235.
- [23] E.T.S. Skibsted, H.F.M. Boelens, J.A. Westerhuis, A.K. Smilde, N.W. Broad, D.R. Rees, D.T. Witte, Net analyte signal based statistical quality control, *Anal. Chem.* 77 (2005) 7103-7114.
- [24] J. Trygg, S. Wold, Advantages of orthogonal inspection in chemometrics, *J. Chemom.* 16 (2002) 119-128.
- [25] J.M. Roger, F. Chauchard, V. Bellon-Maurel, EPO-PLS external parameter orthogonalisation of PLS application to temperature-independent measurement of sugar content of intact fruits, *Chem. Intell. Lab. Syst.* 66, 2003, 191-204.
- [26] T. Vankeirsbilck, A. Vercauteren, W. Baeyens, G. Van der Weken, Applications of Raman spectroscopy in pharmaceutical analysis, *TrAC* 21 (2002) 869-877.
- [27] S. Pieters, J.M. Roger, T. De Beer, M. D'Hondt, B. De Spiegeleer, Y. Vander Heyden, Increasing robustness against spectral background variability of a Raman model for the protein conformational state classification in freeze-dried formulations, submitted manuscript.
- [28] J.C. Kasper, W. Friess, The freezing step in lyophilization: physico-chemical fundamentals, freezing methods and consequences on process performance and quality attributes of biopharmaceuticals, *Eur. J. Pharm. Biopharm.* 78 (2011) 248-263.



## 5.4. References

- [1] European Medicines Agency, EMEA/CHMP/CVMP/QWP/17760/2009 Rev2, Guideline on the use of near infrared spectroscopy (NIRS) by the pharmaceutical industry and the data requirements for new submissions and variations, 2012.  
[http://www.ema.europa.eu/docs/en\\_GB/document\\_library/Scientific\\_guideline/2012/02/WC500122769.pdf](http://www.ema.europa.eu/docs/en_GB/document_library/Scientific_guideline/2012/02/WC500122769.pdf) (accessed on 15/04/2013).
- [2] A.C. Olivieri, N.M. Faber, J. Ferré, R. Boqué, J.H. Kalivas, H. Mark, Uncertainty estimation and figures of merit for multivariate calibration, *Pure Appl. Chem.* 78 (2006) 633-661.
- [3] M. Zeaiter, J.M. Roger, V. Bellon-Maurel, Robustness of models developed by multivariate calibration. Part II: the influence of pre-processing methods, *Trends in Analytical Chemistry* 24 (2005) 437-445.
- [4] J.R. Beattie, J.J. McGarvey, Estimation of signal backgrounds on multivariate loadings improves model generation in face of complex variation in backgrounds and constituents, *J. Raman Spectrosc.* 44 (2013) 329-338.
- [5] J.R. Beattie, Optimising reproducibility in low quality signals without smoothing; an alternative paradigm for signal processing, *J. Raman Spectrosc.* 42 (2011) 1419-1427.
- [6] R. Bro, Multivariate calibration. What is in chemometrics for the analytical chemist?, *Anal. Chim. Acta* 500 (2003) 185-194.
- [7] J.C. Boulet, J.M. Roger, Pretreatments by means of orthogonal projections, *Chemom. Intell. Lab. Syst.* 117 (2012) 61-69.
- [8] A. Bogomolov, Multivariate process trajectories: capture, resolution and analysis, *Chemom. Intell. Lab. Syst.* 108 (2011) 49-63.
- [9] T. Fearn, Standardisation and calibration transfer for near infrared instruments: a review, *J. Near infrared Spec.* 9 (2001) 229-244.
- [10] M. Zeaiter, J.M. Roger, V. Bellon-Maurel, Dynamic orthogonal projection. A new method to maintain the on-line robustness of multivariate calibrations. Application to NIR-based monitoring of wine fermentations. *Chemom. Intell. Lab. Syst.* 80 (2006) 227-235.
- [11] J.F. MacGregor, T. Kourti, Statistical process control of multivariate processes, *Control. Eng. Practice* 3 (1995) 403-414.
- [12] T. Kourti, Process analytical technology beyond real-time analyzers: the role of multivariate analysis, *Crit. Rev. Anal. Chem.* 36 (2006) 257-278.
- [13] S. Albert, R.D. Kinley, Multivariate statistical monitoring of batch processes: an industrial case study of fermentation supervision, *Trends in Biotechnology* 19 (2001) 53-62.
- [14] J.C. Kasper, G. Winter, W. Friess, Recent advances and further challenges in lyophilization, *Eur. J. Pharm. Biopharm.*, 2013, in press.



---

## Chapter 6: SUMMARY, CONCLUSIONS & FUTURE PERSPECTIVES

---

### 6.1. Summary and conclusions

The aim of this thesis was to investigate the feasibility of NIR and Raman spectroscopy for the in-line monitoring of protein unfolding during freeze-drying processes.

In **chapter 1**, the PAT concept, being the motivation behind this research, defines the framework for making freeze-drying processes more efficient, less empirical and more understood. Given the high risk for safety and efficacy issues in the reconstituted product, it is necessary to minimize conformational changes in pharmaceutical proteins during the freeze-drying process. Up to now, no methods existed to continuously in-line monitor this CQA during freeze-drying processes. As NIR and Raman spectroscopy allow ultra-fast, non-invasive in-line measurements of the product during freeze-drying, their potential for monitoring protein unfolding during freeze-drying processes has been studied in this thesis.

To properly evaluate the techniques under study, an adequate reference method was needed to detect protein unfolding in freeze-dried samples. As a freeze-dried product with a native conformational state in the reconstituted product is generally produced by minimizing protein unfolding during the freeze-drying process, this study required thus in essence two types of freeze-dried samples, i.e. those where the freeze-drying process induced obvious (i.e. non-native conformational state), and minimal (i.e. native-like conformational state) changes in the secondary structural element distribution in the freeze-dried product. In **chapter 2** the choice of the reference method, using amide I FTIR spectroscopy, to detect protein unfolding was explained. Compared to a quantitative approach, a qualitative one was preferred because of its higher selectivity to detect changes in the secondary structural element distribution in the presence of varying environmental interferences (e.g. protein hydration state, sample morphology). Hence, using this method freeze-dried samples were categorized into two quality classes, i.e. native-like (acceptable) and non-native (inferior).

In **chapter 2** some practical requirements were defined for NIR and Raman spectroscopy as process analyzers during freeze-drying processes. Both techniques used fiber-optic probes to allow the non-invasive sampling in the freeze-dryer chamber. The core of the product could not be monitored, but this was not considered to be an issue because the outers of the formulation were more susceptible to over-drying (being a potential risk for protein unfolding), while they also experience the same other stress factors (e.g. freezing stress) as the inner core. The short acquisition times ( $< 1$  min) of both techniques allowed a continuous, nearly real-time, acquisition of spectra during the entire process.

For each technique under study, it was investigated (1) whether it can provide information on the desired quality attribute (i.e. determination of a suitable spectral response), (2) whether this information can be obtained directly from experimentally obtained spectra, and (3) whether this information still can be obtained accurately in the presence of expected interferences (e.g. process interferences).

In **chapter 3** the potential of NIR spectroscopy to become an in-line monitoring tool for protein unfolding during freeze-drying processes has been studied. The overwhelming signals for water and ice in the near-infrared region make reflectance NIR spectroscopy unsuitable to be used during cooling, freezing and sublimation in a freeze-drying process. Nevertheless, useful NIR spectra could be acquired during secondary drying, i.e. from the moment that all the ice is sublimated in the measured sample spot (given the fact that sublimation proceeds faster at the outers than in the core of the sample). Hence, the influence of protein dehydration, i.e. the (partial) removal of the hydration shell surrounding the protein molecules, being an important stress factor for the protein's conformational stability during any drying process, could be studied.

Unlike FTIR and Raman spectroscopy, NIR spectroscopy is less suitable for determining the secondary structure in proteins. As it did not provide (enough) specific variations in absorbencies at different frequencies related to changes in secondary structural element distribution, a multivariate data analysis approach was found not useful. However, the frequency of the amide A/II combination band appeared sensitive to the strength of the

hydrogen bonds formed by the protein backbone, which will be different when a protein unfolds. At low water content, as present during the secondary drying phase, NIR spectroscopy also enables monitoring the water elimination. When monitoring these two features in the ice free illuminated sample spot, i.e. the amide A/II peak position versus water elimination, a process trajectory could be developed to relatively determine whether there is protein unfolding in addition to protein dehydration (the latter being the normal process course). The normal trend was consistently followed in different formulations (using no lyoprotectants) where proteins experienced solely dehydration (where no protein unfolding was detectable in the amide I region) during freeze-drying with different secondary drying conditions (time, temperature). On the other hand, when there was protein unfolding, the process trajectories showed consistent deviations from this trend towards higher amide A/II frequencies. Hence, it was concluded that NIR spectroscopy may have a potential for the detection of protein unfolding during the drying phase of the process.

Another interesting observation using this approach was that mechanistic information on protein-lyoprotectant hydrogen bond interactions could be obtained. It could be observed *when* and to what relative *extent* there is hydrogen bond interaction during the secondary drying phase. Interactions between sucrose and the protein backbone were detected directly after sublimation of the illuminated sample spot, and their extent was relatively higher with increasing sucrose concentration. At the end of secondary drying, at constant temperature, the process trajectories still indicated water loss while the amide A/II frequencies remained unchanged. This observation suggested a water substitution effect of sucrose. Hence, NIR spectroscopy may also have some potential for revealing mechanistic process information on the working mechanism of (novel) lyoprotectants.

Given the relative character of the spectral response, i.e. the amide A/II band is influenced by 2 interfering phenomena (i.e. protein (un)folding and (de)hydration), NIR spectroscopy is not suitable for a fast non-destructive determination of protein unfolding in freeze-dried end products (as each product may have a different hydration

status depending on formulation and process conditions, which will influence the amide A/II frequency).

In **chapter 4** it has been shown that Raman spectroscopy can provide information on the protein conformational state (i.e. native-like versus non-native) directly from the experimentally obtained spectra of freeze-dried formulations (off-line). Because of the strong but complex correlation between the Raman spectra and the folded protein structure, the spectra were treated in a multivariate way. Compared to univariate analysis, MVA has the advantage that all useful parts of the spectrum are used, that noise is reduced, and that selective information on the CQA can be obtained from highly unselective data. The tested MVA methods (i.e. unsupervised PCA and supervised PLS-LDA) indicated that the amide III and side chain sensitive regions (i.e. CH<sub>n</sub> bending and C-N stretch + NH<sub>3</sub> deformation) were important for making the differentiation between the two conformational states. Combining those regions led to more accurate models. It was concluded that the technique is able to provide a high amount of predictive variation for protein unfolding. However, the sensitivity of the classification model for detecting mildly denatured proteins was compromised, especially in two types of formulations. Therefore, in **chapter 5**, a variance analysis was performed within the Raman spectral data space. It identified significant spectral background variations among certain batches and formulation types in the studied samples. Next, the robustness of the PLS-LDA model with respect to such spectral background effects was tested via external validations. Based on a small set of well-chosen samples, we were capable of estimating the spectral background subspace, and separate it from the useful Raman spectral space by orthogonal projection. This operation could improve both classification accuracy and sensitivity of the PLS-LDA classification model in the same way as exhaustive calibration did, but without the need for extra reference analyses and by using a more parsimonious model. Hence, one of the causes for the reduced sensitivity of the model was found and could be tackled, improving the model performance.

In a next study in **chapter 5**, it was aspired to investigate the possibility to use Raman spectroscopy for the in-line monitoring of protein unfolding during freeze-drying

processes. A first experiment taught us that the model protein LDH was not being physically denatured by the continuous exposure to the high energetic Raman laser during the entire process. Because there was no possibility to extract samples from the process stream (i.e. for off-line analysis with the reference technique), it was aimed to build an unsupervised in-line statistical model from the process Raman spectra. Since modern freeze-drying processes may not have predefined lengths (e.g. the end points of primary and secondary drying are in real-time determined by PAT-tools), it was aspired to develop a statistical model being independent from the process dynamics. The proposed strategy uses the intra-process variability of a set of NOC batches to define the detrimental subspace of the process data space. To maximize the relevant-to-irrelevant spectral variance ratio, the process spectra of the NOC batches were, prior to building a statistical PCA model, projected orthogonally to this subspace. Hence, the remaining subspace for PCA model building was practically transparent to experimental and process spectral variations. Control charts based on Hotelling  $T^2$  and Q residuals generally confirmed out-of-control validation batches. It appeared that the studied batches went out of control (i.e. detected by a systematic deviation that lasted till the end of the process) already during the freezing phase. However, it was also found that the accuracy of the statistical monitoring was compromised for certain validation batches. A plausible reason for this is that the NOC batches (only 4 in this study) for the model development did not cover all possible intra- and inter-batch variation. Hence, using more NOC batches for model development may increase the robustness of the statistical model. This is planned as a future work.

In conclusion, both NIR and Raman spectroscopy allow obtaining information on protein unfolding from the spectra acquired during (parts of) the freeze-drying process. Therefore, they show interesting potential to be used as in-line monitoring tools for the conformational stability of pharmaceutical proteins during freeze-drying processes. As all spectroscopic techniques require a relatively high protein concentration (e.g. > 5 mg/ml), this will always be a requirement for future applications. The potential strength of NIR spectroscopy for the monitoring of protein unfolding may lay in its sensitivity towards the hydrogen bonding strength of the amide groups in the proteins. It cannot compete with FTIR or Raman spectroscopy to indicate secondary structural changes, but

this unique feature can make NIR an excellent complementary/confirmatory tool when monitoring protein unfolding during protein dehydration (i.e. the secondary drying phase of the freeze-drying process). Both techniques have a different focus, thus they can give a complementary view on what is happening to the protein's conformational state during the process. This can be advantageous in designing a PAT system to gain process understanding and for fault diagnosis. An interesting future work would therefore be to monitor the same process with both techniques simultaneously. Another advantage is that the proposed methods with NIR and Raman spectroscopy are independent from the duration of the process phases, hence they can operate in flexible freeze-drying processes (i.e. with end points not a priori determined).

A continuous monitoring of protein unfolding during the potential stress factor (i.e. the freeze-drying processes) should eventually lead to a better understanding and control of the process and to higher quality assurance. Although both techniques proved having potential for the in-line monitoring of protein unfolding, further research will be necessary to develop true in-line methods from them to allow process understanding and diagnostics. To monitor freeze-drying cycles that minimize protein unfolding, warning and action limits will have to be defined. These will depend on the type of protein (as some proteins are less stable than others) and should be in agreement with a risk analysis (e.g. what is the risk of having non-native proteins in the reconstituted product in relation to the conformational state in the freeze-dried product?). Of course, further development of the methods should require more reference techniques to obtain a more complete view of the protein conformational status.

When information on the protein's physical stability can be continuously and accurately obtained throughout the freeze-drying cycle, this may open possibilities to screen for protein unfolding during any freeze-drying cycle, including the more aggressive ones. As aggressive cycles typically dry above  $T_g'$ , the partially unfolded proteins may be for a considerable period of time exposed to a viscous flow (i.e. they are in a rubbery state) while being dried. So far, there are only a limited number of studies that have off-line investigated the effect of these actions on the protein's physical stability. Although they found no remarkable difference in this CQA when dried aggressively versus normally, it



may provide a higher quality assurance if the protein's physical stability could be continuously monitored in any freeze-drying process, and especially in those that are new and not well known.

A limitation in this work is that only one vial was monitored, even only a part of this vial that is illuminated by the probe. Considering the intra-vial variability, the outer spot that was measured was considered to be the most critical. Given the intra-freeze-dryer variability, one vial can hardly be considered representative for thousands of vials in a freeze-dryer. The technological advances of multi-point NIR and Raman sensors in freeze-dryers address the latter problem. Hence, a next logical step is to implement such methods in multi-point spectroscopic systems. Consequently, spatial information within the freeze-dryer can be obtained on the protein behavior. Moreover, such systems can be easily combined with other PAT tools that monitor critical aspects of the whole batch (e.g. TDLAS, MTM). Moreover, from the same spectra acquired during the process different information can be obtained simultaneously. For instance, they can be supplied to other models as well, e.g. to obtain information on the residual water content (from NIR spectra), the solid state of the excipients (from Raman spectra), etc.

Despite their proven potential, more research with both techniques is necessary to further reveal their practical feasibility for the early detection of protein unfolding, and for gathering process understanding. Some suggestions are made for NIR and Raman spectroscopy in the paragraphs below. It is hoped that someday, they may find their place next to state-of-the-art PAT tools for freeze-drying, and that their use as in-line diagnostic tools may open new perspectives for developing cost-effective freeze-drying cycles with integrated control systems, according to the Process Analytical Technology and Quality by Design concepts.

## **6.2. Suggestions for future research with NIR spectroscopy**

### **6.2.1. Extending the concept to diagnostic method**

For NIR spectroscopy, a proof-of-concept study demonstrated that monitoring the amide A/II frequency versus water elimination can be useful for obtaining information on

protein unfolding and (de)hydration during the freeze-drying process. As a next step, the concept should be confirmed with different model proteins (i.e. with different stabilities to freeze-drying stress) and stabilizers. An interesting future study would also be to monitor the process trajectories of proteins leading to a molten globule state by freeze-drying (this should be confirmed by appropriate off-line techniques). It should allow one to evaluate whether NIR spectroscopy may detect protein unfolding already from changes in the tertiary structure. To become a true diagnostic method, different analytical figures of merit, including accuracy, reproducibility and sensitivity, should be evaluated. Also, warning and action limits should be defined on the process trajectory.

#### **6.2.2. Improving the process trajectories by considering moisture content predictions versus amide A/II frequency monitoring**

The defined process trajectories from the NIR spectra used two variables. One was the frequency shift of the amide A/II band, being related to the strength of the H-bonds formed by the amide groups in the protein, and influenced by both protein folding and protein hydration. The other one was the AWA, being an estimation of the relative unfrozen water loss at the illuminated sample spot throughout drying. The obtained process trajectories may give an idea of how the frequency of the amide A/II band relates to the water removal over the drying time, and the relative character of these features enabled differentiating between native-like or non-native proteins in the studied formulations. It could also tell us something about how the hydration state of the protein molecules evolves throughout drying. However, it would be more interesting if one could predict the actual water content during any time of the secondary drying process in the illuminated sample spot, and define a process trajectory from this variable and the amide A/II frequency. This knowledge would allow making a better comparison between the process trajectories of different runs. Also, this may enable answering some important questions such as: *'At how many % residual moisture does the lyoprotectant make contact to the protein's backbone?'*, and *'At how many % residual moisture is there complete water substitution?'*... This can be practically done by building an in-line PLS model that correlates the parts of the NIR spectra being sensitive to water to the actual moisture content in the sample (e.g. determined by Karl-Fisher titration).

With a sample thief the necessary samples can be taken during the process, to build and validate the in-line MVC model.

### **6.2.3. Testing the concept to other drying processes**

The concept has currently been developed and tested for the drying phase of a freeze-drying process. The removal of the water layer surrounding the protein molecules is present in all drying processes and is always hazardous for protein unfolding. Since the principle of the proposed approach is generic, it would theoretically also be possible to apply it to other drying processes of proteins (such as spray drying, foam drying, air drying...).

## **6.3. Suggestions for future research with Raman spectroscopy**

### **6.3.1. Developing classification models from Raman measurements through glass vials**

Although some publications showed that it is possible to measure (protein) Raman spectra through glass vials with an acceptable background contribution (i.e. not overwhelming the Raman signals), our own experiments through glass vials (type I) led to Raman spectra with an immense background totally obscuring the Raman signals. The background contribution of the glass in the spectra will possibly depend on the type and brand (i.e. the levels of impurities) of glass vial. Therefore, in this thesis, Raman measurements were performed in an open vial or with the product taken out of the vial. This approach has practical limitations. For instance, by opening the vial of the freeze-dried product the sterility is destroyed (i.e. the off-line method is destructive), and by in-line monitoring with the probe head above the vial, the vial cannot be sealed at the end of the process (i.e. it is not applicable for routine production). When it would be possible to acquire useful Raman spectra through glass vials, the real-life potential of the classification Raman model (for in- and off-line use) would greatly improve. The fact that we were able to estimate successfully the background interference space (and could correct for it) for certain formulations is encouraging to try the same approach on Raman spectra acquired through glass vials of brands where the background does not totally obscures the Raman signals.

### **6.3.2. Transfer of the supervised PLS-LDA classification model to in-line use**

Because there was no sample thief available, an unsupervised statistical in-line model was developed to detect protein unfolding during the freeze-drying process. However, when a sample thief would be available, it would also be possible to transfer the off-line PLS-LDA model to in-line use. The problem here can be seen as a method transfer problem. Orthogonal projection or direct standardization methods may possibly allow transferring the supervised model without the need for much reference sampling. However, validation of the approach would require a certain number of well chosen in-line samples for reference analysis.

---

## Annex

---

NIR spectroscopy is an emerging technique for numerous PAT-applications. In this thesis, NIR spectroscopy has been evaluated for a new application, i.e. obtaining real-time information on protein unfolding during freeze-drying processes. Another popular application is the replacement of slow, complex, or costly analysis methods by a MVC model that predicts the CQA from the NIR spectra of the samples. As NIR spectra can be acquired within seconds, and sample preparation is usually not required, the use of such NIR models in the QC lab is appealing. However, the development, validation and maintenance of the NIR model demand investments. One of the factors, requiring sometimes significant investment, is the need to capture all the redundant systematic (e.g. intra- and inter-batch) variations in the calibration set. This is necessary to allow reliable predictions for new samples from novel batches. The following paper proposes a cost-effective strategy for the development of a NIR model to predict API content in tablets, neither requiring exhaustive calibration sets nor frequent model updates.



Contents lists available at SciVerse ScienceDirect

Analytica Chimica Acta

journal homepage: [www.elsevier.com/locate/aca](http://www.elsevier.com/locate/aca)

## Robust calibrations on reduced sample sets for API content prediction in tablets: Definition of a cost-effective NIR model development strategy



Sigrid Pieters<sup>a</sup>, Wouter Saeys<sup>b</sup>, Tom Van den Kerkhof<sup>c</sup>, Mohammad Goodarzi<sup>b</sup>, Mario Hellings<sup>c</sup>, Thomas De Beer<sup>d</sup>, Yvan Vander Heyden<sup>a,\*</sup>

<sup>a</sup> Department of Analytical Chemistry and Pharmaceutical Technology, Center for Pharmaceutical Research, Vrije Universiteit Brussel – VUB, Laarbeeklaan 103, B-1090 Brussels, Belgium

<sup>b</sup> Department of Biosystems, Faculty of Bioscience Engineering, Katholieke Universiteit Leuven – KULeuven, Kasteelpark Arenberg 30, B-3001 Heverlee, Belgium

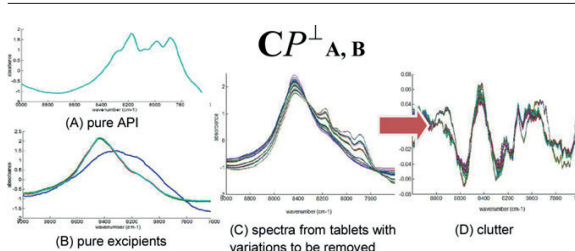
<sup>c</sup> ChemPhar Development Johnson & Johnson, Turnhoutseweg 30, B-2340 Beerse, Belgium

<sup>d</sup> Laboratory of Pharmaceutical Process Analytical Technology, Universiteit Gent, Harelbekestraat 72, B-9000 Ghent, Belgium

### HIGHLIGHTS

- ▶ A cost-effective NIR model development strategy is proposed for API content prediction in tablets.
- ▶ Judicious use of prior spectral information improves PLS model performance.
- ▶ The clutter captures representative intra- and inter-batch spectral variability to be removed.
- ▶ Model requires completeness of the clutter rather than comprehensive calibration sets.

### GRAPHICAL ABSTRACT



### ARTICLE INFO

#### Article history:

Received 25 June 2012

Received in revised form 5 October 2012

Accepted 19 November 2012

Available online 28 November 2012

#### Keywords:

Near infrared spectroscopy

Prior spectral information

Tablets

Orthogonal projection methods

Augmentation methods

### ABSTRACT

Owing to spectral variations from other sources than the component of interest, large investments in the NIR model development may be required to obtain satisfactory and robust prediction performance. To make the NIR model development for routine active pharmaceutical ingredient (API) prediction in tablets more cost-effective, alternative modelling strategies were proposed. They used a massive amount of prior spectral information on intra- and inter-batch variation and the pure component spectra to define a clutter, i.e., the detrimental spectral information. This was subsequently used for artificial data augmentation and/or orthogonal projections. The model performance improved statistically significantly, with a 34–40% reduction in RMSEP while needing fewer model latent variables, by applying the following procedure before PLS regression: (1) augmentation of the calibration spectra with the spectral shapes from the clutter, and (2) net analyte pre-processing (NAP). The improved prediction performance was not compromised when reducing the variability in the calibration set, making exhaustive calibration unnecessary. Strong water content variations in the tablets caused frequency shifts of the API absorption signals that could not be included in the clutter. Updating the model for this kind of variation demonstrated that the completeness of the clutter is critical for the performance of these models and that the model will only be more robust for spectral variation that is not co-linear with the one from the property of interest.

© 2012 Elsevier B.V. All rights reserved.

\* Corresponding author. Tel.: +32 2 477 47 34; fax: +32 2 477 47 35.

E-mail addresses: [yvanvdh@vub.ac.be](mailto:yvanvdh@vub.ac.be), [Yvan.VanderHeyden@vub.ac.be](mailto:Yvan.VanderHeyden@vub.ac.be) (Y.V. Heyden).

## 1. Introduction

Together with the growing popularity of near-infrared (NIR) spectroscopy, the interest to use multivariate prediction models (e.g., PLS) emerged in different industries (food, chemical, pharmaceutical, ...) [1–3]. Compared to HPLC, NIR spectroscopy provides a non-destructive, extremely fast, and hands-on analysis, which can substantially reduce analysis times and costs for the routine assay of active pharmaceutical ingredient (API) in tablets. Multivariate calibration models (e.g., PLS) are typically built in an empirical way. Although this may offer flexibility, it can also be a drawback making the model development, maintenance and update more complex [4]. Consequently, more investment may be required, which must guarantee that a low prediction error is obtained and maintained for future predictions of novel batches.

There are numerous examples where spectral disturbances from various sources, e.g., variations in a process, temperature, humidity, ..., upset the model predictions. In this paper, we specifically consider this problem in tablets produced from a routine production line. Besides measurement variability (path length, temperature, ...), systematic changes in the measured signals in the spectra of tablets may appear, e.g., originating from process and raw material variability (inter- and intra-batch effects). A tableting process involves different subsequent processing steps, such as mixing the ingredients, granulation, compaction and coating. Some tablet production variables, e.g., grain size, compaction pressure, and coating thickness, may introduce spectral variability that is irrelevant for predicting the API content in the tablets [5]. Also, the excipients in the tablet can vary slightly between different batches or samples (excipient homogeneity), while the tablet composition can vary as well when different API target concentration levels are considered in the model. Depending on the relative humidity conditions during their production, packaging, storage and analysis, the water content is another important variable that may upset the NIR model predictions [6].

It is evident that when more relevant variation is covered by the calibration set of the NIR model, lower prediction errors can be obtained on new independent samples [7]. Including all the expected variation in the calibration set is the most intuitive way for doing this, and is still recommended by regulatory authorities [8]. Drawbacks of this approach are that the model complexity may increase rapidly when more 'non-relevant' spectral variability is included in the exhaustive calibration, needing additional latent variables or introducing non-linearities that may require non-linear calibration techniques. A more important practical problem is that a substantial number of well-chosen samples, describing all the expected variability, is needed to obtain robust model performance. It is a non-trivial task to obtain a good estimate of the expected variation in the samples to be predicted, also because there is a practical limit (particularly in terms of costs) to the number of samples to be analyzed with the reference technique. Hence, in most practical cases one selects randomly the calibration samples from 'representative' batches. As a result, existing calibration bases rarely contain all the relevant variability from all the influence factors which can occur in industrial conditions [9], making the models less robust for their long term use and requiring frequently model updates.

It is often overlooked that one of the major advantages of NIR spectroscopy, i.e., its analysis speed and simplicity, provides an excellent opportunity to measure significantly more dosage units than what would be possible with the reference technique, i.e., HPLC. This is especially the case when automated NIR equipment is available. Hence, a massive amount of spectral information can be obtained easily to allow a better understanding of the possible spectral perturbations. The aim of the present study is to investigate whether the use of such spectral information on intra- and

inter-batch variation (without corresponding reference analyses) during model development can improve the NIR model performance for predicting the API content in tablets from novel batches. The prediction performance of different approaches using the prior spectral information was compared to that of PLS models. It was also investigated whether these strategies allowed reducing the variability in the calibration set without compromising the prediction performance. This should lead to the definition of a cost-effective strategy for developing robust calibration models for the routine prediction of API in tablets.

## 2. Theory

There are different ways to incorporate prior information into the calibration model. One distinguishes augmentation and orthogonal correction methods (supervised and unsupervised), while combinations of these are possible as well.

### 2.1. Augmentation methods

#### 2.1.1. Noise augmentation in PLS

The idea of noise augmentation (NA) or ensemble methods [10–13] is to expand the calibration set artificially in order to build PLS models that are more robust to the different kinds of variability expected in the future sample population. An artificial calibration set can be created by augmenting the original one with a high number of spectral signatures, representing the 'noise'. The original spectra in the resulting calibration set should span the chemical variation in the best possible way, whereas the perturbation spectra should represent all the other possible variations that can be expected. One way to estimate the latter is through the measurement of spectra under varying perturbation conditions. Because the 'noise' added to the calibration spectra should be independent from the component of interest, this operation should not change the corresponding reference values.

#### 2.1.2. Prediction – augmented classical least squares (P-ACLS)

In contrast to the inverse modelling approaches (e.g., PLS), classical least squares (CLS) regression is based on an explicit linear additive model (e.g., Lambert-Beer's law in spectroscopy). Eq. (1) depicts the CLS model.

$$\mathbf{J} = \mathbf{PK} + \mathbf{E}_A \quad (1)$$

where  $\mathbf{J}$  is the matrix of the measured intensities,  $\mathbf{P}$  is the matrix of concentration values,  $\mathbf{K}$  is the matrix of the pure component signals at unit concentration, and  $\mathbf{E}_A$  the model error.

The major weakness of CLS is that it requires quantitative knowledge of all the spectrally active components in the calibration set to get an estimate of  $\mathbf{K}$ . Augmented (A)-CLS attempts to obtain a better estimation of  $\mathbf{K}$  by augmenting the predicted pure component matrix with empirically derived spectral shapes, e.g., the loading vectors from PCA on the spectral residuals  $\mathbf{E}_A$  (SRACLS), known pure component spectra [14], or a priori known other variation not included in the calibration set (PACLS) [15,16]. The addition of the spectral shapes both changes and corrects the concentration estimates for the component of interest.

### 2.2. Orthogonal correction methods

#### 2.2.1. Orthogonal projections

There are essentially 2 contributions within the calibration matrix  $\mathbf{X}$ , i.e., one originating from the analyte of interest  $k$  ( $\mathbf{X}_k$ ), and another from all other sources of variance ( $\mathbf{X}_{-k}$ ).

$$\mathbf{X} = \mathbf{X}_k + \mathbf{X}_{-k} \quad (2)$$



Pretreatments based on orthogonal projections aim at removing those spectral patterns, which are 'interfering' with the desired prediction from the data matrix  $\mathbf{X}$ , before calibration on  $\mathbf{y}$ . It is attempted to return the spectra of  $\mathbf{X}$  as  $\mathbf{X}^*$ , containing the most condensed spectral information, i.e., the net analyte signal ( $\mathbf{X}_k$ ) [17]. The information to be removed, i.e., the clutter, can be defined based on pure component spectra of known interferences [18], an experimental design with varying perturbation factor(s) [19], or an (augmented) calibration data set [12]. The column vectors of the so obtained matrix  $\mathbf{S}$  form a basis of the detrimental subspace. Then, an orthogonal projector to  $\mathbf{S}$ , i.e.,  $P_S^\perp$ , can be calculated to correct the initial matrix  $\mathbf{X}$  as follows:

$$\mathbf{X}^* = \mathbf{X}P_S^\perp = \mathbf{X}(\mathbf{I} - \mathbf{S}(\mathbf{S}^T\mathbf{S})^{-1}\mathbf{S}^T) \quad (3)$$

**2.2.1.1. External parameter orthogonalisation (EPO).** This unsupervised orthogonalisation method uses pure spectra (without reference value) to define a basis of the space spanned by the 'interfering' factors, this way estimating the parasitic subspace  $\mathbf{X}_{-k}$  [19]. PCA is applied to  $\mathbf{D}$ , containing spectra collected while the perturbation factor is varying. Retaining only the first  $g_a$  PC's, the column vectors of the matrix of eigenvectors  $\mathbf{G}$  will represent an orthonormal basis of the subspace to be removed. Subsequently, an orthogonal projection is defined to filter the calibration spectra  $\mathbf{X}$  to obtain the 'corrected' ones ( $\mathbf{X}^*$ ).

$$\mathbf{X}^* = \mathbf{X}(\mathbf{I} - \mathbf{G}\mathbf{G}^T) \quad (4)$$

where  $\mathbf{G}$  is a matrix comprising the  $g_a$  first eigenvectors of the square matrix  $[\mathbf{D}^T\mathbf{D}]$ .

Because the original calibration database  $\mathbf{X}$  is adjusted by means of orthogonal projection, the correction is embedded into the model. Hence, there is no need to reapply the correction to new spectra when using the model. Advantages of this method are the high flexibility and the fact that it does not require corresponding  $\mathbf{y}$  values. Because it is based on external a priori information, the success of the unsupervised orthogonalisation will strongly depend on how one is able to identify the detrimental spaces within the variables space, without interfering with the useful space. It will depend on the comprehensiveness of the a priori spectral information and on the empirical tuning for identifying the information to be removed. In practice, the latter can be supported by assessing the RMSECV as a function of  $g_a$  and the number of latent variables, or by the evolution of the Wilks lambda value [19]. Nevertheless, using unsupervised orthogonal projection methods holds a risk of removing too much information, i.e., when there is detrimental information not independent with the net analyte signal [20].

**2.2.1.2. Orthogonal signal correction (OSC).** OSC intends to subtract those factors from the calibration matrix  $\mathbf{X}$  which capture the variability in  $\mathbf{X}$  orthogonal to  $\mathbf{y}$  (supervised orthogonalisation) [21]. It uses a PLS-NIPALS-like algorithm, where the weighted regression vector  $\mathbf{w}$  is adjusted. Thus, OSC pre-processing involves two major steps, i.e. (1) estimation of the vector pair  $(\mathbf{t}, \mathbf{w})$  for which  $\mathbf{t}\mathbf{w}^T$  explains maximum variance in  $\mathbf{X}$  orthogonal to  $\mathbf{y}$ , and (2) removal of the contribution of the identified component from  $\mathbf{X}$ .

$$\mathbf{X}^* = (\mathbf{X} - \mathbf{t}\mathbf{p}^T) \quad (5)$$

Then, the newly obtained  $\mathbf{X}^*$  can be calibrated on  $\mathbf{y}$  by means of PLS. Different approaches have been proposed for estimating the score vector  $\mathbf{t}$ . As the orthogonal projection is not embedded in the calibration model, it has to be applied to new spectra prior to applying the calibration model [17].

**2.2.1.3. Net analyte pre-processing (NAP).** This method was introduced by Goicoechea and Olivieri [22]. To obtain an estimate

of the parasitic subspace  $\mathbf{X}_{-k}$ , the following orthogonal projection of  $\mathbf{X}$  to  $\mathbf{y}$  is performed.

$$\mathbf{X}_{-k\text{est}} = (\mathbf{I} - \mathbf{y}(\mathbf{y}^T\mathbf{y})^{-1}\mathbf{y}^T)\mathbf{X} \quad (6)$$

In a next step,  $\mathbf{X}$  is projected orthogonal to the matrix  $\mathbf{U}$ , consisting of the first  $g_a$  PC's of  $\mathbf{X}_{-k\text{est}}$  to obtain  $\mathbf{X}^*$  for calibration on  $\mathbf{y}$  by means of PLS or CLS.

$$\mathbf{X}^* = \mathbf{X}(\mathbf{I} - \mathbf{U}\mathbf{U}^T) \quad (7)$$

The same transformation is applied to new spectra  $\mathbf{x}$  prior to applying the calibration model.

$$\mathbf{x}^* = (\mathbf{I} - \mathbf{U}\mathbf{U}^T)\mathbf{x} \quad (8)$$

Thus, NAP has in common with OSC that it attempts removing the spectral information in  $\mathbf{X}$  that is orthogonal to  $\mathbf{y}$  (supervised orthogonalisation methods). Yet both methods use different routes to reach this goal. Compared to unsupervised orthogonalisation methods, OSC and NAP allow removing the detrimental subspace in a less empirical way, and may also work efficiently when detrimental and useful information are not independent [20]. A disadvantage is that all the variation to be removed should be present in the calibration base, thus corresponding  $\mathbf{y}$  values are necessary. Because of their close relationship to PLS, it has been repeatedly demonstrated that these methods can reduce the complexity of the PLS regression model, but do not enhance its predictive power [22–24].

### 3. Experimental

#### 3.1. NIR spectroscopy

Tablets were analyzed using a FT-NIR spectrometer (MPA, Bruker, Ettlingen, Germany). Spectra were collected in the 10,000–5700  $\text{cm}^{-1}$  region with a resolution of 8  $\text{cm}^{-1}$  and averaged over 16 scans. The effective sample size was approximately 11% of the tablet. It was assumed that the API was uniformly distributed in the tablet, which was confirmed by studies during method development.

#### 3.2. HPLC

HPLC was used as the reference technique. All HPLC measurements were performed at Janssen Pharmaceutica, Beerse, Belgium, using their developed and validated method (confidential).

#### 3.3. Data analysis

PCA, PLS regression and OSC pre-treatment were performed in Matlab 7.1. (The Mathworks, Natick, MA) using the PLS toolbox 6.2. (Eigenvector Research, Wenatchee, WA). EPO, ACLS and NAP were directly programmed in Matlab. Minitab 16 (Minitab, PA) was used for testing the statistical significance of the predictions by the different models.

##### 3.3.1. Model development and validation

The calibration set consisted of oblong shaped tablets of 6 target API concentration levels, i.e., 0, 25, 50, 100, 150 and 187.5 mg API with respective 0, 7.28, 14.56, 29.12, 38.83 and 48.54% (w/w) per tablet. Tablets at the extreme concentration levels originated from laboratory batches, and were manufactured to extend the concentration range spanning the chemical variability within the specification limits. The tablets at the other concentration levels were manufactured in a production line and represent tablets to be marketed. As the calibration set contained a large concentration range, the tablet composition also varied over the concentration levels.



The NIR spectra were limited to the 9000–7600  $\text{cm}^{-1}$  range and were pre-processed with standard normal variates (SNV). Except for the ACLS and NAP-CLS models, all other calibration models were built with PLS. Mean-centering was always performed prior to PLS modelling. The optimal number of latent variables for each model was selected based on the minimal RMSECV from 'leave-one-batch-out' cross validation. Two independent test sets were used for external model validation. Test set 1 consisted of 54 tablets, originating from 4 new production batches (one for each dose to be marketed) and 2 laboratory batches at the extreme concentration levels. In test set 2 (30 tablets from 4 production batches) strong water variations were introduced by storing the tablets at different conditions (see further in Section 3.3.2). The root mean square error of prediction (RMSEP) was used as the performance criterion to assess and compare the predictive abilities of the different models. The significance of differences in prediction power was assessed by a two-way ANOVA, performed on the absolute values of the prediction errors [25]. Multiple comparisons were performed by the Dunnett's test, using the PLS model as a control to calculate  $p$  values.

### 3.3.2. Available prior information

NIR spectra were recorded from the pure tablet components, i.e., from the API (**A**) and the excipients (**B**). Fig. 1 shows the obtained spectra in the considered spectral range after SNV pre-processing. 10,086 NIR spectra from tablets originating from 27 different production batches (i.e., for doses to be marketed: 3 batches at 7.28% (w/w), 12 batches at 14.56% (w/w), 7 batches at 29.12% (w/w) and 5 batches at 38.83% (w/w)) were measured. They included tablets

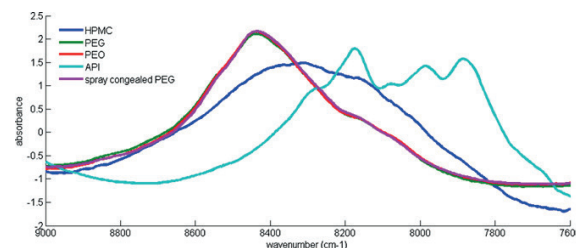


**Fig. 1.** NIR spectra of the pure tablet components (SNV pre-processed) in the range 9000–7600  $\text{cm}^{-1}$ .

produced during pharmaceutical development and clinical trials. They also included characterization batches, produced at the limits of the critical process settings, to increase the spectral variability originating from process variability. Since hundreds of tablets per batch were measured, systematic variations in the spectra due to process variation over time may also be covered. The NIR spectra of the tablets originating from laboratory batches (at the extreme target API concentration levels) were added to this matrix, creating **C** ( $10,213 \times 364$ ). 107 spectra from processed tablets with deliberate strong water variations were measured (Fig. 2). Either the tablets were stored for 30 min at 50 °C (to decrease the water content in the tablets), either for 3 h at 75% RH, or for 16 h at 75% RH (to increase the water content in the tablets).

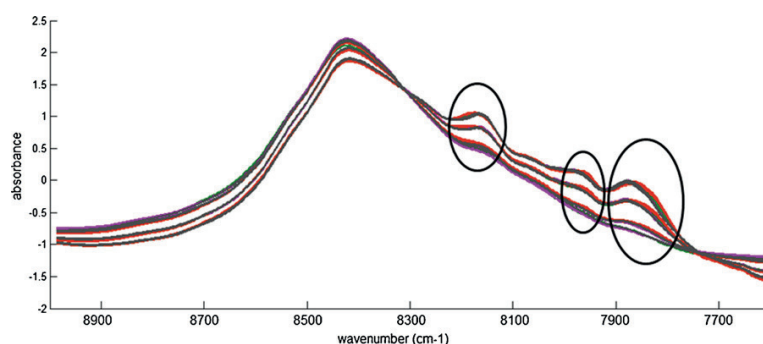


**Fig. 2.** NIR spectra of processed and unprocessed tablets (SNV pre-processed) in the range 9000–7600  $\text{cm}^{-1}$ . Spectra from unprocessed tablets are in grey, from tablets stored for 30 min at 50 °C in green, from tablets stored for 3 h and 16 h at 75% RH in purple and red, respectively. The black ellipses indicate visible shifting of the API absorption signals. (For interpretation of the references to colour in this figure legend, the reader is referred to the web version of the article.)

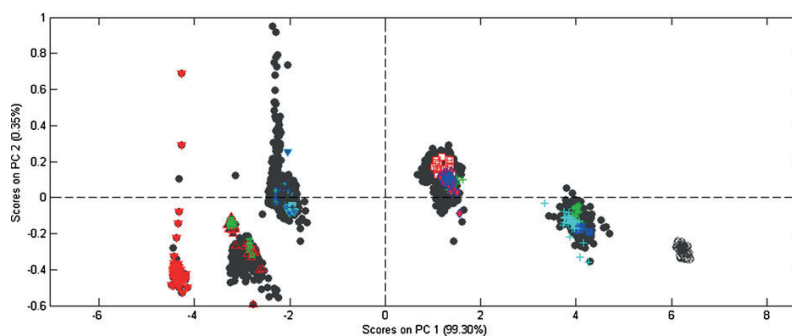


**Fig. 3.** PCA score plot (PC1 versus PC2) from **C** covering the 10,213 spectra of tablets from 27 different batches (in grey). The spectra used in the calibration set 1 are represented by differently coloured markers according to their batch. (For interpretation of the references to colour in this figure legend, the reader is referred to the web version of the article.)

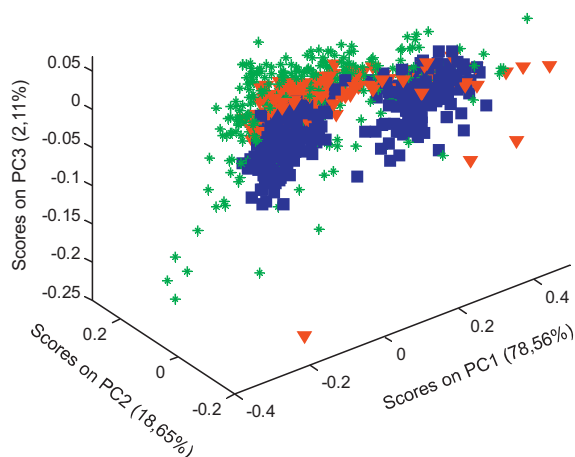


**Fig. 4.** PCA score plot (PC1–PC2–PC3) of NIR spectra (SNV pre-processed) from tablets with 25 mg target API concentration manufactured in a production line. The different batches are indicated with differently coloured markers.

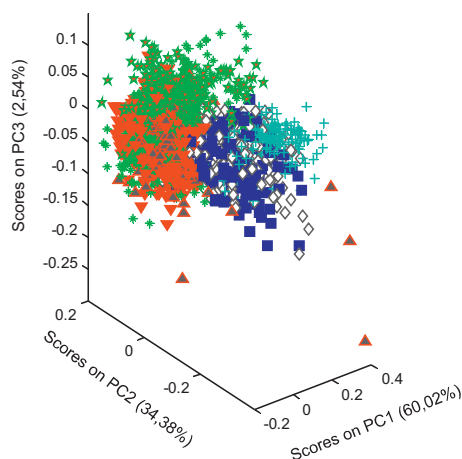


**Fig. 5.** PCA score plot (PC1–PC2–PC3) of NIR spectra (SNV pre-processed) from tablets with 100 mg target API concentration manufactured in a production line. The different batches are indicated with differently coloured markers. (For interpretation of the references to colour in this figure legend, the reader is referred to the web version of the article.)

### 3.4. Strategies for efficient use of the prior information

#### 3.4.1. Identifying the information to be removed (clutter)

The strategies applied in this paper do not require exact knowledge of all perturbation sources, but just need a representative estimate of the spectral variation to be expected in tablets from future batches. This can be obtained by making use of the extremely fast and simple NIR analysis, where far more tablets could be analyzed than what would be possible with HPLC. Fig. 3 shows a PCA score plot (PC1 versus PC2) of samples from randomly selected batches (coloured markers) for calibration of the initial PLS model, and all the prior spectral information **C** ( $10,213 \times 364$ ) are in grey dots. The scores for **C** indicate a generally higher spread for the

production batches, and this was confirmed for the following investigated PC's as well (not shown). The PCA score plots of the spectra of **C** from tablets at each target concentration level also showed clear systematic effects between and within production batches. Examples are shown in Figs. 4 and 5. An interesting example of intra-batch variability is shown in Fig. 4, where the spectra from the batch marked with blue squares showed two separate clusters. This may be due to a systematic effect that occurred over the manufacturing time of the batch. Hence, selecting the samples for calibration holds a risk of not fully covering the spectral intra- and inter-batch variation that may be present in future samples.

As the variation in **C** is partly due to differences in API content (the parameter to be quantified) in each individual tablet, this spectral information cannot be used 'as such' for defining the clutter for the proposed strategies. Many correction methods define the clutter by the difference spectra at various perturbation levels, which works well when the property to be determined can be held constant [17]. Here, it is impossible to obtain individual tablets, even from the same batch, with exactly the same API concentration and tablet composition. Another possibility is using a *y*-gradient method to select the spectra for calculating the difference spectra [26], but no *y*-reference values are available for the massive amount of prior spectral information. For the present case study, we proposed another methodology to obtain a relevant estimate of the clutter. To correct **C** for known chemical variations, the pure spectra from the tablet constituents were used to calculate a basis. Removal of their spectral contributions from **C** was performed by orthogonal projection [18]. After the correction of **C**, the spectra have lost their initial form, leaving only the spectral shapes from other variations (Fig. 6).

Fig. 7 schematically illustrates the different tested strategies for obtaining a clutter. Matrix **B** (tablet excipients) can be defined as a clutter containing the known chemical noise. Considering both **A** and **B** for the orthogonal correction renders a clutter containing only the physical variations and unknown chemical variation (e.g., water content, ...) (**D**). Using **A** yields a clutter containing physical variations and chemical variability caused by all 'interfering' excipients (**E**).

#### 3.4.2. Strategies using EPO

Depending on how the clutter is defined, there are different possibilities to perform EPO corrections on the calibration spectra **X** (Fig. 7). In a similar way as above,  $EPO_{chem}$  directly removes the known interfering chemical variations (**B**) from the **X** spectra. In  $EPO_{glob}$  the expected chemical and other variations were captured in **E** for global EPO correction of **X**. Here, optimization of the dimension of the subspace to be withdrawn was performed by analysing the evolution of the RMSECV as a function of  $g_a$  and the number of LV's [19].

#### 3.4.3. Strategies using data augmentation

Noise augmentation (NA) of the calibration set was obtained by adding the mean-centred spectra of **D** to *n* repetitions of the original calibration spectra **X**. Similarly,  $y_{aug}$  was developed as *n* repetitions of **y**, because the added spectral variations are not supposed to change the corresponding *y* value of each spectrum (Fig. 7). Hence, a calibration set containing 10,213 objects was obtained and used for PLS regression.

Because OSC and NAP need a calibration database to calculate the orthogonal projection, these techniques were applied on the augmented calibration set, i.e.,  $X_{aug}$  and  $y_{aug}$  containing the most complete information. The  $OSC_{aug}$  used the  $X_{aug}$  and  $y_{aug}$  calibration base for calculating the orthogonal correction. The NA-NAP strategies performed NAP on the augmented calibration base  $X_{aug}$

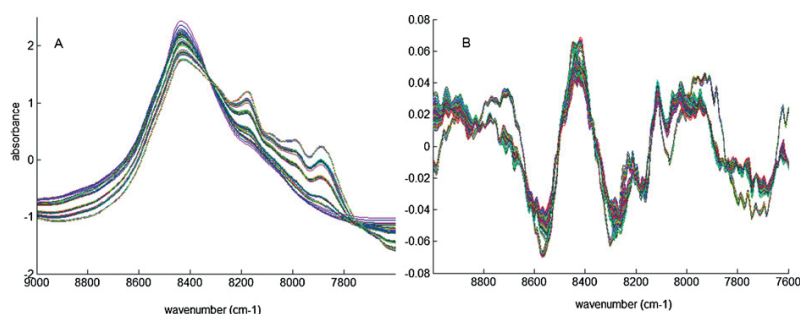


Fig. 6. Spectra before (A) and after (B) orthogonal correction using the pure component spectra of the API and excipients to remove the known chemical variations.

and  $y_{aug}$  this way calculating a projection factor to transform the spectra in  $X$  to  $X^*$  prior to PLS or CLS regression. The optimal number of factors  $g_a$  to be removed was determined via the minimal RMSECV. The test set spectra underwent the same transformation as the calibration spectra.

### 3.4.4. Strategies using ACLS

The SRACLS procedure described in [14] was used to define an augmented pure component matrix  $K$  consisting of the pure spectra from the API (**A**) and the excipients (**B**), and the  $p$  first loading vectors from the residual matrix  $E_A$ . In the PACLS procedure the augmented pure component matrix of the SRACLS procedure was further augmented with the  $k$  first loading vectors from **D**. The optimal  $p$  and  $k$  were determined through cross-validation (minimal RMSECV).

### 3.5. Model update for strong water variations

To assess whether the strategies using prior spectral information can account for strong water variations, 2 different model update strategies were proposed. In *model update 1*, the spectra of such processed tablets were added (with corresponding reference values) to the calibration set 1 to obtain an updated calibration set containing 197 samples (120 initial + 77 processed samples). The prior information contained, just as in the previous section, no spectra of processed tablets. In *model update 2*, the initial training set 1 (120 not-processed tablets) was used for calibration. The prior information matrix containing intra- and inter-batch variability was augmented with spectra from processed tablets to account also for the strong water variations.

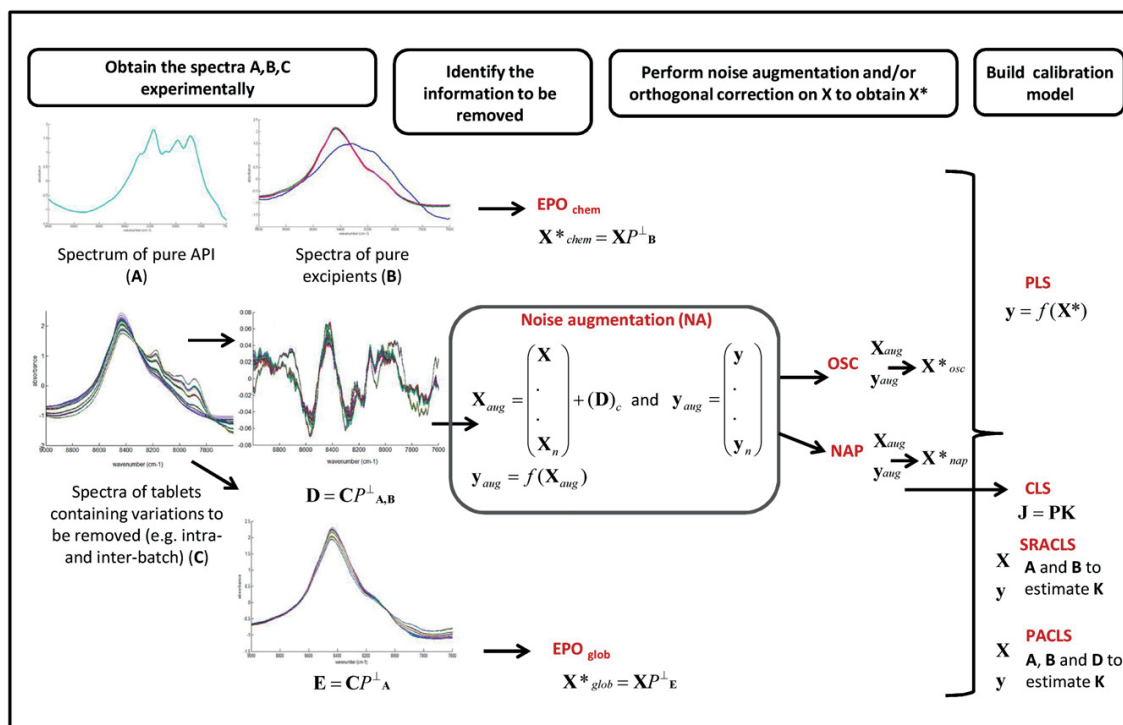


Fig. 7. Flow chart depicting the applied methodologies. **A**, **B** and **C** are matrices containing prior information; the subscript  $c$  represents mean-centred matrices.  $X$  (measured spectral absorbances **J**) and  $y$  (concentrations to be predicted **P**) represent the original calibration set.  $X_{aug}$  and  $y_{aug}$  are the noise augmented calibration set.  $P^{\perp}$  represents orthogonal projection and  $X^*$  is the calibration matrix returned after correction. **K** is the matrix of pure component signals at unit concentration.

#### 4. Results and discussion

##### 4.1. Models using prior information containing intra- and inter-batch variation

In this section, the above discussed strategies were applied to evaluate their capability for filtering the intra- and inter-batch effects hampering the model performance. Test set 1 was used to evaluate the model's ability to withstand unknown variability (external validation). With PLS models covering different amounts of variation in their calibration set as a benchmark, the performance of the investigated modelling strategies was investigated in terms of number of latent variables (LV's), root mean square error of prediction (RMSEP) and its statistical significance (Table 1). The number of factors used for the correction method was also reported. All models were trained on 4 different sample sets, holding different amounts of variation. Set 1 (120 tablets and 12 batches) contained the most intra- and inter-batch variation, while set 4 (18 tablets and 6 batches) contained the least. Sets 2 (60 tablets and 6 batches) and 3 (30 tablets and 6 batches) contained more intra-batch variation compared to set 4. The prior information matrix **C** was considered to be representative for intra- and inter-batch variability in the spectra.

The PLS, NAP-CLS, NAP-PLS and OSC-PLS models did not use any prior information and were added for comparison purposes. They were marked in Table 1 with an asterisk. For all calibration sets the OSC-PLS, NAP-PLS and NAP-CLS models were generally more parsimonious (less LV's) compared to PLS, but did not show improved predictive power. Many papers present similar conclusions on this behaviour of OSC and NAP [22–24]. PLS established higher prediction errors in models calibrated on sample sets containing less variability.

The prediction performances of the ACLS models (SRALCS and PACLS) were much worse than the PLS-based models, making the latter models more suitable for the present case study. It is hypothesized that ACLS models, based on a linear-additive model may have trouble capturing the physical differences between the NIR spectra of powders (pure components) and tablets. They might be more suitable for modelling pure mixtures of different components [14]. Augmenting the calibration set prior to PLS, i.e., by noise addition (NA)-PLS, yielded models with more LV's compared to the original PLS models. This can be attributed to more spectral variation being included in the calibration set. Noise augmentation before PLS regression (NA-PLS), making the calibration matrix very large (10,213 objects) and noisy, could not significantly enhance the prediction performance either, nor could OSC when applied on this augmented calibration matrix (NA-OSC-PLS). NA-NAP-PLS showed a statistically better prediction performance than the PLS model ( $p < 0.05$ ), with a 34–40% lower RMSEP, while needing less latent variables. A similar behaviour of this approach was also seen on all other calibration sets with a progressively smaller size (Table 1).

Compared to NA-PLS, adding the NAP pre-processing seems to be advantageous for making the model more parsimonious and for improving the prediction performance. Nadler and Coifman [27] concluded that PLS may behave differently in two idealized settings: for a noise-free training set the regression vector computed by PLS is, up to normalization, the net analyte signal, while for a noisy infinite training set the regression vector is not purely proportional to the NAS vector, but is optimal under a mean squared error of prediction criterion. Considering the obtained results, it may be speculated that NAP may have a different relationship towards PLS in the augmented calibration set. It would be an interesting topic of further study to find out why the NAP algorithm performs so much better on the large and noisy augmented calibration sets, and actually allows here an improvement in prediction performance.

**Table 1**  
Prediction performance (for test set 1) of the different models calibrated on sample sets with different variation. The matrix with prior intra- and inter-batch variation was **C** (10,213 × 364). The best prediction results are in bold.

Calibration set	Set 1 (120 tablets and 12 batches)				Set 2 (60 tablets and 6 batches)				Set 3 (30 tablets and 6 batches)				Set 4 (18 tablets and 6 batches)			
	Model	# factors	# LV	RMSEP	p-Value <sup>b</sup>	# factors	# LV	RMSEP	p-Value <sup>b</sup>	# factors	# LV	RMSEP	# factors	# LV	RMSEP	p-Value <sup>b</sup>
PLS <sup>a</sup>		7	7	0.586	–	–	4	0.630	–	–	4	0.636	–	4	0.663	–
NAP-CLS <sup>a</sup>		7	–	0.547	0.849	8	–	0.739	0.543	7	–	0.755	7	–	1.126	<0.001 <sup>c</sup>
NAP-PLS <sup>a</sup>		7	4	0.601	1.000	8	5	0.608	1.000	7	4	0.604	7	4	1.123	<0.001 <sup>c</sup>
OSC-PLS <sup>a</sup>		3	4	0.560	1.000	3	5	0.646	0.986	1	3	0.636	1	3	0.663	0.999
NA-PLS		–	8	0.496	0.928	–	5	0.588	1.000	–	6	0.566	–	6	0.585	0.985
SRALCS		5	–	0.659	0.954	10	–	1.254	<0.001 <sup>c</sup>	6	–	0.975	–	–	0.988	<0.001 <sup>c</sup>
PACLS		5–1	–	0.908	<0.001 <sup>c</sup>	8–1	–	1.099	<0.001 <sup>c</sup>	6–1	–	0.945	–	–	1.139	<0.001 <sup>c</sup>
EPO <sub>chem</sub> -PLS		4	5	0.511	0.716	4	4	0.468	0.013 <sup>c</sup>	4	5	0.487	4	5	0.519	0.281
EPO <sub>gr</sub> -PLS		1	6	0.461	0.449	1	7	0.581	1.000	1	6	0.478	1	7	0.516	0.009 <sup>c</sup>
NA-NAP-CLS		10	–	0.572	1.000	12	–	0.527	0.588	11	–	0.546	11	–	0.434	0.026 <sup>c</sup>
NA-NAP-PLS		<b>10</b>	<b>3</b>	<b>0.388</b>	<b>0.027<sup>c</sup></b>	<b>12</b>	<b>2</b>	<b>0.407</b>	<b>0.007<sup>c</sup></b>	<b>11</b>	<b>2</b>	<b>0.382</b>	<b>11</b>	<b>1</b>	<b>0.431</b>	<b>0.015<sup>c</sup></b>
NA-OSC-PLS		2	3	0.488	0.697	1	2	0.546	0.586	1	2	0.533	1	2	0.564	0.727

<sup>a</sup> These models did not use prior information; they used only information from the calibration set.

<sup>b</sup> p-Values (Dunnnett's test) for the significance testing by two-way ANOVA of the predictive ability compared to PLS.

<sup>c</sup> Indicates significantly lower absolute prediction errors on significance level  $\alpha = 0.05$ .

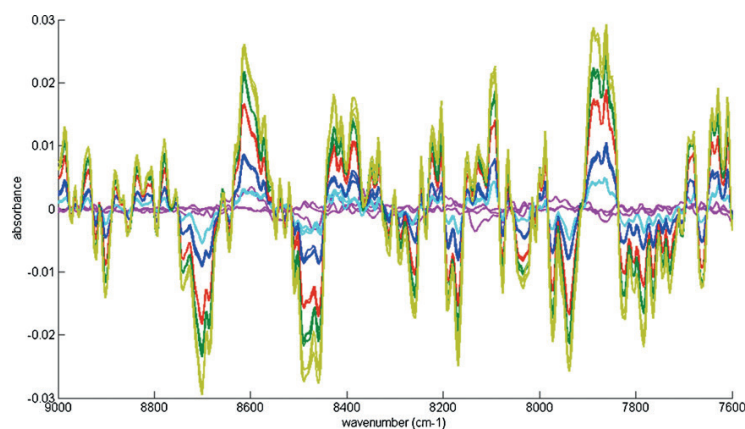


**Fig. 8.** Calibration spectra  $\mathbf{X}_{\text{nap}}^*$  ( $18 \times 364$ ) of set 4 after NA-NAP transformation. These spectra were subsequently calibrated on  $\mathbf{y}$  with PLS. The different colours represent the different API concentration levels.

Compared to NAP-PLS, the NA procedure may add more variability into the calibration database, which is missing when using non-exhaustive calibration. In the NAP-CLS and NAP-PLS models only 7–8 factors were removed by the NAP procedure, whereas the NA-NAP operation removed between 10 and 12 factors, and approximately 1–3 additional factors were needed for subsequent PLS regression. This may approximate the number of perturbation factors to be expected in future tablets. Hence the augmentation step is also necessary to make the model more robust and the completeness of the clutter is an important factor for the performance and robustness of the models.

Except for the model calibrated on set 4 the NA-NAP method performed clearly better when combined with PLS instead of CLS. In these cases, PLS was able to further model the important information. In case of calibration set 4, the NA-NAP operation returned the original calibration spectra  $\mathbf{X}$  into  $\mathbf{X}^*$  containing almost exclusively information on the component to be quantified (Fig. 8), with PLS and CLS giving a comparable result.

Compared to PLS, EPO-PLS based calibrations showed lower RMSEP's and needed a lower number of LV's, and especially for models calibrated on sample sets carrying fewer variability there was a statistical difference between both approaches. Considering only the chemical variations in the correction, i.e.,  $\text{EPO}_{\text{chem}}$ , allowed improving the model performance to some extent. This can be attributed to the correction for the changing tablet compositions

over the API target concentration levels, as well as for excipient inhomogeneities among individual tablets.

#### 4.2. Deliberate water variation (model update)

When the tablets are processed, i.e., stored at different extreme temperature and humidity conditions, the water content in the tablets can change considerably [6]. Compared to the tablets that were stored under normal conditions, those stored long in high humidity conditions (i.e., 75% RH) showed an interesting effect in their NIR spectra, i.e., shifts in the API absorption signals were visible (Fig. 2). These frequency shifts may suggest a different hydrogen bonding state of the API [28]. As this variation affects the PLS model predictions (Table 2), we investigated whether this information might be considered in the calibration base or in the clutter for a model update.

In case the model was updated by adding deliberate water variation to the calibration data base, the NA-NAP-PLS strategy again outperformed the others, and was the only model being statistically significantly better than PLS (Table 2, update 1). With a model requiring only 4 LV's an RMSEP of 0.380 for test set 1 and one of 0.385 for test set 2 were obtained. Hence the model was able to predict perturbed samples reasonably well (test set 2), while also not substantially reducing the prediction performance for normal or unperturbed samples (test set 1). Compared to NA-NAP-CLS,

**Table 2**

Prediction performance (for test sets 1 and 2) after model update for deliberate water variations. The best prediction results are in bold.

Model	Update 1					Update 2				
	# factors	# LV	RMSEP test set 1	RMSEP test set 2	p-Value <sup>b</sup>	# factors	# LV	RMSEP test set 1	RMSEP test set 2	p-Value <sup>b</sup>
PLS <sup>a</sup>	–	8	0.632	0.407	–	–	7	0.586	1.274	–
NAP-CLS <sup>a</sup>	8	–	0.534	0.461	0.883	7	–	0.547	1.488	1.000
NAP-PLS <sup>a</sup>	8	6	0.644	0.302	0.645	7	4	0.601	1.358	1.000
OSC-PLS <sup>a</sup>	5	6	0.632	0.346	0.989	3	4	0.560	1.506	1.000
NA-PLS	–	8	0.548	0.433	0.549	–	5	0.466	0.854	0.844
SRACLS <sup>a</sup>	9	–	0.780	0.466	0.124	5	–	0.659	1.557	1.000
PACLS	9–1	–	0.756	0.417	0.067	5–12	–	5.490	8.323	<0.001 <sup>c</sup>
$\text{EPO}_{\text{chem}}$ -PLS <sup>a</sup>	4	5	0.575	0.376	0.792	4	5	0.511	0.913	0.948
$\text{EPO}_{\text{gl}}$ -PLS	1	7	0.516	0.397	0.284	1	7	0.549	0.977	0.989
NA-NAP-CLS	11	–	0.512	0.517	0.964	13	–	0.567	0.728	0.923
NA-NAP-PLS	<b>11</b>	<b>4</b>	<b>0.380</b>	<b>0.385</b>	<b>0.003<sup>c</sup></b>	13	3	0.488	0.761	0.595
NA-OSC-PLS	4	2	0.498	0.409	0.265	1	2	0.510	0.976	0.966

<sup>a</sup> These models did not use prior information of processed tablets containing deliberate water variations.

<sup>b</sup> p-Values (Dunnnett's test) for the significance testing by two-way ANOVA of the predictive ability compared to PLS.

<sup>c</sup> Indicates significantly lower absolute prediction errors on significance level  $\alpha = 0.05$ .



NA-NAP-PLS allowed a lower RMSEP for both test sets. The NA-NAP-PLS model now required 1 LV more than before model update (Table 1, set 1), which it probably needs to model the shifting of the API absorption signals.

The second model updating strategy included the spectra of the perturbed samples in the prior spectral information matrix. As expected, models using no prior information from processed tablets, i.e., PLS, NAP-CLS, NAP-PLS, OSC-PLS, SRACLS and EPO<sub>chem</sub>-PLS, displayed poor prediction performance for test set 2 (Table 2, update 2). This could be attributed to the fact that they did not take into account the deliberate water variation. Although some of the modelling strategies that used prior information from processed tablets were able to get better prediction errors for test set 2, the overall model performance was low and none of the methods performed significantly better than PLS. Compared to the models updated with strategy 1, none of the methods in model update 2 was able to obtain good prediction results for test set 2. The prediction performance for test set 1 remained reasonably well in all models (except for PACLS), whereas predictions for test set 2 were always poor. The reason for this was found to be that the spectral perturbations due to strong water content variations in **C** (also causing shifting of the API absorption signals) are not completely independent of **y**, and therefore could not be considered in the model update. The proposed method to define the clutter (step 1 of the strategy, see Section 3.4.1) uses unsupervised orthogonal projections with the pure component spectra. These may remove that part of **C**, which is co-linear to **y**, making it not possible to fully consider this kind of spectral variation in the clutter. These results demonstrate that the proposed strategies only allow making the model more robust for spectral variation that is not co-linear with the one from the property of interest. Hence, this variability should still be considered in the calibration set.

## 5. Conclusions

When developing a NIR model for routine quality control that needs to operate over a longer time course, it may not be evident to cover all possible perturbation factors in the calibration set. Because it is difficult to select samples describing intra- and inter-batch variability and to decide when the calibration set is representative, this study explored whether the judicious use of such prior spectral information during model development can improve the performance of NIR models for predicting the API content in tablets. The proposed strategies did neither require exact knowledge of the perturbation levels (only controlled variability of the considered perturbations was necessary), nor needed extra reference analyses.

Rather than exhaustive calibration, a more cost-effective model development approach was aspired. A massive amount of prior spectral information on intra- and inter-batch variation was obtained to allow a more representative view of the possible disturbing (i.e., systematic) effects to be encountered in the NIR spectra of tablets from a routine production. The best approach (NA-NAP-PLS) consists of four essential steps. First, the disturbances to be removed are identified by means of using an orthogonal projection of pure component spectra (API and excipients) to those of the tablets containing representative intra- and inter-batch variability. This way, the known chemical variation is removed from the spectra leaving only the other variations. These mean-centred variations are in a second step added to *n* repetitions of the spectra of **X** for calibration (noise augmentation) to increase the variability in the existing calibration database. In a third step, net analyte pre-processing is used to remove those variations in

**X**<sub>aug</sub> that are orthogonal to **y**<sub>aug</sub>, in order to obtain a better estimate of the NAS. Finally, in a fourth step the orthogonally corrected **X** spectra are regressed to **y** by PLS regression.

Compared to PLS, a statistically significant improvement in prediction performance and a 34–40% reduction in RMSEP was obtained for predicting new tablets with unknown intra- and inter-batch variability. The model needed a minimal amount of calibration samples and latent variables. It would be interesting to further study the behaviour of NAP-PLS in very large and noisy calibration matrices.

Where PLS models need the calibration set to be as complete as possible, models using prior spectral information require completeness of their clutter. This was also demonstrated by updating the model for strong water content variations in the tablets. The latter caused frequency shifts of the API absorption signals that could not be included in the clutter, resulting in reduced performance of the proposed strategies for this kind of variation. It also revealed a limitation of the method: the spectral variance that is co-linear with the wanted variation could not be considered in the clutter and should be considered in the calibration set.

## Acknowledgement

Sigrid Pieters and Wouter Saeys are respectively funded as aspirant and postdoctoral fellow of the Research Foundation – Flanders (FWO).

## References

- [1] J. Luybaert, D.L. Massart, Y. Vander Heyden, *Talanta* 72 (2007) 865–883.
- [2] T. De Beer, A. Burggraef, M. Fonteyne, L. Saerens, J.P. Remon, C. Vervaet, *Int. J. Pharm.* 147 (2011) 32–47.
- [3] D. Cozzolino, W. Cynkar, N. Shah, P. Smith, *Anal. Bioanal. Chem.* 401 (2011) 1475–1484.
- [4] W.F. McClure, *Anal. Chem.* 66 (1994) 43–53.
- [5] M. Blanco, A. Peguero, *J. Pharm. Biomed. Anal.* 52 (2010) 59–65.
- [6] T. Van den Kerkhof, R. De Maesschalck, K. Vanhoutte, M.C. Coene, *J. Pharm. Biomed. Anal.* 42 (2006) 517–522.
- [7] A. Peirs, J. Tirry, B. Verlinden, P. Darius, B.M. Nicolai, *Postharv. Biol. Technol.* 28 (2003) 269–280.
- [8] EMEA/CHMP/CVMP/QWP/17760/2009 Rev 2, 2012 (accessed 28.03.12).
- [9] D.L. Massart, B.M.G. Vandeginste, L.M.C. Buydens, S. De Jong, P.J. Lewi, J. Smeyers-Verbeke, *Handbook of Chemometrics and Qualimetrics: Part A*, Elsevier, Amsterdam, 1997.
- [10] M.J. Saiz-Abajo, B.H. Mevik, V.H. Segtnan, T. Naes, *Anal. Chim. Acta* 533 (2005) 147–159.
- [11] B.H. Mevik, V.H. Segtnan, T. Naes, *J. Chemom.* 18 (2004) 498–507.
- [12] J.A. Fernandez Pierna, F. Chauchard, S. Preys, J.M. Roger, O. Galtier, V. Baeten, P. Dardenne, *Chemom. Intell. Lab. Syst.* 106 (2011) 152–159.
- [13] V.H. Segtnan, B.H. Mevik, T. Isaksson, T. Naes, *Appl. Spectrosc.* 59 (2005) 816–825.
- [14] W. Saeys, K. Beullens, J. Lammertyn, H. Ramon, T. Naes, *Anal. Chem.* 80 (2008) 4951–4959.
- [15] D.M. Haaland, D.K. Melgaard, *Appl. Spectrosc.* 54 (2000) 1303–1312.
- [16] D.M. Haaland, D.K. Melgaard, *Vib. Spectrosc.* 29 (2002) 171–175.
- [17] J.C. Boulet, J.M. Roger, *Chemom. Intell. Lab. Syst.* 117 (2012) 61–69.
- [18] J.C. Boulet, T. Doco, J.M. Roger, *Chemom. Intell. Lab. Syst.* 87 (2007) 295–302.
- [19] J.M. Roger, F. Chauchard, V. Bellon-Maurel, *Chemom. Intell. Lab. Syst.* 66 (2003) 191–204.
- [20] S. Preys, J.M. Roger, J.C. Boulet, *Chemom. Intell. Lab. Syst.* 91 (2008) 28–33.
- [21] S. Wold, H. Antti, F. Lindgren, J. Ohman, *Chemom. Intell. Lab. Syst.* 44 (1998) 175–185.
- [22] H.C. Goicoechea, A.C. Olivieri, *Chemom. Intell. Lab. Syst.* 56 (2001) 73–81.
- [23] W. Ni, S.D. Brown, R. Man, *Chemom. Intell. Lab. Syst.* 98 (2009) 97–107.
- [24] O. Svensson, T. Kourti, J.F. MacGregor, *J. Chemom.* 16 (2002) 176–188.
- [25] H.R. Cederkvist, A.H. Aastveit, T. Naes, *J. Chemom.* 19 (2005) 500–509.
- [26] [http://wiki.eigenvector.com/index.php?title=Decluster\\_Settings\\_Window](http://wiki.eigenvector.com/index.php?title=Decluster_Settings_Window) (accessed 11.04.12).
- [27] B. Nadler, R.R. Coifman, *J. Chemom.* 19 (2005) 45–54.
- [28] S. Pieters, T. De Beer, J.C. Kasper, D. Boulpaep, O. Waszkiewicz, M. Goodarzi, C. Tistaert, W. Friess, J.P. Remon, C. Vervaet, Y. Vander Heyden, *Anal. Chem.* 84 (2012) 947–955.

---

## Curriculum Vitae

---

Sigrid Pieters was born on December 19<sup>th</sup>, 1979 in Aalst, Belgium. In 2003 she graduated as a Pharmacist at the Vrije Universiteit Brussel, and hereafter continued working in private pharmacies. In 2008 she obtained a Master after Master degree in Industrial Pharmaceutical Sciences (interuniversity). She performed her internship at the Pfizer manufacturing plant in Puurs, Belgium, where she obtained know-how on sterile drug product manufacturing. In December 2008 she started working as a pre-doctoral researcher at the department of Analytical Chemistry and Pharmaceutical Technology (FABI), under the supervision of Prof. Y. Vander Heyden. She started performing research in chemometrics in separation science, and afterwards she worked on her PhD dissertation, which was a co-operation between the VUB and the UGent (supervised by Prof. T. De Beer). For this work she obtained a scholarship from the Research Foundation – Flanders (FWO). In 2009, she followed a course on Process Analytical Technology at the Technical University of Denmark (DTU), and in 2012, she had a research stay at Irstea in Montpellier, France. Under the supervision of Dr. J.M. Roger she obtained hands-on experience on using orthogonal projections for making multivariate calibration models more robust.

The results of her research work were published in several international peer-reviewed journals and presented as oral and poster communications at national and international conferences. She also co-promoted 4 master thesis students.





---

## List of publications

---

1. Emerging analytical separation techniques with high-throughput potential for pharmaceutical analysis part I: stationary phase and instrumental developments in LC (review)  
*S. Pieters, B. Dejaegher, Y. Vander Heyden*  
Combinatorial Chemistry and High-Throughput Screening 13 (2010) 510-529 (impact factor 2010 = 2.573)
2. Pressurized capillary electrochromatography in a screening for possible antioxidant molecules in Mallotus fingerprints: Challenges, potentials and prospects  
*S. Pieters, C. Tistaert, G. Alaerts, K. Bodzioch, D. Mangelings, B. Dejaegher, C. Rivière, M. Chau Van, J. Quetin-Leclercq, Y. Vander Heyden*  
Talanta 83 (2011) 1188-1197 (impact factor 2011 = 3.794)
3. Near-infrared spectroscopy for in-line monitoring of protein unfolding and its interactions with lyoprotectants during freeze-drying  
*S. Pieters, T. De Beer, J.C. Kasper, D. Boulpaep, O. Waszkiewicz, M. Goodarzi, C. Tistaert, W. Friess, J.P. Remon, C. Vervaet, Y. Vander Heyden*  
Analytical Chemistry 84 (2012) 947-955 (impact factor 2012 = 5.695)
4. Near-infrared and Raman spectroscopy: Potential tools for monitoring of protein conformational instability during freeze-drying processes  
*S. Pieters, T. De Beer, Y. Vander Heyden*  
American Pharmaceutical Review 15 (2012) 66-73
5. Robust calibrations on reduced sample sets for API content prediction in tablets: definition of a cost-effective NIR model development strategy  
*S. Pieters, W. Saeys, T. Van den Kerkhof, M. Goodarzi, M. Hellings, T. De Beer, Y. Vander Heyden*  
Analytica Chimica Acta 761 (2013) 62-70 (current impact factor = 4.387)
6. Raman spectroscopy and multivariate analysis for the rapid discrimination between native-like and non-native conformational states in freeze-dried protein formulations  
*S. Pieters, Y. Vander Heyden, J.M. Roger, M. D'Hondt, L. Hansen, B. De Spiegeleer, C. Vervaet, J.P. Remon, T. De Beer*  
European Journal of Pharmaceutics and Biopharmaceutics, in press (current impact factor = 3.826)
7. Increasing robustness against spectral background variability of a Raman model for the protein conformational state classification in freeze-dried formulations  
*S. Pieters, J.M. Roger, T. De Beer, M. D'Hondt, B. De Spiegeleer, Y. Vander Heyden*  
submitted
8. Multivariate statistical in-line monitoring of protein unfolding during freeze-drying using Raman spectroscopy  
*S. Pieters, Y. Vander Heyden, L. Hansen, M. D'Hondt, B. De Spiegeleer, J.P. Remon, C. Vervaet, T. De Beer*  
in preparation

9. Improving the capillary electrophoretic analysis of Poliovirus using a Plackett-Burman design  
*I. Oita, H. Halewyck, S. Pieters, B. Dejaegher, B. Thys, B. Rombaut and Y. Vander Heyden*  
Journal of Pharmaceutical and Biomedical Analysis 50 (2009) 655-663 (impact factor 2009 = 2.453)
10. Emerging analytical separation techniques with high-throughput potential for pharmaceutical analysis part II: novel chromatographic modes (review)  
*B. Dejaegher, S. Pieters, Y. Vander Heyden*  
Combinatorial Chemistry and High-Throughput Screening 13 (2010) 530-547 (impact factor 2010 = 2.573)
11. Rational use of stacking principles for signal enhancement in capillary electrophoretic separations of poliovirus samples  
*I. Oita, H. Halewyck, S. Pieters, B. Dejaegher, B. Thys, B. Rombaut and Y. Vander Heyden*  
Journal of Pharmaceutical and Biomedical Analysis 55 (2011) 135-145 (impact factor 2011 = 2.733)
12. Poliovirus separation from cell extracts using capillary electrophoresis: Potential use in vaccine production and control?  
*I. Oita, H. Halewyck, S. Pieters, B. Thys, Y. Vander Heyden, B. Rombaut*  
Journal of Virological methods 185 (2012) 7-17 (impact factor 2012 = 2.011)
13. Similarity analyses of chromatographic fingerprints as tools for identification and quality control of green tea  
*G. Alaerts, J. Van Erps, S. Pieters, M. Dumarey, A.M. van Nederkassel, M. Goodarzi, J. Smeyers-Verbeke, Y. Vander Heyden*  
Journal of Chromatography B 910 (2012) 61-70 (impact factor 2012 = 2.888)
14. Near-infrared spectroscopic evaluation of lyophilized viral vaccine formulations  
*L. Hansen, S. Pieters, J.P. Montenez, R. Daoussi, Y. Vander Heyden, C. Vervaet, J.P. Remon, T. De Beer*  
Biotechnology Progress, in press (current impact factor = 1.853)
15. Particle swarm optimization and genetic algorithm as feature selection techniques for the QSAR modeling of imidazo[1,5-a]pyrido[3,2-e]pyrazines, inhibitors of phosphodiesterase 10A  
*M. Goodarzi, W. Saeys, O. Deeb, S. Pieters, Y. Vander Heyden*  
Chemical Biology and Drug Design, in press (current impact factor = 2.469)
16. Exploration and classification of entire chromatographic fingerprints for identification and quality control of several artemisia species  
*G. Alaerts, S. Pieters, H. Logie, M. Merino-Arévalo, J. Van Erps, L. Schockaert, B. Dejaegher, J. Smeyers-Verbeke, Y. Vander Heyden*  
submitted

